CHEMISTRY JOURNAL OF MOLDOVA. General, Industrial and Ecological Chemistry. 2016, 11(2), 10-16
http://cjm.asm.md
http://dx.doi.org/10.19261/cjm.2016.11(2).15

OVERVIEW OF ECOLOGICAL CHEMISTRY CONFERENCES (1985-2016)

As scientific direction, Ecological Chemistry has been successfully developing in Moldova over the past three decades. Its history began in 1985, when the First International School on Ecological Chemistry of the Environment was organized. More than 80 remarkable scholars from the major research centres of the USSR and 17 foreign countries were among the participants of the event. The main decision made during the event was to develop this scientific direction and the regular organizing of conferences and symposia dedicated to it.

Further, for more than 30 years the Ecological Chemistry has been intensively expanding, being one of the priorities for the sustainable development and international cooperation providing tangible impact to the research and innovation activities in Moldova.

Organization of the ECOLOGICAL CHEMISTRY Conferences in Chisinau, Republic of Moldova transformed into important tradition and represent a series of successful conferences occurred in 1995, 2002, 2005, 2008, 2010 and 2012 being supported by UNESCO, UNEP, CRDF/MRDA, CEI, NATO, ONRG, as well as the local R&D organizations such as the Academy of Sciences of Moldova, Department of Industrial and Ecological Chemistry, Scientific Centre for Ecological and Applied Chemistry, Faculty of Chemistry and Chemical Technology of the Moldova State University, Institute of Chemistry of Academy of Sciences of Moldova, Chemical Society of Republic of Moldova, Moldovan Research and Development Association, etc. The list of the organized Conferences till 2016 and the forthcoming 6th International Conference on Ecological & Environmental Chemistry (2-3 March 2017), number of participants and number of countries are presented in Table 1.

Table 1

The list of the Ecological Chemistry Conferences organized within 1985-2016.

Date	*Title of the Conference*	*No. of Participants*	*No. of Countries*
1985	First School on Ecological Chemistry	80	17
1995	1st International Conference on Ecological Chemistry	150	21
2002	2nd International Conference on Ecological Chemistry	250	22
2005	3rd International Conference on Ecological Chemistry	700	40
2008	4th International Conference and NATO Advanced Research Workshop: The Role of Ecological Chemistry in Pollution Research and Sustainable Development	160	17
2010	International Conference on Ecological Chemistry: Water resources of the Dniester river – premises for the sustainable development of the regional localities	80	4
2010	International Conference: "Water: History, Resources, Perspectives"	200	10
2012	5th International Conference on Ecological Chemistry	300	18
2017 (2-3 March)	*Forthcoming 6th International Conference on Ecological & Environmental Chemistry*	*Registered participants 350*	*25*

Through the years, Ecological Chemistry Conferences became an arena to exchange the latest ideas and promising approaches and opportunities, to present and discuss recent results on the physical-chemical and biochemical aspects of processes, which occur in the ecosystem – soil, air and water, environmental pollution impact to human health and its prevention, environmental engineering and modelling, as well as social and educational implications. The topics of Ecological Chemistry Conferences were adjusted each time to the real needs and their evolution is presented in the Table 2.

The conferences encourage and facilitate the communication among young and experienced scientists, engineers, economists, teachers and professionals working on environmental issues and sustainable development in order to promote healthy style and conditions of life.

The 1st International Conference on Ecological Chemistry organized in 1995 gathered participants from the NIS, EU, USA and Australia and draw up the scientific topics for discussing the latest achievements in the field. The conference materials, which included the books of proceedings and abstracts, were spread to participants during the conference. Among the numerous important reports presented at the conference, the following could be mentioned:

- INTRODUCTION IN ECOLOGICAL CHEMISTRY, *Prof. Gheorghe Duca, Moldova;*
- ECOLOGICAL CATALYSIS: TEORETICAL AND PRACTICAL ASPECTS, *Prof. Tatyana Rakitskaya, Odessa, Ukraine;*

- ENVIRONMENTAL ENGINEERING AND MANAGEMENT OF ECOSYSTEMS: APPLICATION OF BIOLOGICAL, CHEMICAL AND PHYSICAL PROCESSES IN WASTE MANAGEMENT, *Prof. Joseph Malina, USA;*
- WATER RESOURCES MANAGEMENT, *Prof. Paolo Lupino, Italy;*
- MODERN PERFORMANCES ABOUT PROCESSES OF NATURAL WATERS CHEMICAL SELF-PURIFICATION, *Prof. Yurii Skurlatov, Dr. Elena Shtamm, Russia.*

Table 2

International Conferences on Ecological Chemistry Topics Evolution.

1995 - 1st International Conference on Ecological Chemistry	*2002 - 2nd International Conference on Ecological Chemistry*	*2005 - 3rd International Conference on Ecological Chemistry*
A. Natural Self-Purification Processes **B. Transport and Fate of Pollutants in Ecosystems** **C. Remedial Measures to Degrade or Immobilize Pollutants Chemically or Biologically** **D. Impact of Chemical Pollutants and Risk Assessment** **E. Ecological Policy, Law, Education and Training** **F. Environmental Engineering** **G. Environmental Control and Monitoring**	**A. Ecological Chemistry of Water** • *Quality Management and Water Analysis* • *Redox and Catalytic Processes of Self-Purification* • *Drinking Water Quality* • *Wastewater Treatment* **A. Electrochemistry and Ecological Chemistry** **B. Ecological Chemistry of Atmospheric Air** • *Chemical Processes in Atmosphere* • *Impact of Chemistry on the Ozone Layer* • *Effect of Greenhouse Gases* • *Role of Particles on Urban Aerosols* • *Impact of Combustion Gases on Human Health* **C. Soil Contamination and Waste Management** • *Industrial Waste and Landfills* • *Materials Recovery and Recycling* • *Pesticides and other Persistent Organic Pollutants* **D. Environmental Friendly Agricultural Technologies** • *Sustainable Agriculture* • *Pesticides and Fertilizers Management* • *Food Chemistry* **E. Chemical Risk Assessment and Health** • *Impact of Chemicals on Ecosystems* • *Human Health and Environment* • *Biodegradation and Bioaccumulation* **G. Pollution Prevention** • *Product and Process Integrated Environmental Protection* • *Advances in Process and Emission Control*	**A. Ecological Chemistry of Water** • *Monitoring of Water Quality and Environmental Modeling* • *Redox Processes in Natural Water* • *Water Treatment and Supply* **B. Ecological Chemistry of Air** • *Chemical Processes in Atmosphere* • *Air Quality Control and Management* • *Impact of Air Emissions on Human Health* **C. Ecological Chemistry of Soil** • *Soil Contamination and Pollution Prevention* • *Ecological Agriculture* • *Ecological Technology in Agricultural Sector* **D. Waste Management and Cleaner Production** • *Industrial Pollution* • *Solid Waste Management* • *Persistent Organic Pollutants Management* • *Cleaner Production and Sustainable Business* **E. Chemical Risk Assessment** • *Impact of Chemicals on Human Health and Environment* • *Ecotoxicology* • *Chemical Risk Mitigation and Analysis* **F. Ecological Policy and Legislation** • *Ecological Legislation* • *Community Involvement and Education* • *Sustainable Development* **G. Electrochemistry and Ecology** • *Electrochemical methods of environmental protection* • *Ecological problems in electrochemical production* • *Electrochemical methods of natural and waste water treatment and conditioning*

Continuation of Table 2

2008 - 4th International Conference and NATO ARW: The Role of Ecological Chemistry in Pollution Research and Sustainable Development	***2012 - 5th International Conference on Ecological Chemistry***	***2017 - 6th International Conference on Ecological & Environmental Chemistry***
A. Organic Pollutants and POPs in the Environment – Occurrence, Fate and Prevention Measures **B. Water Pollution and Wastewater Treatment** **C. Soil Pollution and Prevention** **D. Waste Management** **E. Risk Assessment, Mitigation Measures and Environmental Awareness**	**A. Ecological chemistry of water** • *Chemical processes and natural waters self-purification* • *Methods of analysis and monitoring of water resources* • *Water treatment and supply* • *Impact of natural waters pollution on the human health* **B. Ecological chemistry of the atmosphere** • *Chemical processes in atmosphere* • *Methods of analysis of gas emissions* • *Mitigation of gas emissions impact on human health* **C. Ecological chemistry of soil** • *Chemical processes in soil* • *Soil degradation processes and their prevention* • *Methods of analysis and mitigation of soils pollution with pesticides* • *Impact of soils pollution on human health and habitat* **D. Ecological chemistry and healthy life style** • *Chemical risk assessment of anthropogenic impact on human health and environment* • *Mathematical modelling and long-term prognosis of human impact on the environment, of trans-boundary transport of pollutants and climate change* • *Medico-biological perspective on ecological chemistry – problems of acute and chronic toxicity, allergies, cancerigenic effects, bioassay* **E. Ecological chemistry and sustainable development** • *Ecological awareness and education* • *Access to ecological information* • *Ecological auditing* • *Public participation in addressing environmental pollution problems* • *Ecological legislation*	**A. Ecological Chemistry** • *Physico-chemical and chemico-biological processes which determine composition, structure and chemical properties of the environment* • *Chemical risk assessment of human health and ecological system* **A. Environmental Chemistry and Engineering** • *Chemistry and processes of treatment of water, air and waste* • *Chemical degradation of soil* **B. Green Chemistry** • *Preventing and reducing the negative impact of chemistry on the environment* • *Design of ecological friendly technologies and chemical products that minimize the use and generation of hazardous substances* **C. Ecological & Environmental Aspects in Chemical Research and Education** • *Ecological & environmental methodological aspects in chemical research and innovation activities* • *Ecological & environmental methodological aspects in chemical education* **D. Yong Scientists Research in Ecological & Environmental Chemistry**
The International Conference "Water: History, Resources, Perspectives" 2010 A. **Physics, chemistry, and the evolution of water** B. **The cultural role of water** • *Water as a symbol* • *Water in traditional culture (folklore, music)* • *Water in literature and poetry* C. **Water and technology** • *The technology of water supply)* • *The technology of water treatment* D. **Environmental aspects of water** • *Quantity and quality of water* • *Water shortage and water-borne diseases as hazards* E. **Water and waters of Moldova**		

The conferences contributed to the fast development of the Ecological Chemistry direction in Moldova. New specializations were created at the Department of Industrial and Ecological Chemistry (DIEC) of Moldova State University resulting in the increase of the number of students. The annual editions of national conferences and trainings in the field of Ecological chemistry for students and young scientists have been organized. During these events, students had the opportunity to present their research results to a large public of experienced scientists. Some trainings and workshops for students and young scientists were organized in Turkey, Romania, Ukraine and other countries, giving them opportunity to familiarize with the latest generation of technologies and practices in the fields of ecological chemistry. Upon the initiative of the students of DIEC, many new ecological non-governmental organizations were founded, such as: CHIMECO, Terra Nostra, UNEP, etc. The projects with great impact for science and society, accomplished by the DIEC staff, were supported by different international foundations - SOROS, ACS, UNDP, UNEP, CRDF, Tacis, REC-Moldova, Novib, GTZ etc. Strong scientific collaborations were established with the researchers from USA, France, Romania, Ukraine, Russia, Armenia, etc.

The Second International Conference on Ecological Chemistry– 2002 was dedicated to 10th Anniversary of the Department of Industrial and Ecological Chemistry of Moldova State University. The most important reports were presented at the plenary session:

- ADVANCES AND PROSPECTS OF ECOLOGICAL CHEMISTRY, *Prof. Gheorghe Duca, Moldova;*
- AQUATIC ECOLOGICAL CHEMISTRY: PAST, PREZENT AND FUTURE, *Prof. Yurii Skurlatov, Russia;*
- GLOBAL TRENDS SHAPING AGRICULTURE, AN ENVIRONMENTAL PERSPECTIVE, *Prof. Seymour Van Gundy, USA;*
- IMPACT OF AIR POLLUTION ON SOIL QUALITY, *Dr. Eiliv Steiness, Norway;*
- MODERN STATE OF THE ACID RAIN PROBLEM, *Prof. Anatolyi Purmali, Russia;*
- ENVIRONMENTAL ENGINERING IS KEY TO SUSTAINABLE DEVELOPMENT, *Prof. Joseph Malina, USA;*
- THE NEW APPROACHES AT A QUANTITATIVE ESTIMATION OF SELFCLEARNING ABILITY OF NATURAL WATERS, *Prof. Gevork Pirumyan, Armenia;*
- APPLICATION OF SLIME BINDING COMPOSITIONS FOR PESTICIDE CONSERVATION, *Prof. Alma Samurzina, Kazakhstan;*
- CONSERVATION OF LAND FOR THE PRODUCTION OF ORGANIC CEREALS, *Iain Tolhurt, UK;*
- BIOETICS AND ECOLOGICAL CHEMISTRY, *Prof. Pietro Cavazini, Italy.*

The 3rd International Conference on Ecological Chemistry organized in 2005 is considered the largest conference because it was attended by more than 700 experienced and young scientists from 40 countries: Albania, Armenia, Austria, Azerbaijan, Belarus, Bulgaria, China, Croatia, Czech Republic, Egypt, Estonia, Germany, Greece, Georgia, France, Hungary, India, Iran, Italy, Israel, Kazakhstan, Kyrgyzstan, Latvia, Moldova, Nigeria, Northern Cyprus, Norway, Pakistan, Poland, Romania, Russia, Serbia and Montenegro, Switzerland, Tajikistan, Turkey, Vietnam, Ukraine, UK, USA, Uzbekistan.

The event received the financial support from UNESCO, U.S.CRDF, ONRG, U.S.NSF, American Chemical Society and the diplomatic missions of the participating countries.

Some of plenary reports are specified below:

- ECOLOGICAL CHEMISTRY. ASCHIEVEMENTS AND PERSPECTIVES, *Prof. Gheorghe Duca, Moldova;*
- CHEMICAL REACTIONS IN THE ATMOSPHERIC WATER, *Prof. Anatolii Purmali, Russia;*
- STRATEGIES FOR SOLVING THE PROBLEM OF ARSENIC POLLUTION IN NATURAL WATER, *Dr. John Malin, USA;*
- ECOLOGICAL CHEMISTRY AS A SCIENCE AND EDUCATION PROCESS, *Prof. Alma Samurzina, Kazakhstan;*
- ELECTROCHEMICAL TECHNICS FOR A CLEANER ENVIRONMENT, *Prof. Maria Jitaru, Romania;*
- THE DEVELOPMENT OF MOLECULAR BIOLOGY IN MOLDOVA TO ADDRESS AGRICULTURAL AND ENVIRONMENTAL ISSUES, *Prof. Seimour Van Gundy, USA;*
- THE ROLE OF BIOTESTING METHODS IN THE EVALUATION OF WATER QUALITY, *Dr. Elena Shtamm, Russia;*
- THE RISK ASSESSMENT OF THE TRANSFORMATION OF NATURAL ECOSYSTEMS OF BELARUSI UNDER THE IMPACT OF ATMOSPHERIC MAN-CAUSED NITROGEN AND SULFUR, *Dr. Vadim Zubritskii, Belarus;*
- ON THE ISSUES OF MODELING OF ENVIRONMENTAL PROCESSES OCCURRING IN RIVER WATER, *Dr. Trahel Vardanian, Armenia.*

The 4th International Conference on Ecological Chemistry organized in 2008 hosted the NATO Advanced Research Workshop:**"The Role of Ecological Chemistry in Pollution Research and Sustainable Development",** gathering experts from 17 countries: Austria, Armenia, Belarus, Germania, Egypt, Italy, Moldova, Romania, The Netherlands, Turkey, Ukraine, Russia, etc. **The main objective of the both event**s was to re-evaluate the state-of-the-art of pollution research in NIS, Middle East and Western European countries and to present promising approaches and strategies for environmentally friendly technologies towards a sustainable development including capacity building by education. The most representative reports are the following:

- TREATMENT OF WINERY SECONDARY PRODUCTS, *Prof. Gheorghe Duca, Chisinau, Moldova;*
- TEACHING SUSTAINABILITY IN CHEMICAL EDUCATION, *Prof. Ali Müfit Bahadir, Braunschweig, Germany;*
- BROMINATED FLAME RETARDANTS IN THE ENVIRONMENT, *Dr. Jacob de Boer, Ijmuiden, The Netherlands;*
- MONITORING AND MEASURES ON POPS IN TURKEY, *Dr. Özcan Ceylan, Istanbul, Turkey;*
- CURRENT STATE IN THE FIELD OF POPs MANAGEMENT IN UKRAINE, *Dr. Svitlana Sukhorebra, Kiev, Ukraine;*
- INTERMEDIATES IN PHOTOCHEMISTRY OF Fe(III)-CARBOXILATE COMPLEXES IN NATURAL WATERS, *Prof. Viktor Plyusnin, Novosibirsk, Russia;*
- THE ROLE OF SOIL ORGANIC MATTER IN LIMITING ORGANIC POLLUTION IN SOILS, *Prof. Nicola Senesi, Italy;*
- HUMIC SUBSTANCES IN MUNICIPAL REFUSE DISPOSED OF IN A LANDFILL, *Prof. Zdenek K. Filip, Czech Republic;*
- FATE AND BEHAVIOUR OF ORGANIC POLLUTANTS WHILE SLUDGE TREATMENT BY GAMMA-IRRADIATION, *Dr. Rawia El-Motaium, Cairo, Egypt;*
- COMPARATIVE STUDY OF KNOWLEDGE IN ENVIRONMENTAL PROBLEMS IN THE CONTEXT OF VARIOUS POPULATION GROUPS IN TWO EU MEMBER STATES, *Prof. Alfa Xenia Lupea, Timisoara, Romania.*

Following the event the book entitled "The Role of Ecological Chemistry in Pollution Research and Sustainable Development" was published by Springer in Series: NATO Science for Peace and Security Series C: Environmental Security, by Editors: Prof. Ali Mufit Bahadir, Germany and Acad. Gheorghe Duca, Moldova.

The scientific works gathered in this book demonstrate clearly the role of the processes defining the composition of the natural environment, its structure and chemical properties corresponding to the biologic value of habitation, the essential impacts of human activity and other related factors on all the environment components, including water, soil and air. The research in ecological chemistry contribute to diminishing of these negative impacts, and promote the rational using of natural resources, their qualified management, broader application of environmentally-friendly production technologies, thus leading to pollution reduction and sustainable development.

The scientific topics addressed at Ecological Chemistry Conferences lead to the organization of a series of events in civil society. One of the most worth mentioning is the **International Conference "Water: History, Resources, Perspectives**", organized in 2010 with considerable support of the Austrian Academy of Sciences and Art. At this event, the interdisciplinary approach and relationship between the humanitarian and natural science focused on folklore, history, terminology usage, management, science and innovation were presented. The most interesting reports are reflected below:

- WATER IN FOLKLORE, *Prof. Thede Kahl, Austria, Germany;*
- MANAGEMENT OF WATER QUALITY, *Acad. Gheorghe Duca, Moldova;*
- TOWARDS BALANCING SAFETY, SECURITY AND SUSTAINABILITY OF WATER GLOBALLY, *Prof. Ashok Vaseashta, USA;*
- SOS: DRINKING WATER, *Acad. Vladislav Gonchearuc, Ukraine;*
- WATER AND ITS ROLE IN VALUING THE GEOGRAPHICAL POSITION OF A STATE, *Dr. Radu Sageata, Paul Serban, Romania;*
- SOME CONSIDERATIONS REGARDING THE RELATIONSHIPS BETWEEN COMPOSITION OF WATER RESOURCES AND APPLIED POTABILISATION TECHNOLOGIES, *Dr. Margareta Nicolau, Romania;*
- SYMBOLIC AND RITUAL SIGNIFICANCE OF WATER IN ORTHODOX SOUTH-EASTERN EUROPE, *Prof. Walter Puchner, Greece;*
- PROTECTION OF THE HUMAN RIGHT TO WATER UNDER INTERNATIONAL LAW: THE NEED FOR ANEW LEGAL FRAMEWORK, *Dr. Jordan Daci, Albania;*
- CONTRIBUTION ON THE SOIL WATER BALANCE OF AN AGRARIAN SITE, *Prof. Othmar Nestroy, Austria;*
- GROUNDWATER CONTAMINATION BY NITRATES, SALINITY AND PESTICIDES: CASE OF THE UNCONFINED AQUIFER OF TRIFFA PLAIN, *Prof. Yassine Zarhloule, Morocco.*

Another important event organized in 2010 is the **International Conference on Ecological Chemistry: "Water resources of the Dniester river – premises for the sustainable development of the regional localities"**, which attracted stakeholders from R&D sector, public authorities and non-governmental organizations. The conference gathered more than 60 representatives of the scientific and the civil society from more than 30 NGOs from Moldova, Transnistria and Ukraine. The main objectives of the event were:

- Promotion and strengthening of collaboration between the representatives of scientific and civil community, and representatives of public authorities in management of Dniester River water quality;
- Raising public awareness about the importance of water quality and its impact on the human health and sustainable development of the localities.

The 5th International conference on Ecological Chemistry, organized on March 2-3, 2012 was dedicated to 20th Anniversary of the Department of Industrial and Ecological Chemistry of the State University of Moldova and was supported by the Academy of Sciences of Moldova, Intergovernmental Foundation for Educational, Scientific and Cultural Cooperation, Moldovan Research and Development Institution, Scientific Centre for Ecological and Applied Chemistry, Department of Industrial and Ecological Chemistry, Faculty of Chemistry and Chemical Technology of Moldova State University, Institute of Chemistry of Academy of Sciences of Moldova and University of Academy of Sciences of Moldova.

The Conference works were focused on promotion of "Healthy Style of Life" by discussing the recent results in the field of ecological chemistry of water, air, soil and promising approaches of sustainable development, as well as social and educational implications. The aim of the conference was to encourage and facilitate the interdisciplinary communication among scientists, engineers, economists, teachers and professionals working on environmental issues and sustainable development. The plenary reports presented at this conference were the following:

- CHEMISTRY VS ECOLOGY, *Acad. Gheorghe Duca, President of the Academy of Sciences of Moldova;*
- REDOX AND FREE-RADICALS PROCESSES IN ENVIRONMENT, *Prof. Yury Skurlatov, Institute of Chemical Physics Russian Academy of Sciences, Russia;*
- SUSTAINABLE WATER MANAGEMENT IN DEVELOPING COUNTRIES, *Prof. Mufit Bahadir, Director of the Institute of Environmental and Sustainable Chemistry, Technical University, Braunschweig, Germany;*
- CHEMISTRY – FRIEND OR ENEMY OF ENVIRONMENT, *Acad. Ionel Haiduc, President of the Romanian Academy, Romania;*
- WATER FOR GLOBAL SAFETY, SECURITY AND ECOLOGICAL SUSTAINABILITY, *Prof. Ashok Vaseashta, Director of the Institutes of Advanced Sciences Convergence and International Clean Water, Marshal University, Huntington, WV, USA;*
- CHEMISTRY, PHYSICS AND BIOLOGY OF WATER, *Acad. Vladislav Goncharuk, Director, A.V. Dumanskii Institute of Colloid Chemistry and Water Chemistry, National Academy of Sciences of Ukraine, Kiev, Ukraine;*
- UNUSUAL PROPERTIES OF WATER, *Prof. Janus Lipkowski, Head of Department of Physical Chemistry of Supramolecular Complexes, Institute of Physical Chemistry, Polish Academy of Sciences, Poland;*
- SOIL DECONTAMINATION FROM ORGANIC POLLUTANTS, *Prof. Nicola Sennesi - Dept. Agriforestrial & Environmental Biology & Chemistry, University of Bari, Italy;*
- COMPUTER-BASED METHODOLOGY TO PREDICT TOXICITY IN ENVIRONMENTAL POLLUTANTS, *Acad. Isaak Bersuker, Professor, Texas University, TX, USA.*

The forthcoming edition of **International conference on Ecological Chemistry** (2-3 March, 2017) will gather more than 300 participants from 25 countries. The conference agenda will include discussions on different approaches in chemistry *versus* ecology, opinions and exchange experience on terminology usage in different countries and regions. The conference will be organized in five scientific sessions entitled *Ecological Chemistry*, *Environmental Chemistry and Engineering, Green Chemistry, Ecological & Environmental Aspects in Chemical Research and Education* and *Young Scientists Research in Ecological & Environmental Chemistry*. The last two sessions are dedicated to teachers and young scientist that will present research works in the field and the ecological & environmental methodological aspects in chemical research, education and innovation sphere. The conference programme will include plenary reports:

- RETROSPECTIVE AND PERSPECTIVE OF ECOLOGICAL AND ENVIRONMENTAL CHEMISTRY, *Acad. Gheorghe Duca, President of the Academy of Sciences of Moldova;*
- ROLE OF OXIDATION-REDUCTION PROCESSES IN FORMATION OF TOXIC PROPERTIES OF A NATURAL AQUEOUS ENVIRONMENT, *Prof. Yurii Skurlatov, Institute of Chemical Physics, Russian Academy of Sciences, Russian Federation;*
- MERCURY AND DICHROMATE FREE DETERMINATION OF CHEMICAL OXYGEN DEMAND (COD), *Prof. Mufit Bahadir, Technisch e Universitaet Braunschweig, Leichtweiss Institute of Hydraulic Engineering and Water Resources, Germany;*
- STATISTICAL DATA ANALYSIS IN ENVIRONMENTAL PROBLEMS, *Prof. Asaf Haji Oglu Hajiyev, Secretary General, Parliamentary Assembly of the Black Sea Economic Cooperation (PABSEC);*
- ECOLOGICAL CHEMISTRY THROUGH POPULAR SCIENTIFIC ARTICLES, *Prof. Ketevan Kupatadze, Ilia State University, Tbilisi, Georgia;*
- GENETIC DAMAGE IN BIOINDICATOR ORGANISMS AND HEAVY METALS CONTENT IN ECOGENOTOXIC STUDIES, *Prof. Rouben Aroutiounian, National Academy of Sciences of Armenia;*
- POWER GENERATION FROM LOW-GRADE FUELS AND WASTES PROCESSING USING FILTRATION COMBUSTION, *Prof. Serghey ALDOSHIN, First Vice President of the Russian Academy of Sciences, Institute of Problems of Chemical Physics, Russian Federation;*
- NANO TECHNOLOGICAL INNOVATIONS SUPPORTING WATER SAFETY AND SECURITY, *Prof. Ashok Vaseahta, International Clean Water Institute, Manassas, VA, USA;*
- QUO VADIS SEPARATION SCIENCES? NEW SOLUTIONS AND CHALLENGES IN ENVIRONMENT MONITORING, *Prof. Boguslaw Buszewski, Faculty of Chemistry, Nicolaus Copernicus University in Torun, Poland;*

- OBTAINING OF LIGNOCELLULOSE BIOSORBENTS MODIFIED WITH INORGANIC NANOCLUSTERS, *Prof. Mykola Kartel, Chuiko Institute of Surface Chemistry, NAS of Ukraine, Kiev, Ukraine;*
- TECHNOLOGY OF BIOFUEL PRODUCTION FROM ALTERNATIVE RENEWABLE RAW MATERIALS SOURCES, *Prof. Alexander Garabadzhiu, Saint-Petersburg State Institute of Technology, Russian Federation;*
- PREDICTIVE ASSESSMENT OF THE HUMAN AND ENVIRONMENTAL TOXICITY OF CHEMICAL SUBSTANCES, *Prof. Gerrit Schüürmann, Department of Ecological Chemistry at the Helmholtz-Centre for Environmental Research in Leipzig, Germany;*
- ASSESSING LONG-TERM VARIATION OF OCEAN ACIDIFICATION DUE TO ANTHROPOGENIC CARBON PENETRATION IN SEAWATER, *Prof. Catherine Goyet, Perpignan University, France.*

Concluding remarks

Importance of theoretical and practical contributions of Ecological Chemistry Conferences to general scientific knowledge and implementation of environmentally friendly processes, benefits of healthy lifestyle, and proceeding from the strong necessity to promote the further development of this discipline are focused to the following preconditions:

- Maintaining the promotion and support of the interdisciplinary approach to ecological chemistry in strengthening of research-education-innovation in order to reduce the negative anthropogenic impacts on the human health and the environment.
- Strengthening fundamental and applied research of physical, chemical, and biological processes associated with the natural and anthropogenic pollution of environment and various interactions between the living organisms and natural environment.
- Enlarging the medico-biological research in the framework of ecological chemistry, including methods of prognosis of acute and chronic toxicity, allergic and carcinogenic effects, as well as assessment of the factors that may cause these conditions and prevent their development.
- Advanced study of various factors that describe the dynamics of eco-chemical processes in the environment, which lead to solving of ecological problems in different sphere of human activities.
- Improving of water quality indicators using combined methods of bio-testing based on toxicity parameters and standardization with subsequent inclusion in the measurement system of permissible level of impact to the state of water ecosystems and security of drinking water.
- Continuous studies on the phenomena of self-purification processes, in order to keep the natural systems in equilibrium state, and to stimulate their efficiency in pollutants diminution in environment.
- The developing of efficient methods for mathematical modelling and long-term prognosis of human impact on environment, of trans-boundary transport and transformations of pollutants, of climate change, as well as design of new technologies of waste treatment and reuse.
- Elaboration of advanced and environmental friendly methods for extraction of useful substances from the municipal and agricultural wastes, and deepened research of their structure, physical, chemical, and biological properties to facilitate their use in different sectors of economy.
- Promote the education of all ages population by introducing the main aspects of Ecological Chemistry in the educational programs and curricula and its enlargement to the rural area.

Traditionally the resolutions and recommendations draw up at the end of each edition of Ecological Chemistry conferences raise awareness and needs to study and prevent the negative impact of pollutions on human health and environment, and to bring into attention of the Governmental bodies and Authorities involved in the environment protection about the latest achievements and ideas in ecological chemistry.

It is important to continue supporting awareness campaigns using mass-media, press, TV, radio, on environment protection at national, regional and international levels. Also, continuous promotion of Ecological Chemistry principles and achievements through the strengthening of international collaboration for the sustainable use of natural resources and habitat protection, information exchange, development of bilateral and multilateral projects with involvement of key-persons from research, education, civil society and business.

Academician Gheorghe DUCA
President of the Academy of Sciences of Moldova

Dr. Lidia ROMANCIUC
Director of the Centre of International Projects

CHEMISTRY JOURNAL OF MOLDOVA. General, Industrial and Ecological Chemistry. 2016, 11(2), 17-25
http://cjm.asm.md
http://dx.doi.org/10.19261/cjm.2016.11(2).03

RECENT TRENDS IN ALGINATE, CHITOSAN AND ALGINATE-CHITOSAN ANTIMICROBIAL SYSTEMS

Ivancic Albert

Faculty of Chemistry and Chemical Technology, Moldova State University, 60, Alexei Mateevici str., Chisinau MD2009, Republic of Moldova
Institute of Chemistry of Academy of Sciences of Moldova, 3, Academiei str., Chisinau MD2028, Republic of Moldova
e-mail: ivancicalbert@gmail.com; phone: (+373 68) 344 034

Abstract. Natural polysaccharides alginate and chitosan have been used extensively, separately or in mixtures (systems), in manufacturing of pharmaceutical products (antimicrobial) and not only. Alginates usually serve as basis for antimicrobial systems, while chitosan, in certain proportions, enhances their physicochemical and antimicrobial properties. Focusing on the recent literature (mostly since 2000), this review outlines the main synthetic approaches for the preparation of systems based on both polymers as well as identify potential areas of their application as antimicrobial agents. Various techniques used for systems preparation like microparticles, films, fibers, nanoparticles, sponges, applications and usefulness of these systems as carriers of antimicrobial compounds will also be discussed.

Keywords: alginate, chitosan, antimicrobial system, ionotropic gelation, drug.

Received: August 2016/ Revised final: October 2016/ Accepted: October 2016

Introduction

Nowadays, new systems with antimicrobial properties, that are more potent, less toxic to humans, with prolonged action and preferentially based on natural compounds, are of high interest. Consequently, antimicrobial systems based on natural polymers, such as alginates and chitosan, which fulfil the above mentioned properties and are relatively accessible and ecological as they can be obtained from various agro-industrial waste; are being studied increasingly. According to the available data, this review intends to consolidate for the first time the knowledge about the most popular alginate/chitosan antimicrobial systems, though more attention being paid to the alginate-chitosan systems with encapsulated antimicrobial compounds, namely the synthesis techniques, some physicochemical and bioactive properties as well as areas of use.

Alginates represent anionic polysaccharides, linear copolymers with homopolymeric blocks of 1,4-linked *β*-D-mannuronate and *α*-L-guluronate residues [1,2] (Figure 1), spread as a mixture of calcium, sodium and potassium salts of alginic acid in the cell walls of all brown algae (*Phaeophyceae*) [1,2,3] and several bacteria (*e.g. Azotobacter vinelandii*) [3].

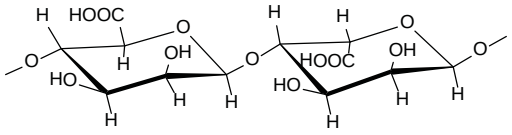

Figure 1. Alginic acid fragment (*β*-D-mannuronate and *α*-L-guluronate (1-4)-linked).

Alginates have the property to form gel in the presence of certain divalent (or multivalent) cations, particularly calcium ions, and entrap other materials in this gel [2]. The rheological properties of the formed gel depend on the ratio mannuronate:guluronate; rich in guluronate alginates, produce strong and brittle gels, while rich in mannuronate alginates produce weaker but more elastic gels [2,4]. Calcium alginate gels are generally non-toxic [5], biocompatible [5-7], likewise alginic acid and sodium alginate gels [5]. Also, calcium alginate systems show some antioxidant and antimicrobial properties [8], while sodium alginate systems demonstrated good antioxidant properties [9,10], but do not have antibiotic activity on the microorganisms studied in the paper [9]. Alginate gels have non-adhesive to cell properties [11].

Alginates in the form of various systems, like gels [2-5,12,13], water/oil soluble films [13-23], fibers [8,24-26] and others [13,18,27-29], have found application in the fields such as medicine and pharmaceuticals [5,8,12,14,16,22,24,26-29], food industry [4,15,17-21,23] and textiles [2,24-26].

Chitosan represents natural, cationic aminopolysaccharide copolymer [30] consisting of randomly distributed units of D-glucosamine and N-acetyl-D-glucosamine linked *β*-1,4 (Figure 2), obtained by partial deacetylation of chitin contained in the exoskeletons or cuticles of many invertebrates [30-32], cell walls of some fungi, mushroom [31] and yeasts [31,32].

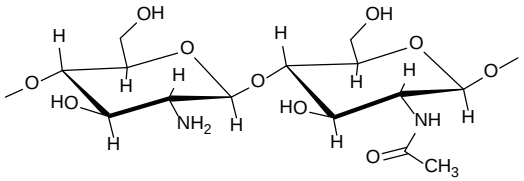

Figure 2. Chitosan fragment (D-glucosamine and N-acetyl-D-glucosamine (1-4)-linked).

Chitosan has multiple useful properties like non-toxicity [32], biocompatibility [13,32-34], antimicrobial activity [13,32-45], biodegradability [13,32-34], antioxidant activity [13,35,41,44], haemostatic properties [30,46,47] and others [13,30]. Chitosan easily can be moulded in diverse forms: hydrogel [13,32,33], powder [13,34], paste [13,34], film [13,32-34,40,41,45], fibers [32,34], sponge [13,32], scaffold [32-34] and others [13,30,33,38,42-44], which have found application, alone or in combination with other compounds, in the fields of medicine [13,30,32-34,36-43,46,47], textile [32], food industry [33,35,40,44,45], water treatment [33], etc.

Several papers were drafted in the field of development and analysis of alginate or chitosan based systems containing antibacterial substances. Compared to other works written in this field, the present paper highlights the possibility of obtaining alginate/chitosan or alginate-chitosan with antimicrobial substances systems, of different chemical nature. Based on alginate were obtained and analysed antimicrobial systems containing: silver ions [8,26], nanocrystalline silver [8], ethylenediaminetetraacetic acid [16], 3-(trimethoxysilyl)propyl-octadecyldimethylammonium chloride [28], lysozyme [12,16], lactoperoxidase [20], nisin [16-18], lysosomes [29], grape fruit seed extract [16,19], essential oils [21-23] and others. Like alginates, chitosan was used as matrix for various antimicrobial systems with: copper ions and nanoparticles [13], silver nanoparticles [13,44], silver oxide [45], lomefloxacin [42], ofloxacin [43], lysozyme [44], nisin, natamycin, peptide P34 [40], essential oils [41], etc. Obtained systems showed more pronounced antimicrobial activity than alginate/chitosan and antimicrobial compounds apart.

Due to the opposite charges, alginate (-) and chitosan (+) form polyelectrolyte complexes, that can be moulded in the form of various systems. Based on a literature review of the last fifteen years of research in this field, it was identified that the most studied alginate-chitosan systems are: a) microparticles; b) films; c) fibers; d) nanoparticles; e) sponges.

Microparticles

Alginate-chitosan microparticles are especially used in the pharmaceutical, for sustained-release of antimicrobial compounds. Microparticles provide stability, mask an unpleasant taste and odour, and reduce toxic side effects of encapsulated bioactive substances.

Microparticles can be obtained using one of the methods: ionotropic gelation of alginate with calcium ions in the presence of chitosan, tripolyphosphate cross-linking method or both of them. Using first method were obtained alginate-chitosan microsystems with antimicrobial compounds like: amoxicillin [48,49], nitrofurantoin [50], metronidazole [51], polymyxin B [52], cefaclor [53], rifampicin, isoniazid, pirazinamid [54,56] (Figure 3). By the use of the tripolyphosphate cross-linking method were obtained alginate-chitosan microcapsules with metronidazole [57]. Alginate-chitosan beads with sulfathiazole [58] were obtained by mixing elements of both methods.

Encapsulation of amoxicillin in alginate-chitosan mucoadhesive microcapsules as gastroretentive delivery system, resulted in enhanced stability [48] and controlled release of antimicrobial drug in the simulated gastric fluid, compared to amoxicillin plain drug. [48,49] Reducing approximately two times and more of concentration of used chitosan (0.5% w/v and lower) to obtain antimicrobial alginate-chitosan microparticles resulted in selective sustained-release of active principle (nitrofurantoin [50], polymyxin B [52], rifampicin, isoniazid and pyrazinamide [54,56]) in simulated intestinal fluid, while the release in simulated gastric fluid was very slow. Cefaclor release from alginate-chitosan microparticles in simulated gastric fluid is intensifying with increasing of alginate concentration up to 7% w/v (chitosan concentration - 0.5% w/v) [53]. Similar release profile was observed for systems containing antituberculosis drug rifampicin and for which obtaining was used 1% alginate and 1.5% chitosan [55]. Alginate-chitosan beads with metronidazole were obtained; due to high contents of chitosan (5% w/v) float on gastric juice and consequently are retained in the stomach where they gradually release antibiotic compound [51]. In vivo studies have shown that the encapsulation of rifampicin, isoniazid and pyrazinamide in alginate-chitosan microcapsules resulted in an increase of about 13-15 times in their biological half-life compared to non-encapsulated substances, leading to an increased duration of action of the antituberculous compounds [56].

Using tripolyphosphate cross-linking method were obtained metronidazole containing alginate-chitosan microcapsules, characterized by good mucoadhesive property and prolonged release in simulated intestinal fluid due to ionic cross-link between negatively charged tripolyphosphate and positively charged chitosan molecules [57].

Alginate-chitosan microsystems with sulfathiazole were obtained using the stages: 1. ionotropic gelation of alginate with calcium chloride in presence of chitosan and sulfathiazole; 2. treatment of obtained beads with sodium tripolyphosphate solution; 3. beads irradiation with microwave radiation. Obtained beads showed release-retarding properties in the simulated gastric fluid, due to alginate-chitosan complexation and alginate cross-linking, especially after microwave treatment [58].

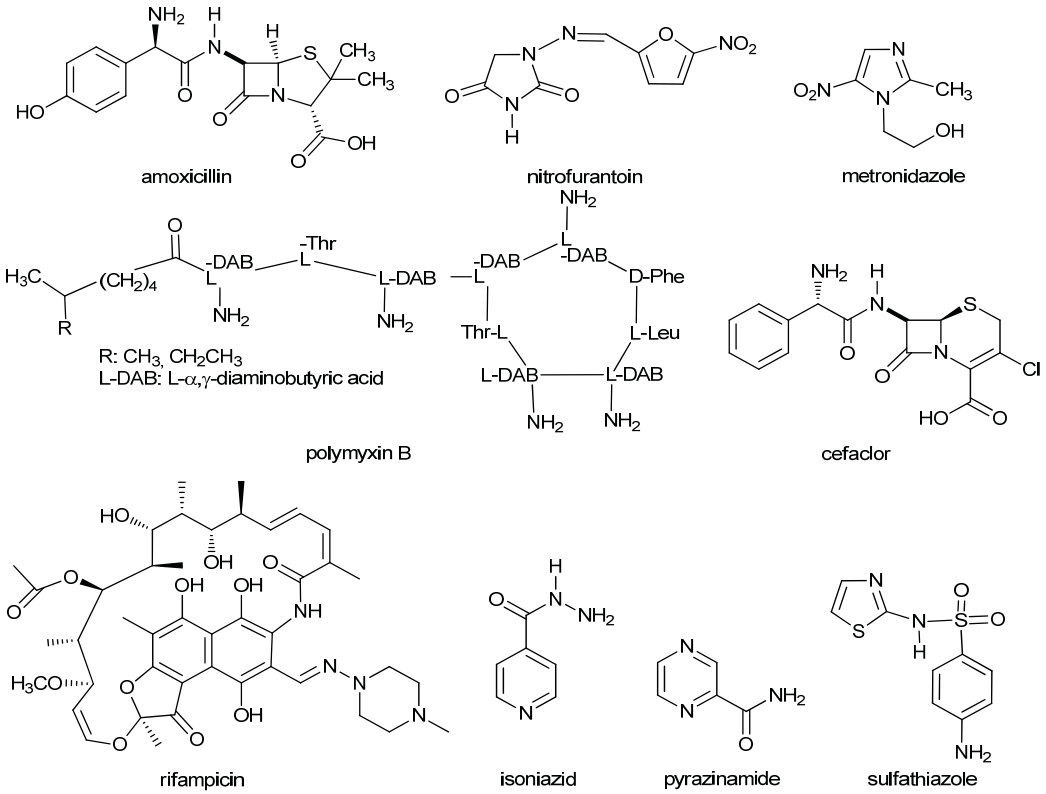

Figure 3. Structures of some antimicrobial compounds encapsulated in alginate-chitosan microparticles.

Films

As microsystems, alginate-chitosan films show some antimicrobial properties either due to mechanical blockage of microorganisms on the surface of films or due to antimicrobial effect of the chitosan itself [59,60]. Inclusion of antimicrobial substances like: silver nanoparticles [61], copper ions [62], natamycin [63,64], minocycline [65], ciprofloxacin [66], silver sulfadiazine [67] and chlorhexidine [68] (Figure 4) leads to increased antimicrobial properties of alginate-chitosan films which allows their use in various fields such as: wound dressings materials development [59-61,66,67], antibacterial functional coatings with controlled release [62,65], pharmaceutical forms with sustained release [67,68], scaffolds for tissue engineering [60], food packaging [61,63,64] and water treatment [62].

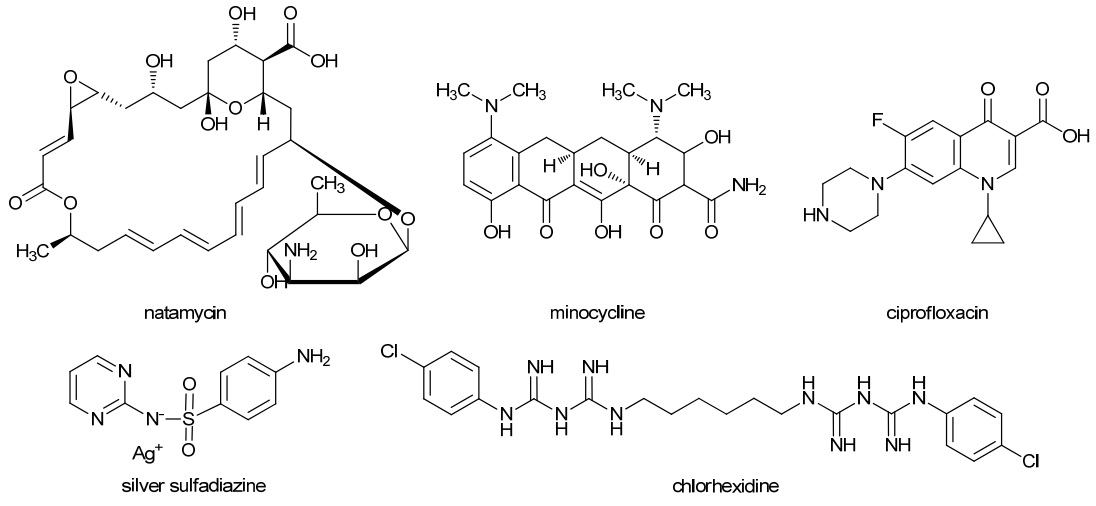

Figure 4. Structures of some antimicrobial compounds incorporated in alginate-chitosan films.

Films can be obtained without [61,62,67,68] or using calcium chloride [59,60,63-66] to cross-linking alginate. Structurally, antimicrobial membranes may consist of a homogenous alginate-chitosan mixture [59-64,67,68] or two and more individual layers of alginate and chitosan which adhere to each other [62,65,66].

Fibers

As it was already mentioned, alginate and chitosan can be moulded in form of fibers. Using alginate-chitosan mixtures can be obtained fibers with advanced useful properties, compared to individual polymers. Wet spinning technique [69-75] is the most common method for manufacturing these fibers. Using this method, it can be obtained fibers consisting entirely of alginate-chitosan mixture [70,75], alginate coated with chitosan [69,71-73] (Figure 5) or *vice versa* - chitosan coated with alginate [74] (Figure 6).

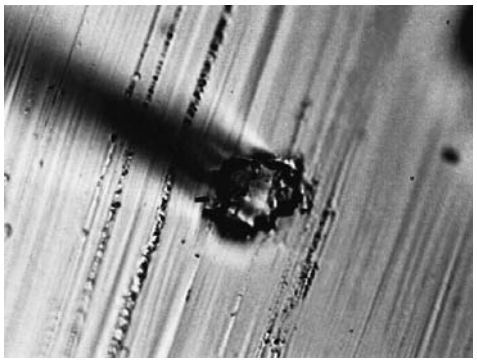

Figure 5. Microscopic cross view of chitosan-alginate fiber stained by ninhydrin (adapted from [73]).

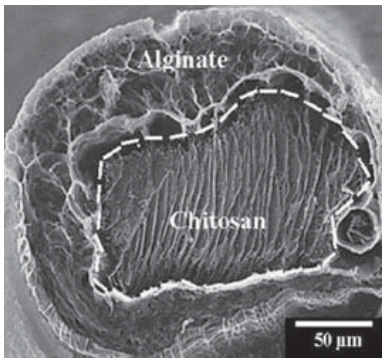

Figure 6. LV-SEM image of alginate-chitosan fiber cross section (adapted from [74]).

Due to chitosan and antimicrobial compounds (sulfathiazole [71]), alginate-chitosan fibers show antimicrobial activity - inhibit the growth of various bacteria that inhabit the skin of mammals, such as *Staphylococcus aureus* [69,70,72], *Escherichia coli* [70,71], *Micrococcus luteus*, *Staphylococcus epidermidis* [69]. This property together with the ability to carry cationic [74] and anionic [75] drugs, allow antimicrobial alginate-chitosan fibers to be a potential candidate for wound dressing materials.

Nanoparticles

A preliminary review of the literature showed the possibility of encapsulation into alginate-chitosan nanoparticles of various chemical structures of antimicrobial compounds like: benzoyl peroxide [76], gatifloxacin [77], levofloxacin [78], daptomycin [79], nisin [80] (Figure 7) and *Ocimum sanctum* methanolic extract [81].

Nanoparticles were prepared using ionotropic gelation (with or without some modifications) [76-81], freeze-drying and spray-drying methods [82]. In the majority of cases, the nanoparticles obtained by ionotropic gelation method are stables (zeta potential – $\zeta < -30$ mV or $\zeta > +30$ mV) [77,80,81], have a nearly spherical shape, with sizes ranging from < 100 nm [76,78,81] to 200-900 nm [77,79,80]. Freeze-drying and spray-drying methods allow obtaining of nanoparticles, together with microparticles, which have irregular shapes (fibrids-like) and sizes around 900 nm and larger, while spray-dried systems show higher antimicrobial activity than freeze-dried ones [82]. Pristine and drug loaded alginate-chitosan nanoparticles show antimicrobial activity against: *Staphylococcus aureus* [79-82], *Escherichia coli* [81,82], *Propionibacterium acnes* [76], *Staphylococcus epidermidis*, *Staphylococcus capitis*, *Staphylococcus hominis*, *Staphylococcus lundunensis*, *Staphylococcus haemolyticus*, *Staphylococcus warneri* [79], *Bacillus cereus*, *Pseudomonas aeruginosa*, *Bacillus cereus* [81]. Drug loaded nanoparticles release antimicrobial compound over an extended period of time (4 hours and more) [77-80], keeping the antimicrobial activity even after 30 laundering cycles of fabrics treated with nanoparticles [81]. Due to this properties, alginate-chitosan antimicrobial nanoparticles can be potentially usable in medicine: as potential carrier systems with sustained release of antimicrobial drugs [76-79] and as components in developing of fabrics for medical use [81,82]; in food industry as preservatives [80].

Sponges

Alginate-chitosan sponge represent a tridimensional porous scaffold, prepared by freeze-drying technique of mixture [83] or consecutively deposited one above the other layers of alginate and chitosan [84-86]. Pore sizes range from <100 µm [85, 86], 200-400 µm [83] and approximately 500 µm [84], as a function of various factors such as cross-linking time with Ca^{2+} ions - with its increasing pore sizes being reduced [83] (Figure 8). In the same time with increasing of calcium ions concentration the release rate of antimicrobial compound from systems decreases, because of this, systems containing the lowest concentration of calcium ions (5%), in the conditions of the experiment, showed shortest time in reducing of number of viable bacteria cells to zero [85].

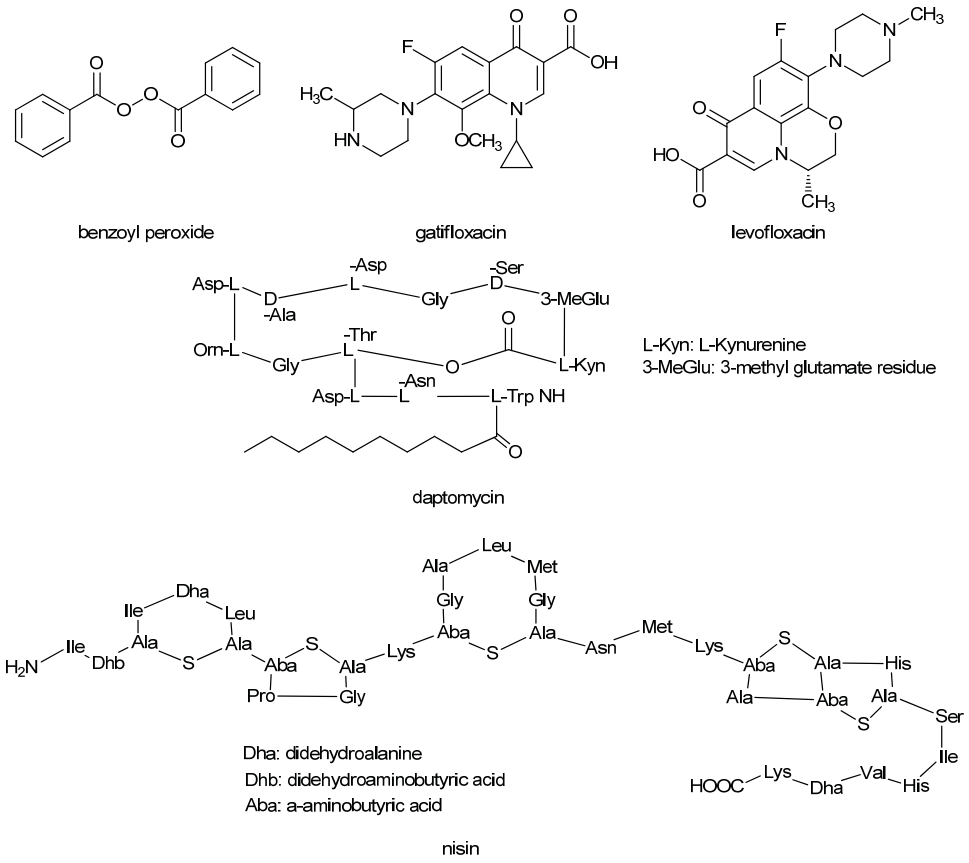

Figure 7. Structures of some antimicrobial compounds encapsulated in alginate-chitosan nanoparticles.

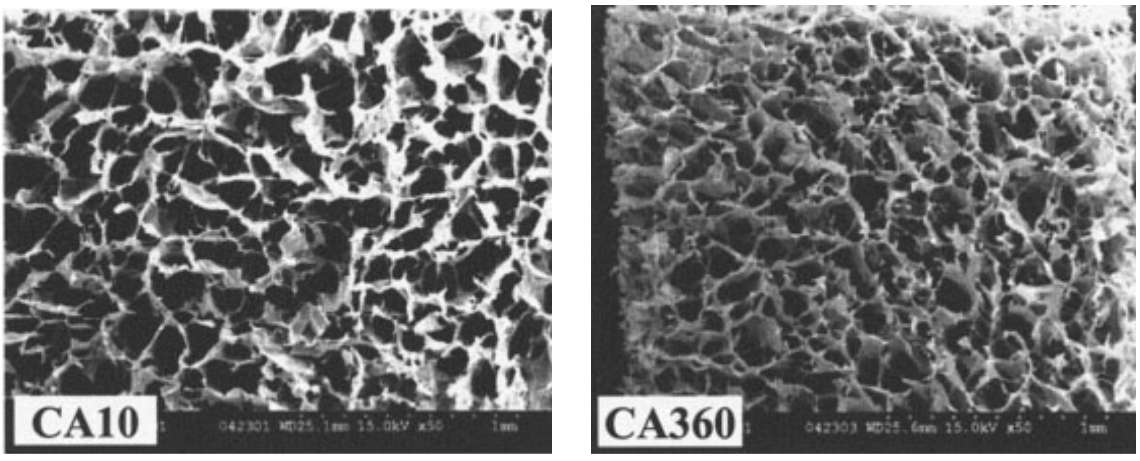

Figure 8. SEM images of alginate-chitosan sponges prepared with cross-linking time 10 min (left) and 360 min (right) (adapted from [83]).

In the alginate-chitosan sponges were encapsulated antimicrobial compounds like: silver sulfadiazine [83,86], gentamicin [84] and ciprofloxacin [85]; in result, increased the antimicrobial activity against: *Staphylococcus aureus* [83-86], *Pseudomonas aeruginosa* [83,86] and *Escherichia coli* [85], compared to pristine alginate-chitosan sponges.

All of the studied alginate-chitosan antimicrobial sponges demonstrated sustained release of antimicrobial drugs from 4 hrs [85] to 30 days [84]. Due to these properties, alginate-chitosan antimicrobial sponges can be potentially used in wound dressing manufacturing [83,85,86] and in tissue engineering applications [84].

Conclusions

The most studied alginate-chitosan antimicrobial systems in the literature: microparticles, films, fibers, nanoparticles and sponges, have been analyzed and classified. Based on their properties, areas of potential application like medicine, pharmaceutics, food industry, fabrics production, were identified. Although a considerable amount of research has been conducted in this field, further work is required because chemists are still faced with the challenge of developing a universal methodology that is compatible with a large variety of alginate-chitosan antimicrobial systems.

Acknowledgements

The author thanks the Moldavian State Program project (No. 16.00353.50.06A) for financial support and Dr. hab., Prof. Macaev Fliur for helpful discussions.

References

1. Andrade, L.R.; Salgado, L.T.; Farina, M.; Pereira, M.S.; Mourão, P.A.S.; Amado Filho, G.M. Ultrastructure of acidic polysaccharides from the cell walls of brown algae. Journal of Structural Biology, 2004, 145(3), pp. 216–225.
2. Kakita, H.; Kamishima, H. Some properties of alginate gels derived from algal sodium alginate. Journal of Applied Phycology, 2008, 20(5), pp. 543-549.
3. Thomas, S.; Visakh, P.M.; Mathew, A.P. Eds. Advances in natural polymers. Springer-Verlag: Berlin, 2013, pp. 193-254.
4. Llanes, F.; Ryan, D.H.; Marchessault, R.H. Magnetic nanostructured composites using alginates of different M/G ratios as polymeric matrix. International Journal of Biological Macromolecules, 2000, 27(1), pp. 35-40.
5. Glicksman, M. Ed. Food Hydrocolloids. Chemical Rubber Company Press: Boca Raton, 1983, pp. 115–154.
6. Becker, T.A.; Kipke, D.R; Brandon, T. Calcium alginate gel: a biocompatible and mechanically stable polymer for endovascular embolization. Journal of Biomedical Materials Research, 2001, 54(1), pp. 76-86.
7. Becker, T.A.; Preul, M.C.; Bichard, W.D.; Kipke, D.R.; McDougall, C.G. Calcium alginate gel as a biocompatible material for endovascular arteriovenous malformation embolization: six-month results in an animal model. Neurosurgery, 2005, 56(4), pp. 793-801.
8. Wiegand, C.; Heinze, T.; Hipler, U.C. Comparative in vitro study on cytotoxicity, antimicrobial activity, and binding capacity for pathophysiological factors in chronic wounds of alginate and silver-containing alginate. Wound Repair and Regeneration, 2009, 17(4), pp. 511-521.
9. Zhao, X.; Li, B.; Xue, C.; Sun, L. Effect of molecular weight on the antioxidant property of low molecular weight alginate from Laminaria japonica. Journal of Applied Phycology, 2012, 24(2), pp. 295–300.
10. Tusi, S.K.; Khalaj, L.; Ashabi, G.; Kiaei, M.; Khodagholi, F. Alginate oligosaccharide protects against endoplasmic reticulum- and mitochondrial-mediated apoptotic cell death and oxidative stress. Biomaterials, 2011, 32(23), pp. 5438-5458.
11. Pilar Rauter, A.; Lindhorst, T.K. Eds. Carbohydrate Chemistry. Chemical and Biological Approaches. Royal Society of Chemistry Publishing: Cambridge, 2011, pp. 227-258.
12. Jin, Z.; Harvey, A.M.; Mailloux, S.; Halámek, J.; Bocharova, V.; Twiss, M.R.; Katz, E. Electrochemically stimulated release of lysozyme from an alginate matrix cross-linked with iron cations. Journal of Materials Chemistry, 2012, 22(37), pp. 19523-19528.
13. Said-Galiev, E.E.; Gamzazade, A.I.; Grigor'ev, T.E.; Khokhlov, A.R.; Bakuleva, N.P.; Lyutova, I.G.; Shtykova, E.V.; Dembo, K.A.; Volkov, V.V. Synthesis of Ag and Cu–chitosan metal–polymer nanocomposites in supercritical carbon dioxide medium and study of their structure and antimicrobial activity. Nanotechnologies in Russia, 2011, 6(5), pp. 341–352.
14. Stenberg, K.G.; Hubinette, F. Water-soluble films comprising low-viscosity alginates. USA Patent, 2014, No. US8759282.
15. Olivas, G.I.; Barbosa-Cánovas, G.V. Alginate–calcium films: Water vapor permeability and mechanical properties as affected by plasticizer and relative humidity. LWT - Food Science and Technology, 2008, 41(2), pp. 359–366.
16. Chaa, D.S.; Choib, J.H.; Chinnana, M.S.; Parkb, H.J. Antimicrobial films based on Na-alginate and k-carrageenan. LWT - Food Science and Technology, 2002, 35(8), pp. 715–719.
17. Chacko, J.; Lalpuria, M.; Floros, J.D.; Anantheswaran, R.C. Controlled release of nisin from biopolymer films. 11th International Congress on Engineering and Food: Athens, 2011, vol. 1, pp. 105-106.
18. Millette, M.; Le Tien, C.; Smoragiewicz, W.; Lacroix, M. Inhibition of Staphylococcus aureus on beef by nisin-containing modified alginate films and beads. Food Control, 2007, 18(7), pp. 878–884.
19. Aloui, H.; Khwaldia, K.; Sánchez-González, L.; Muneret, L.; Jeandel, C.; Hamdi, M.; Desobry, S. Alginate coatings containing grapefruit essential oil or grapefruit seed extract for grapes preservation. International Journal of Food Science & Technology, 2014, 49(4), pp. 952–959.
20. Yener, F.Y.G. Development of antimicrobial protective food coating materials from edible alginate films.

M.Sc. Thesis, Graduate School of Engineering and Science of Izmir Institute of Technology, Izmir, Turkey, 2007.
21. Oussalah, M.; Caillet, S.; Salmiéri, S.; Saucier, L.; Lacroix, M. Antimicrobial effects of alginate-based film containing essential oils for the preservation of whole beef muscle. Journal of Food Protection, 2006, 69(10), pp. 2364-2369.
22. Liakos, I.; Rizzello, L.; Scurr, D.J.; Pompa, P.P.; Bayer, I.S.; Athanassiou, A. All-natural composite wound dressing films of essential oils encapsulated in sodium alginate with antimicrobial properties. International Journal of Pharmaceutics, 2014, 463(2), pp.137-145.
23. Villalobos-Carvajal, R.; Benavides, S.; Reyes, J.E. Effects of mechanism of gelation on physical, mechanical and antibacterial properties of alginate films with oregano essential oil incorporated. 11th International Congress on Engineering and Food: Athens, 2011, vol. 1, pp. 113-114.
24. Qin, Y. Alginate fibres: an overview of the production processes and applications in wound management. Polymer International, 2008, 57(2), pp. 171-180.
25. Moussavi, P.H. Production of fibers based on alginate. Ph.D. Thesis, University of Leeds, Leeds, UK, 1991.
26. Percival, S.L.; Slone, W.; Linton, S.; Okel, T.; Corum, L.; Thomas, J.G. The antimicrobial efficacy of a silver alginate dressing against a broad spectrum of clinically relevant wound isolates. International Wound Journal, 2011, 8(3), pp. 237–243.
27. Olderøy, M.Ø.; Xie, M.; Andreassen, J.P; Strand, B.L.; Zhang, Z.; Sikorski, P. Viscoelastic properties of mineralized alginate hydrogel beads. Journal of Materials Science: Materials in Medicine, 2012, 23(7), pp. 1619-1627.
28. Kim, Y.S.; Kim, H.W.; Lee, S.H.; Shin, K.S.; Hur, H.W.; Rhee, Y.H. Preparation of alginate–quaternary ammonium complex beads and evaluation of their antimicrobial activity. International Journal of Biological Macromolecules, 2007, 41(1), pp. 36–41.
29. Park, H.J.; Min, J.; Ahn, J.M.; Cho, S.J.; Ahn, J.Y.; Kim, Y.H. Effect of pH on the formation of lysosome-alginate beads for antimicrobial activity, Journal of Microbiology and Biotechnology, 2015, 25(2), pp. 234-237.
30. Sonia, T.A.; Sharma, C.P. Chitosan and its derivatives for drug delivery perspective. Advances in Polymer Science, 2011, 243, pp. 23–54.
31. Ramawat, K.G.; Mérillon, J.M. Polysaccharides. Bioactivity and Biotechnology. Springer International Publishing: Gewerbestrasse, 2015, pp. 219-246.
32. Francesko, A.; Tzanov, T. Chitin, chitosan and derivatives for wound healing and tissue engineering. Advances in Biochemical Engineering/Biotechnology, 2011, 125, pp. 1-27
33. Honarkar, H.; Barikani, M. Applications of biopolymers I: chitosan. Monatshefte für Chemie - Chemical Monthly, 2009, 140, pp. 1403–1420.
34. Chen, M.C.; Mi, F.L.; Liao, Z.X.; Sung, H.W. Chitosan: its applications in drug-eluting devices. Advances in Polymer Science, 2011, 243, pp. 185–230.
35. Prabu, K.; Natarajan, E. In vitro antimicrobial and antioxidant activity of chitosan isolated from podophthalmus vigil. Journal of Applied Pharmaceutical Science, 2012, 2(9), pp. 075-082.
36. Liu, N.; Chen, X.G.; Park, H.J.; Liu, C.G.; Liu, C.S.; Meng, X.H.; Yu, L.J. Effect of MW and concentration of chitosan on antibacterial activity of Escherichia coli. Carbohydrate Polymers, 2006, 64, pp. 60–65.
37. Zheng, L.Y.; Zhu, J.F. Study on antimicrobial activity of chitosan with different molecular weights. Carbohydrate Polymers, 2003, 54(4), pp. 527-530.
38. Chávez de Paz, L.E.; Resin, A.; Howard, K.A.; Sutherland, D.S.; Wejse, P.L. Antimicrobial effect of chitosan nanoparticles on Streptococcus mutans biofilms. Applied and Environmental Microbiology, 2011, 77(11), pp. 3892–3895.
39. Champer, J.; Patel, J.; Fernando, N.; Salehi, E.; Wong, V.; Kim, J. Chitosan against cutaneous pathogens. AMB Express, 2013, 3(1), p. 37.
40. Cé, N.; Noreña, C.P.Z.; Brandelli, A. Antimicrobialactivity of chitosan films containing nisin, peptide P34, and natamycin. CyTA - Journal of Food, 2012, 10(1), pp. 21-26.
41. Altiok, D.; Altiok, E.; Tihminlioglu, F. Physical, antibacterial and antioxidant properties of chitosan films incorporated with thyme oil for potential wound healing applications. Journal of Materials Science: Materials in Medicine, 2010, 21(7), pp. 2227–2236.
42. Abdelrahman, A.A.; Salem, H.F.; Khallaf, R.A.; Ali, A.M.A. Modeling, Optimization, and In Vitro Corneal Permeation of Chitosan-Lomefloxacin HCl Nanosuspension Intended for Ophthalmic Delivery. Journal of Pharmaceutical Innovation, 2015, 10(3), pp. 254–268.
43. Singh, J.; Dutta, P.K. Preparation, antibacterial and physicochemical behavior of chitosan/ofloxacin complexes. International Journal of Polymeric Materials and Polymeric Biomaterials, 2010, 59(10), pp. 793–807.

44. Zimoch-Korzycka, A.; Jarmoluk, A. The use of chitosan, lysozyme, and the nano-silver as antimicrobial ingredients of edible protective hydrosols applied into the surface of meat. Journal of Food Science and Technology, 2015, 52(9), pp. 5996–6002.
45. Tripathi, S.; Mehrotra, G.K.; Dutta, P.K. Chitosan–silver oxide nanocomposite film: Preparation and antimicrobial activity. Bulletin of Materials Science, 2011, 34(1), pp. 29–35.
46. Pogorielov, M.; Kalinkevich, O.; Deineka, V.; Garbuzova, V.; Solodovnik, A.; Kalinkevich, A.; Kalinichenko, T.; Gapchenko, A.; Sklyar, A.; Danilchenko, S. Haemostatic chitosan coated gauze: in vitro interaction with human blood and in-vivo effectiveness. Biomaterials Research, 2015, 19(1), pp. 22-32.
47. Song, H.F.; Chen, A.Z.; Wang, S.B.; Kang, Y.Q.; Ye, S.F.; Liu, Y.G.; Wu, W.G. Preparation of chitosan-based hemostatic sponges by supercritical fluid technology. Materials, 2014, 7(4), pp. 2459-2473.
48. Arora, S.; Budhiraja, R.D. Chitosan-alginate microcapsules of amoxicillin for gastric stability and mucoadhesion. Journal of Advanced Pharmaceutical Technology & Research, 2012, 3(1), pp. 68-74.
49. Sahasathian, T.; Praphairaksit, N.; Muangsin, N. Mucoadhesive and floating chitosan-coated alginate beads for the controlled gastric release of amoxicillin. Archives of Pharmacal Research, 2010, 33(6), pp. 889-899.
50. Hari, P.R.; Chandy, T.; Sharma, C.P. Chitosan/calcium alginate microcapsules for intestinal delivery of nitrofurantoin. Journal of Microencapsulation: Micro and Nano Carriers, 1996, 13(3), pp. 319-329.
51. Murata, Y.; Sasaki, N.; Miyamoto, E.; Kawashima, S. Use of floating alginate gel beads for stomach-specific drug delivery. European Journal of Pharmaceutics and Biopharmaceutics, 2000, 50(2), pp. 221-226.
52. Coppi, G.; Iannuccelli, V.; Sala, N.; Bondi M. Alginate microparticles for Polymyxin B Peyer's patches uptake: microparticles for antibiotic oral administration. Journal of Microencapsulation, 2004, 21(8), pp. 829–839.
53. Rasool, B.K.; Fahmy, S.A. Development of coated beads for oral controlled delivery of cefaclor: In vitro evaluation. Acta Pharmaceutica, 2013, 63(1), pp. 31–44.
54. Sabitha, P.; Vijaya Ratna, J.; Ravindra Reddy, K. Design and Evaluation of controlled release chitosan-calcium alginate microcapsules of anti tubercular drugs for oral use. International Journal of ChemTech Research, 2010, 2(1), pp. 88-98.
55. Lacerda, L.; Parize, A.L.; Fávere, V.; Laranjeira, M.C.M.; Stulzer, H.K. Development and evaluation of pH-sensitive sodium alginate/chitosan microparticles containing the antituberculosis drug rifampicin. Materials Science and Engineering C, 2014, 39, pp. 161–167.
56. Pandey, R.; Khuller, G.K. Chemotherapeutic potential of alginate–chitosan microspheres as anti-tubercular drug carriers. Journal of Antimicrobial Chemotherapy, 2004, 53, pp. 635–640.
57. Garud, A.; Garud, N. Preparation and evaluation of chitosan microcapsules of metronidazole using tripolyphosphate cross-linking method. Dhaka University Journal of Pharmaceutical Sciences, 2010, 9(2), pp. 125-130.
58. Wong, T.W.; Chan, L.W.; Kho, S.B.; Sia Heng, P.W. Design of controlled-release solid dosage forms of alginate and chitosan using microwave. Journal of Controlled Release, 2002, 84(3), pp. 99–114.
59. Rodrigues, A.P.; Saraiva Sanchez, E.M.; da Costa, A.C.; Moraes, A.M. The influence of preparation conditions on the characteristics of chitosan-alginate dressings for skin lesions. Journal of Applied Polymer Science, 2008, 109(4), pp. 2703–2710.
60. Zorzi Bueno, C.; Moraes, Â.M. Development of porous lamellar chitosan-alginate membranes: Effect of different surfactants on biomaterial properties. Journal of Applied Polymer Science, 2011, 122(1), pp. 624–631.
61. Sharma, S.; Sanpui, P.; Chattopadhyay, A.; Ghosh, S.S. Fabrication of antibacterial silver nanoparticle-sodium alginate-chitosan composite films. RSC Advances, 2012, 2, pp. 5837–5843.
62. de Paiva, R.G.; de Moraes, M.A.; de Godoi, F.C.; Beppu, M.M. Multilayer biopolymer membranes containing copper for antibacterial applications. Journal of Applied Polymer Science, 2012, 126(S1), pp. E17–E24.
63. da Silva, M.A.; Krause Bierhalz, A.C.; Kieckbusch, T.G. Physical-chemical properties of alginate/chitosan composite films containing natamycin as antimicrobial agent. 11th International Congress on Engineering and Food: Athens, 2011, vol. 2, pp. 1007-1008.
64. da Silva, M.A.; Iamanaka, B.T.; Taniwaki, M.H.; Kieckbusch, T.G. Evaluation of the antimicrobial potential of alginate and alginate/chitosan films containing potassium sorbate and natamycin. Packaging Technology and Science, 2013, 26(8), pp. 479–492.
65. Lv, H.; Chen, Z.; Yang, X.; Cen, L.; Zhang, X.; Gao, P. Layer-by-layer self-assembly of minocycline loaded chitosan/alginate multilayer on titanium substrates to inhibit biofilm formation. Journal of Dentistry, 2014, 42(11), pp. 1464–1472.
66. Han, F.; Dong, Y.; Song, A.; Yin, R.; Li, S. Alginate/chitosan based bi-layer composite membrane as potential sustained-release wound dressing containing ciprofloxacin hydrochloride. Applied Surface Science, 2014, 311, pp. 626–634.

67. Meng, X.; Tian, F.; Yang, J.; He, C.N.; Xing, N.; Li, F. Chitosan and alginate polyelectrolyte complex membranes and their properties for wound dressing application. Journal of Materials Science: Materials in Medicine, 2010, 21(5), pp. 1751–1759.
68. Juliano, C.; Cossu, M.; Pigozzi, P.; Rassu, G.; Giunchedi, P. Preparation, in vitro characterization and preliminary in vivo evaluation of buccal polymeric films containing chlorhexidine. AAPS PharmSciTech, 2008, 9(4), pp. 1153-1158.
69. Miraftab, M.; Barnabas, J.; Kennedy, J.F.; Masood, R. Antimicrobial properties of alginate–chitosan (Alchite) fibers developed for wound care applications. Journal of Industrial Textiles, 2011, 40(4), pp. 345-360.
70. Watthanaphanit, A.; Supaphol, P.; Tamura, H.; Tokura, S.; Rujiravanit, R. Wet-spun alginate/chitosan whiskers nanocomposite fibers: Preparation, characterization and release characteristic of the whiskers. Carbohydrate Polymers, 2010, 79(3), pp. 738–746.
71. Sibaja, B.; Culbertson, E.; Marshall, P.; Broughton, R.M.; Aguilar Solano, A.; Esquivel, M.; Parker, J.; De La Fuente, L.; Auad, M.L. Preparation of alginate-chitosan fibers with potential biomedical applications. Carbohydrate Polymers, 2015, 134, pp. 598-608.
72. Knill, C.J.; Kennedy, J.F.; Mistry, J.; Miraftab, M.; Smart, G.; Groocock, M.R.; Williams, H.J. Alginate fibres modified with unhydrolysed and hydrolysed chitosans for wound dressings. Carbohydrate Polymers, 2004, 55(1), pp. 65–76.
73. Tamura, H.; Tsuruta, Y.; Tokura, S. Preparation of chitosan-coated alginate filament. Materials Science and Engineering: C, 2002, 20(1), pp. 143–147.
74. Mirabedini, A.; Foroughi, J.; Romeo, T.; Wallace, G.G. Development and characterization of novel hybrid hydrogel fibers. Macromolecular Materials and Engineering, 2015, 300(12), pp. 1217–1225.
75. Watthanaphanit, A.; Supaphol, P.; Furuike, T.; Tokura, S.; Tamura, H.; Rujiravanit, R. Novel chitosan-spotted alginate fibers from wet-spinning of alginate solutions containing emulsified chitosan-citrate complex and their characterization. Biomacromolecules, 2009, 10(2), pp. 320–327.
76. Friedman, A.J.; Phan, J.; Schairer, D.O.; Champer, J.; Qin, M.; Pirouz, A.; Blecher-Paz, K.; Oren, A.; Liu, P.T.; Modlin, R.L.; Kim, J. Antimicrobial and anti-inflammatory activity of chitosan–alginate nanoparticles: a targeted therapy for cutaneous pathogens. Journal of Investigative Dermatology, 2013, 133(5), pp. 1231–1239.
77. Motwani, S.K.; Chopra, S.; Talegaonkar, S.; Kohli, K.; Ahmad, F.J.; Khar, R.K. Chitosan–sodium alginate nanoparticles as submicroscopic reservoirs for ocular delivery: Formulation, optimization and in vitro characterization. European Journal of Pharmaceutics and Biopharmaceutics, 2008, 68(3), pp. 513–525.
78. Balaji, R.A.; Raghunathan, S.; Revathy, R. Levofloxacin: formulation and in-vitro evaluation of alginate and chitosan nanospheres. Egyptian Pharmaceutical Journal, 2015, 14(1), pp. 30-35.
79. Costa, J.R.; Silva, N.C.; Sarmento, B.; Pintado, M. Potential chitosan-coated alginate nanoparticles for ocular delivery of daptomycin. European Journal of Clinical Microbiology & Infectious Diseases, 2015, 34(6), pp. 1255–1262.
80. Zohri, M.; Alavidjeh, M.S.; Haririan, I.; Ardestani, M.S.; Ebrahimi, S.E.S.; Sani, H.T.; Sadjadi, S.K. A comparative study between the antibacterial effect of nisin and nisin-loaded chitosan/alginate nanoparticles on the growth of Staphylococcus aureus in raw and pasteurized milk samples. Probiotics and Antimicrobial Proteins, 2010, 2(4), pp. 258–266.
81. Rajendran, R.; Radhai, R.; Kotresh, T.M.; Csiszar, E. Development of antimicrobial cotton fabrics using herb loaded nanoparticles. Carbohydrate Polymers, 2013, 91(2), pp. 613–617.
82. Wiśniewska-Wrona, M.; Kucharska, M.; Struszczyk, M.H.; Cichecka, M.; Wilbik-Hałgas, B.; Szymonowicz, M.; Paluch, D.; Guzińska, K.; Rybak, Z. Hemostatic, resorbable dressing of natural polymers- hemoguard. AUTEX Research Journal, 2016, 16(1), pp. 29-34.
83. Yu, S.H.; Mi, F.L.; Wu, Y.B.; Peng, C.K.; Shyu, S.S.; Huang, R.N. Antibacterial activity of chitosan–alginate sponges incorporating silver sulfadiazine: effect of ladder-loop transition of interpolyelectrolyte complex and ionic crosslinking on the antibiotic release. Journal of Applied Polymer Science, 2005, 98(2), pp. 538–549.
84. Mehta, A.S.; Singh, B.K.; Singh, N.; Archana, D.; Snigdha, K.; Harniman, R.; Rahatekar, S.S.; Tewari, R.P.; Dutta, P.K. Chitosan silk-based three dimensional scaffolds containing gentamicin encapsulated calcium alginate beads for drug administration and blood compatibility. Journal of Biomaterials Applications, 2015, 29(9), pp. 1314-1325.
85. Öztürk, E.; Ağalar, C.; Keçeci, K.; Denkbaş, E.B. Preparation and characterization of ciprofloxacin-loaded alginate/chitosan sponge as a wound dressing material. Journal of Applied Polymer Science, 2006, 101(3), pp. 1602-1609.
86. Kim, H.J.; Lee, H.C.; Oh, J.S.; Shin, B.A.; Oh, C.S.; Park, R.D.; Yang, K.S.; Cho, C.S. Polyelectrolyte complex composed of chitosan and sodium alginate for wound dressing application. Journal of Biomaterials Science, Polymer Edition, 1999, 10(5), pp.543-556.

CHEMISTRY JOURNAL OF MOLDOVA. General, Industrial and Ecological Chemistry. 2016, 11(2), 26-33
http://cjm.asm.md
http://dx.doi.org/10.19261/cjm.2016.11(2).01

ADSORPTION OF STRONTIUM IONS FROM WATER ON MODIFIED ACTIVATED CARBONS

Mihai Ciobanu*, Victor Botan, Tudor Lupascu, Tatiana Mitina, Maria Rusu

Institute of Chemistry of Academy of Sciences of Moldova, 3, Academiei str., Chisinau MD-2028, Republic of Moldova
**e-mail: mihai_ciobanu2002@yahoo.co.uk*

Abstract. Adsorption of strontium ions from aqueous solutions on active carbons CAN-7 and oxidized CAN-8 has been studied. It has been found that allure of the adsorption isotherms for both studied active carbons are practically identical. Studies have shown that the adsorption isotherms for strontium ions from aqueous solutions are well described by the Langmuir and Dubinin-Radushkevich equations, respectively. The surface heterogeneity of activated carbons CAN-7 and oxidized CAN-8 has been assessed by using Freundlich equation.

Keywords: adsorption, strontium ions, modified activated carbon.

Received: April 2016/ Revised final: November 2016/ Accepted: November 2016

Introduction

Moldovan ground waters usually contain various pollutants, and most frequently encountered are hydrogen sulphide also ions of iron, manganese, strontium and ammonium (ammonia). When strontium ions are present in potable water in concentrations higher than maximum allowable, they slow down the growth in height of children and replace the calcium ions from bone, causing various diseases. In some wells the content of strontium ions may reach 48 mg/L, a value that exceeds the maximum allowable adopted in European countries (5 mg/L) [1] and in Russia (7 mg/L, [2]). Thus, the problem of removing the strontium ions in ground water becomes very important.

There are a series of publications devoted to the study of the processes of strontium ions adsorption from aqueous solutions on different carbonaceous adsorbents [3-5]. In these works, the processes of adsorption were studied at different temperatures as a function of pH and contact time. A series of isotherms of adsorption of strontium ions from aqueous solutions on activated carbons obtained from nuts (pecan) shells have been presented [5], which show not only the variation of the maximum values of absorbance as a function of pH, but also the presence of jump, followed by a significant increase in adsorption. It is worth mentioning here the recently presented results [6], namely the mass spectrum of activated carbon obtained by chemical activation with ortho-phosphoric acid from the shells of pecan nuts is conclusive for the presence of various types of functional groups on the surface of carbonaceous adsorbent.

This paper aims to study the process of adsorption of strontium ions from water on activated carbons obtained from vegetable by-products that are subsequently modified in order to assess the possibility of removing the strontium ions from the ground water.

Materials and methods

Experimental procedure

Activated carbon CAN-7 was obtained from Greek walnut shells that are waste of the food industry. The technology of obtaining this adsorbent includes walnut shells impregnation with ortho-phosphoric acid with further heating thereof up to 80ºC and then activation at 460ºC. Activated carbon CAN-8 was obtained from nut shells by physico-chemical method. Activation was carried out with water vapour at a temperature of 960ºC. The obtained activated carbon was modified *via* oxidation with 20% nitric acid at a temperature of 80ºC. Quality indices of the initial activated carbon CAN-8 were published by us earlier [7].

Measurements

Structure parameters of activated carbons CAN-7 and oxidized CAN-8 (CAN-8ox) were determined from adsorption-desorption isotherms of nitrogen measured at 1MP Autosorb facility.

The Fourier Transform Infrared spectroscopic (FTIR) analysis of activated carbon samples was performed using the Fourier Transform Infrared Spectrometer (Perkin Elmer FTIR, Spectrum 100, USA). The IR spectra were recorded in the wave number range of 4000-400 cm^{-1}. Prior to the FTIR analysis the samples were dried and the dilutions in KBr have been used (0.15 wt%) [8].

Adsorption isotherms were determined in static conditions at different initial concentrations of strontium ions in solution and at the same mass of activated carbon, at temperature of 20ºC. The initial concentration of $Sr(NO_3)_2$ in model solution was 100 mg/L, pH=6.2. The fraction of activated carbons used in the study was 0.8-1.0 mm. The process of strontium ions adsorption on activated carbon has been studied also on real water (Calarasi, Republic of Moldova), containing in addition to the Sr^{2+} ions (9.96 mg/L), also Ca^{2+} (37 mg/L) and Mg^{2+} (16 mg/L) ions, and pollutants that are often encountered in deep waters. The equilibrium concentrations of strontium ions were determined on spectrophotometer AAS-1.

Results and discussion

Structure parameters, the specific surface and pore volume of the activated carbons used in the present study, are presented in Table 1. According to presented data, activated carbon CAN-7 has a relatively high proportion both of small pores (micropores) and larger sized pores (mesopores).

Adsorption isotherm of strontium ions on the activated carbon CAN-7 is shown in Figure 1. Adsorption isotherm presents the specific jump registered in the previous studies [5]. The obtained adsorption isotherm is of the type VI, according to the classification proposed by Brunauer *et al.* [9]. Such type of adsorption isotherms is not often encountered in literature. Of course, the description of this isotherm by the known patterns can present some difficulties because of the complicated processes occurring at active carbon-solution interface. Here, as a confirmation, the data come from mass spectrometric measurements of activated carbon obtained from the nut shells (pecan) [6], from which carbonyl, carboxylic and phenol groups, aromatic bridges, as well as protonated aromatic carbon and aliphatic carbon are distinguished on the surface of the studied adsorbent.

Adsorption isotherm of strontium ions on the activated carbon CAN-7 in coordinates of Freundlich equation is shown in Figure 2. Presented data (Figure 2) attest a more pronounced deviation of the points from a line at relatively low equilibrium concentrations (R=9.1), which obstruct in some degree the precise determination of *n* index, characterizing the heterogeneity of surface of active carbon CAN-7. Nevertheless, *n* index has been calculated, being equal to 0.65.

Table 1

Structure parameters of activated carbons CAN-7 and oxidized CAN-8ox.

Sample	W_{01}	W_{02}	E_{01}	E_{02}	X_{01}	X_{02}	Vs	V_{meso}	S_{meso}	S_{sp}
	cm³/g		*kJ/mol*		*nm*		*cm³/g*		*m²/g*	
CAN-7	0.24	0.16	15.72	6.49	0.64	1.54	0.64	0.24	210	725
CAN-8ox	0.17	0.06	25.08	9.09	0.40	1.10	0.42	0.19	90	650

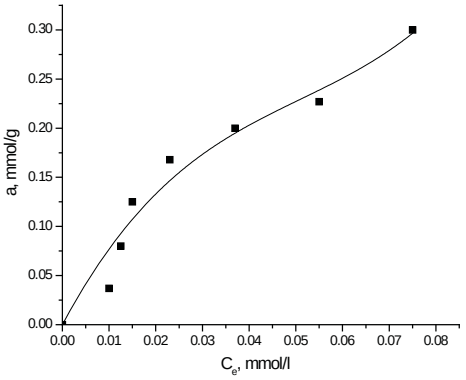

Figure 1. Adsorption isotherm of strontium ions on the activated carbon CAN-7.

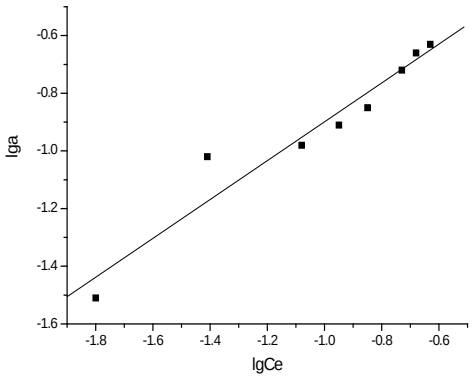

Figure 2. Adsorption isotherm of strontium ions on activated carbon CAN-7 in coordinates of Freundlich equation.

The adsorption isotherm of strontium ions on active carbon CAN-7 in coordinates of Langmuir equation is shown in Figure 3. The data presented in Figure 3 show that the process of adsorption of strontium ions can take place in active centres, even if the points on the isotherm do not stand strictly on straight line, allowing us to conclude that the isotherm depicted in Figure 1 is of Langmuir type.

Figure 4 illustrates the adsorption isotherm for strontium ions on active carbon CAN-7, in coordinates of the Dubinin-Serpinschi-1 (DS-1) equation [10]. From Figure 4 it is evident that adsorption of strontium ions occurs not only in the centres of adsorption, thereby DS-1 equation does not adequately describe the process.

The obtained results allow us to assume that adsorption of the strontium ions from aqueous solutions occurs in the centres of activated carbon CAN-7, both due to ion exchange and other interactions. The mechanism of Cu^{2+} ions interaction with the oxidized surface of the activated carbon has been schematically represented [11]:

$>C\text{-}H + Cu^{2+} \rightarrow >C\text{-}H\cdot\cdot\cdot Cu^{2+}$ (dipole-dipole interaction) Scheme 1

$>C\text{-}COOH + Cu^{2+} \rightarrow >C\text{-}COOCu^{+} + H^{+}$ Scheme 2

The same mechanism could be attributed to the adsorption of strontium ions on activated carbon CAN-7. Adsorption and diffusion processes of strontium ions in the sorbent's micropores are discussed by Qadeer *et al*. [12], being schematically represented in Scheme 3. Scheme 4 represents the adsorbed and diffused strontium in microporous structure of carbonaceous adsorbent (X) [13].

$Sr^{2+} + H_2O = Sr(OH)^+ + H^+$ Scheme 3

$Sr(OH)^+ + X = Sr(OH)X$ Scheme 4

Sveshnikova *et al*. specified that Rb^+ and Cs^+ ions adsorbed on the activated carbon, which was obtained by the treatment with orthophosphoric acid, do not desorb after the hydrochloric acid treatment [14]. This is an indication on the formation of stable chemical compounds between the mentioned ions and functional groups from the adsorbent's surface, obtained after treatment of activated carbon with orthophosphoric acid.

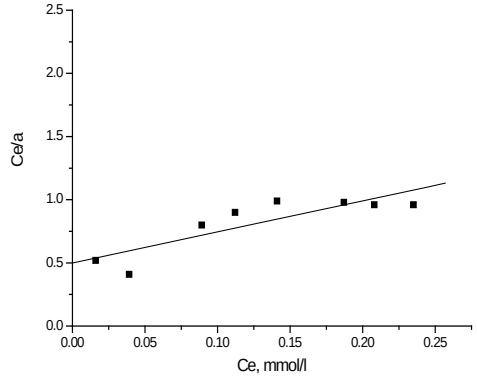

Figure 3. Adsorption isotherm of strontium ions on active carbon CAN-7, in coordinates of Langmuir equation.

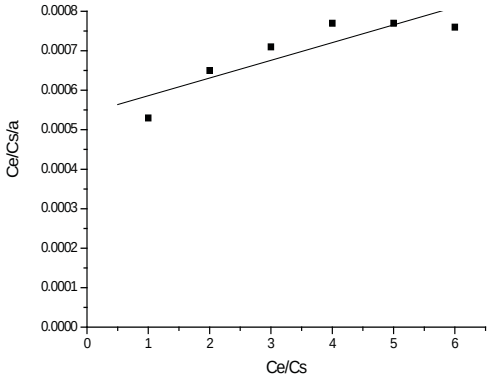

Figure 4. Adsorption isotherm of strontium ions on active carbon CAN-7, in coordinates of DS-1 equation.

Figure 5 presents the FTIR spectra of the initial active carbon CAN-7 and of the sample of active carbon with adsorbed strontium ions CAN-7-Sr. The absorption band at 1175 cm^{-1} in the FTIR spectrum of the initial active carbon CAN-7 suggests the presence of the phosphates and polyphosphates (P=O and C-O-P groups) on its surface.

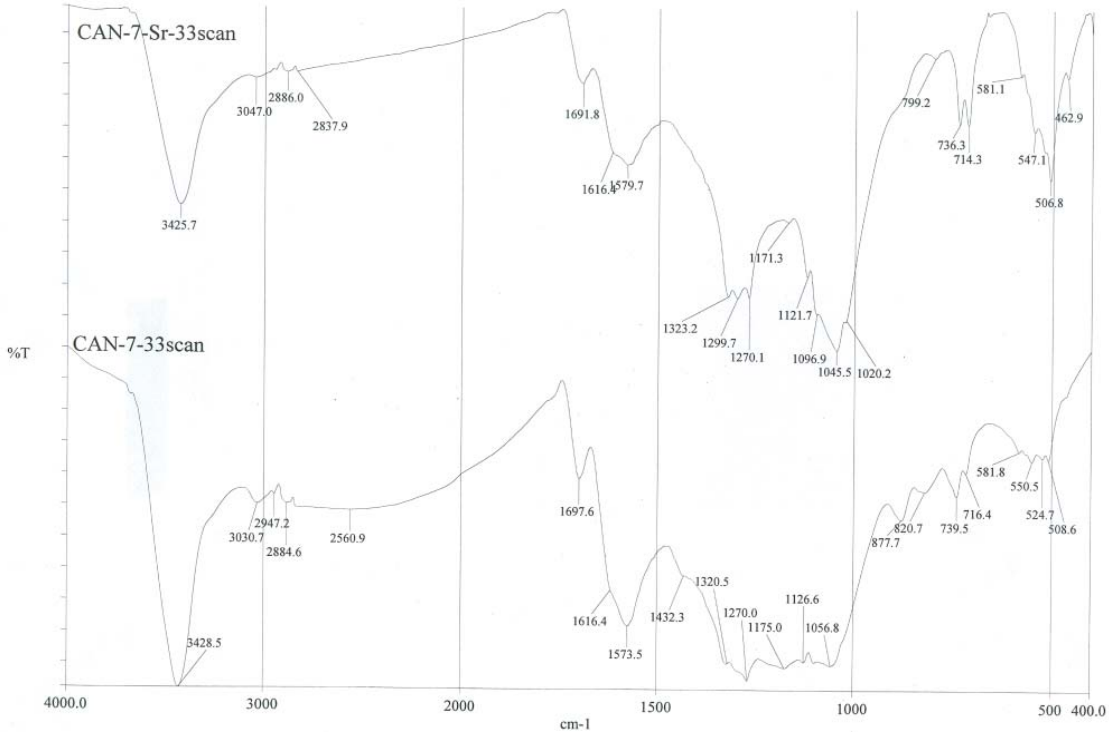

Figure 5. FTIR spectra of initial sample (CAN-7) and sample with adsorbed strontium ions (CAN-7-Sr).

The FTIR spectra of the initial CAN-8ox active carbon and the sample of active carbon with adsorbed strontium ions CAN-8ox-Sr^{2+} are shown in Figure 6. According to the data provided by Figure 6, we find that the oscillation band of C=O groups from -COOH (1733.4 cm^{-1}) in CAN-8ox disappear or is significantly diminished after sorption of strontium ions, but in the spectrum become stronger the bands corresponding to symmetrical (1384.6 cm^{-1}) and asymmetric (1570.5 cm^{-1}) oscillations of carboxyl ions, by analogy with the data in the published works [15]. The oscillation band of the carboxylic groups in the FTIR spectrum of CAN-8ox-Sr^{2+} sample moves toward region of lower frequencies (from 1733.4 cm^{-1} to 1712.7 cm^{-1}), which proves the ionization of carboxylic groups.

It should be noted, that cationic exchange capacity of active carbon obtained by activation with orthophosphoric acid is similar to that of oxidized active carbon containing acid functional groups (carboxylic, lactonic, phenolic) [16]. In contrast to the active carbon oxidized with H_2O_2, HNO_3, O_3, O_2 and air, the active carbon modified with orthophosphoric acid does not require an additional step of oxidation, for rendering the ion exchange properties.

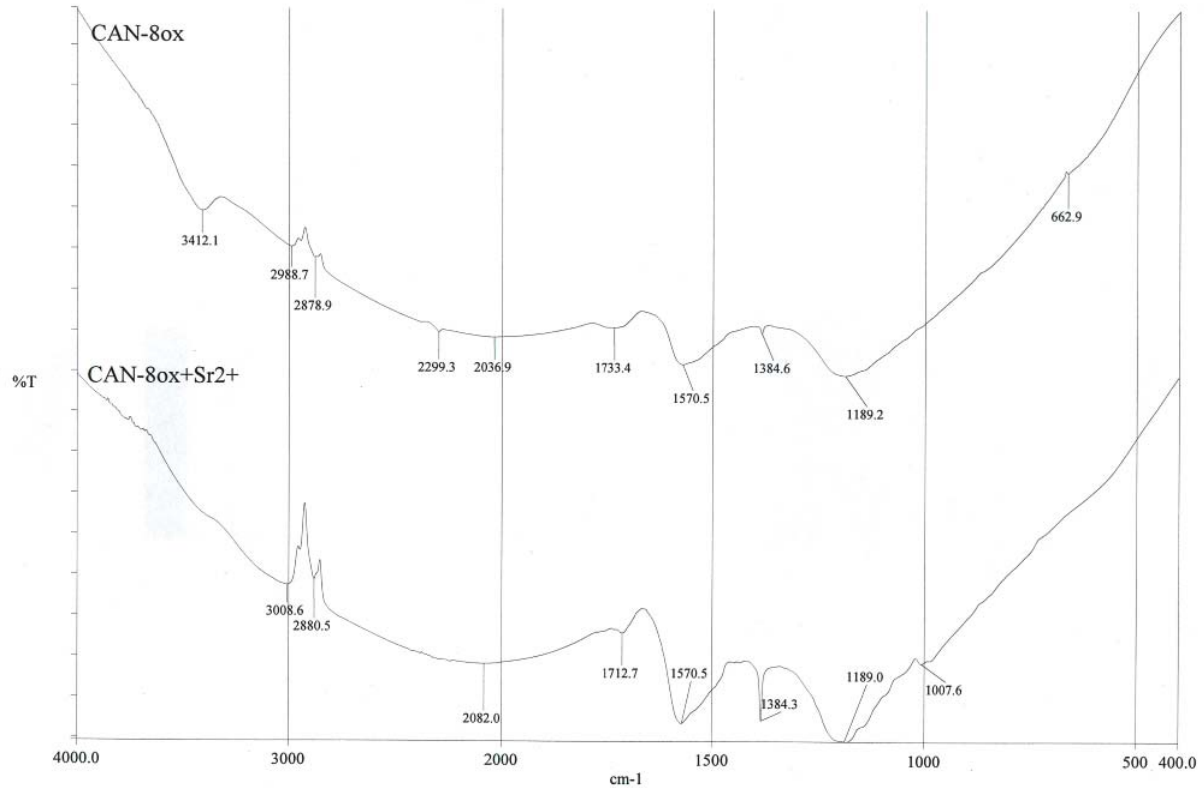

Figure 6. FTIR spectra of initial active carbon (CAN-8ox) and of the sample with adsorbed strontium ions (CAN-8ox + Sr^{2+}).

It was found that the surface of activated carbon, obtained by treating the starting material with orthophosphoric acid, is negatively charged in the range of 1.5-11.0 pH values, as a result of dissociation of functional groups that are present on the surface, according to the equation [15]:

$$QH = Q^- + H^+$$

Thus, the cation exchange capacity of the obtained activated carbon in the range of studied pH values was higher than that of activated carbon produced from the same raw material and subsequently oxidized. The same authors [17] reported on the formation of the complexes of composition 1:2 $(Q_i)_2Cu$, as a result of sorption of the Cu^{2+} ions on the surface of the activated carbon obtained by treatment with orthophosphoric acid. It is mentioned, that phosphate groups on the surface of the adsorbent bind 90% of all amount of adsorbed Cu^{2+} ions.

Perhaps in the case of adsorption of Sr^{2+} ions from aqueous solutions on CAN-7 active carbon, the adsorption process occurs due to the dipole-dipole interaction [10], but also due to the ion exchange. This explains the shape of the isotherm (Figure 1) at very low equilibrium concentrations and the influence of pH on the adsorption process described in literature [5].

Comparison of the values of adsorption of strontium ions on CAN-8ox and CAN-7 (Figure 7), allowed us to establish a big difference in the adsorption capacity of these adsorbents, namely CAN-7 active carbon has a higher adsorption capacity than CAN-8ox activated carbon.

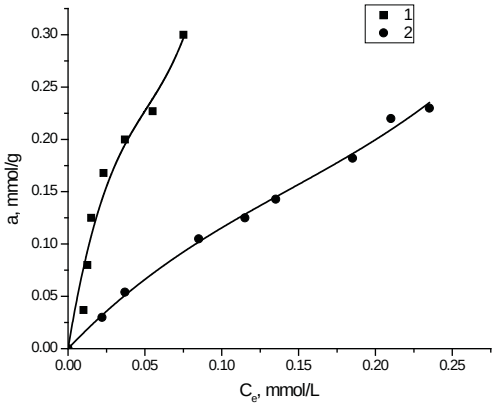

Figure 7. Adsorption isotherms of strontium ions on active carbons: (1) CAN-7; (2) CAN-8ox.

The adsorption isotherm of strontium ions from aqueous solutions on CAN-8ox activated carbon is shown in Figure 8, in the linear coordinates of Langmuir equation. According to Figure 8, a great deviation of experimental points from a straight line (R=0.66) has been attested showing that the adsorption of strontium ions on both CAN-8ox and CAN-7 active carbons takes place not only in the active centres.

The adsorption isotherm of strontium ions from aqueous solution on CAN-8ox active carbon is depicted in Figure 9, in coordinates of DS-1 equation. From the presented data one can conclude that even if DS-1 equation roughly describes the adsorption isotherm for strontium ions on CAN-8ox active carbon, the experimental data points do not sit well on a straight line in the coordinates of DS-1 linear equation (R=0.67).

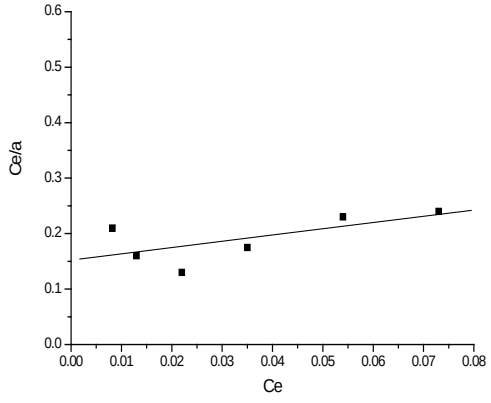

Figure 8. Adsorption isotherm of strontium ions on active carbon CAN-8ox, in coordinates of Langmuir equation.

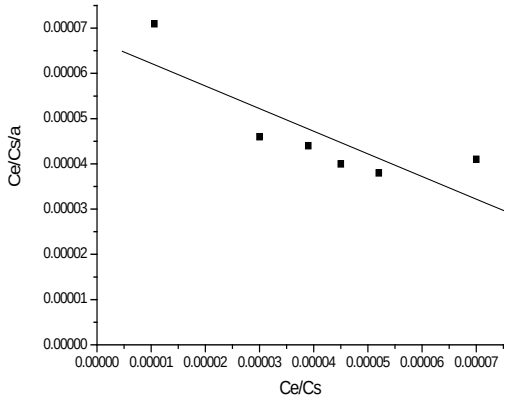

Figure 9. Adsorption isotherm of strontium ions carbon CAN-8ox, in coordinates of DS-1 equation.

Figure 10 illustrates the adsorption isotherm of strontium ions from aqueous solutions on activated carbon CAN-8ox in coordinates of Freundlich equation. From the presented data some variation of data points from a straight line is noticed. The index *n* value is 0.86.

According to the literature data, the heterogeneity of adsorbent surface enhances with the decrease of the value of adsorbent surface *n* index in Freundlich equation [18]. Comparison of the *n* index values obtained for active carbon CAN-7 containing the adsorbed strontium ions (Figure 2) with the data presented in Figure 10, offers a conclusive evidence on the higher surface heterogeneity of CAN-7, than that of CAN-8ox activated carbon. This can be explained

by the appearance of some new groups, such as P=O and C-O-P, characteristic for phosphates and polyphosphates, on the surface of activated carbon CAN-7 obtained by treatment with orthophosphoric acid that increase the heterogeneity of the surface of CAN-7 adsorbent.

Figure 11 presents the adsorption isotherm of strontium ions from aqueous solutions on CAN-7 activated carbon in coordinates of Dubinin-Radushkevich equation (*e*-Polanyi potential) Eq.(1):

$$e = RT \ln(1 + \frac{1}{Ce}) \quad (1)$$

where *e* is Polanyi potential;

R - gas constant;

T- temperature;

Ce – equilibrium concentration of strontium ions in solution.

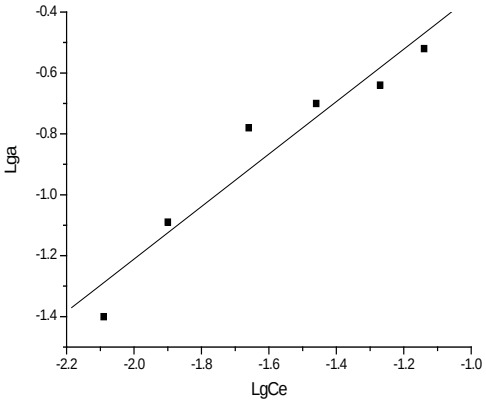

Figure 10. Adsorption isotherm of strontium ions on active carbon CAN-8ox, in coordinates of Freundlich equation.

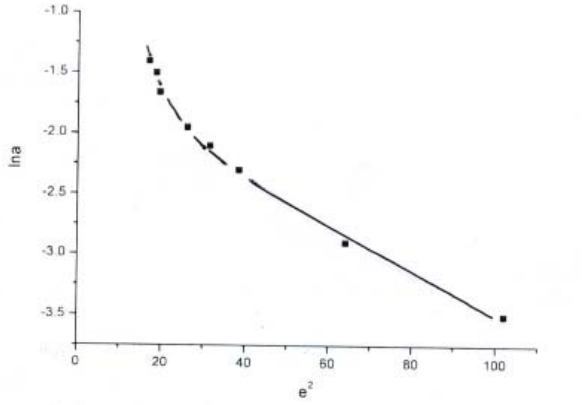

Figure 11. Adsorption isotherm of strontium ions on activated carbon CAN-7, in coordinates of Dubinin-Radushkevich equation (*e- Polanyi potential*).

The adsorption isotherm of strontium ions from aqueous solutions on activated carbon CAN-7 in coordinates of Dubinin-Radushkevich equation (*A*- differential molar free energy of adsorption, Eq.(2)) is illustrated in Figure 12.

$$A = RT \ln(\frac{Cs}{Ce}) \quad (2)$$

where *A* is differential molar free energy of adsorption;

R - gas constant;

T- temperature;

Ce – equilibrium concentration of strontium ions in solution;

Cs – water solubility of strontium nitrate.

According to the data reported in Figure 12, Dubinin-Radushkevich equation well describes the process of strontium ions adsorption on activated carbon CAN-7 only over the equilibrium concentrations range of 0.016-0.084 mmol/L. The deviation of data points from a straight line demonstrates that in the range of equilibrium concentrations 0.084-0.235 mmol/L adsorption of strontium ions occurs in mesopores and in this concentration range Dubinin-Radushkevich equation can not be applied.

Figure 13 depicts the adsorption isotherm of strontium ions from aqueous solutions on CAN-8ox activated carbon in coordinates of Dubinin-Radushkevich equation. In accordance with the experimental data included in Figure 13, Dubinin-Radushkevich equation well describes the process of strontium ions adsorption on CAN-8ox activated carbon.

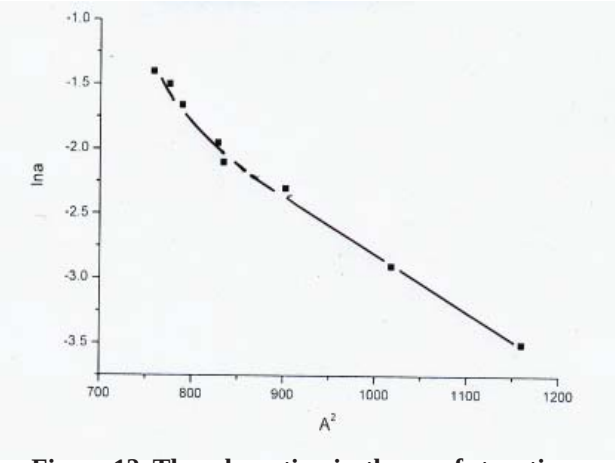

Figure 12. The adsorption isotherm of strontium ions on activated carbon CAN-7 in the coordinates of Dubinin-Radushkevich equation (*A- differential molar free energy of adsorption*).

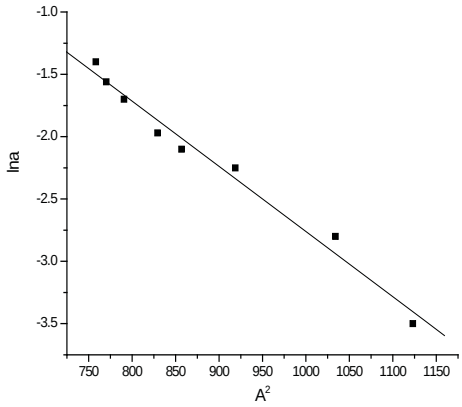

Figure 13. The adsorption isotherm of strontium ions on activated carbon CAN-8ox in the coordinates of Dubinin-Radushkevich equation (*A- differential molar free energy of adsorption*).

Figure 14 shows the isotherm of adsorption of strontium ions on CAN-7 activated carbon from real water, containing in addition to the Sr^{2+} ions (9.96 mg/L), also Ca^{2+} (37 mg/L) and Mg^{2+} (16 mg/L) ions, and pollutants that are often encountered in deep waters.

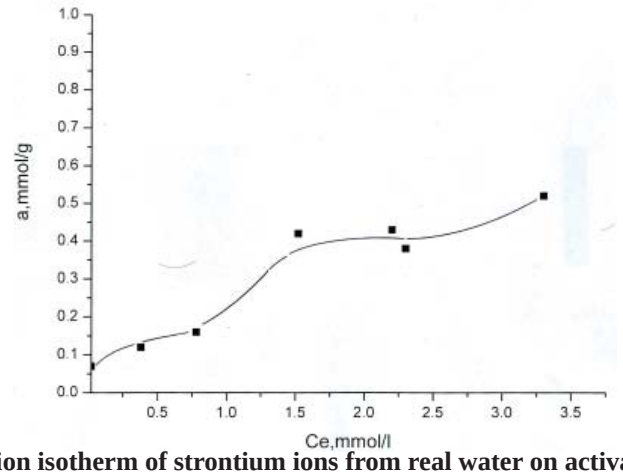

Figure 14. Adsorption isotherm of strontium ions from real water on activated carbon CAN-7.

The presented data reveal that the activated carbons CAN-7 and CAN-8ox can be successfully employed in removing the strontium, calcium and magnesium ions from real water. However, the competitive process of adsorption must be taken into account that is in favour of calcium ions, according to the series of adsorption capacity: $NH_4^+ < Na^+ < Rb^+ < Cs^+ < Mg^{2+} < Cd^{2+}$, $Mn^{2+} < Sr^{2+} < Ca^{2+} < Zn^{2+}$, $Fe^{2+} < Ni^{2+}$, $Al^{3+} < Y^{3+} \leq Cr^{3+} \leq Be^{2+} < Cu^{2+} < Fe^{3+}$ [15]. Thus, in order to efficiently remove strontium ions in water by the adsorption method, it must not contain calcium ions at all, or contain their small amount.

Conclusions

The study of adsorption of strontium ions from aqueous solutions on active carbons CAN-7 and CAN-8ox has demonstrated a similarity in allure of the obtained isotherms: both adsorption isotherms have inflection points.

Dubinin-Radushkevich equation well describes the adsorption of strontium ions from aqueous solutions on active carbons CAN-8ox and CAN-7, in the range of equilibrium concentrations 0.016-0.084 mmol/L.

The process of adsorption of strontium ions from aqueous solutions on activated carbon CAN-7, obtained by chemical activation with orthophosphoric acid, takes place due to the interaction of strontium ions with P=O and C-O-P groups, with formation of stable compounds, but also by ion exchange.

From the mixture with substantial amounts of calcium and magnesium ions, adsorption of strontium ions from water decrease in a certain extent, still remaining considerable.

References

1. The potential regulatory implications of strontium. American Water Works Association, http://www.awwa.org/Portals/0/files/legreg/documents/2014AWWAStrontiumBriefingPaper.pdf.
2. The quality control of the sanitary-epidemiological rules and standards of SanPiN 2.1.4.1074-01. Russian Ministry of Health, Russian Federation, Moscow, 2002, 62 p. (in Russian).
3. Ahmadpour, A.; Zabihi, M.; Tahmasbi, M.; Rohani Bastami M.T. Effect of adsorbents and chemical treatments on the removal of strontium from aqueous solutions. Journal of Hazardous Materials, 2010, 182, pp. 552-556.
4. Yakout S.M.; Elsherif, E. Batch kinetics isotherm and thermodynamic studies of adsorption of strontium from aqueous solutions onto low cost rice-straw based carbons. Carbon–Science and Technology, 2010, 1, pp. 144-153.
5. Shawarbkeh, R.A.; Rockstraw, D.A.; Bheda, R.K. Copper and strontium adsorption by a novel carbon material manufactured from pecan shells. Carbon, 2002, 40, pp. 781-786.
6. Cheng, H.N.; Waetelle, L.H.; Klasson, K.T.; Edwards, J.C. Solid-state NMR and ESP studies of activated carbons produced from pecan shells. Carbon, 2010, 48, pp. 2455-2469.
7. Lupascu, T.; Ciobanu, M.; Botan, V.; Nistor, A. Catalytic oxidation of methylene blue. Chemistry Journal of Moldova, 2010, 5(2), pp. 37-40.
8. Shepel, D.; Goreacioc, T.; Lupascu, T.; Filippov, M.; Rusu, M. Method of infrared spectra registration of activated carbons in potassium bromide pellets. Chemistry Journal of Moldova, 2015, 10(1), pp. 113-115.
9. Brunauer, S.; Deming, L.; Deming, W; Teller, E. On the theory of the Van der Waals adsorption of gases. Journal of American Chemical Society, 1940, 62(7), pp. 1723-1732.
10. Dubinin, M.M.; Serpinsky, V.V. On the issue of the equation of adsorption isotherms of water vapors on active charcoal. Reports of the Academy of Science of USSR, 1954, 99(6), pp. 1033-1036 (in Russian).
11. Biniak, S.; Pacula, M.; Szymanski, G.S.; Swiatkowski, A. Effect of activated carbon surface oxygen-and/or nitrogen-containing groups on adsorption of cooper (ii) ions from aqueous solution. Langmuir, 1999, 15, pp. 6117-6122.
12. Qadeer, R.; Hanif, J.; Hanif, I. Kinetics of strontium ions adsorption on activated charcoal from aqueous solutions. Journal of the Chemical Society of Pakistan, 1995, 17(2), pp. 74-77.
13. Qadeer, R.; Hanif, J.; Saleem, M.; Afzal, M. Selective Adsorption of strontium on activated charcoal from electrolytic aqueous solutions. Collection of Czechoslovak Chemical Communications, 1992, 57(10), pp. 2065-2072.
14. Sveshnikova, D.A.; Gafurov, M.M.; Ataev, M.B.; Rabaldanov, K.Sh.; Asvarov, A.Sh.; Ramazanov, A.Sh.; Kunjueva, K.G. Sorption of rubidium and caesium ions on chemically modified active carbons. Chemistry, Physics and Technology of Surface, 2013, 4(1), pp. 27-36 (in Russian).
15. Tarkovskaja, I.A. Oxidized carbon. Naukova dumka: Kiev, 1981, 197 p. (in Russian).
16. Puzii, A.M.; Poddubnaja, O.I.; Stavitskaja, S.S. Acid-base properties of carbon sorbents determined by potentiometric titration. Russian Journal of Applied Chemistry, 2004, 77(8), pp. 1279-1283 (in Russian).
17. Puzii, A.M. Methods for the preparation, structure and physicochemical properties of phosphorylated carbon adsorbents. Theoretical and Experimental Chemistry, 2011, 47(5), pp. 265-278.
18. Dobrovolski, R.; Jaroniec, M.; Kosmulski M. Study of Cd(II) adsorption from aqueous solution on activated carbon. Carbon, 1986, 24(1), pp. 15-20.

CHEMISTRY JOURNAL OF MOLDOVA. General, Industrial and Ecological Chemistry. 2016, 11(2), 34-45
http://cjm.asm.md
http://dx.doi.org/10.19261/cjm.2016.11(2).12

SEASONAL CHANGES OF MACRO- AND MICROELEMENTS CONTENT IN SOILS OF GREEN TEA FARMING FROM RIZE (TURKEY)

Fatih İslamoğlu*, Özlem Buçan, Oktay Torul, Naciye Erdoğan

Department of Chemistry, RecepTayyip Erdogan University, 53100 Rize, Turkey
**e-mail: fatih.islamoglu@erdogan.edu.tr*

Abstract. During 2014 year, 60 soil samples at the point of 30 soil samples in the spring and 30 soil samples in autumn were taken from the localities of Fındıklı (41°16'14.40"N - 41°08'24.13"E), Pazar (41°10'50.06"N - 40°53'11.35"E) and Sabuncular (41°04'20.79"N - 40°43'13.51"E) from Rize (Turkey), where green tea has been cultivated. The value of pH, content of the organic matter, and amount of macro- and microelements amount were determined in sampled soils and the seasonal changes were investigated. According to the obtained results, it was established that, in general, the values of pH, as well as the content of macro- and microelements in spring were higher than those recorded in autumn.

Keywords: soil samples, macroelements, microelements, pH, organic matter.

Received: August 2016/ Revised final: October 2016/ Accepted: November 2016

Introduction

Soil is a natural organic structure, having both mineral and organic constituents, in addition to biological, physical, and chemical features. Hence, the soil properties cannot be a simple reflexion on the connected features of all soil components. Chemical elements in soil refer to as trace elements (TEs), because of their occurrence at concentrations less than 100 $mg \cdot kg^{-1}$. Many of these elements are present at concentrations much lower than this value. The most of trace elements, which have environmental and human/animal health significance, are metals, such as: cadmium, chromium, cobalt, copper, gold, lead, manganese, mercury, molybdenum, nickel, palladium, platinum, rhodium, silver, thallium, tin, vanadium and zinc. Other significant TEs belong to the metalloid (*e.g.* boron, arsenic, and antimony), non-metal (*e.g.* selenium), actinoid (*e.g.* uranium) and halogen (*e.g.* iodine and fluorine) groups of elements [1]. The combination of soils is exceedingly different and, although, controlled by many different agents, the climatic conditions and the parent material predominate most ordinarily. Soil is a combination of solid (mineral and organic section), liquid, and gaseous phases. Furthermore, not only the chemical combination of soil, but also its mineral structure and the expression of distribution are significant factors, influencing soil properties.

Trace elements have also been termed "toxic metals", "trace metals" or "heavy metals", although none of these terms is entirely satisfactory from a chemical viewpoint. "Heavy metals" is the most popularly used and widely recognized term for a large group of elements with a density greater than 6 $g \cdot cm^{-1}$, but all TEs are metals [2]. Similarly, the term "toxic metals" is not suitable as TEs become toxic to living organisms only when they are at excess levels. For this reason, TEs are also frequently referred as potentially toxic trace elements (PTEs); this term is more comprehensive and appropriate than toxic or heavy metals. The term "trace element" is utilitarian as it clasps metals, metalloids, non-metals and other elements in the soil–plant–animal system, but it is somewhat indefinite, because it can incorporate any element notwithstanding of its function.

Seven elements, such as: chlorine, manganese, iron, zinc, boron, copper and molybdenum, are important nutrients required in trace amounts for plant growth, as well as human and animal health, although chlorine and iron within soils and plants are not TEs, because their average concentration is generally greater than 100 $mg \cdot kg^{-1}$. These elements are necessary for maintaining the life processes in plants and/or animals, including humans and, therefore, they are important micronutrients [2]. Cobalt, chromium, fluorine, iodine, nickel and selenium found in plants are not important nutrients as such, but animals have developed a dependency on these elements for use in their metabolic procedures. Cobalt is also required by microorganisms for atmospheric-nitrogen obsession and by ruminants for their rumen bacteria. Although the biological role of these elements is not fully understood, they are considered as important beneficial TEs [3]. There is little evidence to suggest that arsenic, cadmium, lead and mercury play a nutritive role in higher plants and animals [4].

The aim of this work was (i) determination of the pH value, organic matter content, amount of the macro- and microelements and (ii) evaluation of seasonal changes of these parameters in soils sampled from Rize (Turkey), where the green tea has been cultivated.

Materials and methods

Materials

In this study, 60 soil samples at the point of 30 soil samples in spring and 30 soil samples in autumn were taken from the localities of Fındıklı, Pazar and Sabuncular, where the green tea has been cultivated in Rize (Turkey) during 2014 year. Localities Fındıklı (41°16'14.40"N - 41°08'24.13"E), Pazar (41°10'50.06"N - 40°53'11.35"E) and Sabuncular (41°04'20.79"N - 40°43'13.51"E) are given by the coordinates in Figure 1.

Figure 1. Studied regions on the map.

Preparation of soil samples

Four basic stages, which help to determine the representativeness and reliability of approach, were defined as follows: Stage 1 - pre-sampling assessment and plan; Stage 2 - soil sampling; Stage 3 - soil pre-analysis treatment (which includes soil preparation and storage); and Stage 4 - soil analysis [1]. The samples were collected from the three different sampling points (Sabuncular, Pazar and Fındıklı in Rize (Turkey)) during two different seasons (April (I) and November (II)). The most soil samples are collected using a specific corer or auger. These primary samples are subsequently either combined (composite/aggregated) or kept and analysed separately (Figure 2).

The logistics, costs, obtained information and interpretation that is likely to be gained from both of these two approaches is very different [1]. The number and relative position of the sampling points depend on the scope of sampling and, thus, on the particular sampling strategy chosen, which can be selected on a statistical basis [1]. When these primary samples are mixed together, a composite/aggregate sample is obtained. A sample ready for the laboratory can be obtained either directly from the primary sample or from the composite sample [1].

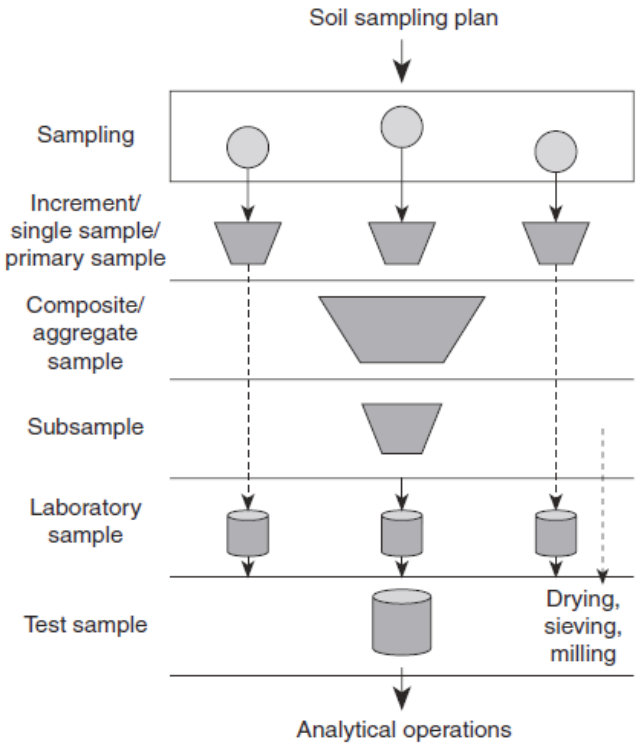

Figure 2. Sampling operations [5].

Methods

All chemicals used in this study were purchased from Merck and were of analytical grade. The value of pH, organic matter content, amount of the macro- and microelements were determined in all soil samples. Each determination was repeated 3 times.

pH value

The pH measurement was carried out after pH meter electrodes were plunged in the suspension of soil, according to the recommendations presented in [6-7].

Organic matter content

Organic matter in soil sample was digested by oxidation with acid-dichromate solution. The excess of dichromate was titrated with $KMnO_4$ solution, using ferrous(II) sulphate solution as indicator [8].

Nitrogen content

The soil sample was subjected to digestion with concentrated H_2SO_4 and solubilisation mixture (Na_2SO_4 or K_2SO_4 + $CuSO_4 \cdot 5H_2O$ + $FeSO_4 \cdot 7H_2O$). The soil extract was titrated with boric acid in micro-*Kjeldahl* apparatus and the nitrogen content was calculated by the corresponding formula [8].

Phosphorus content

Phosphorus content in soil samples was determined after digestion by extraction solution (NH_4F + 0.5N HCl). Phosphorus content was determined in filtrate solution after adding ammonium molybdate in the presence of aqueous tin(II) chloride, at 660 nm wave length [8].

Potassium content

Potassium content was determined, after digestion of soil sample by ammonium acetate, in flame photometer device [8].

Calcium content

Solution after digestion by ammonium acetate was titrated with 0.01N EDTA in the presence of ammonium purpurate in alkaline medium. The calcium content was calculated by the corresponding formula [8].

Calcium + magnesium content

Solution after digestion by ammonium acetate was titrated with 0.01N EDTA in the presence of eriochrom black - T indicator. The magnesium content was calculated by the corresponding formula [8].

Iron, manganese, zinc and copper content

The soil sample was subjected to digestion with DTPA solution (diethylene triaminepentaacetic acid + $CaCl_2$ + triethanolamine). The content of iron, manganese, zinc and copper was determined in soil extracts by using atomic absorption spectrometry (AAS) at 248.3 nm, 279.5 nm, 213.9 nm and 324.7 nm respectively.

Replaceable aluminium

Aluminium was determined by atomic absorption spectrometry (AAS) at 309.3 nm wavelength, after soil treatment with a solution of potassium chloride.

Devices

For this study the following devices were used: pH meter (Thermo Orion, X01162), spectrophotometer (Shimadzu, UV-1800), nitrogen distillation apparatus (Gerhardt, 7145110018), flame photometer (BWB XP flame photometer), age incinerator (Gerhardt, 7043130020), shaker (Selecta, 480151), atomic absorption spectrometry (GBC, Avanta T) and precision balances (Precisa, XB620M).

Results and discussion

In this study, soil samples were taken from the region of Sabuncular, Pazar and Fındıklı in Rize (Turkey) during April and November, 2014. A total of 30 soil samples was obtained from 10 different manufacturers in each region. Twelve separate analyses of each of these soil samples were performed (a total of 360).

pH value

The pH value of the tea agricultural land in Rize ranged from mild to exceptionally acidic. The pH value ranged from 3.42 to 6.12. It was determined that the pH value in the most cases was below of 4.50. In 86.6% of the soil samples the value of pH was recorded between 4.50 and 6.00, which is considered ideal for tea growing. In 76.6% of samples the exceptionally acidic pH value was registered, while 23.4% of samples had the ideal value of pH. The results for each zone and season are given in the Tables 1-3.

According to the results presented in Tables 1-3, the higher values of pH were observed in soil sampled during April. Organic fertilizers used in spring are considered as one of the reasons. It has led to the rise of pH due to the properly processing of the soil containing the applied organic fertilizer, by rainfall. In the autumn, the effect of organic fertilizer is reduced. Secondly, the drop in the pH value during November is caused by pollution through rainwater contaminated with organic fertilizer. It has led to the emergence of a significant negative effect that can be considered in the literature of the uncontrolled use of agricultural chemicals in our country and uncontrolled of manufacturers in this topic. Our tea producers have applied ammonium sulphate ($(NH_4)_2SO_4$) fertilizer in excessive quantity and one-sidedly despite all warnings. Consequently, more than 95% of our tea soils in 30 years have gained an excessive level of acidity and the pH of soil has dropped below the lower limit of pH (4.5). As a result, it appears to be compatible with the average values of pH obtained in April for tea cultivation, considering pH value of 4.5 - 6.0. The pH variation in soils of Sabuncular region is presented in Figure 3.

Table 1

Results of soil samples analyses, taken from the green tea farming in the region of Sabuncular during April (I) and November (II).

Altitude (m)	*Month*	*pH*	*Organic matter content (%)*	*N (g/kg)*	*P (g/kg)*	*K (g/kg)*	*Ca (g/kg)*	*Mg (g/kg)*	*Fe (g/kg)*	*Mn (g/kg)*	*Zn (mg/kg)*	*Cu (mg/kg)*	*Al (g/kg)*
	I	5.39	7.54	3.77	0.0653	0.1030	3.3040	2.5470	0.1365	0.0485	3.9890	1.2260	0.0503
430	II	4.47	3.52	1.76	0.0444	0.0667	2.4000	2.7380	0.2188	0.0428	2.8090	1.0320	0.0595
	I	5.14	14.56	7.28	0.1133	0.2010	6.8240	4.5830	0.2997	0.0810	4.4790	4.9100	0.0422
520	II	4.67	10.66	5.33	0.1113	0.1353	5.2240	4.3890	0.2396	0.1121	6.5300	5.8070	0.0595
	I	5.21	7.98	3.99	0.0214	0.0663	3.3600	2.7940	0.1188	0.0807	3.2580	0.9960	0.1075
550	II	4.35	3.46	1.73	0.0162	0.0267	2.9840	1.8590	0.1423	0.0479	1.7040	0.8940	0.1273
	I	5.59	6.26	3.13	0.0055	0.1030	5.3360	3.6840	0.0734	0.0577	3.4880	2.3920	0.0355
640	II	4.93	2.14	1.07	0.0048	0.0250	3.6800	2.9540	0.1315	0.0788	3.7790	2.1700	0.0421
	I	4.76	6.76	3.38	0.0147	0.0947	1.3360	1.3970	0.2124	0.0309	3.1040	1.9790	0.6694
680	II	3.91	3.36	1.68	0.0112	0.0440	0.9600	0.9860	0.2630	0.0603	2.2010	1.2620	0.6763
	I	5.52	7.26	3.63	0.0549	0.0983	4.9040	1.9860	0.1620	0.0853	5.5930	4.8280	0.0225
700	II	4.38	3.54	1.77	0.0336	0.0650	3.6800	1.3740	0.1840	0.1042	6.5420	3.5110	0.0347
	I	4.50	17.26	8.63	0.1286	0.1253	5.4400	1.6950	0.3941	0.0158	3.3890	1.2010	0.1540
750	II	3.72	13.52	6.76	0.0781	0.0780	4.0000	1.2940	0.2753	0.0104	4.4530	3.0270	0.1952
	I	4.77	7.38	3.69	0.0649	0.1383	3.6240	3.8290	0.2296	0.0558	4.0810	3.1110	0.2514
770	II	4.23	5.50	2.75	0.0444	0.0947	2.2400	1.7380	0.2589	0.0780	4.9390	2.9680	0.2881
	I	4.32	11.86	5.93	0.0540	0.1290	2.9360	2.7430	0.4081	0.0219	2.4970	1.0690	0.4772
770	II	3.70	8.08	4.04	0.0256	0.0663	1.9760	1.3820	0.2806	0.0252	2.9710	1.5320	0.4973
	I	4.63	8.62	4.31	0.0653	0.1670	2.7760	1.3820	0.2760	0.0515	3.6360	2.7490	0.3717
770	II	3.73	5.44	2.72	0.0362	0.0970	1.5440	1.0930	0.2812	0.1006	4.2060	2.4970	0.4126

Table 2

Results of soil samples analyses, taken from the green tea farming in the region of Pazar during April (I) and November (II).

Altitude (m)	*Month*	*pH*	*Organic matter content (%)*	*N (g/kg)*	*P (g/kg)*	*K (g/kg)*	*Ca (g/kg)*	*Mg (g/kg)*	*Fe (g/kg)*	*Mn (g/kg)*	*Zn (mg/kg)*	*Cu (mg/kg)*	*Al (g/kg)*
160	I	5.44	9.82	4.91	0.0136	0.6703	47.3040	5.3480	0.0539	0.0407	2.6310	1.5440	0.0411
	II	4.34	2.74	1.37	0.0087	0.4653	31.8960	3.6280	0.1911	0.1428	1.1680	1.6800	0.0595
165	I	5.10	6.32	3.16	0.0592	0.6617	8.4800	1.1250	0.1737	0.0362	4.0700	3.4670	0.2954
	II	4.21	5.62	2.81	0.0474	0.5807	5.1760	0.7690	0.3174	0.0565	1.3870	3.6900	0.0595
170	I	5.12	8.24	4.12	0.0502	0.3093	2.8800	12.9470	0.0854	0.0360	2.1170	1.3280	0.0533
	II	4.16	4.14	2.07	0.0076	0.2087	1.3360	11.2570	0.2429	0.0638	3.0090	0.5510	0.1273
175	I	4.94	6.98	3.49	0.0172	0.0767	1.2800	2.5750	0.0444	0.0235	0.6930	0.3200	0.7886
	II	3.68	4.20	2.1	0.0034	0.0350	0.6960	0.9480	0.1359	0.0192	0.7740	0.1940	0.0421
270	I	4.34	8.76	4.38	0.0109	0.2350	0.9040	0.9780	0.0528	0.0356	1.5590	0.1640	0.4952
	II	4.01	4.42	2.21	0.0030	0.0890	0.7440	0.4580	0.1425	0.0246	3.1640	0.2930	0.6763
290	I	4.90	7.42	3.71	0.0547	0.0713	5.6000	1.1450	0.0925	0.0235	1.6650	0.7070	0.6666
	II	4.19	5.58	2.79	0.0242	0.0460	4.6960	0.9480	0.1387	0.0354	1.0480	0.3160	0.0347
310	I	4.97	7.24	3.62	0.0132	0.3193	8.8000	2.3670	0.0819	0.0395	3.6540	1.3310	0.5787
	II	3.88	4.88	2.44	0.0085	0.2427	5.3840	1.4830	0.1413	0.1033	1.3620	0.5090	0.1952
315	I	5.25	8.40	4.2	0.0362	0.4853	2.6640	4.6360	0.0591	0.0240	1.3510	1.5400	0.0937
	II	4.13	3.54	1.77	0.0078	0.2110	1.4400	3.8290	0.1047	0.1016	1.8450	1.3000	0.2881
320	I	5.18	6.42	3.21	0.0134	0.0683	13.6000	1.9680	0.0795	0.0390	1.6750	1.1780	0.1672
	II	4.89	5.02	2.51	0.0042	0.0570	10.3440	0.9790	0.1782	0.0750	0.6250	0.5270	0.4973
330	I	5.45	4.44	2.22	0.0338	0.7950	11.8960	14.5680	0.0399	0.0399	1.4270	0.6990	0.1129
	II	5.13	2.78	1.39	0.0203	0.7113	8.2160	11.2840	0.0783	0.1369	2.7000	1.2510	0.4126

Table 3

Results of soil samples analyses, taken from the green tea farming in the region of Fındıklı during April (I) and November (II).

Altitude (m)	*Month*	*pH*	*Organic matter content (%)*	*N (g/kg)*	*P (g/kg)*	*K (g/kg)*	*Ca (g/kg)*	*Mg (g/kg)*	*Fe (g/kg)*	*Mn (g/kg)*	*Zn (mg/kg)*	*Cu (mg/kg)*	*Al (g/kg)*
	I	5.07	3.38	1.69	0.0282	0.1227	4.5840	2.4020	0.1262	0.0282	3.2210	2.6770	0.0465
200	II	4.35	2.40	1.2	0.0047	0.0680	2.8240	1.5560	0.0656	0.0763	3.6480	0.2700	0.0595
	I	6.12	7.44	3.72	0.0289	0.5257	10.6640	2.6260	0.1879	0.0228	4.7910	7.5810	0.0168
235	II	5.12	4.16	2.08	0.0239	0.3190	7.0960	1.2980	0.0779	0.0666	1.0250	0.1840	0.0357
	I	4.59	6.88	3.44	0.0300	0.2233	3.5760	0.5200	0.2360	0.0034	2.4320	2.7000	0.1528
240	II	3.63	4.70	2.35	0.0279	0.1027	2.0800	0.4860	0.2808	0.0140	1.4650	0.1050	0.1975
	I	4.37	7.28	3.64	0.0497	0.1007	2.1840	0.1310	0.1654	0.0114	2.6460	2.8660	0.3745
250	II	3.42	2.22	1.11	0.0117	0.0767	1.1760	0.0340	0.1726	0.0215	2.8920	1.5520	0.4435
	I	5.26	4.30	2.15	0.0293	0.1557	2.7200	0.6470	0.1362	0.0084	3.2370	3.3060	0.1042
255	II	4.44	3.26	1.63	0.0211	0.0780	1.5440	0.2630	0.1702	0.0261	3.5500	1.5460	0.1236
	I	4.55	9.78	4.89	0.0073	0.0710	1.0160	0.2630	0.0797	0.0085	2.3680	1.1230	0.3293
260	II	3.76	4.56	2.28	0.0047	0.0583	0.4240	0.1460	0.0449	0.0177	2.5580	0.5010	0.3631
	I	5.41	6.38	3.19	0.0080	0.4993	5.4960	0.9040	0.1258	0.0317	3.3710	2.5580	0.0397
280	II	4.92	3.64	1.82	0.0076	0.3343	4.6960	0.2920	0.0717	0.0527	0.6980	1.4710	0.0463
	I	5.02	5.04	2.52	0.0085	0.4133	5.7600	0.8410	0.1203	0.0309	2.5830	1.7250	0.0886
285	II	4.55	3.20	1.6	0.0065	0.3433	3.6240	0.6470	0.0682	0.0833	3.4430	0.6380	0.1222
	I	4.95	6.54	3.27	0.0159	0.3360	3.4640	0.8070	0.0790	0.0191	2.1480	2.0380	0.1307
320	II	3.84	4.10	2.05	0.0104	0.2427	1.9760	0.5830	0.0959	0.0448	2.5260	0.8580	0.1531
	I	5.56	7.40	3.7	0.0483	0.4333	8.8560	1.9450	0.1998	0.0177	4.7500	4.9620	0.0430
340	II	4.43	4.76	2.38	0.0057	0.3093	6.0240	1.0990	0.0693	0.0430	0.8800	0.0480	0.0580

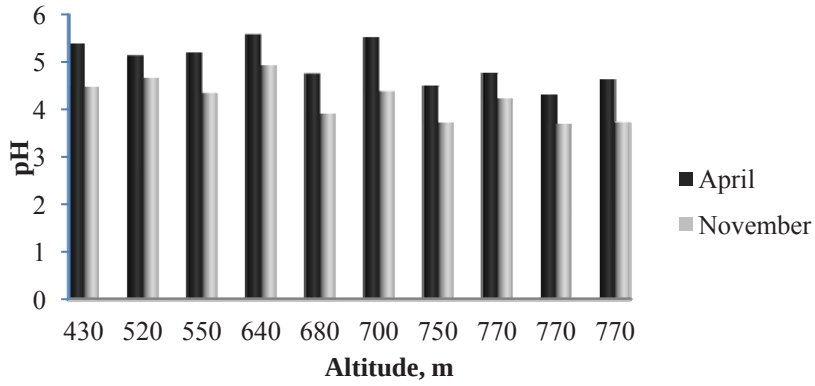

Figure 3.
Variation of pH value in soil sampled from Sabuncular region.

Organic matter content

In 13.3% of soil sampled during April the organic matter content was at high level, while in 86.7% of samples was at very high level. During November there were registered the following results: in 16.7% of samples the organic matter content was at medium level, in 73.3% - at high level and in 10.0% - at very high level. Similar results were identified in another study in Rize [9]. The values of organic matter content vary widely in soil of tea garden during April and November. This is explained by the fact that each month is characterized by abundant rainfall and low temperatures. Dynamics of organic matter content registered in Sabuncular region is shown in Figure 4.

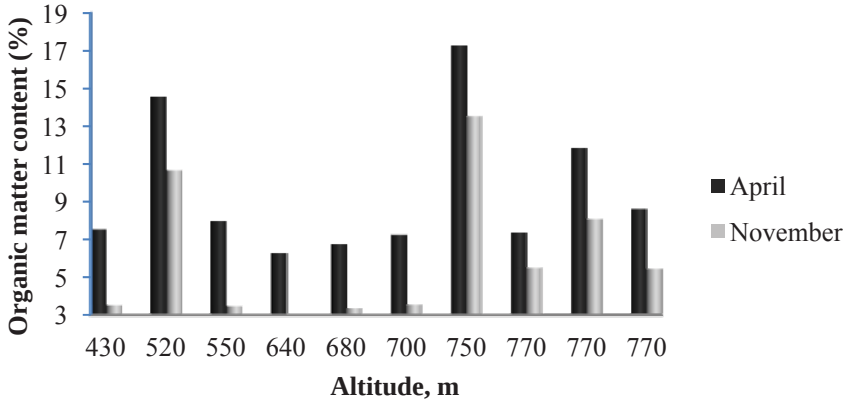

Figure 4.
Variation of organic matter content in soil sampled from Sabuncular region.

Nitrogen content

The nitrogen content in soil samples ranged from 1.1 g/kg to 8.6 g/kg. In 10% of soil sampled during April the nitrogen content was at high level, while in 90% of samples was at very high level. During November there were registered the following results: in 16.7% of samples the nitrogen content was at medium level, in 56.7% - at high level and in 10.0% - at very high level. The nitrogen ratio was similar to organic matter content. Thus, we can conclude that nitrogen is originated from organic matter in the soil.

A dynamics of nitrogen content in a study conducted between 1978 - 1982 years for 1667 soil samples at same region was reported [10]. Also, Müftüoğlu *et al.* determined the nitrogen content of the tea garden soils, classifying them as group of low, medium, high and very high [11]. There were identified the following groups: 3.78% low, 16.09% medium, 40.59% high and 39.53% very high in a study of soil samples [12]. It appears that these values are compatible with our results. The variation of nitrogen content recorded in Sabuncular region is presented in Figure 5.

Phosphorus content

The phosphorus content in soil sampled in April and November ranged from 0.0030 g/kg to 0.1286 g/kg. Comparing the obtained results with results performed in another study in the same region, which include research of 1815 soil samples [10], the increasing of phosphorus content in the soil was observed.

The phosphorus amount in samples taken in November was lower than the phosphorus content in samples collected in April. The reason is a reduction of pH value in soils. In soil phosphorus reacts with Al, Fe, Mn and insoluble hydrated oxides of these elements under acidic conditions, with Ca and Mg - in alkaline conditions. Phosphorus is a nutrient, being the most affected by the soil reaction. From the soil, plants often use the HPO_4^{-2} and $H_2PO_4^-$ form of phosphorus. Plants utilize phosphorus in the form of $H_2PO_4^-$ when pH value is lower than 6.71 and in the form of HPO_4^{-2}

when pH value is higher than 6.71. The solubility of the phosphate increases when the amount of alkali metal salts in the soil augments, depending on pH value. As a result, the plant benefits the phosphorus at pH values in limits of 5-7. Phosphorus content variation identified in Sabuncular region is shown in Figure 6.

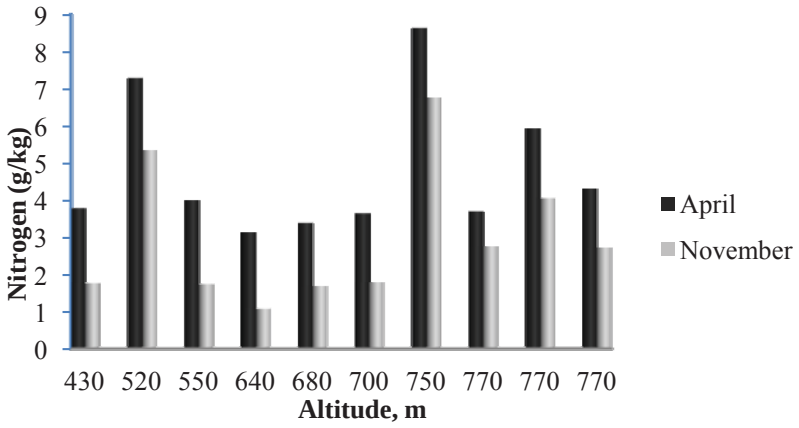

Figure 5.
Variation of nitrogen content in soil samples from Sabuncular region.

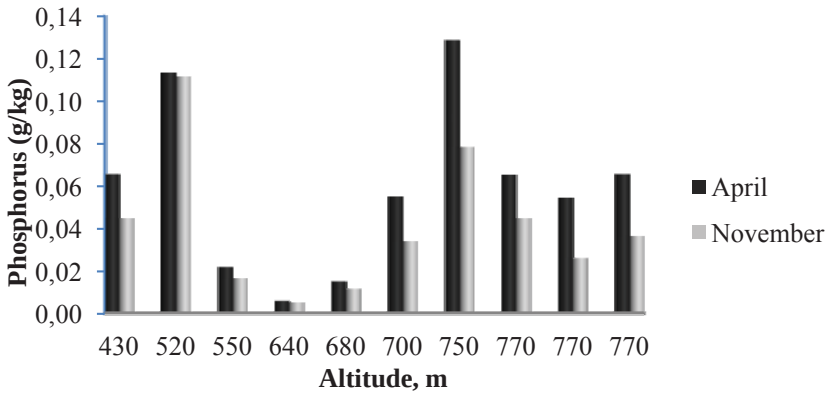

Figure 6.
Variation of phosphorus content in soil samples from Sabuncular region.

Potassium content

In soil sampled during April in 46.7% of samples the potassium content was at low level, while in 26.7% of samples was at sufficient level, and in 26.6% - at high level. During November there were registered the following results: in 16.7% of samples the potassium amount was at very low level, in 46.7% - at low level, in 26.6% - at sufficient level and in 10.0% - at very high level. By comparing our results with the results of another study in the same region, which include research of 1678 soil samples [13], it is observed an increasing the potassium amount in the soil.

Potassium content in the samples taken in November was lower than the potassium levels in April. It can be stated that decreasing the pH value, increasing the precipitation quantity and freeze-thaw phenomena in the soil are the reasons for this fact. It is not exactly determined that increasing the potassium level in the soil depends on the pH value. It is accepted as a general rule that the potassium level increases in the conditions of high pH [14]. Potassium amount dynamics in soils sampled from Pazar region is presented in Figure 7.

Calcium content

The calcium content in soil sampled in April and November ranged from 0.424 g/kg to 47.304 g/kg. Calcium content values in soil samples were higher than the normal values during both seasons. In 36.7% of the samples taken in the spring and in 40.0% of the samples taken in the autumn the calcium content had the desirable values. The dynamics of calcium content in soils sampled in Pazar region is shown in Figure 8.

Magnesium content

In soil sampled during April in 3.3% of samples the magnesium content was at sufficient level, while in 33.4% of samples was at high level, in 60.0% - at very high level. During November there were registered the following results: in 10.0% of samples the magnesium amount was at sufficient level, in 50.0% - at high level, in 33.3% - at very high level. The values of magnesium content in the soil samples were higher than the normal values during both seasons. In 3.3% of the samples taken in the spring and in 10.0% of the samples taken in the autumn the magnesium content had the desirable values. A dynamics of magnesium content in soils sampled in Pazar region is shown in Figure 9.

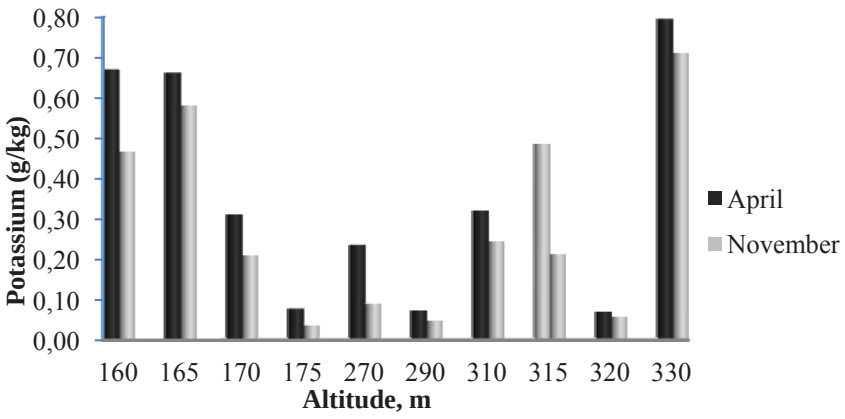

Figure 7.
Variation of potassium content in soil samples from Pazar region.

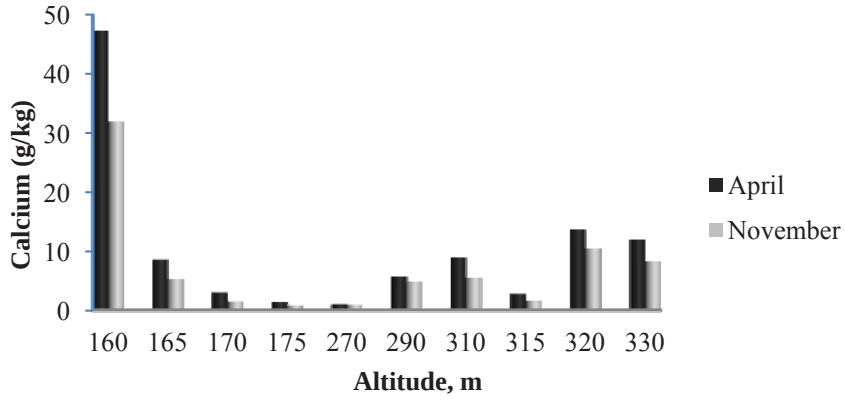

Figure 8.
Variation of calcium content in soil samples from Pazar region.

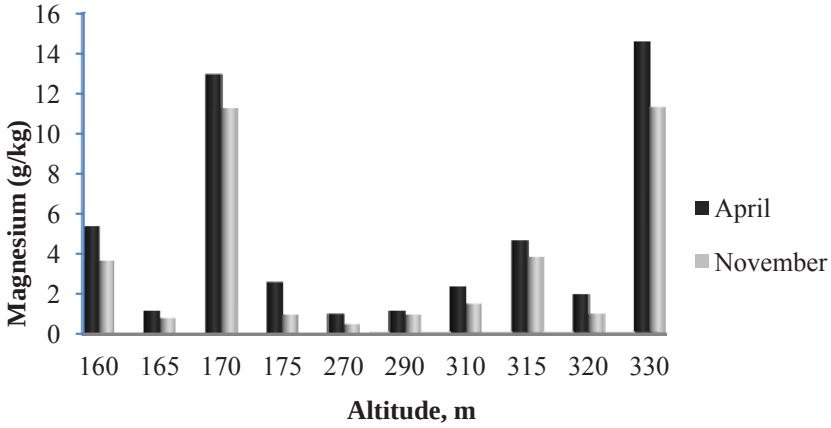

Figure 9.
Variation of magnesium content in soil samples from Pazar region.

Iron content

The iron content of samples taken in April was at medium level in 6.7% of samples, at a high level in 40.0% of samples and at a very high level in 53.3% of samples. In November the iron amount was registered at medium level in 3.3% of samples, at a high level in 26.7% of samples and at a very high level in 70.0% of samples. In 40.0% of samples taken in the spring and in 26.7% of samples collected in the autumn the iron content had the desirable values. The reason is the decline of pH value between the two seasons. The higher values of pH in the spring cause the iron content decreasing, whereas the fall in pH values in autumn causes the iron content increasing above the normal values.

It was determined that the values of iron content ranged between 0.0036–0.0448 g/kg in a study conducted in 8 gardens between the years of 1977-1978 in the same region [14]. Taking into account these data, it seems to be an increase in values of iron amount in our tea land. Toxic effects causing an excess of soluble iron in plants, which lack of useful iron content, contribute to excessive iron deficiency in some soils. The variation of iron content in soil sampled in Pazar region is presented in Figure 10.

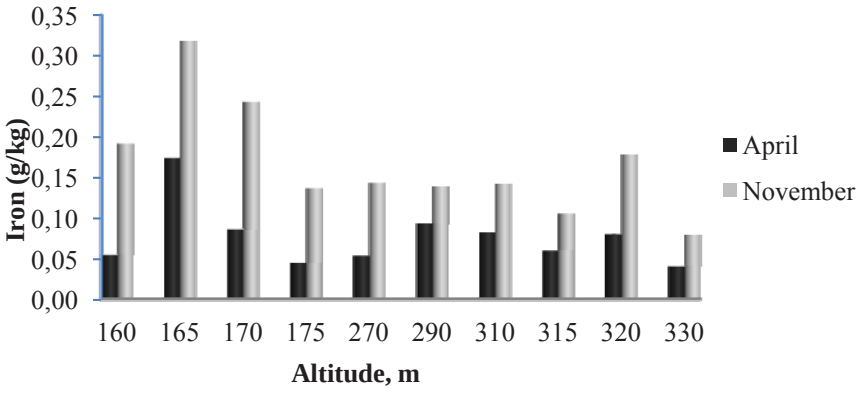

Figure 10.
Variation of iron content in soil samples from Pazar region.

Manganese content

The manganese content in samples taken in April was at medium level in 76.7% of samples and at a very high level in 23.3% of sample. In November the manganese content in 36.7% of samples was at medium level, in 40.0% of samples – at high level and in 23.3% of samples – at very high level. In 23.0% of samples taken in the spring and in 40.0% of samples taken in the autumn the manganese amount had the desirable values. It is determined the manganese values ranged between 0.0019–0.0405 g/kg in a study conducted in 8 gardens between the years of 1977-1978 in the same region [15]. As a result, an increase in the value of manganese content was observed in samples taken in November. The variation of the manganese amount in soil sampled in Fındıklı region is shown in Figure 11.

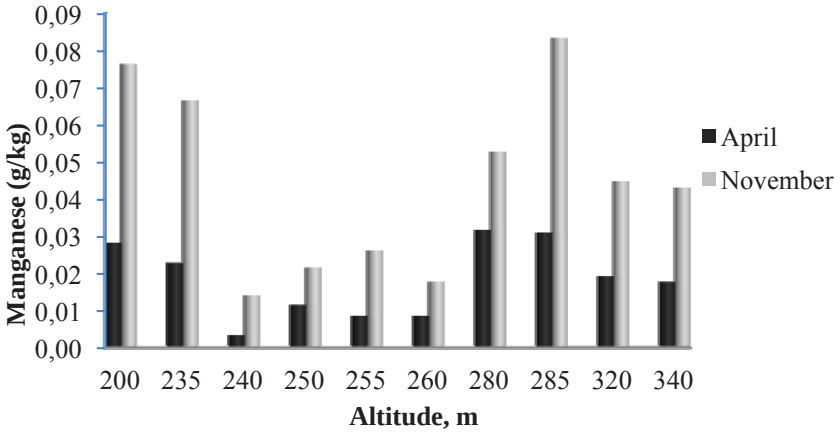

Figure 11.
Variation of manganese content in soil samples from Fındıklı region.

Zinc content

The zinc content in samples taken in April was at medium level in 20.0% of samples and at a very high level in 80.0% of samples. In November the zinc amount was at medium level in 40.0% of samples and at a high level in 60.0% of samples. In 80.0% of samples taken in the spring and in 60.0% of samples taken in the autumn the zinc amount had the desirable values. The amount of zinc ranged between 0.12–4.05 mg/kg in a study conducted in 8 gardens between the years of 1977-1978 in the same region [15]. As a result, a decrease in the value of zinc content was observed in samples collected in November. The variation of zinc content in soil sampled in Fındıklı region is shown in Figure 12.

Copper content

The copper content in samples taken in April was in 16.7% of samples at medium level, in 80.0% - at a high level and in 3.3% - at a very high level. In November the copper content was in 46.7% of samples at medium level and in 53.3% - at a high level. The copper content ranged between 0.06–5.93 mg/kg in a study conducted in 8 gardens between the years of 1977-1978 in the same region [15]. As a result, an increase in the value of the copper amount was observed in soil sampled during two seasons. Dynamics of the copper amount in soil sampled in Fındıklı region is presented in Figure 13.

Aluminium content

The aluminium content in samples taken in April was at low level in 63.3% of samples and at medium level in 36.7%. In 53.3% of samples it was at low level and in 46.7% at medium level during November. The variation of aluminium content in soil sampled in Fındıklı region is shown in Figure 14.

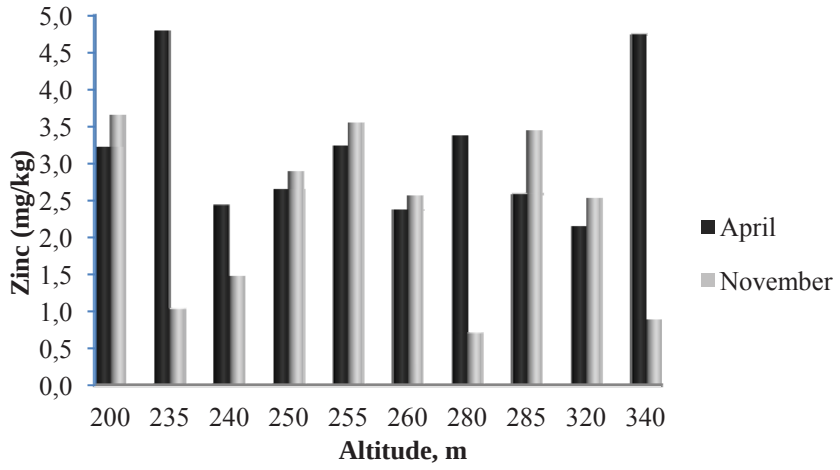

Figure 12.
Variation of zinc content in soil samples from Fındıklı region.

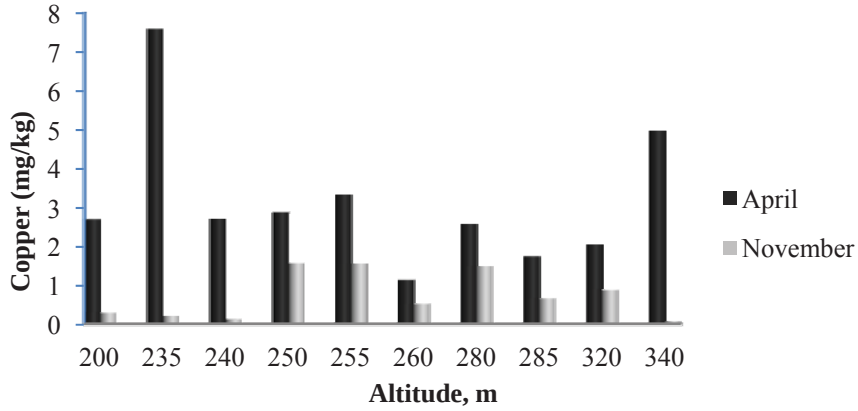

Figure 13.
Variation of copper content in soil samples from Fındıklı region.

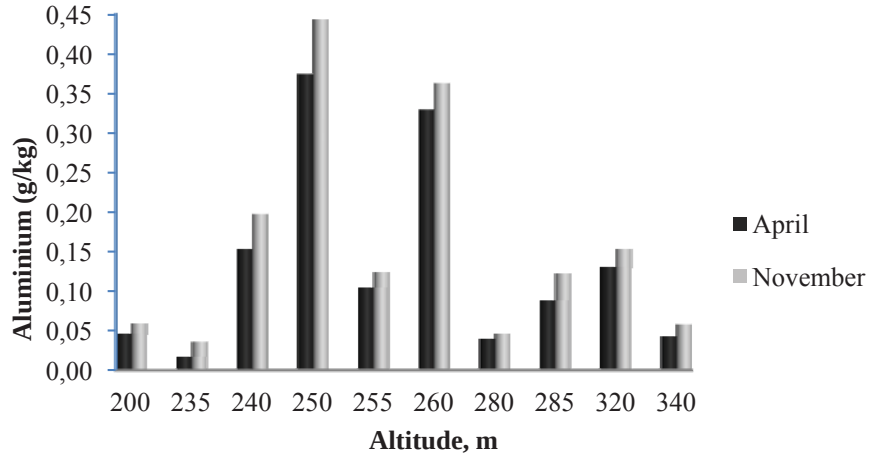

Figure 14.
Variation of aluminium content in soil samples from Fındıklı region.

Conclusions

Commercial fertilizers, especially on the basis of nitrogen and phosphorus, are often used unconsciously in tea growing areas in Turkey. Soil reaction has been gradually acidic and the soil productivity began to be lost as a result of manufacturers, especially using ammonium sulphate fertilizer alone and overmuch. The amount of products to be received per unit area will be high-quality as long as soil fertility status is at an appropriate level. Therefore, the promotion and protection of soil productivity level is important.

Despite the depletion or decrease in the use of ammonium sulphate fertilizer in many platforms and the expression used for the location of compound fertilizer, tea manufacturers have not outgrown their habits but continued to use ammonium sulphate fertilizer for years. In order to avoid the acidity increasing of the soil it is recommended to use composite fertilizer (with ammonium sulphate) instead of using ammonium sulphate alone.

References

1. Hooda, P.S. Trace Elements in soils. John Wiley and Sons Ltd.: Chichester, 2010, pp. 53-56.
2. Bennett, W.F. Ed. Nutrient Deficiencies & Toxicities in Crop Plants. APS Press: New York, 1993, pp. 28-32.
3. Johnston, A.E. Trace elements in soil: status and management in Essential Trace Elements for Plants. Animals and Humans NJF Seminar: Iceland, 2005, pp. 71-74.
4. Adriano, D.C. Trace elements in the terrestrial environment. Springer: New York, 1986, pp. 43-45.
5. De Zorzi, P.; Barbizzi, S.; Belli, M.; Ciceri, G.; Fajgelj, A.; Sansone, U.; Van Der Perk, M. Terminology in soil sampling. Pure and Applied Chemistry, 2005, 77, pp. 827-841.
6. Kalra, Y.P. Determination of pH of soils by different methods: Collaborative study. Journal of AOAC International, 1995, 78, pp. 310-321.
7. Noli, F.; Tsamos, P. Concentration of heavy metals and trace elements in soils, waters and vegetables and assessment of health risk in the vicinity of a lignite-fired power plant. Science of the Total Environment, 2016, 563, pp. 377-385.
8. Bremner, J.M.; Mulvaney, C.S. Methods of soil analysis. Part 2. Chemical and microbiological properties. Academic Press:USA, 1982, pp. 595-624.
9. Sarimehmet, M.; Müftüoğlu, N.M. Status of organic matter at tea agricultural soil in Eastern Black Sea region. Journal of Ege University Faculty of Agriculture, 1993, 30, pp. 49-56.
10. Sarimehmet, M.; Müftüoğlu, N.M. Status of nitrogen at tea agricultural soil in Eastern Black Sea region. Journal of Ege University Faculty of Agriculture, 1993, 30, pp. 57-64.
11. Müftüoğlu, N.M.; Yüce, E.; Turna, T.; Kabaoğlu, A.; Özer, S.P.; Tanyel, G. Assessment of soil and plant properties in tea agriculture made areas. Journal of Ege University Faculty of Agriculture, 2010, 45, pp. 309-316.
12. Müftüoğlu, N.M.; Özer, S.P.; Tanyel, G.; Kabaoğlu, A. Changes occurring depend on time at some plant nutrientin eastern black sea region soils made tea agricultural. Journal of Ege University Faculty of Agriculture, 2012, 47, pp. 167-168.
13. Sarimehmet, M.; Müftüoğlu, N.M.; Yılmaz, E. Determination of plant nutrient content and physical structure in our country the tea soil, Tea Authority Headquarters. Tea Research Institute Working Paper, 1982, pp. 71-92.
14. Bilen, S.; Yıldırım S. Effects of Plant Nutrient availability on soil reaction, Journal of Atatürk University, Faculty of Agriculture, 1993, 24, pp. 156-166.
15. Kacar, B.; Przemeck, E.; Özgümüş, A.; Turan, C.; Katkat, A.V.; Kayıkçıoğlu, İ. A study on the microelement necessity of tea plants and soils in Turkey. Ankara:Tubitak, 1979, pp. 67-68 (in Turkish).

CHEMISTRY JOURNAL OF MOLDOVA. General, Industrial and Ecological Chemistry. 2016, 11(2), 46-51
http://cjm.asm.md
http://dx.doi.org/10.19261/cjm.2016.11(2).08

ANTIOXIDANT AND ANTIMICROBIAL PROPERTIES OF *STEVIA* LEAVES EXTRACTS AND SILVER NANOPARTICLES COLLOIDS

Iryna Laguta[a*], Teteiana Fesenko[a], Oksana Stavinskaya[a], Oksana Dzjuba[b], Lesya Shpak[b]

[a]*Chuiko Institute of Surface Chemistry of National Academy of Sciences of Ukraine, 17, General Naumov Street, Kiev-03164, Ukraine*
[b]*M.M. Gryshko National Botanic Garden of National Academy of Sciences of Ukraine, 1, Timiryazevska Street, Kiev-01014, Ukraine*
[*]*e-mail: icvmtt34@gmail.com*

Abstract. Three extracts of *Stevia rebaudiana* (Bertoni) were prepared using various types of raw materials: leaves of plants grown *ex situ*, leaves of plants grown *in vitro*, callus culture formed on damaged leaves. Composition of the extracts, their activity in the synthesis of silver nanoparticles colloids, as well as antioxidant and antimicrobial properties of the extracts and the colloids were investigated.

Keywords: *Stevia* leaves extract, silver nanoparticles colloid, antioxidant activity, antimicrobial properties.

Received: October 2016/ Revised final: November 2016/ Accepted: November 2016

Introduction

Recently detailed investigation of plants phytoconstituents and extracts has attracted a great attention. A variety of plants was considered as a source of biologically active substances with various valuable properties [1-3]. For example, *Acacia arabica* was used to extract tannins for the production of natural dyes for textile industry. *Atropa belladonna*, *Nicotiana tabaccum*, *Cinchona* tree were found to contain pharmacologically active substances such as atropine, nicotine, quinine. *Madagascar periwinkle* was used as a source of anticancer alkaloids. Essential oils extracted from the fruits, flowers, barks, stem, leaves, roots and other parts of various plants are widely used in cosmetic industry and aromatherapy.

For medicine, biology and food industry, bioactive compounds endowed with redox properties, as well as antimicrobial activity, are of especial interest. Plants may be a source of effective antioxidants of natural origin, such as: flavonoids, phenolic acids, phenolic diterpenes, and tannins. All these compounds may be used in pharmacology and cosmetology to produce the preparations with antioxidant, anti-inflammatory, immunomodulation action [1]. Many of plants may also contain such phytoconstituents as terpenoids, alkaloids, coumarins, fatty acids with clear antimicrobial activity [4]. According to the published data, they may be used, in particular, as antimicrobial drugs, antimicrobial agents in food packaging and preservatives in the cosmetic industry [2, 4-7]. An additional way of using the plant extracts with redox properties for medical or biological applications is represented by "green" synthesis of silver nanoparticles (AgNPs), which are known to be very effective antimicrobial agent. Green synthesis of metal nanoparticles (NPs) where plant constituents are employed is also of interest for various fields of science and technologies due to wide application of the NPs in electronics, material science, physics and catalysis [8]. Use of plant extracts for NPs production appears to provide the synthesis with beneficial requirements: mild temperature and pH, non-toxic and cheap reducing/stabilizing agents.

In spite of wide diversity of utilization and application, the extracts of plants grown in the traditional way may also posses certain drawbacks. The formation of metabolites in the plants grown *ex situ* may be affected by unfavourable ambient conditions; this, in turn, may lead to violation of the synthesis of valuable metabolites and accumulation of toxic substances in the plants. Cultivation of the plant tissues under aseptic conditions is an alternative method for production of pure bioactive compounds. Pureness of bioactive compounds and independence of the metabolites yields on climate conditions and negative ambient effects are the advantages of this method.

The present communication reports on study of the extracts of *Stevia rebaudiana* (Bertoni) obtained from the leaves of the plants grown *ex situ* and *in vitro* as well as from the callus tissue culture formed on damaged leaves. *Stevia rebaudiana* (Bertoni) is a herbaceous perennial shrub. The *Stevia* leaves contain a complex mixture of sweet diterpene glycosides [9] as well as such bioactive substances as: flavonoids, phenolic acids, fatty acids, proteins, and vitamins [10]. The availability of compounds with redox properties makes *Stevia* plants an interesting raw material for preparation of biologically active extracts and for green synthesis of NPs colloids. To the best of our knowledge, comprehensive investigation of these plant extracts from the different types of raw materials as well as the use of such extracts for the green synthesis of metal NPs has not been reported. Our work was also aimed at study of the activity of the *Stevia rebaudiana* (Bertoni) extracts in synthesis of silver nanoparticles and characterization of the antioxidant/ antimicrobial properties of the extracts and the synthesized colloids.

Experimental

Stevia plants were grown in M.M. Gryshko National Botanic Garden of National Academy of Sciences of Ukraine. Three types of raw material were used to prepare the *Stevia* extracts. Extract 1 and Extract 2 were produced

using leaves of the plants grown *ex situ* and *in vitro*, respectively. Extract 3 was prepared from callus. To grow plants *in vitro*, sterilized seeds were placed in glass flasks containing Murashige and Skoog basal medium and exposed to artificial light for 16 hours per day. To obtain callus, transverse incisions were made on fresh leaves, without reaching the edge of the leaf. Then these leaves were placed on a modified Murashige and Skoog basal medium additionally containing 40 mg/L of iron(III) chloride and up to 0.2 mg/L of vitamins B1, B6 and thidiazuron.

The ***biologically active substances*** were extracted from the leaves and callus with a 70% ethanol aqueous solution according to a procedure described in the literature [11]. To 1 g of finely chopped leaves or callus, 100 mL of 70% ethanol were added, then the mixtures were placed into steam bath for 30 minutes. After cooling, the extract was adjusted to the initial volume and filtered.

The ***total concentration of phenolic compounds*** in the extracts was evaluated by using the Folin–Ciocalteau method. For measuring the total phenol index [12], 11.5 mL of distilled water, 5 mL of 20% sodium carbonate solution, 1.25 mL of Folin-Ciocalteau reagent (Merck) and 6.25 mL of water were consecutively added to 1 mL of extract. The solution was stirred for 30 min, then the absorbance at 750 nm was measured, and the total phenol index was calculated in accordance with the described protocol [12]. Using the data on total phenol index for the well known antioxidant, ascorbic acid (for 0.5 mM solution of ascorbic acid the total phenol index was equal to [13]), the equivalent concentration of ascorbic acid in the extracts was calculated.

For determining the ***total content of flavonoids***, we used the method based on the ability of the compounds to form a coloured complex with aluminium chloride. To 1 mL of extract, prepared as above-described and placed in a volumetric flask, 5 mL of 2% solution of $AlCl_3$ (Sigma-Aldrich) in 95% ethanol was added, and then 95% ethanol was added to reach the volume of 25 mL. The mixture was stirred for 30 min and the optical density of the solution at 410 nm was measured. To prepare a blank solution, 0.1 mL of concentrated acetic acid was added to 1 mL of extract, followed by the dilution of the mixture by 95% ethanol to the total volume of 25 mL. For obtaining the reference samples, rutin (Sigma-Aldrich) solutions of different concentrations were prepared using 95% ethanol as solvent [14]. Total content of flavonoids is given as equivalent content of rutin in dry raw material.

High performance liquid chromatography (HPLC) method was used for ***identification and quantification of steviol glycosides and hydroxycinnamic acids***. The analysis was performed using an automatic four-channel liquid chromatograph Agilent 1100 with diode-matrix detector and chemical analyzer (Agilent Technologies, Germany). For preparation of the extracts for analysis, air-dried leaves or callus were finely chopped, poured over with methanol in the 1 g : 20 mL ratio, kept for 24 h in the dark and filtered using dense (0.2 μm) teflon filter. For estimating the quantity of steviol glycosides and hydroxycinnamic acids, the areas of appropriate signals were compared with the ones for reference substances (stevioside, rebaudioside, caffeic acid).

For preparation of the AgNPs, 9 mL of 1 mM $AgNO_3$ (Merck) aqueous solution were added to 1 mL of extract. The Extract/$AgNO_3$ reaction mixture was stirred for 2 hours at temperature of 40°C, then the solution was cooled to room temperature and the UV spectra of the obtained colloid were recorded. For all the Extract/$AgNO_3$ reaction mixtures, changing the colour of the mixtures from yellow to brown, which indicates the formation of AgNPs, was observed in about 30 minutes after beginning of the reaction.

UV/Vis spectra of plant extracts and AgNPs colloids were recorded on a Perkin Elmer Lambda 35 UV/Vis double beam Spectrophotometer at 25°C in the wavelength range of 200-800 nm. Scanning speed was 480 nm/min, cuvette path length was 10 mm.

The ***antioxidant activity*** of the extracts and AgNPs colloids was evaluated using 2,2-diphenyl-1-picrylhydrazyl (DPPH) radical scavenging method [15]. A 0.15 mM solution of DPPH (Sigma-Aldrich) in 70% ethanol was prepared. To 2 mL of the DPPH solution 2 mL of 70% ethanol and 1 mL of original or diluted extract/colloid were consecutively added. The concentration of stable radicals in reaction mixture was determined from the change in optical density at the absorption maximum of 520 nm. For characterization of the antioxidant ability of the extracts and colloids, percentages of the reduced DPPH radicals for the reaction time of 30 min (DPPH-30 values) were determined. For diluted *Stevia* extracts, the kinetics of radical inhibition during 2 hours was also investigated.

To characterize ***antimicrobial properties*** of the extracts and colloids, we studied their ability to inhibit the growth of the test culture in a standard meat-peptone broth (MPB) medium, with *Bacillus cereus* cells as a test culture. A volume of 4 mL of MPB, 0.5 mL of extract/colloid (original or diluted by 2-10 times) and 0.5 mL of *Bacillus cereus* cells suspension were placed in a test tube, the concentration of the cells in the reaction medium was 0.5 million cells/mL. Reference samples were prepared by the same way, but 0.5 mL of extract/colloid was substituted for 0.5 mL of MPB or 0.5 mL of ethanol solution of different concentration. The content of tubes was mixed and incubated at 30°C for 24 h. The concentration of *Bacillus cereus* cells in the suspension was determined from UV spectra, using the concentration-dependent absorbance of *Bacillus cereus* cells at λ = 540 nm. Percentage of the inhibited by extracts/colloids cells were calculated as a difference in concentration of *Bacillus cereus* cells in the studied suspension and control samples. The presented results are the average of three independent measurements.

Results and discussion

Table 1 shows the total phenol index, equivalent concentration of ascorbic acid and results of DPPH-30 test for *Stevia* extracts prepared from the leaves of the plants grown *ex situ* and *in vitro* and from callus culture (Extract 1-3, respectively). Table 2 gives the data regarding the content of phytoconstituents with antioxidant

and antimicrobial properties in the *Stevia* raw material. Three main groups of bioactive compounds were revealed in the plants and extracts: steviol glycosides, flavonoids and hydroxycinnamic acids. Flavonoids and hydroxycinnamic acids are phenolic compounds with high redox properties, while steviol glycosides are known to possess distinctive antimicrobial activity. In addition to the above-mentioned compounds, small amounts of fatty acids, reducing sugars and terpenoids were also detected in the extracts during our previous experiment by means of laser desorption/ionization mass spectrometry method.

Table 1

Antioxidants properties of *Stevia* extracts.

Raw material used for extract preparation	*Extract designation*	*Total phenol index**	*Equivalent concentration* of ascorbic acid, mM*	*DPPH-30*, %*
Leaves of plant grown *ex situ*	Extract 1	10.8±0.2	5.4±0.1	~100
Leaves of plant grown *in vitro*	Extract 2	4.0±0.1	2.0±0.1	~100
Callus	Extract 3	8.0±0.1	4.0±0.1	~100

**Indicated scattering of the data corresponds to 90% confidence interval*

Table 2

Content of phytoconstituents in the *Stevia* raw material.

Raw material used for extract preparation	*Content of bioactive compounds*, %*		
	Flavonoids	*Steviol glycosides*	*Hydroxycinnamic acids*
Leaves of plant grown *ex situ*	0.92±0.05	2.8±0.1	1.0±0.1
Leaves of plant grown *in vitro*	0.60±0.05	1.9±0.1	3.3±0.1
Callus	0.11±0.05	≤ 0.1	8.3±0.1

**Indicated scattering of the data corresponds to 90% confidence interval*

As one can see from the Tables 1 and 2, all the extracts have high content of phenols, which is equivalent to a concentration of ascorbic acid of 2-5 mM. The highest content of phenols, flavonoids, and steviol glycosides were observed for the leaves of the grown *ex situ* plants and for the appropriate Extract 1. Callus and Extract 3 are characterized by the highest content of hydroxycinnamic acids and by significant value of total phenol index, the content of flavonoids and steviol glycosides being negligible. As to the plants grown *in vitro*, they contain the smallest amount of phenols and intermediate amount of flavonoids and steviol glycosides.

All original extracts were found to possess antioxidant ability that was sufficient to inhibit practically 100% of DPPH radicals for 30 minutes (Table 1). To reveal the distinction in the antioxidant properties of the extracts, the DPPH test was also performed using the diluted by 200 times extracts (Figure 1). As one can conclude from the Figure 1, the activity of diluted extracts in reaction with DPPH radicals during 2 h is represented by the series: Extract 1 ≈ Extract 3>>Extract 2. Thus, antioxidant activity of the extracts correlates with total phenols content, rather than flavonoids content (Table 1). At the same time, composition of the extracts appears to contribute to the reaction kinetics: high amount of flavonoids in Extract 1 leads to faster reduction of DPPH radicals during first 10 min of the reaction, as compared to Extract 3 (Figure 1). Antimicrobial properties of the extracts are illustrated by Table 4 data and will be discussed below.

All the extracts revealed significant activity in the AgNPs synthesis. Figure 2 gives the UV spectra for Extract/$AgNO_3$ reaction mixtures in 2 h after the start of the reaction. As one can see from the Figure 2, all the spectra include the absorbance band with the maximum at around 450 nm, which is characteristic of AgNPs plasmon resonance. The smallest intensity of the band is characteristic for Extract 2/$AgNO_3$ reaction mixture and close to each other are the bands for Extract 1/$AgNO_3$ and Extract 3/$AgNO_3$ mixtures. The different efficiency of the extracts in the synthesis of AgNPs may be explained by the distinctions in the extracts composition; as one can conclude from the comparison of Figures 1 and 2, this efficiency correlates with the antioxidant activity of the extracts, which was determined by using DPPH test. Indeed, Extract 2 is characterized by the smallest content of phenols and by the lowest rate of DPPH inhibition; it also has the less activity in AgNPs synthesis. Extract 1 has the highest content of phenols and flavonoids, which are very effective redox agents [16], and during first two hours of the reactions, shows the fastest reduction of both DPPH radicals and Ag^+ ions. Extract 3 from the callus culture is similar to Extract 1 by its redox properties and exhibits the similar activity in AgNPs synthesis.

Table 3 gives the data on antioxidant and antimicrobial properties for AgNPs colloids that were synthesized using *Stevia* leaves extracts. As it was above-mentioned, all original extracts possessed antioxidant ability sufficient to inhibit ~100% of DPPH radicals under standard DPPH-30 test conditions. The same observation appears to be true for the appropriate colloids: in spite of partial consumption of reducing agents for the reduction of Ag^+ ions, all colloids still possess high antioxidant ability and practically reduce 100% of DPPH radicals for 30 min (Table 3). All colloids are also very effective antimicrobial agents inhibiting 80-85% of *Bacillus cereus* cells.

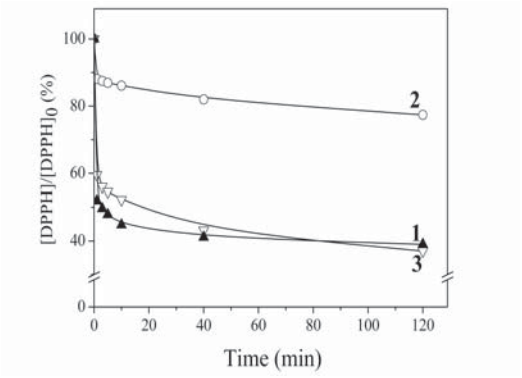

Figure 1. Inhibition of DPPH radicals by diluted *Stevia* extracts.
(1)–Extract 1 from the leaves of plants grown *ex situ*;
(2)–Extract 2 from the leaves of plants grown *in vitro*;
(3)–Extract 3 from callus culture.

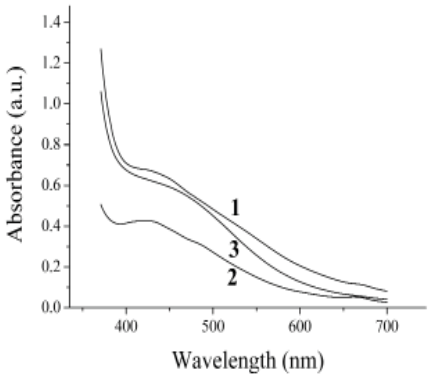

Figure 2. UV spectra of Extract/$AgNO_3$ reaction mixtures.
(1)–Extract 1/$AgNO_3$; (2) – Extract 2/$AgNO_3$;
(3)–Extract 3/$AgNO_3$.
Time of reaction: 2 h.

Table 3

Antioxidant and antimicrobial properties of AgNPs colloids.

Raw material used for extract preparation	*Colloid designation*	*Colloid characteristics*	
		DPPH-30, %*	*Inhibition* of Bacillus cereus cells, %*
Leaves of plant grown *ex situ*	Extract 1/ AgNPs colloid	~100	85±7
Leaves of plant grown *in vitro*	Extract 2/ AgNPs colloid	~100	80±7
Callus	Extract 3/ AgNPs colloid	~100	80±5

**Indicated scattering of the data corresponds to 90% confidence interval*

Table 4 gives the data on antimicrobial properties for diluted *Stevia* extracts and for appropriate AgNPs colloids. In general, antimicrobial properties of Extract/AgNPs colloids must be a result of antimicrobial action both of extract and silver ions/NPs. However, antimicrobial properties of ethanol extracts may be caused by action of both of extract constituents and ethanol itself.

Table 4

Antimicrobial properties of diluted colloids, extracts, and ethanol solutions.

Sample	*Raw material used for extract / colloid preparation*	*Dilution, times*	*Percentages of ethanol in solution/ extract/ colloid*	*Percentages* of cells inhibited by solution/ extract/ colloid*
70 % ethanol	—	10	7	0
70 % ethanol	—	5	14	20±4
70 % ethanol	—	2	35	63±5
Extract 1	Leaves of plant grown *ex situ*	2	35	60±8
Extract 2	Leaves of plant grown *in vitro*	2	35	65±7
Extract 3	Callus	2	35	58±5
Extract 1	Leaves of plant grown *ex situ*	5	14	30±5
Extract 2	Leaves of plant grown *in vitro*	5	14	35±6
Extract 3	Callus	5	14	23±5
Extract 1	Leaves of plant grown *ex situ*	10	7	0
Extract 2	Leaves of plant grown *in vitro*	10	7	0
Extract 3	Callus	10	7	0
Extract 1/AgNPs colloid	Leaves of plant grown *ex situ*	2	3.5	70±3
Extract 2/AgNPs colloid	Leaves of plant grown *in vitro*	2	3.5	65±7
Extract 3/AgNPs colloid	Callus	2	3.5	60±7
Extract 1/AgNPs colloid	Leaves of plant grown *ex situ*	5	1.4	55±3
Extract 2/AgNPs colloid	Leaves of plant grown *in vitro*	5	1.4	55±3
Extract 3/AgNPs colloid	Callus	5	1.4	50±7

**Indicated scattering of the data corresponds to 90% confidence interval*

The data of Table 4 show that the twice-diluted extracts suppress 58-65% of the *Bacillus cereus* cells, while ethanol in the appropriate concentration inhibits the same percentages of the cells. Five-fold diluted extracts suppressed cells growth to a higher extent than five-fold diluted 70% ethanol (23-35% cells suppressed instead of 20%). Thus, the difference of 3-15% may be attributed to antimicrobial effect of the extracts constituents. The stronger inhibition of *Bacillus cereus* cells by diluted Extract 1 and Extract 2 (Table 4) appears to occur due to the higher content of constituents, such as: steviol, glycosides and flavonoids, which are known to possess high antimicrobial activity [17-19]. Since original extracts in Extract/AgNPs colloids are diluted by ten times and ten-fold diluted extracts practically did not suppress the growth of cells (Table 4), antimicrobial properties of the colloids are caused by inhibiting effect of silver ions/NPs. All colloids exhibited similar antimicrobial activity with the distinctions being about the accuracy of measurements.

Conclusions

Leaves of *Stevia* plants grown *ex situ* and *in vitro* as well as callus culture formed on damaged leaves were found to be valuable raw material for extraction of bioactive compounds with antioxidant and/or antimicrobial properties. Steviol glycosides, hydroxycinnamic acids and flavonoids were the main groups of bioactive compounds revealed in the extracts, with the content of compounds and properties of the extracts being dependent on the type of raw material.

All extracts have demonstrated high redox properties and significant activity in the synthesis of AgNPs. The activity of the extracts in the reactions with both DPPH radicals and Ag^+ ions correlated with their total phenol content and changed in the series: Extract from the leaves of plants grown *ex situ* ≈ Extract from callus culture >> Extract from the leaves of plants grown *in vitro*.

All extracts suppressed the growth of *Bacillus cereus* cells, the effect being more significant for the extracts from the leaves of plants grown *ex situ* and *in vitro* with the higher content of steviol glycosides and flavonoids. All colloids were very effective antimicrobial agents, seemingly due to the action of AgNPs and still possessed high antioxidant properties.

Thus, *Stevia rebaudiana* extracts and Extract/AgNPs colloids showed both antioxidant and antimicrobial activity, the properties of extracts and colloids being dependent on the type of raw material used for extracts/colloids preparation. The high redox properties of the extract from callus culture tissue indicate a great potential of biotechnological methods for production of pure bioactive compounds and extracts for biological and medical applications.

References

1. Brewer, M.S. Natural antioxidants: Sources, compounds, mechanisms of action, and potential applications. Comprehensive Reviews in Food Science and Food Safety, 2011, 10, pp. 221–247.
2. Gurib-Fakim, A. Medicinal plants: Traditions of yesterday and drugs of tomorrow. Molecular Aspects of Medicine, 2006, 27, pp. 1–93.
3. Shahid-ul-Islam; Shahid, M.; Mohammad, F. Perspectives for natural product based agents derived from industrial plants in textile applications - a review. Journal of Cleaner Production, 2013, 57, pp. 2–18.
4. Lupascu, L.; Rudic, V.; Cotos, V.; Lupascu, T. Antimicrobial activity of the autochthonous compound Enoxil. Journal of Biomedical Science and Engineering, 2010, 3, pp. 758-762.
5. Cowan, M.M. Plant products as antimicrobial agents. Clinical Microbiology Reviews, 1999, 12(4), pp. 564–582.
6. Malhotra, B.; Keshwani, A.; Kharkwal, H. Antimicrobial food packaging: potential and pitfalls. Frontiers in Microbiology, 2015, 6, pp. 611-620.
7. Herman, A.; Herman, A.P.; Domagalska, B.W.; Młynarczyk, A. Essential oils and herbal extracts as antimicrobial agents in cosmetic emulsion. Indian Journal of Microbiology, 2013, 53(2), pp. 232–237.
8. Iravani, S. Green synthesis of metal nanoparticles using plants. Green Chemistry, 2011, 13, pp. 2638-2650.
9. Goyal, S.; Samsher, S.; Goyal, R. *Stevia (Stevia rebaudiana*) a bio-sweetener: a review. International Journal of Food Sciences and Nutrition, 2010, 61, pp. 1–10.
10. Gupta, E.; Purwar, S.; Sandaram, S.; Gai, G.K. Nutritional and therapeutic values of *Stevia rebaudiana:* A review. Journal of Medicinal Plants Research, 2013, 7, pp. 3343–3353.
11. Komarova, M.N.; Nikolaeva, L.A.; Regir, V.G. Phytochemical analysis of medicinal plants: guidelines for laboratory studies, St. Petersburg: State Chemical-Pharmaceutical Academy, 1998, 60 p. (in Russian).
12. Alonso, A.M.; Domianguez, C.; Guillean, D.; Barroso, C.G. Determination of antioxidant power of red and white wines by a new electrochemical method and its correlation with polyphenolic content. Journal of Agricultural and Food Chemistry, 2002, 50, pp. 3112–3115.
13. Stavinskaya, O.M.; Kuzema, P.O.; Laguta, I.V.; Pakhlov, E.M.; Kazakova, O.O.; Chernyavskaya, T.V. Interaction of ascorbic acid with hydrophilic-hydrophobic silicas. Annales Universitatis Mariae Curie-Sklodowska, 2007, 62, pp. 124-135.

14. Andreeva, V.Yu.; Kalinkina, G.I. Development of method of quantitative determination of flavonoids in *Alchemilla vulgaris*. Khimiva rastitel'nogo syr'ya, 2000, 1, pp. 85–88 (in Russian).
15. Brand-Williams, W.; Cuvelier, M.E.; Berset, C. Use of a free radical method to evaluate antioxidant activity. LWT - Food Science and Technology, 1995, 28(1), pp. 25–30.
16. Rice-Evans, C.A.; Miller, N.J.; Paganga, G. Structure-antioxidant activity relationships of flavonoids and phenolic acids. Free Radical Biology and Medicine, 1996, 20, pp. 7933–7956.
17. Puri, M.; Sharma, D. Antibacterial activity of stevioside towards food-borne pathogenic bacteria. Engineering in Life Sciences, 2011, 11, pp. 326–329.
18. Cushnie, T.P.T.; Lamb, A.J. Antimicrobial activity of flavonoids. International Journal of Antimicrobial Agents, 2005, 26, pp. 343–56.
19. Desbois, A.P.; Smith, V.J. Antibacterial free fatty acids: activities, mechanisms of action and biotechnological potential. Applied Microbiology and Biotechnology, 2010, 85, pp. 1629–1642.

CHEMISTRY JOURNAL OF MOLDOVA. General, Industrial and Ecological Chemistry. 2016, 11(2), 52-57
http://cjm.asm.md
http://dx.doi.org/10.19261/cjm.2016.11(2).11

SYNTHESIS AND STRUCTURAL CHARACTERISTICS OF BIS(CITRATE)GERMANATES(IV) $(Hbipy)_2[Ge(HCit)_2]\cdot 2H_2O$ AND $[CuCl(bipy)_2]_2[Ge(HCit)_2]\cdot 8H_2O$

Inna Seifullina[a], Elena Martsinko[a*], Elena Chebanenko[a], Olha Pirozhok[a], Viktoriya Dyakonenko[b], Svitlana Shishkina[b,c]

[a]*I.I. Mechnikov Odessa National University, Odessa 65082, Ukraine*
[b]*SSI "Institute for Single Crystals", National Academy of Sciences of Ukraine, 60, Nauki Ave., Kharkiv 61001, Ukraine*
[c]*V.N. Karazin Kharkiv National University, 4 Svobody sq., Kharkiv 61077, Ukraine*
**e-mail: lborn@ukr.net*

Abstract. The crystalline compounds $(Hbipy)_2[Ge(HCit)_2]\cdot 2H_2O$ (**1**) and $[CuCl(bipy)_2]_2[Ge(HCit)_2]\cdot 8H_2O$ (**2**) (where H_4Cit is citric acid, bipy is 2,2′-bipyridine) were obtained for the first time and their structures were determined by the single-crystal X-ray diffraction method. Compounds were characterized by IR spectroscopy, thermogravimetric (TGA) and elemental analyses. Both compounds are formed with complex bis(citrate)germanate anion and protonated 2,2'-bipyridine or $[Cu(bipy)_2Cl]^+$ as cations in compounds **1** and **2**, respectively.

Keywords: germanium(IV) compound, citric acid, 2,2'-bipyridine, copper(II) complex, structure.

Received: November 2016/ Revised final: December 2016/ Accepted: December 2016

Introduction

Citric acid is the most interesting vital biological ligand for a range of metal ions in coordination chemistry. It is the direct participant of the Krebs cycle and is present in blood plasma [1]. This acid has many useful properties and applications in medicine, pharmaceutical and food industries.

In the past time, we have synthesized and studied a number of mixed-ligand and mixed-metal coordination compounds of germanium(IV) with citric acid [2–7]. The pharmacological activity of some of these compounds has been approved [8]. The complexes of germanium(IV) are interesting materials for modern technics [9,10]. We have obtained the Eu^{2+}-doped Li_2CaGeO_4 material with luminescent properties by thermolysis of the complex precursor $[Ca(H_2O)_6][Ge(HCit)_2]$ [10].

Addition of nitrogen-containing heterocyclic organic molecules such as 2,2′-bipyridine into composition of coordination compounds of germanium(IV) with citric acid can modify its properties. Similar compound with tris(oxalato-O,O')germanate anion $(Hbipy)_2[Ge(C_2O_4)_3]$ has been isolated after a mild hydrothermal synthesis and its structure has been elucidated [11]. The chelate $[GeCl(bipy)(HCit)]\cdot 2.5CH_3CN$ has also been synthesized by the reaction between the adduct $[GeCl_4(bipy)]$ and citric acid in acetonitrile solution [12].

The objectives of the present work was to synthesize homo- and heterometallic complexes on the basis of bis(citrate)germanate and 2,2′-bipyridine, to determine their composition, thermal stability and structure.

Experimental

General

Chemicals were readily available from commercial sources and used as received without further purification: germanium(IV) oxide (GeO_2, 99.99%, Aldrich), citric acid monohydrate ($H_4Cit\cdot H_2O$, ≥99%, Aldrich), 2,2'-bipyridine (bipy, ≥98%, Fluka), copper(II) chloride dihydrate ($CuCl_2\cdot 2H_2O$, ≥99%, Aldrich).

Instrumentation

Elemental analyses for germanium and copper were performed using inductively coupled plasma atomic emission spectroscopy with an Optima 2000 DV instrument (Perkin Elmer); chlorine was quantified by mercurometry, analyses for C, H, and N were performed in Elemental Analyzer CE-440. Thermogravimetric analyses (TGA) were carried out using a Q-1500D with a heating rate of 10°C/min in air in the temperature range of 20-1000°C. The IR absorption spectra of the ligand and the complexes were collected from KBr pellets on a Frontier spectrophotometer (Perkin Elmer) in the 400–4000 cm^{-1} range. The most important absorption bands in the IR spectra of complexes and **2** were attributed in compliance with the literature data [13-16], including data for the germanium(IV) coordination compounds with citric acid [2-7] (*s*. - strong, *m*. – middle, *w*. – weak).

Crystal data for structures **1** and **2** were measured on an Xcalibur-3 diffractometer (graphite monochromated Mo-K_α radiation, CCD detector, φ and ω-scanning). The structures were solved by the direct method using SHELXTL package [17]. Full-matrix least-squares refinement against F^2 in anisotropic approximation was used for non-hydrogen atoms. Positions of hydrogen atoms were located from the electron density difference maps and refined by ''riding" model with $U_{iso} = nU_{eq}$ of the carrier atom (n = 1.5 for hydroxyl groups and n = 1.2 for other hydrogen atoms). CCDC 1513407-1513408 contain the supplementary crystallographic data for **1** and **2**. These data can be obtained free of charge

via http://www.ccdc.cam.ac.uk/conts/retrieving.html, or from the Cambridge Crystallographic Data Centre, 12 Union Road, Cambridge CB2 1EZ, UK; fax: (+44) 1223-336-033; or e-mail: deposit@ccdc.cam.ac.uk [18]. Full use of the CCDC package was also employed for searching in the CSD Database.

Synthesis

$(Hbipy)_2[Ge(HCit)_2]\cdot 2H_2O$ (1). A mixture of 0.084 g GeO_2 (0.8 mmol), 0.336 g $H_4Cit\cdot H_2O$ (1.6 mmol) and 0.256 g bipy (1.6 mmol) was added to 100 mL of hot water. The resulting mixture was heated at stirring to completely dissolve the reagents and evaporated (80-90°C) in a water bath to a volume of 10 mL (~2 h). A white residue of complex **1** was precipitated in one day. The yield constituted 65% (with respect to Ge). Single crystals of **1** suitable for X-ray analysis were withdrawn from the reaction medium.

Calculated elemental composition (based on single-crystal data for $C_{32}GeH_{32}N_4O_{16}$, M=801.20; in %): C 47.93, Ge 9.06, N 6.99, H 3.99. Found for the as-synthesized bulk material (in %): C 47.89, Ge 9.00, N 6.54, H 3.65.

TGA data (weight losses inside parentheses): 150-220°C, endothermic peak 170°C (-5.0%); 220-260°C, endothermic peak 240°C (-20.0%); 260-320°C, endothermic peak 280°C (-45.0%); 480-620°C, exothermic peak 500°C (-17.0%).

Selected IR data for **1** (in cm^{-1}): ν(O-H) = 3471m; ν(C-H, bipy ring) = 3100w, 2930w; ν(C=O, uncoordinated carbonyl groups) = 1697s; $\nu_{as}(COO^-)$ = 1643s; ν(C-C, skeletal vibration bipy ring) = 1582s, 1518m, 1478w; $\nu_s(COO^-)$ = 1377s; ν(C-N, bipy) = 1340m; ν(C-O) = 1198s, 1079w; ν(C-H) = 1087w, 1036w, 995w, 949w, 900w; ν(Ge-O) = 698m, 668m.

Crystal data for **$(Hbipy)_2[Ge(HCit)_2]\cdot 2H_2O$ (1).** (M=801.20 g/mol): monoclinic, space group $P2_1/c$, a = 11.121(1) Å, b= 21.365(3)Å, c = 7.346(1)Å, β = 108.27(1), V = 1657.4(4)Å^3, Z= 2, T = 294K, μ(MoKα) = 1.010mm^{-1}, $Dcalc$= 1.605g/cm^3, 10794 reflections measured (6.144° ≤ 2Θ ≤ 50°), 2918 unique (R_{int} = 0.084, R_{sigma} = 0.079) which were used in all calculations. The final R_1 was 0.070 (I > 2σ(I)) and wR_2 was 0.178 (all data).

$[CuCl(bipy)_2]_2[Ge(HCit)_2]\cdot 8H_2O$ (2). In the first step, 0.0523 g GeO_2 (0.5 mmol) and 0.21 g $H_4Cit\cdot H_2O$ (1 mmol) were added to the 50 mL of water. The mixture was heated up to 80°C and stirred until the reagents were completely dissolved, then concentrated on a water bath to 10 mL (~1 h) and cooled. In the second step, a mixture of 0.171 g $CuCl_2\cdot 2H_2O$ (1 mmol) and 0.312 g bipy (2 mmol) in 10 mL of ethanol, previously heated for 10 min and cooled, was added to the obtained solution. The resulting solution was stirred for 5.0 min without heating and then filtered. A blue precipitate of complex **2**, which contained crystals suitable for X-ray crystallography, was formed in 2 days. The yield of the product was 75%.

Calculated elemental composition (based on single-crystal data for $C_{52}Cl_2Cu_2GeH_{58}N_8O_{22}$, M=1417.63; in %): C 44.02, Cl 5.01, Cu 9.03, Ge 5.12, N 7.90, H 4.09. Found for the as-synthesized bulk material (in %): C 43.22, Cl 4.49, Cu 9.00, Ge 5.02, N 7.85, H 4.00.

TGA data (weight losses inside parentheses): 80-180°C, endothermic peak 100°C (-10.0%); 270-330°C, endothermic peak 280°C (-44.0%); 330-370°C, exothermic peak 350°C (-6.0%); 530-670°C, exothermic peak 570°C (-14.0%); 670-820°C, exothermic peak 770°C (-7.7%).

Selected IR data for **2** (in cm^{-1}): ν(O-H) = 3442s; ν(C-H, aromatic) = 3118w, 2930w; ν(C=O, uncoordinated carbonyl groups) = 1680m; $\nu_{as}(COO^-)$ = 1640s; ν(C-C, skeletal vibration bipy ring) = 1602s, 1500w, 1478w; $\nu_s(COO^-)$ = 1393m; ν(C-N, bipy) = 1317m; ν(C-O) = 1176m, 1063w; ν(C-H) = 1085w, 1033w, 995w, 955w, 908w; ν(Ge-O) = 672m, 644m.

Crystal data for **$[CuCl(bipy)_2]_2[Ge(HCit)_2]\cdot 8H_2O$ (2)** (M = 1417.63 g/mol): triclinic, space group $P^{\bar{1}}$, a = 8.7182(4)Å, b = 12.5675(5)Å, c = 13.9109(5)Å, α = 75.413(3), β = 81.155(3), γ = 88.650(3), V = 1457.3(1)Å^3, Z = 1, T = 293K, μ(MoKα) = 1.414 mm^{-1}, $Dcalc$ = 1.615g/cm^3, 10339 reflections measured (5.84° ≤ 2Θ ≤ 49.992°), 5101 unique (R_{int} = 0.056, R_{sigma} = 0.090) which were used in all calculations. The final R_1 was 0.055 (I > 2σ(I)) and wR_2 was 0.130 (all data).

Results and discussion

The newly-synthesized complexes represent stable in air crystalline compounds with the molar ratio Ge : citrate : bipy = 1:2:2 (**1**) and Ge : citrate : Cu: bipy = 1:2:2:4 (**2**).

During the study of thermal stability of the synthesized complexes, we have established that their thermolysis could be divided into distinct stages. At the first stage, the endotherm peak is observed within the range of 150-220°C (for **1**) and 80–180°C (for **2**). The wide temperature range and corresponding weight loss, which has been recorded in TGA, allow us to conclude that the complexes include molecules of crystallization water (2 and 8 H_2O molecules in **1** and **2**, respectively).

The presence of water of crystallization in their structures was confirmed by IR spectroscopy. Their IR spectra contain absorption bands due to the ν(O-H) stretching vibrations at 3471 (**1**) and 3442 cm^{-1} (**2**).

The weight loss values derived from thermogravimetric curves of **1** show that at the second stage in the 220–260°C temperature range the endothermic peak occurs, which corresponds to the removal of one bipy molecule. In the temperature range of 260–320°C one more 2,2'-bipyridine molecule is removed simultaneously with the decarboxylation of the coordinated citrate ion in complex **1**. The main difference in the thermolysis of **2** is the contemporaneous release from 270 to 330°C of four molecules of 2,2'-bipyridine. Then, a number of exothermic effects is observed, that is connected to the oxidative thermal destruction of compounds **1** and **2**.

According to the weight loss calculations and to the data from the previous researches [2,3,5,6], the final thermo-destruction products of complexes at 1000°C are GeO_2 (for **1**) and Cu_2GeO_4 (for **2**).

IR spectra of **1** and **2** contain the absorption bands ν(C=O), ν_{as}(COO$^-$) and ν_s(COO$^-$), that indicate the presence of nonequivalent coordinated and free carboxyl groups in complexes. Due to the absorption bands of ν(C–O) at 1079 (for **1**) and 1063 cm^{-1} (for **2**), it is suggested that alcoholic OH groups of the citrate ligands were deprotonated and coordinated to germanium atom. The stretching vibrations Ge-O are located at 698 and 668 cm^{-1} (for **1**) and at 672 and 644 cm^{-1} (for **2**).

X-ray diffraction study has shown that compounds **1** and **2** are of onium-type, where $[Ge(HCit)_2]^{2-}$ is the complex anion. This anion is located in the particular position, where the Ge atom coordinates coincide with the symmetry center of coordinates. The cation is 2,2'-bipyridine molecule with one protonated nitrogen atom in compound **1** and $[Cu(bipy)_2Cl]^+$ complex in compound **2**. Complexes **1** and **2** are hydrates with two (compound **1**) and eight (compound **2**) water molecules.

In the centrosymmetric anion of complexes **1** and **2** the coordination polyhedron of Ge atom is a distorted octahedron, which is formed from three pairs of three different types of O atoms in two tridentate bis(chelating) $HCit^{3-}$ ligands: hydroxyl (atom O(3)), α-carboxylate (atom O(1)), β-carboxylate (atom O(4)) (Figure 1). Bond length Ge-O changes within a range 1.803(3) – 1.947(3) Å in **1** and 1.812(3) – 1.944(3) Å in **2**, bond angles O-Ge-O 87.51(15) – 92.15(15)° in **1** and 88.26(14) – 91.74(14)° in **2**. This differences are discussed in the previous works dedicated to bis(citrate)germanate complexes [2-7].

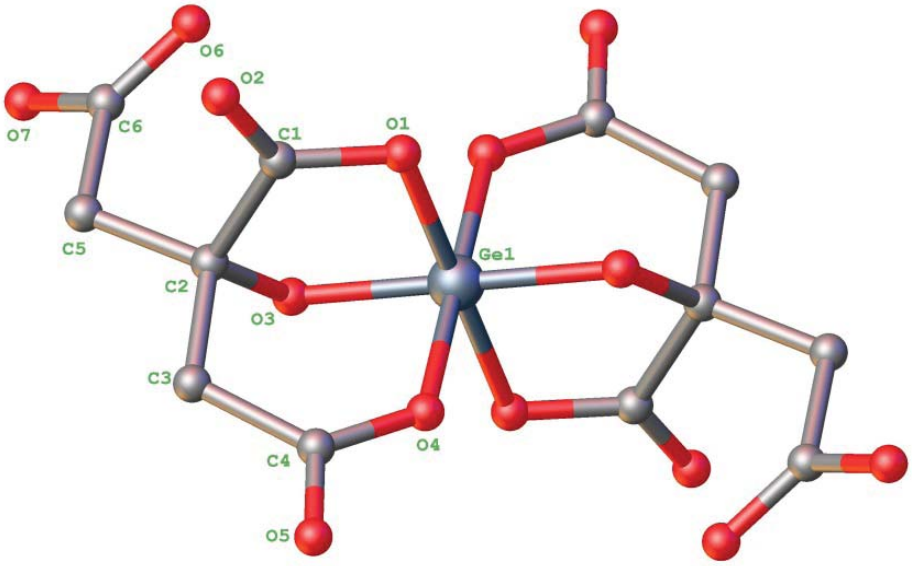

Figure 1. Molecular structure of $[Ge(HCit)_2]^{2-}$ anion in 1 and 2 (the H atoms are omitted for clarity).

Owing to the developing of bis(citrato)germanate anion, five- and six-membered metallocycles are formed. The Ge-O(3)-C(2)-C(3)-C(4)-O(4) six-membered cycle adopts a sofa conformation in both compounds (the atom O (3) deviates from the mean plane of the remaining atoms of the cycle by -0.8 Å in **1** and **2**; the puckering parameters are listed in Table 1). The five-membered ring has an envelope conformation. The O(3) atom deviates from the mean squared plane of the remaining atoms by -0.5 Å in both compounds.

Table 1

Puckering parameters in the structures of 1 and 2.

Compound	*S*	*Θ, (°)*	*Ψ, (°)*
1	0.98	44.3	22.30
2	0.58	59.2	21.03

The localization of the positive charge on the 2,2'-bipyridine molecule (Figure 2) has been confirmed by the detection of the hydrogen atom at N(2) from the electron density difference maps and the N(2)-C(12) bond elongation up to 1.344(7) Å in comparison with its mean value of 1.339 Å [19].

The Cu atom coordination polyhedron in complex cation $[CuCl(bipy)_2]^+$ of structure **2** is a distorted trigonal bipyramid (Figure 3). The N(1), N(3), Cl(1) atoms are located in the equatorial positions and in the N(2) and N(4) atoms coordinate the copper atom in axial positions. The Cu(1)-N bond lengths vary within 1.986(4) Å ÷ 2.096(3) Å, the Cu(1)-Cl bond length is 2.354(2) Å (Table 2). The valence angles have values within 111.5(2)° ÷ 127.7(2)° in the equatorial direction (ideal value is 120°) and within 79.7(2)° ÷ 98.4(3)° in the axial direction (ideal value is 90°).

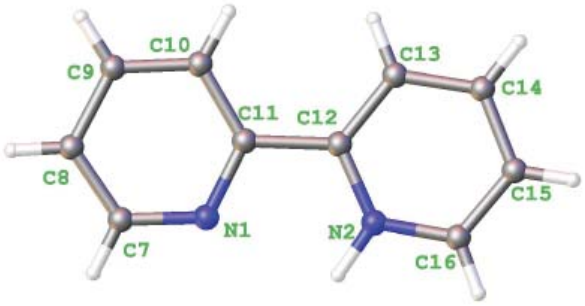

Figure 2. Molecular structure of protonated 2,2'-bipyridine fragment.

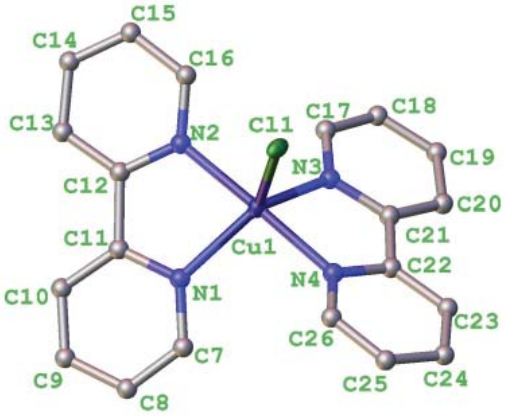

Figure 3. Molecular structure of $[CuCl(bipy)_2]^+$ cation.

Table 2

Bond lengths (Å) and bond angles (°) in structures of 1 and 2 (^{1}-x, 1-y, -z).

Bond lengths (Å)/ bond angles (°)	***1***	***2***
Ge(1)-O(4)	1.947(3)	1.944(3)
Ge(1)-O(1)	1.897(3)	1.891(3)
Ge(1)-O(3)	1.803(3)	1.812(3)
Cu(1)-N(1)		2.087(4)
Cu(1)-N(2)		1.989(4)
Cu(1)-N(3)		2.096(4)
Cu(1)-N(4)		1.986(4)
Cu(1)-Cl(1)		2.354(3)
O(1)-Ge(1)-O(4)^1	89.6(2)	89.9(1)
O(1)-Ge(1)-O(4)	90.4(2)	90.2(1)
O(3)^1-Ge(1)-O(1)^1	87.9(1)	88.3(1)
O(3)-Ge(1)-O(1)^1	92.2(1)	91.7(1)
O(3)-Ge(1)-O(1)	87.9(1)	88.3(1)
O(3)^1-Ge(1)-O(4)	89.7(2)	90.0(1)
O(3)-Ge(1)-O(4)	90.3(2)	90.1(1)
N(1)-Cu(1)-Cl(1)		127.7(1)
N(1)-Cu(1)-N(2)		79.9(2)
N(1)-Cu(1)-N(3)		120.8(2)
N(2)-Cu(1)-Cl(1)		91.5(1)
N(2)-Cu(1)-N(3)		99.8(2)
N(3)-Cu(1)-Cl(1)		111.5(1)
N(4)-Cu(1)-Cl(1)		90.8(1)
N(4)-Cu(1)-N(2)		177.7(2)
N(4)-Cu(1)-N(3)		79.7(2)

The cation, anion and water molecules in the crystal compound **1** are connected with the intermolecular hydrogen bonds (Table 3) and form a three-dimensional net (Figure 4). In the case of compound **2** the cations and anions are bonded by intermolecular hydrogen bonds through the bridging water molecules and form layers along the *ac* crystallographic plane (Figure 5).

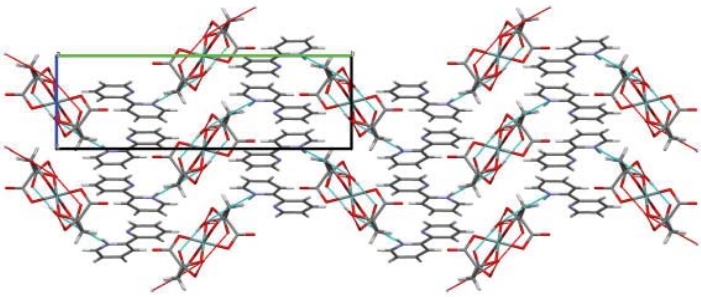

Figure 4. Crystallografic structure of 1 (projection along the crystallographic axis *a*).

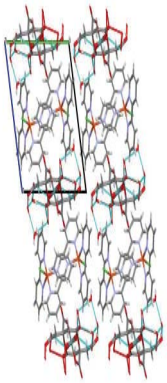

Figure 5. Crystallographic structure of 2 (projection along the crystallographic axis *a*).

Table 3

Geometric parameters of the hydrogen bonds in the structures 1 and 2.

D-H…A	*d(H…A), Å*	*d(D…A), Å*	*D-H…A(°)*
	*Complex **1***		
N(2)-H(2)…O(5)	1.86	2.724(6)	144.0
C(15)-H(15)…O(1)[1]	2.37	3.250(7)	158.2
O(7)-H(7A)…O(8)[2]	1.80	2.605(6)	168.2
O(8)-H(8A)…O(6)[3]	2.07	2.915(6)	172.9
O(8)-H(8B)…O(5)	2.06	2.825(6)	149.6
	*Complex **2***		
O(7)-H(7A)…O(9)	1.77	2.563(6)	163.1
O(10)-H(10B)…O(5)	1.92	2.756(5)	168.4
O(8)-H(8A)…O(6)	1.98	2.822(6)	171.2
O(8)-H(8B)…O(5)[4]	2.09	2.913(6)	163.8
O(11)-H(11A)…O(10)	2.08	2.924(7)	167.2
O(11)-H(11B)…Cl(1)	2.66	3.308(5)	132.7

[1]-1+x,+y,-1+z; [2]1+x,+y,+z; [3]1-x,1-y,2-z; [4]-x,1-y,-z

Conclusions

It is necessary to point out, that when organic cation $(Hbipy)^+$ is displaced with the $[CuCl(bipy)_2]^+$, the structure of complex anion almost remains, but in the case of **2** the distortion becomes a little higher. At the same time the crystal structure of complexes changes completely: three-dimensional net, in which cations, anions and water molecules are connected by the intermolecular hydrogen bonds is characteristic for **1** and alternating layer of anions and cations, connected with the bridging water molecules identifies complex **2**.

References

1. Koenigsberger, L.; Koenigsberger, E.; May, P.M.; Hefter, G.T. Complexation of iron(III) and iron(II) by citrate. Implications for iron speciation in blood plasma. Journal of Inorganic Biochemistry, 2000, 78, pp. 175–184.
2. Seifullina, I.I.; Pesaroglo, A.G.; Minacheva, L.Kh.; Martsinko, E.E.; Sergienko, V.S. Bis(citrato)germanate complexes with organic cations: crystal structure of $(HNic)_2[Ge(HCit)_2]\cdot 3H_2O$. Russian Journal of Inorganic Chemistry, 2006, 51, pp. 1892–1899.
3. Seifullina, I.I.; Ilyukhin, A.B.; Martsinko, E.E.; Sergienko, V.S.; Chebanenko, E.A. Products of reaction between bis(citrate)hydroxogermanic acid and organic molecules. Molecular and crystal structure of $(HNad)_2[Ge(HCit)_2]\cdot 4H_2O$. Russian Journal of Inorganic Chemistry, 2015, 60, pp. 33–37.
4. Pesaroglo, A.G.; Martsinko, E.E.; Minacheva, L.Kh.; Seifullina, I.I.; Sergienko**,** V.S. The coordination polymer triaquabarium-μ-bis(citrato)germanate trihydrate: synthesis, properties, molecular and crystal structure of $\{[Ge(\mu\text{-}HCit)_2Ba(H_2O)_3]\cdot 3H_2O\}_n$. Russian Journal of Inorganic Chemistry, 2010, pp. 1366–1372.
5. Martsinko, E.E.; Minacheva, L.Kh.; Pesaroglo, A.G.; Seifullina, I.I.; Churakov, A.V.; Sergienko, V.S. Bis(citrato)germanates of bivalent 3d metals (Fe, Co, Ni, Cu, Zn): crystal and molecular structure of $[Fe(H_2O)_6][Ge(HCit)_2]\cdot 4H_2O$. Russian Journal of Inorganic Chemistry, 2011, 56, pp. 1243–1249.
6. Martsinko, E.E.; Minacheva, L.Kh.; Chebanenko, E.A.; Seifullina, I.I.; Sergienko, V.S.; Churakov, A.V. The conditions of formation of heterometallic complexes in the $GeCl_4$ ($SnCl_4$)–citric acid–$M(CH_3COO)_2$–H_2O systems. The crystal and molecular structures of $[M(H_2O)_6][Ge(HCit)_2]\cdot 4H_2O$ (M = Mg, Mn, Co, Cu, Zn) and $[M(H_2O)_6][Sn(HCit)_2]\cdot 4H_2O$ (M = Mg, Co, Ni). Russian Journal of Inorganic Chemistry, 2013, 58, pp. 515–522.
7. Martsinko, E.E.; Minacheva, L.Kh.; Chebanenko, E.A.; Ilyukhin, A.B.; Seifullina, I.I.; Sergienko, V.S. Ammonium and potassium citratogermanates(iv): synthesis, chemical compositions, and structures. The crystal structures of $(NH_4)[Ge(OH)(H_2Cit)_2]\cdot H_2O$ and $K_4[Ge(HCit)_2(H_2Cit)]\cdot 3H_2O$. Russian Journal of Coordination Chemistry, 2013, 39, pp. 629–635.
8. Seifullina, I.I.; Martsinko, E.E.; Afanasenko, E.V. Design and synthesis of new homo- and heterometal coordination compounds of germanium(IV) for preparation of low toxic drugs with a wide therapeutic action. Odessa National University Herald. Chemistry, 2015, 4, pp. 6-17.
9. Smola, S.; Rusakova, N.; Martsinko, E.; Seifullina, I.; Korovin, Yu. Spectroscopic Properties of the Ln-Ge complexes with diethylentriaminepentaacetic acid. Chemistry Journal of Moldova. General, Industrial and Ecological Chemistry, 2007, 2, pp. 83–87.
10. Berezovskaya, I.V.; Efryushina, N.P.; Seifullina, I.I.; Martsinko, E.E.; Zadneprovski, B.I.; Stryganyuk, G.B.; Voloshinovskii, A.S.; Levshov, S.M.; Dotsenko, V.P. Luminescence properties of Eu^{2+} and Ce^{3+} ions in calcium lithio-germanate Li_2CaGeO_4. Ceramics International, 2013, 39, pp. 6835–6840.
11. Zheng, S.T.; Zhang, J.; Yang, G.Yu. Hydrothermal synthesis and structure of a novel hybrid germanium vanadate: $(2,2'\text{-bpy})_2(V^VO_2)_2(H_2GeO_4)\ 6H_2O$. Inorganic Chemistry Communications, 2004, 7, pp. 861–863.
12. Willey, G.R.; Somasunderam, U.; Aris, D.R.; Errington, W. Ge(IV)–citrate complex formation: synthesis and structural characterization of $GeCl_4$(bipy) and GeCl(bipy)(HCit) (bipy = 2,2′-bipyridine, H_4Cit = citric acid). Inorganica Chimica Acta, 2001, 315, pp. 191–195.
13. Nakamoto, K. IR spectra and Raman spectra of inorganic and organic coordinative compounds. Mir: Moscow, 1991, 536 p. (in Russian).
14. Nakanisi, K. Infrared spectra and structure of organic compounds. Mir: Moscow, 1965, 216 p. (in Russian).
15. Bellami, L. Infrared spectra of complex molecules. IL: Moscow, 1963, 590 p. (in Russian).
16. Tarasevich, B.N. Infrared spectra of basic class of organic compounds. Reference materials: Moscow, 2012, 54 p. (in Russian).
17. Sheldrick, G.M. A short history of SHELX. Acta Crystallographica Section A, 2008, A64, pp. 112-122.
18. CCDC, The Cambridge Crystallographic Data Centre, 12 Union Road, Cambridge, CB2 1EZ, UK, 44 1223 336408. E-mail: deposit@ccdc.cam.ac.uk.
19. Burgi, H.-B.; Dunitz, J.D. Structure correlation. VCH: Weinheim, 1994, vol. 2, pp. 741-784.

CHEMISTRY JOURNAL OF MOLDOVA. General, Industrial and Ecological Chemistry. 2016, 11(2), 58-67
http://cjm.asm.md
http://dx.doi.org/10.19261/cjm.2016.11(2).07

SYNTHESIS, SPECTRAL AND THEORETICAL CHARACTERIZATION OF 5,6-DICHLORO/DIMETHYL-2-(2′,3′/2′,4′/2′,5′/3′,4′/3′,5′-DIMETHOXYPHENYL)-1*H*-BENZIMIDAZOLES

Demet Gürbüz[a], Aydin Tavman[a*], Adem Cinarli[a], Ismail Boz[b]

[a]*Istanbul University, Faculty of Engineering, Department of Chemistry, 34320, Avcilar, Istanbul, Turkey*
[b]*Istanbul University, Faculty of Engineering, Department of Chemical Engineering, 34320, Avcilar, Istanbul, Turkey*
[*]*e-mail: atavman@istanbul.edu.tr; phone: (+90) 21 247 370 70; fax: (+90) 21 247 371 80*

Abstract. 5,6-Dichloro/dimethyl-2-(2′,3′/2′,4′/2′,5′/3′,4′/3′,5′-dimethoxyphenyl)-1*H*-benzimidazoles were synthesized and characterized by using analytical data, FT-IR, FT-Raman, NMR, ESI-MS and fluorescence spectroscopy. The optimized molecular geometry, zero point energy, dipole moment, ESE, band gap and charge distributions were calculated by Gaussian 09 using Density Functional Theory (DFT, RB3LYP) with 6-31++G(d,p) basis set. According to the calculations, the molecules have structures with various torsion angles between the benzimidazole and benzene rings from 9.7º to 47.8º. The calculated energy values with ZPE correction and DFT show that the methyl derivatives are more stable than the chloro forms. 3′,4′-Dimethoxy derivatives have higher decomposition points in comparison with the other compounds in series. The chlorine atoms of 5,6-dichloro-2-(2′,3′/2′,4′/2′,5′/3′,4′/3′,5′-dimethoxyphenyl)-1*H*-benzimidazoles are positively charged whereas the C5 and C6 carbon atoms are negatively charged due to the attached chlorine atoms, in virtue of the electron withdrawing characteristic of the imidazole part of the benzimidazole ring. Also, some calculated prominent bond lengths and bond angles were discussed.

Keywords: dimethoxyphenylbenzimidazoles, spectral characterization, density functional theory, charge distribution, geometry optimization.

Received: June 2016/ Revised final: November 2016/ Accepted: November 2016

Introduction

Various benzimidazole derivatives display a wide range of biological activity. For instance, vitamin B12 has 5,6-dimethylbenzimidazole moiety as coordinated to the Co(II) ion [1,2]. On the other hand, various drugs and pharmaceutical compositions contain benzimidazole derivatives. Perhaps the most important one is an antisecretory agent, omeprazole [5-methoxy-2-(4-methoxy-3,5-dimethylpyridin-2-yl-methylsulphinyl)-1*H*-benzimidazole] [3]. The other important benzimidazol derivatives that are used as drugs are: thiabendazole [4,5], albendazole, mebendazole, flubendazole [6,7] astemizole [8] and fenbendazole [9]. The high therapeutic properties of the related drugs have encouraged the medicinal chemists to synthesize a large number of novel chemotherapeutic agents [10–12]. They displayed many biological activities, such as: antiviral [13] and antitumoral [14]; antifungal and antimycotic [15]; antihistaminic and antiallergic [16]; antimicrobial [17–20] and antihelminthic activity [21]; all are unique characteristics known for benzimidazole derivatives [10]. These compounds are also extensively used in industrial processes as corrosion inhibitors for metal and alloy surfaces [22,23]. These different applications have attracted many experimentalists and theorists to investigate the spectroscopic and structural properties of benzimidazole [24–26] and some its derivatives [27].

In this study, 5,6-dichloro/dimethyl-2-(2′,3′/2′,4′/2′,5′/3′,4′/3′,5′-dimethoxyphenyl)-1*H*-benzimidazoles (**1**–**10**, Figure 1) were synthesized and characterized by analytical and spectroscopic methods, such as: FT-IR, FT-Raman, ^{1}H- and ^{13}C-NMR, fluorescence spectra and ESI-MS. In addition, the optimized structure and charge distribution of the molecules are investigated using the Gaussian09 program applying Density Functional Theory (DFT) method.

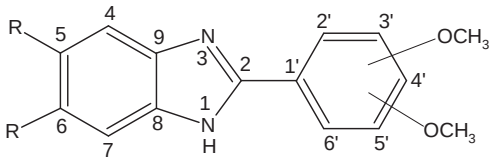

Figure 1. Schematic view of the compounds in the study.

1) R = Cl; 2′,3′-dimethoxy
2) R = Cl; 2′,4′-dimethoxy
3) R = Cl; 2′,5′-dimethoxy
4) R = Cl; 3′,4′-dimethoxy
5) R = Cl; 3′,5′-dimethoxy
6) R= CH_3; 2′,3′-dimethoxy
7) R= CH_3; 2′,4′-dimethoxy
8) R= CH_3; 2′,5′-dimethoxy
9) R= CH_3; 3′,4′-dimethoxy
10) R= CH_3; 3′,5′-dimethoxy

Compounds **1**, **2**, **5**, **6**, **7** and **10** are reported for the first time in this study. Mukhopadhyay and Tapaswi reported some methoxy/dimethoxyphenylbenzimidazoles including **3**, **4**, **8** and **9** [28]. Our research was focused on the investigation of the effect of electropositive (methyl) and electronegative (chloro) substituents on the characteristics of a series of compounds.

Results and discussion

Some physicochemical and spectral data of compounds are presented in Experimental section. We present only the Raman and fluorescence data for the known molecules (**3**, **4**, **8** and **9**) for which these data are absent in the literature. The other spectral and physicochemical data are omitted. It was observed that compounds decomposed before they started to melt. 3′,4′-Dimethoxy derivatives (**4** and **9**) have higher decomposition points as compared to the others. Compound **5**, 5,6-dichloro-2-(3′,5′-dimethoxyphenyl)-1*H*-benzimidazole, has the lowest decomposition point (125°C). It was also observed that the colour of the dichloro derivatives (**1**–**5**) is darker than the dimethyl derivatives (**6**–**10**) probably because of the intramolecular charge transfer transitions.

FT-IR and FT-Raman spectra

FT-IR and FT-Raman spectral data of compounds are given in Experimental section. FT-IR and FT-Raman spectra of compound **8** were also presented in Figure 2 as an example for comparison of the IR and Raman spectra. The characteristic ν(N–H) vibration frequencies of compounds exhibit a medium broad band at ca. 3200 cm^{-1} in the IR spectra. The ν(C=C) frequencies for the ring residue are expected to appear at around 1600 cm^{-1} with their own characteristics for the compounds in the IR spectra. Similarly, the (C=N) asymmetric stretching frequencies are expected to appear at *ca*. 1590 cm^{-1}.

The C–Cl stretching vibration was observed in the range of 656 – 670 cm^{-1} for **1** – **5** as medium band in the FT-IR spectra [29]. The characteristic ν(C–H) modes of ring residues are observed in the range of 3038 – 3093 cm^{-1}, particularly in the Raman spectra of compounds (Figure 2). The aliphatic ν(C–H) bands appeared as weak or medium in the range of 2800 – 2970 cm^{-1} both in the IR and Raman spectra. The strong bands above 1600 cm^{-1} and the medium bands around 1590 cm^{-1} in the Raman spectra are considered to belong to C=N and C=C bonds, respectively. The corresponding to these frequencies bands in the IR spectra are weak in most of compounds. The FT-Raman spectra of compounds **1**–**5** are smooth; however, those of **6**–**10** are not smooth, probably due to disturbing fluorescence effect.

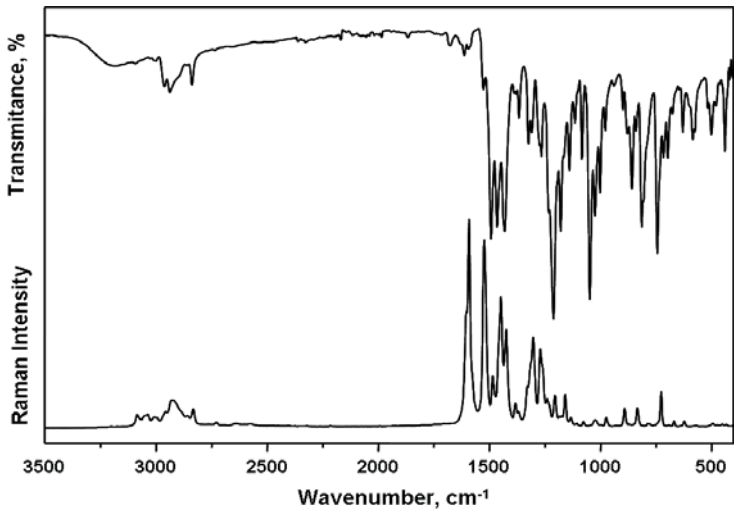

Figure 2. FT-IR and FT-Raman spectra of compound 8.

NMR spectra

The ^{1}H- and ^{13}C-NMR (Attached Proton Test, APT) spectral data of compounds are given in Experimental section. In addition, ^{1}H-NMR spectrum of **2** is presented in Figure 3. Mukhopadhyay and Tapaswi reported the ^{1}H- and ^{13}C-NMR spectral data of compounds **3**, **4**, **8** and **9** [28]. Our NMR data of these compounds are mostly in line with those of the present study.

The NH protons appear in the 11.66 – 12.86 ppm range as a broad singlet in most of compounds in DMSO-d_6. Chemical shifts of NH peaks of compounds **4** and **5** could not be detected. Reason of this probably is the tautomeric equilibrium of the hydrogen atom in the imidazole ring between the two nitrogen atoms [30,31]. This fluxional behaviour causes acidic character of NH proton. Consequently, NH protons of **4** and **5** that have higher acidic character than in the other compounds disappear; NH protons of the other compounds appear as broad singlet.

It is observed that the protons H4 and H7 have very close chemical shifts. These protons are almost identical and they are affected by the methyl or chloro substituents at the neighbouring carbon atoms (C5 and C6). They appear as a singlet (in **1**, **5**, **7** and **8**) or a broad singlet (in **2**, **3**, **4** and **9**) as expected, in the range of 7.78 – 7.85 ppm and 7.32 – 7.47 ppm for the chloro and methyl derivatives, respectively. In compounds **6** and **10** they give separate singlets. The methoxy and methyl protons give singlet in the range of 3.79 – 4.02 and 2.30 – 2.39 ppm, respectively.

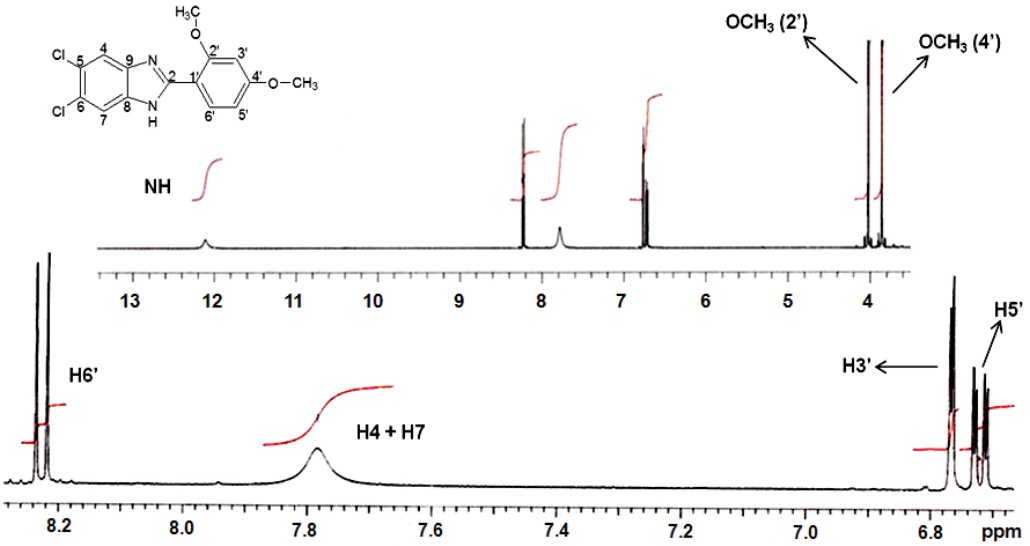

Figure 3. Fragment of ^{1}H-NMR spectrum for compound 2 and expanded view of the aromatic region

In the APT spectra of compounds, the signal at the highest ppm values should belong to N–C=N (C2) carbon atom *e.g.* for compound **2** it is found at 163.31 ppm. The methoxy and methyl carbon atoms appear in the ranges of 56.10 – 61.61 and 19.24 – 20.81 ppm, respectively. The signals around 150 ppm are assigned to C8, C9, C**'** and the carbon atoms attached to the methoxy group (for example C2' and C3'carbon atoms in **1**).

ESI-MS spectra

The ESI-MS data of molecular ions of compounds with the relative abundance and the calculated isotopic patterns [32] for **1** and **6** (one compound from both groups) are given in Experimental section.

Compound **1** {5,6-dichloro-2-(2′,3′-dimethoxyphenyl)-1*H*-benzimidazole, $C_{15}H_{12}Cl_2N_2O_2$} has two chlorine atoms whereas compound **6** {2-(2′,3′-dimethoxyphenyl)-5,6-dimethyl-1*H*-benzimidazole, $C_{17}H_{18}N_2O_2$} has no chlorine. Five distinct isotopic patterns were observed in the ESI-MS spectra of **1** since chlorine has two isotopes: ^{35}Cl (75.8 %): ^{37}Cl (24.2 %) (3:1). Three distinct isotopic patterns appeared in the ESI-MS spectra of **6**. The experimental ESI-MS data of compounds are compatible with the calculated ones.

Fluorescence spectra

Excitation and emission spectra of compounds were obtained in ethanol at room temperature (excitation wavelength: 354 nm; concentration: ~10^{-4} M). The fluorescence spectra of **2** and **8** are shown in Figure 4.

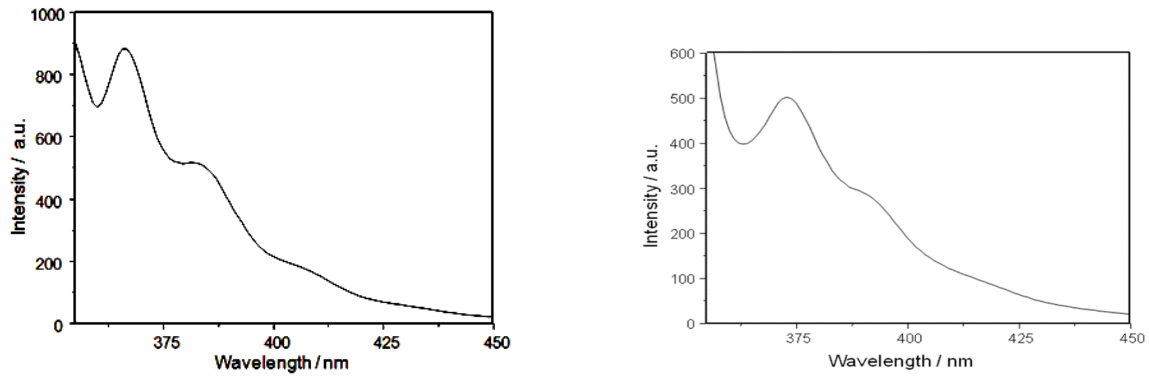

Compound 2 **Compound 8**

Figure 4. Fluorescence spectra for compounds 2 and 8.

Compounds exhibit dual or triple fluorescence in ethanol. Most of compounds display dual fluorescence in ethanol with a medium band and a shoulder. Compounds **2**, **3** and **5** exhibit triple fluorescence emissions in ethanol. These bands probably result from: 1- the normal Stokes shift originating from a locally excited π^* electronic state; 2- intramolecular charge transfer and; 3-monocation protonated at the benzimidazole nitrogen atom N3 as a result of the interaction with the solvent (H-bonding). The fluorescence spectra of **1** and **6** are similar to each other. Compounds **2**–**5** are blue-shifted with respect to **1**. Compound **7** is blue-shifted in comparison to **6** whereas the fluorescence spectra of the other methyl derivatives are similar to that of **6**.

Theoretical aspects: geometry optimization

The calculated HOMO (highest occupied molecular orbital), LUMO (lowest unoccupied molecular orbital) levels, band gap, energy (based on DFT and ZPE methods), dipole moment, electronic spatial extend (ESE) and dihedral angle values for compounds are given in Table 1. The geometry optimization studies of the compounds reveal that all molecules belong to C_1 symmetry point group. The optimized structures of compounds are shown in Figure 5. According to the optimized structures, **1**, **2**, **3**, **6**, **7** and **8** (2,3-, 2,4- and 2,5-dimethoxy derivatives) have torsion angles (dihedral angle; *i.e.* N1-C2-C1'-C6') between the benzimidazole and benzene rings in the 41.9 – 47.8° range; while compounds **4**, **5**, **9** and **10** (3,4- and 3,5-dimethoxy derivatives) are less twisted (torsion angles in the range of 9.7 – 16.7°). Another major dihedral angles involving N3-C2-C1'-C6' (134.3 – 138.3° for **1**, **2**, **3**, **6**, **7** and 163.3 – 170.3° for **4**, **5**, **9** and **10**) and N1-C2-C1'-C2' (135.6 – 140.9° for **1**, **2**, **3**, **6**,**7** and 163.3 – 170.2° for **4**, **5**, **9** and **10**) support this conclusion.

Some considerable bond lengths are the following: N3–C2: 1.315 – 1.319 Å; NH1–C2: 1.387 – 1.390 Å; C2–C1': 1.468 – 1.474 Å; Cl–C: around 1.750 Å; $H_3C–C_{arom}$: around 1.510 Å. It is significant that the NH1–C2 bond length is longer than N3–C2 as expected. Some important bond angles values are as follows (as ranges): N3-C2-NH: 112.07 – 112.34°; N3-C2-C1': 124.95 – 127.69° (this angle is lower in 3,4- and 3,5-dimethoxy derivatives and higher in the other derivatives); NH-C2-C1': 120.23 – 122.97° (higher in 3,4- and 3,5-dimethoxy derivatives, lower in the others); C2-C1'-C2': 118.45 – 122.45° (lower in 3,4- and 3,5-dimethoxy derivatives, higher in the others); C2-C1'-C6': 118.92 – 122.65° (higher in 3,4- and 3,5-dimethoxy derivatives, lower in the others); C8-N3-C2: around 105.40° and C9-NH-C2: around 107.25°. From this, it can be concluded that the positions of the methoxy groups affect the N3-C2-C1', NH-C2-C1', C2-C1'-C2' and C2-C1'-C6' bond angles in considerable values.

The calculated band-gaps of the compounds are in the range of 4.304 – 4.698 eV (Table 1). The band gap of the 2,4-, 2,5- and 3,4-dimethoxy derivatives involving the chloro groups (**2**–**4**) are slightly lower than those of the corresponding dimethyl derivatives (**7**–**9**).

Table 1

Some theoretical values for compounds 1–10.

Compound	*LUMO (eV)*	*HOMO (eV)*	*Band gap (eV)*	*Dipole moment (D)*	*ESE[a] (a.u.)*	*Dihedral angle (°)*	*Energy (Hartrees)*	
							TE[b]	*ZPE[c]*
1	-1.564	-6.262	4.698	6.92	10581.9	46.0	-1759.20	153.12
2	-1.389	-5.881	4.492	7.55	11285.7	41.9	-1759.20	153.30
3	-1.573	-5.900	4.327	7.68	10820.1	43.6	-1759.21	153.23
4	-1.681	-5.985	4.304	7.89	12285.2	10.7	-1759.20	153.08
5	-1.735	-6.153	4.418	8.24	12019.0	9.7	-1759.21	153.16
6	-1.080	-5.759	4.679	3.04	8582.7	46.0	-918.66	199.85
7	-0.909	-5.487	4.578	3.85	9215.6	44.5	-918.61	199.78
8	-1.119	-5.521	4.402	2.78	8456.7	47.8	-918.66	199.84
9	-1.195	-5.531	4.336	4.79	10023.8	10.6	-918.66	199.79
10	-1.284	-5.681	4.397	4.08	9498.7	16.7	-918.67	199.87

[a]*ESE- Electronic Spatial Extent;*

[b]*TE-Total energy from DFT calculations;*

[c]*ZPE- Zero point energy from DFT calculations.*

The electronic spatial extent (*ESE*) is defined as the area covering the volume around the molecule beyond and is a measure of the sensitivity of the molecule to the electric field [33]. The *ESE* values of the compounds increase in the following order: **8**<**6**<**7**<**10**<**9**<**3**<**1**<**2**<**5**<**4**. Since the studied molecules are clustered in two groups, it is seen that the rich in electrons dichloro derivatives have higher *ESE* values in comparison with dimethyl derivatives. Among all compounds, 5,6-dichloro-2-(3′,4′-dimethoxyphenyl)-1*H*-benzimidazole **4** has the highest *ESE* value and 2-(2′,5′-dimethoxyphenyl)-5,6-dimethyl-1*H*-benzimidazole **8** has the lowest value. The highest *ESE* value in the 5,6-dimethyl derivatives belongs to **9** (3′,4′-dimethoxy). It is observed that 3′,4′-dimethoxy derivatives (**4** and **9**) have highest molecular volume values at their groups.

Theoretical stability order of **1**–**10** was based on the zero point energies (*ZPE*). The geometry of each compound was optimized by *DFT* methods. The energies of the each optimized geometry are shown in Table 1. According to *ZPE*

calculations, the order of stability is **10**>**6**>**8**>**9**>**7**>**2**>**3**>**5**>**1**>**4**. The *ZPE* and *DFT* calculations show that the more stable forms exist within methyl species in vacuum.

As expected, the calculated dipole moment values of the dichloro derivatives (**1**–**5**) are higher than those of the dimethyl derivatives. The compound that has the highest dipole moment value is 5,6-dichloro-2-(3′,5′-dimethoxyphenyl)-1*H*-benzimidazole (**5**) with the value of 8.24 D. 2-(2′,5′-Dimethoxyphenyl)-5,6-dimethyl-1*H*-benzimidazole (**8**) has the lowest dipole moment among the studied compounds (2.78 D).

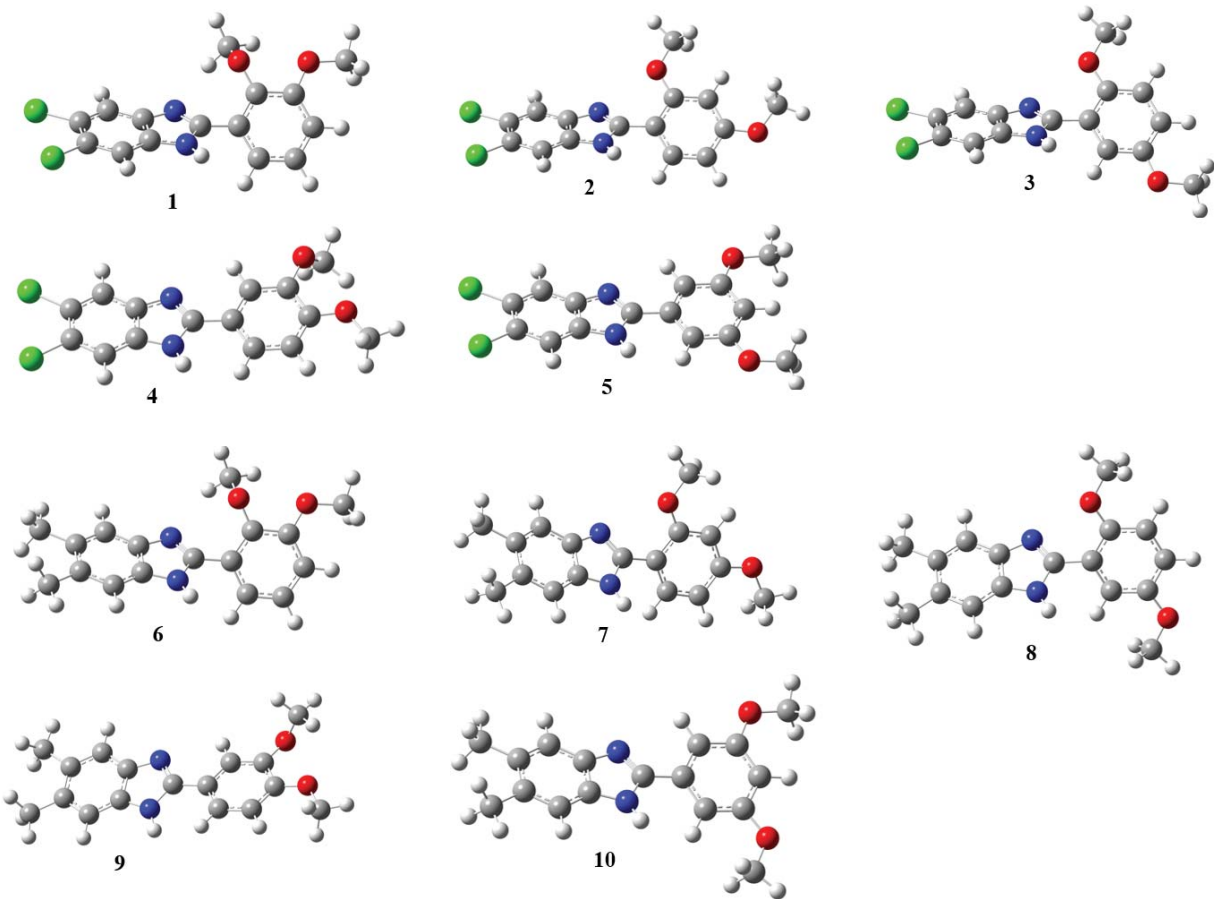

Figure 5. The optimized structures of compounds.

Atomic charges (charge distribution)

The charge distributions of compounds were calculated and are listed in Table 2. A full natural bond orbitals (NBO) analysis is obtained in Gaussian using the POP=NBO keyword. Natural Population Analysis (NPA) phase of NBO is used to show atomic partial charges which are obtained through summation over natural atomic orbitals (NAOs). The atomic charges calculated from NPAs are tabulated in Table 2. A distinguished feature of the results is that carbon atoms in methyl groups have partial negative charges. The exemplary charge distributions for **1** and **6** are depicted in Figure 6.

It is known that partial charges on atoms in a molecule arise from differences in electron affinity. Charge is transferred from one atom to the next through the covalent bond joining them. Groups of tightly bonded atoms are often electrically neutral with the partial charge on one atom balanced by the negative partial charge on the other atom [34]. Electronic charge density distribution in molecular systems has been described in terms of the topological properties [35].

It is very interesting that the chlorine atoms in compounds **1**–**5** are slightly positively charged, whereas C5 and C6 carbon atoms are negatively charged, due to the attached chlorine atoms. This unusual finding is interpreted in the light of the presence of the benzimidazole moiety. It has a conjugated system and two nitrogen atoms with high negative charges that withdraws electron from the chlorine atoms (Figure 6, Table 2).

The charge distribution shows that the more positive charge is concentrated on C2. In all compounds, C6' atom is negatively charged and the partial positive charge resides at C8 and C9. The carbon atoms bonded to the methoxy groups are positively charged, as expected. Atomic charge of the NH nitrogen (N1) is more negative than that of the C=N nitrogen atom (N3).

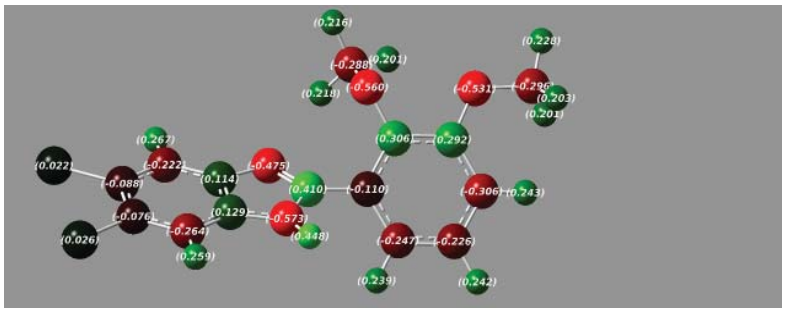

compound 1

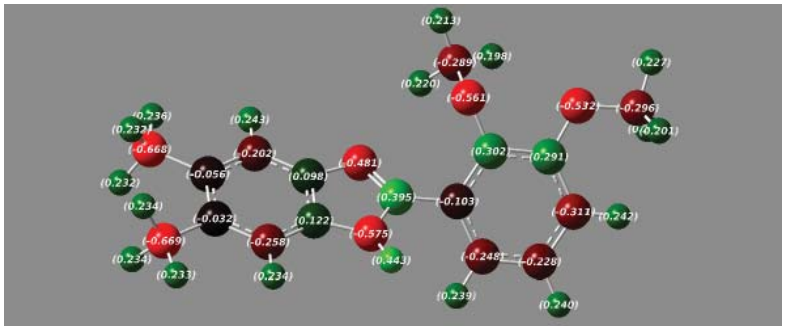

compound 6

Figure 6. Atomic charges of compounds 1 and 6 with numerical values.

Table 2

Atomic charges values (e).

	Compounds									
Atoms	***1***	***2***	***3***	***4***	***5***	***6***	***7***[a]	***8***	***9***	***10***
N1[b]	-0.573	-0.576	-0.574	-0.572	-0.569	-0.575	-0.468	-0.579	-0.573	-0.574
C2	0.410	0.409	0.402	0.402	0.417	0.395	0.558	0.389	0.387	0.389
N2	-0.475	-0.464	-0.456	-0.482	-0.477	-0.481	-0.256	-0.461	-0.485	-0.478
C4	-0.222	-0.223	-0.221	-0.224	-0.208	-0.202	-0.559	-0.214	-0.203	-0.214
C5	-0.088	-0.089	-0.089	-0.088	-0.094	-0.056	0.786	-0.051	-0.056	-0.048
C6	-0.076	-0.078	-0.076	-0.083	-0.076	-0.032	0.471	-0.033	-0.039	-0.035
C7	-0.264	-0.266	-0.265	-0.252	-0.266	-0.258	-0.490	-0.260	-0.247	-0.260
C8	0.129	0.128	0.129	0.123	0.132	0.122	0.309	0.121	0.117	0.124
C9	0.114	0.112	0.111	0.116	0.107	0.098	-0.368	0.102	0.100	0.105
C1’	-0.110	-0.179	-0.105	-0.106	-0.082	-0.103	0.365	-0.101	-0.098	-0.066
C2’	0.306	0.392	0.328	-0.214	-0.261	0.302	0.574	0.326	-0.217	-0.235
C3’	0.292	-0.408	-0.298	0.273	0.351	0.291	-0.563	-0.297	0.271	0.334
C4’	-0.306	0.357	-0.291	0.295	-0.396	-0.311	-0.222	-0.246	0.289	-0.364
C5’	-0.226	-0.314	0.292	0.311	0.338	-0.228	0.785	0.291	-0.311	0.348
C6’	-0.247	-0.168	-0.244	-0.216	-0.287	-0.248	-1.475	-0.294	-0.220	-0.349
$Cl(CH_3)_{(5)}$[c]	0.022	0.019	0.021	0.023	0.023	-0.668	-0.642	-0.668	-0.668	-0.668
$Cl(CH_3)_{(6)}$[d]	0.026	0.022	0.024	0.025	0.026	-0.669	-0.636	-0.669	-0.669	-0.669
$\underline{O}CH_3$[e]	-0.560	-0.516	-0.521	-0.563	-0.531	-0.561	-0.285	-0.522	-0.565	-0.533
$\underline{O}CH_3$[e]	-0.531	-0.531	-0.540	-0.532	-0.537	-0.532	-0.334	-0.540	-0.535	-0.539
$O\underline{C}H_3$	-0.288	-0.298	-0.296	-0.289	-0.298	-0.289	-0.146	-0.296	-0.288	-0.288
$O\underline{C}H_3$	-0.296	-0.298	-0.296	-0.297	-0.297	-0.296	-0.174	-0.296	-0.296	-0.296

[a]*Mulliken charges- Atomic charges of **7** could not be obtained by NBO method;*

[b]*NH;*

[c,d]*-CH_3 for **6**–**10**;*

[e]*-OCH_3 groups were given as order 2,3; 2,4; 2,5; 3,4 and 3,5-positions.*

The dimethoxy carbon atoms are partially negatively charged and the methoxy oxygen atom is negatively charged in all of compounds, as shown in the charge distribution figures of **1** and **6** (Figure 6). Unexpectedly, in dimethyl derivatives (**6**–**10**) the methyl carbon atoms also have considerable negative charge (around -0.67 *e*).

Conclusions

It is known that various benzimidazole derivatives are an important class of compounds due to the demonstrated biological activity. In this study, ten benzimidazole derivatives including dimethoxy or dimethyl groups, 5,6-dichloro/dimethyl-2-(2′,3′/2′,4′/2′,5′/3′,4′/3′,5′-dimethoxyphenyl)-1*H*-benzimidazoles (**1**–**10**) were synthesized in high yields. They were characterized using FT-IR, FT-Raman, NMR, ESI-MS, and fluorescence spectroscopy. It was found that compounds **2**, **3** and **5** show triple fluorescence whereas the other compounds present dual fluorescence. In addition, the optimized molecular geometry, bond lengths, bond angles, energy, dipole moment, ESE, band gap and charge distributions of compounds were calculated by using Gaussian 09 using DFT method (RB3LYP) with 6-31++G(d,p) basis set. The dihedral angles between the benzimidazole and benzene rings vary from 9.7º to 47.8º. The calculated energy values based on ZPE and DFT show that the order of stability is **10**>**6**>**8**>**9**>**7**>**2**>**3**>**5**>**1**>**4**. According to this order the methyl derivatives (**6**–**10**) are more stable than the chloro forms. 3′,4′-Dimethoxy derivatives (**4** and **9**) have higher melting points in comparison with the other compounds in series. The chloro derivatives have higher dipole moment as compared to the methyl derivatives, due to the electronegativity of chlorine atoms. 5,6-Dichloro-2-(3′,5′-dimethoxyphenyl)-1*H*-benzimidazole (**5**) has the highest dipole moment value of 8.24 D and 2-(2′,5′-dimethoxyphenyl)-5,6-dimethyl-1*H*-benzimidazole (**8**) has the lowest dipole moment (2.78 D). According to the calculated atomic charges, the chlorine atoms in the compounds **1**–**5** are positively charged whereas C5 and C6 carbon atoms are negatively charged, due to the attached chlorine atoms. This was explained by the presence of the benzimidazole moiety exerting the electron withdrawing effect.

Experimental

General experimental procedure

All chemicals and solvents were of reagent grade and were used without further purification. Elemental analysis (C, H, N) data were obtained with a ThermoFinnigan Flash EA 1112 analyser. Decomposition points were determined using an Electro thermal melting-point apparatus. ^{1}H- and ^{13}C-NMR (APT) spectra were run on a Varian Unity Inova 500 NMR spectrometer. The residual DMSO-d_6 signal was also used as an internal reference. Fluorescence spectra were performed on a Shimadzu RF-5301 PC Spectrofluorophotometer. The Electron Spray Ionization-Mass Spectrometry (ESI-MS) analyses were carried out in positive ion modes using a ThermoFinnigan LCQ Advantage MAX LC/MS/MS. FT-IR spectra were recorded on a Bruker Optics Vertex 70 spectrometer using Attenuated Total Reflection (ATR) techniques between 400 and 4000 cm^{-1}. The FT-Raman spectra were also recorded on the same instrument with a R100/R RAMII Raman module equipped with Nd:YAG laser source operating at 1064 nm line with 200 mW power and a spectral resolution of ±2 cm^{-1}.

Synthesis of compounds

Compounds **1–10** were prepared according to the procedures found in the literature [36,37].

5,6-Dichloro-2-(2′,3′-dimethoxyphenyl)-1*H*-benzimidazole (1). For synthesis of **1**, 2,3-dimethoxybenzaldehyde (332 mg, 2 mmol) reacted with an equivalent amount of $NaHSO_3$ (208 mg, 2 mmol) at room temperature in ethanol (10 mL) for 4–5 hours. The resultant mixture was treated with 4,5-dichlorobenzene-1,2-diamine (354 mg, 2 mmol) in dimethylformamide (5 mL) and gently refluxed for 2-3 hours. The reaction mixture was then poured into iced water (100 mL). A precipitate of compound (**1**) was formed; it was filtered and crystallized from ethanol (600 mg, 93%). Brown solid. m.p.: 195 °C (decomp.). Anal. calcd. for $C_{15}H_{12}Cl_2N_2O_2$ (M_r=323.17), *w*/%, are: C, 55.75; H, 3.74; N, 8.67. Found: C, 53.50; H, 4.64; N, 8.86. ^{1}H NMR (DMSO-d_6) δ/ppm: 12.59 (br s, 1H, NH), 7.85 (s, 2H, H4+H7), 7.82 (dd, J = 9.3, 8.3 Hz, 1H, H5'), 7.22 (m, 2H, H4'+H6'), 3.89 (s, 3H, $OCH_{3(2')}$), 3.86 (s, 3H, $OCH_{3(3')}$); ^{13}C NMR (APT, 125 MHz, DMSO-d_6) δ/ppm: 153.54, 151.84, 147.75, 125.06, 123.12 (quaternary carbons), 125.24, 121.89, 121.86, 115.71, 61.61, 56.77 (H-bonded carbons). IR (ATR, $\bar{\nu}$/cm^{-1}): 3178 m,br, 2938 m, 2835 m, 1581 m, 1525 m, 1481 s, 1436 m, 1264 s, 1231 s, 1059 m, 966 s, 871 m, 742 s, 663 m, 531 m, 436 m. Raman ($\bar{\nu}$/cm^{-1}): 3071 w, 2935 w, 2836 w, 1600 s, 1521 s, 1442 m, 1411 m, 1322 w, 1284 w, 1228 m, 1118 w, 972 w, 875 w, 781 w, 733 w, 664 w. Fluorescence spectra (EtOH, c = 1·10^{-4} mol/L) λ_{max}/nm: 373 m,br, 392 sh. MS *m*/*z*: 323.4 (100%, $[M]^+$), 325.4 (66.9%, $[M+2]^+$), 324.4 (15.4%, $[M+1]^+$), 326.4 (10.6%, $[M+3]^+$), 327.3 (10.3%, $[M+4]^+$); Calculated [32]: 322.03 (100%), 323.03 (16.2%), 324.02 (63.9%), 325.03 (10.4%), 326.02 (10.2%), 327.02 (1.7%).

Compounds **2**–**5** were synthesized in a similar manner to the synthesis of **1**.

5,6-Dichloro-2-(2′,4′-dimethoxyphenyl)-1*H*-benzimidazole (2). 2,4-Dimethoxybenzaldehyde (517 mg, 2 mmol) was employed for synthesizing compound **2.** Yield: 258 mg, 80%. Reddish brown solid. m.p.: 222 °C (decomp.). Anal. calcd. for $C_{15}H_{12}Cl_2N_2O_2$ (M_r=323.17), *w*/%, are: C, 55.75; H, 3.74; N, 8.67. Found: C, 55.56; H, 4.01; N, 8.76. ^{1}H NMR (DMSO-d_6) δ/ppm: 12.11 (s, br, 1H, NH), 8.23 (d, J = 8.8 Hz, 1H, H6'), 7.78 (s, br, 2H, H4+H7), 6.77 (d, J = 2.4 Hz, 1H, H3'), 6.72 (dd, J = 8.8, 2.4 Hz, 1H, H5'), 4.02 (s, 3H, $OCH_{3(2')}$), 3.86 (s, 3H, $OCH_{3(4')}$); ^{13}C NMR (APT, 125 MHz, DMSO-d_6) δ/ppm: 163.31, 159.09, 152.49, 124.43, 110.71, 99.30 (quaternary carbons), 131.82, 107.25, 107.22, 99.35, 99.33, 56.72, 56.23 (H-bonded carbons). IR (ATR, $\bar{\nu}$/cm^{-1}): 3386 m, 3305 m, 3099 w, 2938 w, 2834 w, 1612 s, 1582 m, 1470 m, 1418 m, 1285 s, 1257 s, 1215 s, 1178 m, 1093 m, 1033 s, 937 w, 863 m,

820 s, 726 m, 669 m, 522 m, 486 m, 424 m. Raman ($\overline{\nu}$/cm^{-1}): 3078 w, 2936 w, 2831 w, 1609 s, 1573 m, 1530 s, 1445 m, 1413 m, 1287 w, 1249 m, 1224 w, 1133 w, 1092 w, 966 w, 726 w, 664w, 619 w. Fluorescence spectra (EtOH, c = 1·10^{-4} mol/L) λ_{max}/nm: 365 m, 382 sh, 408 sh.

5,6-Dichloro-2-(2´,5´-dimethoxyphenyl)-1*H*-benzimidazole (3). Raman ($\overline{\nu}$/cm^{-1}): 3080 w, 2936 w, 2831 w, 1590 m, 1520 s, 1479 m, 1442 m, 1413 m, 1359 w, 1262 m, 1218 m, 1174 w, 1083 w, 973 w, 887 m, 819 w, 737 w, 674 w, 620 w (cm^{-1}). Fluorescence spectra (EtOH, c = 1·10^{-4} mol/L) λ_{max}/nm: 365 m, 381 m, 409 sh.

5,6-Dichloro-2-(3´,4´-dimethoxyphenyl)-1*H*-benzimidazole (4). Raman ($\overline{\nu}$/cm^{-1}): 3068 w, 3005 w, 2939 w, 2836 w, 1603 s, 1544 m, 1496 m, 1439 m, 1417 sh, 1269 m, 1228 w, 1095 w, 975 w, 888 w, 765 w, 664 w. Fluorescence (ethanol, c = 1·10^{-4} mol/L): (λ_{max}/nm): 365 m,br, 382 sh.

5,6-Dichloro-2-(3´,5´-dimethoxyphenyl)-1*H*-benzimidazole (5). 3,5-Dimethoxybenzaldehyde (332 mg, 2 mmol) was employed for synthesizing compound **5.** Yield: 485 mg, 75%. Light brown solid. m.p.: 126°C (decomp.); Anal. calcd. for $C_{15}H_{12}Cl_2N_2O_2$ (M_r=323.17), *w*/%, are: C, 55.75; H, 3.74; N, 8.67. Found: C, 55.58; H, 3.90; N, 8.75. ^{1}H NMR (DMSO-d_6) δ/ppm: 7.78 (s, 2H, H4+H7), 7.73 (d, J = 1.9 Hz, 1H, H6'), 7.72 (d, J = 1.9 Hz, 1H, H2'), 7.12 (s, 1H, H4'), 3.87 (s, 3H, $OCH_{3(5')}$), 3.83 (s, 3H, $OCH_{3(3')}$); ^{13}C NMR (APT, 125 MHz, DMSO-d_6) δ/ppm: 154.74, 151.59, 149.66, 124.87, 122.37 (quaternary carbons), 120.57, 120.53, 112.57, 110.67, 110.64, 56.37, 56.31 (H-bonded carbons). IR (ATR, $\overline{\nu}$/cm^{-1}): 3178 m,br, 3139 m,br, 2937 m, 2838 m, 1679 w, 1614 m, 1594 m, 1475 m, 1413 m, 1351 m, 1251 m, 1204 m, 1161 m, 1098 m, 1056 s, 963 m, 851 m, 723 m, 656 m, 501 m, 429 m. Raman ($\overline{\nu}$/cm^{-1}): 3068 w, 3017 w, 2936 w, 2839 w, 1606 s, 1534 s, 1442 m, 1414 m, 1281 m, 1250 m, 1095 w, 1052 w, 992 m, 885 w, 786 w, 658 w. Fluorescence spectra (EtOH, c = 1·10^{-4} mol/L) λ_{max}/nm: 365 m,br, 381 sh, 392 m,br.

2-(2´,3´-Dimethoxyphenyl)-5,6-dimethyl-1*H*-benzimidazole (6). Compound **6** was synthesized in a similar manner to that described for synthesis of compound **1**. 4,5-Dimethylbenzene-1,2-diamine (272 mg, 2 mmol) was used for the synthesis of compounds **6**–**10** instead of 4,5-dichlorobenzene-1,2-diamine. Yield: 503 mg, 89%. Light yellow solid. m.p.: 149°C (decomp.); Anal. calcd. for $C_{17}H_{18}N_2O_2$ (M_r=282.34), *w*/%, are: C, 72.32; H, 6.43; N, 9.92. Found: C, 72.48; H, 6.61; N, 10.14. ^{1}H NMR (DMSO-d_6) δ/ppm: 11.97 (s, 1H, NH), 7.85 (dd, J = 6.8, 1.9 Hz, H6'), 7.47 (s, 1H, H4), 7.44 (s, 1H, H7), 7.26 (dd, J = 7.8, 1.9 Hz, H4'), 7.21 (dd, J = 7.8, 6.8 Hz, H5'), 3.95 (s, 3H, $OCH_{3(2')}$), 3.90 (s, 3H, $OCH_{3(3')}$), 2.39 (s, 3H, $CH_{3(5)}$), 2.38 (s, 3H, $CH_{3(6)}$); ^{13}C NMR (APT, 125 MHz, DMSO-d_6) δ/ppm: 153.55, 152.85, 148.38, 147.33, 134.43, 130.80, 124.42 (quaternary carbons), 124.99, 124.55, 123.66, 121.78, 114.62, 112.84, 61.40, 56.70, 20.77 (H-bonded carbons). IR (ATR, $\overline{\nu}$/cm^{-1}): 3594 m, 3157 m,br, 2937 m, 2837 w, 1659 m, 1583 m, 1525 m, 1482 m, 1438 m, 1264 s, 1227 m, 1136 m, 1061 m, 1002 s, 855 m, 797 m, 744 m, 711 m, 499 m, 440 m. Raman ($\overline{\nu}$/cm^{-1}): 3083 w, 3042 w, 2935 w, 2839 w, 1603 s, 1521 s, 1465 m, 1442 m, 1417 m, 1386 w, 1307 m, 1256 m, 1238 m, 1159 w, 1130 w, 982 w, 885 w, 784 w, 730 m. Fluorescence spectra (EtOH, c = 1·10^{-4} mol/L) λ_{max}/nm: 372 m,br, 392 sh. MS *m*/*z*: 283.2 (100%, [M+1]$^+$), 284.2 (12.7%, [M+2]$^+$), 285.3 (1.7%, [M+2]$^+$); Calculated [32]: 282.14 (100%), 283.14 (18.4%), 284.14 (1.6%).

2-(2´,4´-Dimethoxyphenyl)-5,6-dimethyl-1*H*-benzimidazole (7). Compound **7** was synthesized in a similar manner to **2**. 4,5-Dimethylbenzene-1,2-diamine (272 mg, 2 mmol) was used instead of 4,5-dichlorobenzene-1,2-diamine. Yield: 520 mg, 92%. Beige solid. m.p.: 207 °C (decomp.); Anal. calcd. for $C_{17}H_{18}N_2O_2$ (M_r=282.34), *w*/%, are: C, 72.32; H, 6.43; N, 9.92. Found: C, 72.10; H, 6.52; N, 10.19. ^{1}H NMR (DMSO-d_6) δ/ppm: 11.66 (br s, 1H, NH), 8.20 (d, J = 8.3 Hz, 1H, H6'), 7.33 (s, 2H, H4+H7), 6.72 (d, J = 2.4 Hz, 1H, H3'), 6.68 (dd, J = 8.8, 2.4 Hz, 1H, H5'), 3.99 (s, 3H, $OCH_{3(4')}$), 3.84 (s, 3H, $OCH_{3(2')}$), 2.30 (s, 6H, $2CH_3$); ^{13}C NMR (APT, 125 MHz, DMSO-d_6) δ/ppm: 162.38, 158.56, 149.02, 130.35, 112.07 (quaternary carbons), 131.33, 106.87, 106.85, 99.26, 99.24, 56.47, 56.13, 20.79, 20.76 (H-bonded carbons). IR (ATR, $\overline{\nu}$/cm^{-1}): 3224 m,br, 2963 m, 2937 m, 2833 m, 1611 m, 1581 m, 1447 m, 1423 s, 1279 s, 1208 s, 1170 m, 1078 m, 1040 m, 834 m, 686 m, 509 m, 463 m, 404 m. Raman ($\overline{\nu}$/cm^{-1}): 3093 w, 3043 w, 2939 w, 2831 w, 1609 s, 1577 w, 1534 s, 1448 m, 1427 m, 1383 w, 1335 w, 1307 m, 1259 m, 1159 w, 1121 w, 960 m, 730 m, 554 w. Fluorescence spectra (EtOH, c = 1·10^{-4} mol/L) λ_{max}/nm: 364 m,br, 380 m,br.

2-(2´,5´-Dimethoxyphenyl)-5,6-dimethyl-1*H*-benzimidazole (8). Raman ($\overline{\nu}$/cm^{-1}):3088 w, 3040 w, 2927 w, 2836 w, 1610 sh, 1595 s, 1525 s, 1487 w, 1449 m, 1427 m, 1385 w, 1307 m, 1273 m, 1207 w, 1159 w, 1027 w, 977 w, 895 w, 837 w, 730 m. Fluorescence spectra (EtOH, c = 1·10^{-4} mol/L) λ_{max}/nm: 374 m,br, 392 sh.

2-(3´,4´-Dimethoxyphenyl)-5,6-dimethyl-1*H*-benzimidazole (9). Raman ($\overline{\nu}$/cm^{-1}): 3078 w, 3047 w, 2920 m, 2836 w, 1631 w, 1606 s, 1549 m, 1499 m, 1461 m, 1417 m, 1363 w, 1317 m, 1291 m, 1235 w, 1164 w, 1133 w, 992 w, 768 w, 730 w. Fluorescence spectra (EtOH, c = 1·10^{-4} mol/L) λ_{max}/nm: 375 m,br, 392 m,br.

2-(3´,5´-Dimethoxyphenyl)-5,6-dimethyl-1*H*-benzimidazole (10). Compound **10** was synthesized in a similar manner to **5**. 4,5-Dimethylbenzene-1,2-diamine (272 mg, 2 mmol) was used instead of 4,5-dichlorobenzene-1,2-diamine. Yield: 440 mg, 78%. Dirty white solid. m.p.: 251 °C (decomp.); Anal. calcd. for $C_{17}H_{18}N_2O_2$ (M_r=282.34), *w*/%, are: C, 72.32; H, 6.43; N, 9.92. Found: C, 72.25; H, 6.59; N, 10.06. ^{1}H NMR (DMSO-d_6) δ/ppm: 12.86 (br s, 1H, NH), 7.37 (s, 2H, H2'+H6'), 7.33 (s, 1H, H4), 7.32 (s, 1H, H7), 6.61 (s, 1H, H6'), 3.84 (s, 6H, $2OCH_3$), 2.33 (s, 6H, $2CH_3$); ^{13}C NMR (APT, 125 MHz, DMSO-d_6) δ/ppm: 161.48, 150.83, 143.05, 134.12, 132.96, 132.00, 130.66 (quaternary carbons), 161.47, 119.61, 111.97, 104.77, 102.40, 56.14, 56.10, 20.73, 19.24 (H-bonded carbons). IR (ATR, $\overline{\nu}$/cm^{-1}): 3018 w, 2966 w, 2832 w, 1607 m, 1593 s, 1464 m, 1417 m, 1304 m, 1253 m, 1202 m, 1159 s, 1049 s, 844 m, 854 m, 721 m, 677 m, 572 m, 436 m. Raman ($\overline{\nu}$/cm^{-1}): 3038 w, 2920 m, 2834 w, 1603 s, 1562 w, 1537 m, 1455 m, 1420 m, 1379 w, 1307 s, 1259 m, 1164 w, 1047 w, 991 m, 802 w, 730 m. Fluorescence spectra (EtOH, c = 1·10^{-4} mol/L) λ_{max}/nm: 375 m,br, 392 m,br.

Computational method

GAUSSIAN 09 software package was used for theoretical calculations [38]. The quantum chemical calculations were performed by applying DFT (RB3LYP) method with the standard 6-31++G(d,p) basis set. The default options for the self-consistent field convergence and threshold limits in the optimization were used.

Acknowledgements

This work was supported by the Scientific Research Projects Unit of Istanbul University, Grant no. 7011.

References

1. Bonnett, R. The chemistry of the vitamin B_{12} group. Chemical Reviews, 1963, 63, pp. 573–605.
2. Brink, N.G.; Folkers, K. Vitamin B_{12}. X. 5,6-Dimethylbenzimidazole, a degradation product of vitamin B_{12}. Journal of the American Chemical Society, 1950, 72, pp. 4442–4443.
3. Sastry, C.S.P.; Naidu, P.Y.; Murty, S.S.N. Spectrophotometric methods for the determination of omeprazole in bulk form and pharmaceutical formulation. Talanta, 1997, 44, pp. 1211–1217.
4. Delescluse, C.; Piechock, M.P.; Ledirac, N.; Hines, R.H.; Li, R.; Gidrol, X.; Rahmani, R. Induction of cytochrome P450 1A1 gene expression, oxidative stress, and genotoxicity by carbaryl and thiabendazole in transfected human HepG2 and lymphoblastoid cells. Biochemical Pharmacology, 2001, 61, pp. 399–407.
5. Mothilal, K.K.; Karunakaran, C.; Rajendran, A.; Murugesan, R. Synthesis, X-ray crystal structure, antimicrobial activity and photodynamic effects of some thiabendazole complexes. Journal of Inorganic Biochemistry, 2004, 98, pp. 322–332.
6. Cardoso, E.J.; Luna, A.F.; Urizar, J.P. *In vitro* activity of two phenyl-carbamate derivatives, singly and in combination with albendazole against albendazole-resistant *Giardia intestinalis*. Acta Tropica, 2004, 92, pp. 237–244.
7. Savlik, M.; Polaskova, P.; Szotakova, B.; Lamka, J.; Skalova, L. The effects of flubendazole and mebendazole on cytochromes P4501A in pheasant hepatocytes. Research in Veterinary Science, 2005, 79, pp. 139–147.
8. Almeida, R.G.; Florio, J.C.; Spinosa, H.S.; Bernardi, M.M. Comparative effects of maternal prenatal and postnatal exposures to as temizole on reproductive parameters of rats. Neurotoxicology and Teratology, 2002, 24, pp. 255–265.
9. Gronvold, J.; Svendsen, T.S.; Kraglund, H.O.; Bresciani, J.; Monrad, J. Effect of the antiparasitic drugs fenbendazole and ivermectin on the soil nematode *Pristionchusmaupasi*. Veterinary Parasitology, 2004, 124, pp. 91–99.
10. Infante-Castillo, R.; Rivera-Montalvo, L.A.; Hernandez-Rivera, S.P. Theoretical DFT, vibrational and NMR studies of benzimidazole and alkyl derivatives. Journal of Molecular Structure, 2008, 877, pp. 10–19.
11. Karpinka, M.M.; Matysiak, J.; Niewiadomy, A. Synthesis of novel 4-(1H-benzimidazol-2-yl)benzene-1,3-diols and their cytotoxic activity against human cancer cell lines. Archives of Pharmaceutical Research, 2011, 34, pp. 1639–1647.
12. Karpinska, M.M.; Matysiak, J.; Niewiadomy, A.; Wietrzyk, J.; Klopotowska, D. Synthesis and biological activity of novel 4- and 6-(1-alkyl/aryl-1H-benzimidazol-2-yl)benzene-1,3-diols. Monatsheftefür Chemie, 2012, 143, pp. 269–276.
13. Cheng, J.; Xie, J.; Luo, X. Synthesis and antiviral activity against Coxsackie virus B3 of some novel benzimidazole derivatives. Bioorganic & Medicinal Chemistry Letters, 2005, 15, pp. 267–269.
14. Charlson, A.J. The methanesulfonylation of 2-benzimidazolemethanol and alpha-(2-benzimidazolyl)benzyl alcohol. Carbohydrate Research, 1973, 29, pp. 89–98.
15. Walker, K.A.M.; Braemer, A.C.; Hitt, S.; Jones, R.E.; Mathews, T.R. A new potent antifungal agent. Journal of Medicinal Chemistry, 1978, 21, pp. 840–842.
16. Nakano, H.; Inoue, T.; Kawasaki, N.; Miyataka, H.; Matsumoto, H.; Taguchi, T.; Inagaki, N.; Nagai, H.; Satoh, T. Synthesis and biological activities of novel antiallergic agents with 5-lipoxygenase inhibiting action. Bioorganic & Medicinal Chemistry, 2000, 8, pp. 373–380.
17. Sheng, J.; Nguyen, P.T.M.; Baldeck, J.D.; Olsson, J.; Marquis, R.E. Antimicrobial actions of benzimidazoles against the oral anaerobes *Fusobacteriumnucleatum* and *Prevotella intermedia*. Archives of Oral Biology, 2006, 51, pp. 1015–1023.
18. Tavman, A.; Agh-Atabay, N.M.; Neshat, A.; Gücin, F.; Dülger, B.; Haciu, D. Structural characterization and antimicrobial activity of 2-(5-H/methyl/chloro-1*H*-benzimidazol-2-yl)-4-bromo/nitro-phenol ligands and their $Fe(NO_3)_3$ complexes. Transition Metal Chemistry, 2006, 31, pp. 194–200.
19. Tavman, A.; Agh-Atabay, N.M.; Güner, S.; Gucin, F.; Dülger, B. Investigation of Raman, FT-IR, EPR spectra and antimicrobial activity of 2-(5-H/Me/Cl-1*H*-benzimidazol-2-yl)-phenol ligands and their $Fe(NO_3)_3$ complexes. Transition Metal Chemistry, 2007, 32, pp. 172–179.
20. Tavman, A.; Boz, I.; Birteksöz, A.S. Spectral characterization and antimicrobial activity of 2-(5-chloro/nitro-1*H*-benzimidazol-2-yl)-4-bromo/nitro-phenols and their zinc(II) complexes. Spectrochimica Acta A, 2010, 77, pp. 199–206.

21. Los, R.; Wesolowska-Trojanowska, M.; Malm, A.; Karpinska, M.M.; Matysiak, J.; Niewiadomy, A.; Glaszcz, U. A new approach to the synthesis of 2-aryl-substituted benzimidazoles, quinazolines, and other related compounds and their antibacterial activity. Heteroatom Chemistry, 2012, 23, pp. 265–275.
22. Mavrova, A.T.; Anichina, K.K.; Vuchev, D.I.; Tsenov, J.A.; Denkova, P.S.; Kondeva, M.S.; Micheva, M.K. Antihelminthic activity of some newly synthesized 5(6)-(un)substituted-1*H*-benzimidazol-2-ylthioacetylpiperazine derivatives. European Journal of Medicinal Chemistry, 2006, 41, pp. 1412–1420.
23. Thibault, S. Comparison of inhibitory properties of nitrogen compounds on the corrosion of cooper in low-acid environment. Corrosion Science, 1977, 17, pp. 701–709 (in French).
24. Mohan, S.; Sundaraganesan, N.; Mink, J. FTIR and Raman studies on benzimidazole. Spectrochimica Acta A, 1991, 47, pp. 1111–1115.
25. Klots, T.D.; Devlin, P.; Collier, W.B. Heteroatom derivatives of indene: V. Vibrational spectra of benzimidazole. Spectrochimica Acta A, 1997, 53, pp. 2445–2456.
26. Morsy, M.A.; Al-Khadi, M.A.; Suwaiyan, A. Normal vibrational modes and assignment of benzimidazole by *ab initio* and density functional calculations and plolarized infrared and Raman spectroscopy. The Journal of Physical Chemistry A, 2002, 106, pp. 9196–9203.
27. Yurdakul, S.; Yilmaz, C. Vibrational spectroscopic investigations of (benzimidazole)$_2$Ni(CN)$_4$ and Cd(benzimidazole)Cl$_2$ complexes. Vibrational Spectroscopy, 1999, 21, pp. 127–132.
28. Mukhopadhyay, C.; Tapaswi, P.K. PEG-mediated catalyst-free expeditious synthesis of 2-substituted benzimidazoles and bis-benzimidazoles under solvent-less conditions. Tetrahedron Letters, 2008, 49, pp. 6237–6240.
29. Sundaraganesan, N.; Anand, B.; Jian, F.-F.; Zhao, P. FT-Raman and FT-IR spectra, ab initio and density functional studies of 3,4-dichlorobenzyl alcohol. Spectrochimica Acta A, 2006, 65, pp. 826–832.
30. Aghatabay, N.M.; Neshat, A.; Karabiyik, T.; Somer, M.; Haciu, D.; Dulger, B. Synthesis, characterization and antimicrobial activity of Fe(II), Zn(II), Cd(II) and Hg(II) complexes with 2,6-bis(benzimidazol-2-yl) pyridine ligand. European Journal Medicinal Chemistry, 2007, 42, pp. 205–213.
31. Tavman, A.; Ulkuseven, B.; Agh-Atabay, N.M. 1,2-Bis-(2-benzimidazolyl)-1,2-ethanediol and 1,4-bis-(2-benzimidazolyl)-1,2,3,4-butanetetraol $PdCl_2$ complexes. Transition Metal Chemistry, 2000, 25, pp. 324–328.
32. Patiny, L.; Borel, A. ChemCalc: a building block for tomorrow's chemical infrastructure. Journal of Chemical Information and Modelling, 2013, 53, pp. 1223–1228.
33. Bober, L.; Kawczak, P.; Baczek, T. Pharmacological classification and activity evaluation of furan and thiophene amide derivatives applying semi-empirical *ab initio* molecular modelling methods. International Journal of Molecular Sciences, 2012, 13, pp. 6665–6678.
34. Thilagavathy, R.; Kavitha, H.P.; Amrutha, R.; Venkatrama, B.R. Structural parameters, charge distribution and vibrational frequency analysis using theoretical SCF methods. Elixir International Journal, 2011, 40, pp. 5514–5516.
35. Kulkarni, G.U.; Gopalan, R.S.; Rao, C.N.R. Experimental and theoretical electronic charge densities in molecular crystals. Journal of Molecular Structure (Theochem), 2000, 500, pp. 339–362.
36. Tavman, A.; Ulküseven, B. Zinc(II) complexes of 2-(2-hydroxy-5-bromo/nitro-phenyl)-5-methyl/chloro/nitro-1*H*-benzimidazoles. Main Group Metal Chemistry, 2001, 24, pp. 205–210.
37. Ridley, H.F.; Spickett, R.G.W.; Timmis, G.M. A new synthesis of benzimidazoles and aza-analogs. Journal of Heterocyclic Chemistry, 1965, 2, pp. 453–456**.**
38. Gaussian 09, Frisch, M.J.; Trucks, G.W.; Schlegel, H.B.; Scuseria, G.E.; Robb, M.A.; Cheeseman, J.R.; Scalmani, G.; Barone, V.; Mennucci, B.; Petersson, G. A.; Nakatsuji, H.; Caricato, M.; Li, X.; Hratchian, H.P.; Izmaylov, A.F.; Bloino, J.; Zheng, G.; Sonnenberg, J.L.; Hada, M.; Ehara, M.; Toyota, K.; Fukuda, R.; Hasegawa, J.; Ishida, M.; Nakajima, T.; Honda, Y.; Kitao, O.; Nakai, H.; Vreven, T.; Montgomery, Jr.J.A.; Peralta, J. E.; Ogliaro, F.; Bearpark, M.; Heyd, J.J.; Brothers, E.; Kudin, K. N.; Staroverov, V.N.; Kobayashi, R.; Normand, J.; Raghavachari, K.; Rendell, A.; Burant, J. C.; Iyengar, S.S.; Tomasi, J.; Cossi, M.; Rega, N.; Millam, J.M.; Klene, M.; Knox, J.E.; Cross, J.B.; Bakken, V.; Adamo, C.; Jaramillo, J.; Gomperts, R.; Stratmann, R.E.; Yazyev, O.; Austin, A.J.; Cammi, R.; Pomelli, C.; Ochterski, J.W.; Martin, R.L.; Morokuma, K.; Zakrzewski, V.G.; Voth, G.A.; Salvador, P.; Dannenberg, J.J.; Dapprich, S.; Daniels, A.D.; Farkas, Ö.; Foresman, J.B.; Ortiz, J.V.; Cioslowski, J.; Fox, D.J. Gaussian, Inc., Wallingford CT, 2009.

CHEMISTRY JOURNAL OF MOLDOVA. General, Industrial and Ecological Chemistry. 2016, 11(2), 68-73
http://cjm.asm.md
http://dx.doi.org/10.19261/cjm.2016.11(2).02

EXTRACT OF BARBERRY AS ENTIRELY GREEN CATALYST FOR THE SYNTHESIS OF STRUCTURALLY DIVERSE 3,4,5-SUBSTITUTED FURAN-2(5*H*)-ONES

Nourallah Hazeri[a*], Razieh Doostmohammadi[a], Belgheis Adrom[a], Mojtaba Lashkari[b], Malek Taher Maghsoodlou[a]

[a]*Faculty of Science, University of Sistan and Baluchestan, Zahedan P.O. Box 98135-674, Iran*
[b]*Faculty of Science, Velayat University, Iranshahr P.O. Box 9911131311, Iran*
**email: nhazeri@chem.usb.ac.ir; n_hazeri@yahoo.com*

Abstract. An eco-friendly and environmentally benign synthesis of 3,4,5-substituted furan-2(5*H*)-ones employing Iranian seedless barberry, known as Zereshk, (*Berberis integerrima* "Bidaneh", *Berberidaceae*) as a biocatalyst, was developed. For the first time, we found that the barberry juice could be effectively used for three-component condensation reaction of aldehydes, amines, and dialkyl acetylenedicarboxylates. The merits of this method include the environmentally friendly reaction conditions, simple operation, broad substrate, satisfying yields, and the generation of less waste rather than the conventional chemical reagents.

Keywords: three-component reaction, dialkyl acetylenedicarboxylates, furan-2(5*H*)-ones, aldehydes, barberry juice.

Received: August 2016/ Revised final: October 2016/ Accepted: October 2016

Introduction

In recent years, organic research has been mainly focused on the development of greener and eco-friendlier processes that involve the use of alternative reaction media to replace toxic and expensive catalysts or volatile and hazardous solvents like benzene, toluene and methanol, commonly used in organic synthesis. Nowadays, many organic transformations are carried out in water. Water is a unique solvent because it is readily available, inexpensive, nontoxic, and environmentally benign. The applications of an aqueous extract of different fruit juices have witnessed a rapid development. This growing interest in fruit juice is mainly rooted in its biocatalysts, nonhazardous, environmentally benign character, and cost effectiveness [1-3].

In recent years, chemical reactions using plant cell cultures and part of plants as biocatalysts received great attention [4-6]. This crescent interest is due to the wide biotechnological potential of the enzymatic reactions. The biocatalytical alteration using edible plants [7], plant root [8], plant tubers [9], edible plants [10] and plant leaves [11] extract can be applied in many organic reactions. Fruit juice is also a natural product that is used as biocatalysts in organic synthesis. Fruit juice is now being routinely used in organic synthesis as homogeneous catalysts for various selective transformations of simple and complex molecules [12].

Furanones are the five-membered heterocyclic compounds possessing lactone ring in their structures. These heterocycles are the core structures of many bioactive natural products, as well as synthetic drugs, such as rubrolide, sarcophine, benfurodil hemisuccinate, etc. The *5H*-Furan-2-one derivatives exhibit many pharmacological and biological activities including antifungal, antibacterial, anti-oxidants, anti-inflammatory, anti-microbial and anti cancer agents [13–17].

As a part of our efforts to develop new synthetic methods in heterocyclic chemistry [18-20], herein we report, for the first time, a three-component reaction of aldehydes, amines and dialkyl acetylenedicarboxylates for the synthesis of 3,4,5-substituted furan-2(5*H*)-one derivatives in barberry juice as an eco-friendly catalyst (Scheme 1). This approach offers an alternative method of construction of furanone architectures with potential biological activities based on a concise, rapid, and environmentally friendly vision.

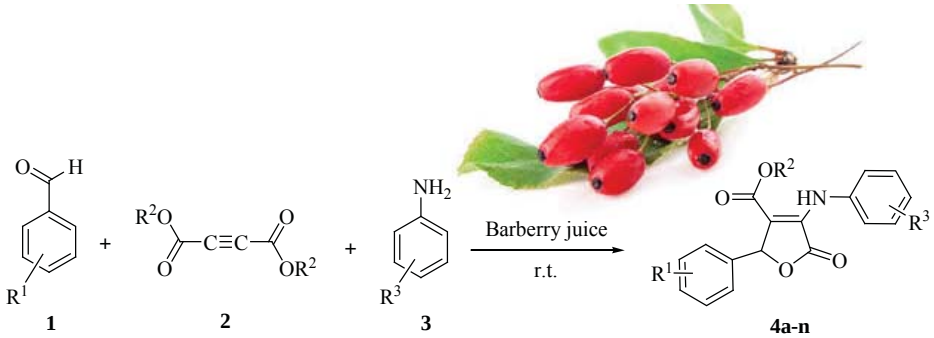

1 **2** **3** **4a-n**

Scheme 1. Synthesis of furan-2(5*H*)-one derivatives.

Results and discussion

In continuation of our work following the principles of green chemistry [17-20], we have developed a simple, efficient, and green protocol for the preparation of 3,4,5-substituted furan-2(5*H*)-one, using an extract of barberry as a green and inexpensive catalyst and solvent. Our approach reduces the use of hazardous organic solvents and uses simple and mild conditions with inherently lower costs.

Different types of barberry are well known around the world for several benefits, such as medical, ornamental and food uses. Iranian seedless barberry (*Berberis integerrima* ''Bidaneh'') is commercially cultivated for its fruit in Iran, especially in South Khorasan province. Currently, there are over 11,000 ha of cultivated seedless barberry, annually producing more than 9200 tonnes of dried fruit [21]. Some studies have found that barberry has some important bioactive components in roots and/or fruits, such as calcium, sodium, sulphur, iron, zinc, vitamin C, carbohydrates, organic acids and alkaloids, *e.g.* berberine and palmatine [22, 23].

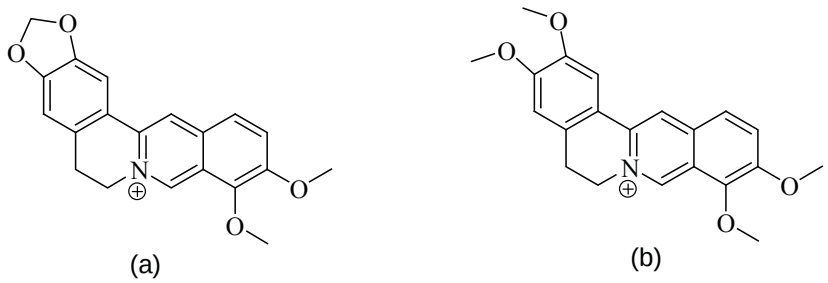

Figure 1. Chemical structures of berberine (a) and palmatine (b).

Among active components of barberry, the alkaloid berberine (Figure 1) occurring in bark of root, stem and unripe fruit, is considered the most important active constituent of the plant. Berberine, a yellow colour bitter substance [24], belongs to a large and diverse group of alkaloids called benzylisoquinolines [25]. Soluble sugars and berberine content of the barberry are one of its most important properties, since the value of the barberry is dependent on this content. The sugars were applied as an efficient and homogenous catalyst for multicomponent reaction in excellent yields [26,27].

Our further experiments have been designed to check the activities of some components of barberry juice on the synthesis of 3,4,5-substituted furan-2(5*H*)-one. For this purpose in separate experiments, components of barberry juice with the highest percentage, such as glucose, fructose, and vitamin C were selected. Investigations showed that the reaction occurred in the presence of all above components in good yield. Since the juice contains so many vitamins, ions and reducing sugars with different ratio and varieties, regarding to the mentioned experiment, it seems that a set of above agents are effective in occurring of this three component reaction.

At the beginning, a test reaction was performed using benzaldehyde **1** (1.0 mmol), aniline **3** (1.0 mmol) and dimethyl acetylenedicarboxylate **2** (1.0 mmol) in 5 mL juice of barberry at room temperature, in order to establish the real effectiveness of the catalyst/solvent, and the product was obtained in good yields.

In order to compare the strength of the juice of barberry and a catalyst with juice of various summer fruits, a model reaction was carried out between benzaldehyde **1** (1.0 mmol), aniline **3** (1.0 mmol) and dimethyl acetylenedicarboxylate **2** (1.0 mmol), using various fruit juices as catalysts at room temperature, and the results were summarized in Table 1.

Table 1

Optimization of catalyst for the synthesis of furan-2(5*H*)-ones.

Entry	*Solvent*	*pH*	*Time (h)*	*Isolated yield (%)*
1	H_2O	6.8	24	-
2	melon juice	5.8	6	50
3	blackberry juice	3.9	15	25
4	grapes juice	2.9	12	40
5	pomegranate juice	3.0	15	25
6	strawberries juice	3.2	24	-
7	peach juice	3.3	10	42
8	verjuice juice	3.5	16	38
9	**barberry juice**	**5.6**	**3**	**92**

Reaction conditions: benzaldehyde (1.0 mmol), aniline (1.0 mmol), dimethyl acetylenedicarboxylate (1.0 mmol) in various media at room temperature.

To explore the scope and generality of the presented multicomponent reaction protocol for the synthesis of 3,4,5-substituted furan-2(5*H*)-one under the optimized conditions, a variety of aromatic aldehydes containing electron donating or electron withdrawing substituents in the aromatic ring, such as -Me, -Cl, -OMe and -NO_2 were reacted with dialkyl acetylenedicarboxylate and various anilines to furnish diverse furan-2(5*H*)-one. The results were summarized in Table 3. In all cases, aromatic aldehydes with substituents carrying either electron-donating or electron-withdrawing groups reacted successfully and gave the products in high yields. It was found that aromatic aldehydes with electron-withdrawing groups reacted faster than those with electron-donating groups, as would be expected. The results were shown in Table 2.

Table 2

Synthesis of furan-2(5*H*)-one derivatives.

Entry	*R^1*	*R^2*	*R^3*	*Time (h)*	*Isolated yield (%)*	*Product*	*M.p. (°C)*	
							This work	*Lit. [Ref]*
1	Ph	CH_3	4-F-C_6H_4	2.5	70	4a	293–295	293–295 [13]
2	Ph	CH_3	4-Cl-C_6H_4	1.5	75	4b	150–152	149–152 [17]
3	Ph	CH_3	3-NO_2-C_6H_4	2.5	85	4c	178-181	179-182 [17]
4	4-NO_2-C_6H_4	CH_3	Ph	0.5	94	4d	128-130	130-131 [17]
5	Ph	CH_3CH_2	Ph	0.5	90	4e	163–165	164–166 [12]
6	4-Me-C_6H_4	CH_3CH_2	Ph	1	90	4f	119–121	120–121 [12]
7	4-OMe-C_6H_4	CH_3	Ph	1.5	67	4g	239–242	239–242 [17]
8	4-Me-C_6H_4	CH_3	Ph	2	85	4h	181–183	181–183 [13]
9	4-Cl-C_6H_4	CH_3	Ph	2	75	4i	149–152	149–152 [12]
10	Ph	CH_3	4-Me-C_6H_4	1	90	4j	284–287	284–287 [12]
11	Ph	CH_3CH_2	4-Me-C_6H_4	1	80	4k	185–186	188–191 [12]
12	Ph	CH_3CH_2	3-NO_2-C_6H_4	3	84	4l	208-210	208 [28]
13	4-Me-C_6H_4	*tert*-buthyl	Ph	2	90	4m	176-178	175-178 [28]
14	Ph	CH_3	Ph	0.5	96	4n	158-160	159–162 [13]
15	3-NO_2-C_6H_4	CH_3	Ph	1	95	4o	200–202	203–205 [13]
16	Ph	*tert*-buthyl	4-Me-C_6H_4	6	85	4p	185-187	-
17	Ph	*tert*-buthyl	4-Cl-C_6H_4	10	84	4q	169-171	-
18	Ph	*tert*-buthyl	4-F-C_6H_4	10	83	4r	170-173	-

A proposed mechanism for the discussed transformation can be combined with the nucleophilic Michael addition, iminium-enamine tautomerization and *γ*-lactonization [16-20] (Scheme 2).

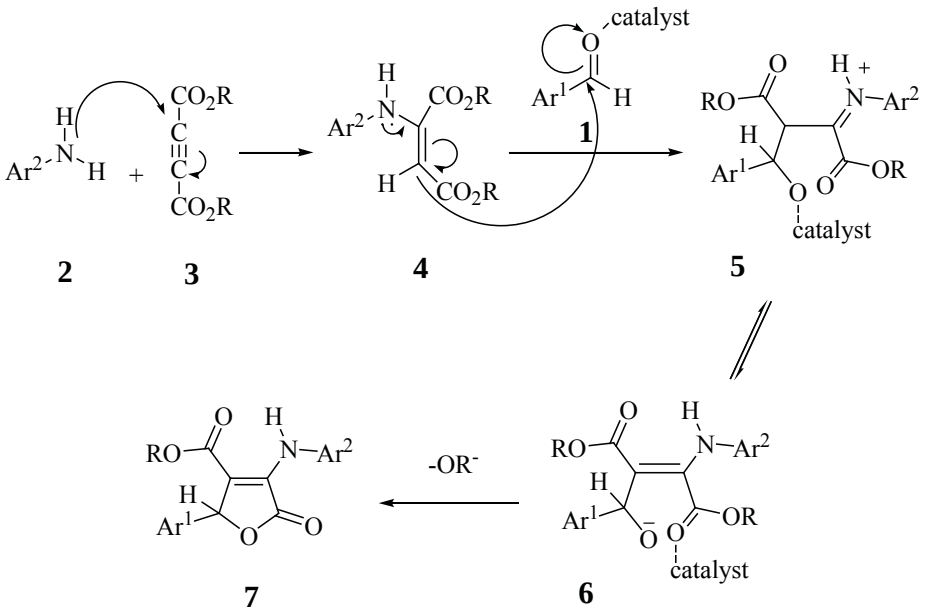

Scheme 2. Suggested mechanism for synthesis of furan-2(5*H*)-ones.

The structures of new compounds presented in Table 3 were deduced on the basis of IR, ^{1}H and ^{13}C NMR spectroscopy, mass spectrometry, and elemental analysis. The mass spectrum of compound *tert*-butyl 4-(*p*-tolylamino)-2,5-dihydro-5-oxo-2-phenylfuran-3-carboxylate **4p**, displayed the molecular ion peak at *m/z* = 365 that is consistent with the proposed structure. The ^{1}H NMR spectrum of this product exhibited a singlet at δ = 1.35 ppm and singlet at δ = 2.25 ppm for *tert*-butyl protons of the carboxylate group and one sharp singlet arising from benzylic proton at δ = 5.63 ppm. The aromatic protons of product were observed at δ = 7.06-7.35 ppm. A broad singlet for the NH group at δ = 9.09 ppm indicated intra-molecular hydrogen bond formation with the vicinal carbonyl group. The ^{13}C NMR spectrum of this product showed 16 distinct resonances consistent with the proposed structure. The IR spectrum indicated one sharp peak at 3305 cm^{-1} for NH within the product. To compare the applicability and efficiency of barberry juice with the reported catalysts in the literature for the synthesis of 3,4,5-substituted furan-2(5*H*)-ones, we have tabulated the results of these catalysts in Table 3. As shown in Table 4, barberry juice can act as an efficient catalyst in terms of reaction time and yield of products.

Table 3

Comparison of using barberry juice and the reported catalysts for the synthesis of 3,4,5-substituted furan-2(5*H*)-ones 4n.

Entry	*Product*	*Catalyst*	*Time (h)*	*Yield (%)*	*Reference*
1	**4n**	nano-ZnO	2.5	94	[16]
2		$Al(HSO_4)_3$	8	84	[15]
3		$SnCl_2.2H_2O$	6.5	90	[14]
4		$[Bu_4N][HSO_4]$	5	92	[19]
5		PPA/SiO_2	1	90	[18]
6		sucrose	9	97	[27]
7		barberry juice	0.5	96	This work

Conclusions

In conclusion, we have found that the aqueous extract of barberry is as an efficient, economical, and environmentally-friendly catalyst for the synthesis of 3,4,5-substituted furan-2(5*H*)-ones. The high yield of products in a short reaction time with high purity, mild reaction conditions, and a simple workup procedure make this procedure attractive. The use of barberry juice both as a solvent and biodegradable catalyst is the attractive feature of this protocol. Furnishing pure products by simple filtration makes an aqueous approach possible for large scale preparation of furan-2(5*H*)-ones.

Experimental

Melting points and IR spectra of all compounds were measured on an Electrothermal 9100 apparatus and a JASCO FTIR 460 Plus spectrometer respectively. The ^{1}H and ^{13}C NMR spectra were obtained on Bruker DRX-400 Avance instruments with $CDCl_3$ as a solvent. Mass spectra were recorded on an Agilent Technology (HP) spectrometer operating at an ionization potential of 70 eV. Samples of fruits were blended using a laboratory electrical blender (Model 32BL79, Waring, USA). All reagents and solvents obtained from Fluka and Merck were used without further purification**.**

Plant material

Eight samples of fruits were purchased from the local commercial market, collected in the period between July and August (2013) in the region of the South of Sistan and Baluchestan and South Khorasan, Iran. The purchased samples were washed and drained. The skins of them except blackberry and barberry were peeled and the rest of the fruit was cut into 3 cm cubes. The seeds were then removed and all flesh parts were blended using a laboratory electrical blender (Model 32BL79, Waring, USA). The obtained juice was vacuum- filtered and then transferred into a beaker**.**

General procedure for the synthesis of furan-2(5H)-one derivatives

The mixture of aldehyde (1.0 mmol), amine (1.0 mmol), dialkyl acetylenedicarboxylate (1.0 mmol) and 5 mL juice of barberry were stirred at room temperature. After completion of the reaction (monitored by thin-layer chromatography, TLC), the reaction products were collected by filtration. The products were washed with water/ethanol (1:1, 3×2 mL) to give the corresponding pure compounds. The catalyst remained in the water/ethanol filtrate.

Methyl 2,5-dihydro-5-*oxo*-2-phenyl-4-(phenylamino)furan-3-carboxylate (4n). White solid: 0.296 g (96 %); m.p. 158-160 °C; IR (KBr): 3260, 3208, 1702, 1661 cm^{-1}; ^{1}H NMR (400 MHz, $CDCl_3$) δ, ppm: 3.77 (s, 3H, OCH_3), 5.76 (s, 1H, $H_{benzylic}$), 7.13 (t, J = 7.3 Hz, $1H_{aromatic}$), 7.24-7.31 (m, 6H), 7.52 (d, J = 8 Hz, 2H, $H_{aromatic}$), 8.90 (br, 1H, NH).

***Tert*-butyl 4-(*p*-tolylamino)-2,5-dihydro-5-*oxo*-2-phenylfuran-3-carboxylate (4p).** Colorless solid; 0.287 g (85 %); m.p. 185-187 °C; IR (KBr): 3305, 3030, 1690, 1666 cm^{-1}; ^1H NMR (400 MHz, $CDCl_3$) δ, ppm: 1.35 (s, 9H, CH_3), 2.25 (s, 3H, CH_3), 5.63 (s, 1H, $H_{benzylic}$), 7.06-7.35 (m, 9H, $H_{aromatic}$), 9.09 (br, 1H, NH); ^{13}C NMR (100 MHz, $CDCl_3$) δ, ppm: 165.1 and 162.9 (CO of ester), 157.0, 135.6, 135.4, 133.7, 129.5, 128.4, 128.5, 127.6, 122.5, 114.3 (10 $C_{aromatic}$), 83.2 (C-O), 61.8 ($C_{benzylic}$), 27.9 (3 CH_3), 20.9 (CH_3); MS m/z (%): 57 (42), 77 (25), 102 (39), 130 (100), 158 (42), 175 (24), 263 (29), 291 (39), 309 (52), 365 (M^+, 28).

***Tert*-butyl 4-(4-chlorophenylamino)-2,5-dihydro-5-*oxo*-2-phenylfuran-3-carboxylate (4q).** Colourless solid; 0.268 g (84 %); m.p. 169-171 °C; IR (KBr): 3315, 3095, 2975, 1690, 1655 cm^{-1}; ^1H NMR (400 MHz, $CDCl_3$) δ, ppm: 1.36 (s, 9H, CH_3), 5.64 (s, 1H, $H_{benzylic}$), 7.18-7-47 (m, 9H, $H_{aromatic}$), 9.36 (br, 1H, NH); ^{13}C NMR (100 MHz, $CDCl_3$) δ, ppm: 165.0, 162.9 (C_{ester}), 156.6, 134.96, 134.95, 131.0, 129.0, 128.68, 128.60, 127.5, 123.3, 114.6 (10 $C_{aromatic}$ and C_{vinyl}), 83.5 (C-O), 61.6 ($C_{benzylic}$), 27.9 (CH_3); MS m/z (%): 57 (48), 77 (34), 102 (46), 130 (100), 158 (32), 175 (76), 284 (36), 329 (92), 311 (45), 385 (M^+, 33), 387 (M^++2, 12), 389 (M^++4, 0.5).

***Tert*-butyl 4-(4-fluorophenylamino)-2,5-dihydro-5-*oxo*-2-phenylfuran-3-carboxylate (4r).** Colourless solid; 0.232 g (83 %); m.p. 170-173 °C; IR (KBr): 3260, 3145, 2970, 1689, 1650 cm^{-1}; ^1H NMR (400 MHz, $CDCl_3$) δ, ppm: 1.35 (s, 9H, CH_3), 5.61 (s, 1H, $H_{benzylic}$), 6.94-7.43 (m, 9H, $H_{aromatic}$) 9.37 (br, 1H, NH); ^{13}C NMR (100 MHz, $CDCl_3$) δ, ppm: 165.1, 162.9 (CO_{ester}), 160.2 (d, J_{CF} =245.9 Hz), 156.8, 135.0, 132.3 (d, J_{CF} =3.0 Hz), 128.6, 128.5, 127.6, 124.4 (d, J_{CF} =8.4 Hz), 115.8 (d, J_{CF} =22.6 Hz), 114.5 (10 $C_{aromatic}$ and C_{vinyl}), 83.3 (C-O), 62.0 ($C_{benzylic}$), 27.9 (CH_3); MS m/z (%): 57 (76), 77 (30), 102 (43), 130 (100), 158 (41), 175 (76), 268 (42), 295 (29), 313 (88), 361 (51), 369 (M^+, 29).

Supplementary information

Supplementary data are available free of charge at http://cjm.asm.md as PDF file.

Acknowledgments

We gratefully acknowledge the financial support from the Research Council of the University of Sistan and Baluchestan.

References

1. van der Plas, H.C.; Tramper, J.; Linko, P. Eds. Biocatalysts in Organic Syntheses. 1st Edition. Elsevier: Amsterdam, 1985, 25 p.
2. Baldassare, F.; Bertoni, G.; Chiappe, C.; Marioni, F. Preparative synthesis of chiral alcohols by enantioselective reduction with daucus carota root as biocatalyst. Journal of Molecular Catalysis B: Enzymatic, 2000, 11, pp. 55−58.
3. Koeller, K.M.; Wong, C.H. Enzymes for chemical synthesis. Nature, 2001, 409(6817), pp. 232−240.
4. Giri, A.; Dhinga, V.; Giri, C.C.; Singh, A.; Ward, O.P.; Narasu, M.L. Biotransformations using plant cells, organ cultures and enzyme systems: current trends and future prospects. Biotechnology Advances, 2001, 19(3), pp. 175-199.
5. Villa, R.; Molinari, F.; Levati, M.; Aragozzini, F. Stereoselective reduction of ketones by plant cell cultures. Biotechnology Letters, 1998, 20(12), pp. 1105-1108.
6. Bruni, R.; Fantin, G.; Medici, A.; Pedrini, P.; Sacchetti, G. Plants in organic synthesis: an alternative to baker's yeast. Tetrahedron Letters, 2002, 43(18), pp. 3377-3379.
7. Comasseto, J.V.; Omori, A.T.; Porto, A.L. M.; Andrade, L.H. Preparation of chiral organochalcogeno-*α*-methylbenzyl alcohols via biocatalysis. The role of *Daucus carota* root. Tetrahedron Letters, 2004, 45(3), pp. 473-476.
8. Yadav, J.S.; Reddy, T.; Nanda, S.; Rao, A.B. Stereoselective synthesis of (*R*)-(−)-denopamine, (*R*)-(−)-tembamide and (*R*)-(−)-aegeline via asymmetric reduction of azidoketones by *Daucus carota* in aqueous medium. Tetrahedron: Asymmetry, 2002, 12(24), pp. 3381-3385.
9. Mironowicz, A. Biotransformations of racemic acetates by potato and topinambur tubers. Phytochemistry, 1998, 47(8), pp. 1531-1534.
10. Andrade, L.H.; Utsunomiya, S.; Omori, A.T.; Porto, A.L.M.; Comasseto, J.V. Edible catalysts for clean chemical reactions: Bioreduction of aromatic ketones and biooxidation of secondary alcohols using plants. Journal of Molecular Catalysis B: Enzymatic, 2006, 38(2), pp. 84-90.
11. Silver, G.M.; Fall, R. Enzymatic synthesis of isoprene from dimethylallyl diphosphate in aspen leaf extracts. Plant Physiology, 1991, 97(4), pp. 1588-1591.
12. Pore, S.; Rashimkar, G.; Mote, K.; Salunkhe, R. Aqueous extract of the pericarp of *Sapindus trifoliatus* fruits: Anovel 'green' catalyst for the aldimine synthesis. Chemistry & Biodiversity, 2010, 7, pp. 1796-1800.
13. Narayana Murthy, S.; Madhav, B.; Vijay Kumar, A.; Rama Rao, K.; Nageswar, Y.V.D. Facile and efficient synthesis of 3,4,5-substituted furan-2(5*H*)-ones by using *β*-cyclodextrin as reusable catalyst. Tetrahedron, 2009, 65(27), pp. 5251-5256.
14. Nagarapu, L.; Kumar, U.N.; Upendra, P.; Bantu, R. Simple, Convenient method for the synthesis of substituted furan-2(5*H*)-one derivatives using tin(ii) chloride. Synthetic Communications, 2012, 42(14), pp. 2139-2148.

15. Mohammad Shafiee, M.R.; Mansoor, S.S.; Ghashang, M.; Fazlinia, A. Preparation of 3,4,5-substituted furan-2(5*H*)-ones using aluminum hydrogen sulfate as an efficient catalyst. Comptes Rendus Chimie, 2014, 17(2), pp. 131-134.
16. Tekale, S.U.; Kauthale, S.S.; Pagore, V.P.; Jadhav, V.B.; Pawar, R.P. ZnO nanoparticle-catalyzed efficient one-pot three-component synthesis of 3,4,5-trisubstituted furan-2(5*H*)-ones. Journal of the Iranian Chemical Society, 2013, 10(6), pp. 1271-1277.
17. Ramesh, S.; Nagarajan, R. Efficient one-pot multicomponent synthesis of (carbazolylamino)furan-2(*5H*)-one and carbazolyltetrahydropyrimidine derivatives. Synthesis, 2011, 20, pp. 3307–3317.
18. Doostmohammadi, R.; Hazeri, N. Application of silica gel-supported polyphosphoric acid (PPA/SiO_2) as a reusable solid acid catalyst for one-pot multi-component synthesis of 3,4,5-substituted furan-2(5*H*)-ones. Letters in Organic Chemistry, 2013, 10(3), pp. 199-203.
19. Doostmohammadi, R.; Maghsoodlou, M.T.; Hazeri, N.; Habibi-Khorassani, S.M. An efficient one-pot multi-component synthesis of 3,4,5-substituted furan-2(5*H*)-ones catalyzed by tetra-*n*-butylammonium bisulfate. Chinese Chemical Letters, 2013, 24(10), pp. 901-903.
20. Adrom, B.; Hazeri, N.; Maghsoodlou, M.T.; Mollamohammadi, M. Ecofriendly and efficient multicomponent method for preparation of 1-amidoalkyl-2-naphthols using maltose under solvent-free conditions. Research on Chemical Intermediates, 2015, 41(7), pp. 4741-4747.
21. Rezaei, M.; Ebadi, A.; Reim, S.; Reza, F.; Balandary, A.; Farrokhi, N.; Hanke, M.V. Molecular analysis of Iranian seedless barberries via SSR. Scientia Horticulturae, 2011, 129(4), pp. 702-709.
22. Gundogdu, M. Determination of antioxidant capacities and biochemical compounds of *Berberis vulgaris L*. fruits. Advances in Environmental Biology, 2013, 7(2), pp. 344-348.
23. Pozniakovskiĭ, V.M.; Golub, O.V.; Popova, D.G.; Kovalevskaia, I.N. The use of barberry berries in human nutrition. Voprosy pitaniia, 2003, 72(4), pp. 46-49 (in Russian).
24. Arayne, S.M.; Sultana, N.; Bahadur, S.S.; Pak. J. The berberis story: *Berberis vulgaris* in therapeutics. Pakistan Journal of Pharmaceutical Sciences, 2007, 20(1), pp. 83-92.
25. Kutchan, T.M. Alkaloid biosynthesis-the basis for metabolic engineering of medicinal plants. The Plant Cell, 1995, 7(7), pp. 1059-1070.
26. Mousavi, M.R.; Hazeri, N.; Maghsoodlou, M.T.; Salahi, S.; Habibi-Khorassani, S.M. Entirely green protocol for the synthesis of *β*-aminoketones using saccharose as a homogenous catalyst. Chinese Chemical Letters, 2013, 24(5), pp. 411-414.
27. Hazeri, N.; Maghsoodlou, M.T.; Mahmoudabadi, N.; Doostmohammadi, R.; Salahi, S. Sucrose as an environmental and economical catalyst for the synthesis of 2(*5H*) furanone. Current Organocatalysis, 2014, 1(1), pp. 45-60.
28. Adrom, B.; Maghsoodlou, M.T.; Lashkari, M.; Hazeri, N.; Doostmohammadi, R. Efficient one-pot three-component synthesis of 3,4,5-substituted furan-2(*5H*)-ones catalyzed watermelon juice. Synthesis and Reactivity in Inorganic, Metal-Organic, and Nano-Metal Chemistry, 2016, 46(3), pp. 423-427.

CHEMISTRY JOURNAL OF MOLDOVA. General, Industrial and Ecological Chemistry. 2016, 11(2), 74-83
http://cjm.asm.md
http://dx.doi.org/10.19261/cjm.2016.11(2).10

REMOVAL OF METHYLENE BLUE BY ADSORPTION ONTO *RETAMA RAETAM* PLANT: KINETICS AND EQUILIBRIUM STUDY

Dalila Badis[a], Zoubir Benmaamar[b*], Othmane Benkortbi[a], Houcine Boutoumi[c], Houria Hamitouche[b], Amele Aggoun[c]

[a]*Biomaterials and Transport Phenomena Laboratory, University of Dr Yahia Fares, Ain d'hab, Medea 26000, Algeria*
[b]*Hydrogen Energetical Application Laboratory, University of Blida1, Soumaa, Blida 9000, Algeria*
[c]*Chemical Engineering Laboratory, University of Blida1, Soumaa, Blida 9000, Algeria*
**e-mail: benmaamarzoubir@yahoo.fr*

Abstract. The feasibility of using medicinal plants species *Retama raetam* as a low cost and an eco-friendly adsorbent for the adsorption of cationic dye methylene blue from simulated aqueous solution has been investigated. Adsorption kinetics of methylene blue onto *Retama raetam* plants was studied in a batch system. The effects of pH and contact time were examined. The methylene blue maximum adsorption occurred at pH 8 and the lowest adsorption occurred at pH 2. The apparent equilibrium was reached after 120 min. Optimal experimental conditions were determined. Adsorption modelling parameters for Freundlich and Langmuir isotherms were determined and, based on R^2, various error distribution functions were evaluated as well. Adsorption isotherm was best described by non linear Freundlich isotherm model. Thermodynamic studies show that adsorption was spontaneous and exothermic. For determining the best-fit-kinetic adsorption model, the experimental data were analyzed by using pseudo-first-order, pseudo-second-order, pseudo-third-order, Esquivel, and Elovich models. Linear regressive and non-linear regressive method was used to obtain the relative parameters. The statistical functions were estimated to find the suitable method that fit better the experimental data. Both methods were appropriate for obtaining the parameters. The linear pseudo-second-order (type 9 and type 10) models were the best to fit the equilibrium data. The present work showed that plant *Retama raetam* can be used as a low cost adsorbent for the removal of methylene blue from water.

Keywords: *Retama raetam*, methylene blue, removal, modelling, adsorption.

Received: June 2016/ Revised final: November 2016/ Accepted: November 2016

Introduction

The textile industry is one of industrial waste water source. This contaminated water is very toxic for the humans and animals [1]. Methylene blue is used in colouring paper, dyeing cottons, wools, silk, leather and coating for paper stock. Although methylene blue is not strongly hazardous, it can cause some harmful effects, such as heartbeat increase, vomiting, shock, cyanosis, jaundice, quadriplegia, and tissue necrosis in human organisms [2].

Chemical coagulation–flocculation [3], different types of oxidation processes [4], biological process [5], membrane-based separation processes [6] and adsorption [7] were the treatments used in the purification of waters. The most efficient method used for the quickly removal of dyes from the aqueous solution is the physical adsorption [8]. Biosorbents, such as wood sawdust [9], waste-biomass [10], delonix regia [11], agricultural solid waste [12], are able to remove efficiently the colour from water.

Retama raetam plants can be used as biosorbent. This species belonging to the *Fabaceae* family has a very productive vertical and horizontal root system, which can reach 20 m. This, in turn, increases substantially the stabilization of the soil. Moreover, the *Retama* species contributes to the biofertilisation of poor grounds, because of their aptitude to associate with fixing nitrogen bacteria *Rhizobia*. Therefore, the genus of *Retama* is included in a re-vegetation program for degraded areas in semi-arid Mediterranean environments [13].

Retama raetam is a common plant in the North African and East Mediterranean region. In Algeria, it is located in Sahara and Atlas regions and is used in folk medicine under the common name "R'tam" to reduce the blood glucose and skin inflammations, while in Lebanon it is used as folk herbal medicine against joint aches and in Morocco against skin diseases. Previous pharmacological studies on the plant have revealed its various medicinal properties: antibacterial, antifungal, antihypertensive, antioxidant, antiviral, diuretic, hypoglycaemic, hepatoprotective, nephroprotective and cytotoxic effects. *Retama* species have been reported to contain flavonoids and alkaloids [14].

However, there are no reported studies on the adsorption of cationic dyes by *Retama raetam*. This work aims to understand the potential of *Retama raetam* for removal of methylene blue dye from simulated aqueous solution in batch mode. The adsorption efficiency of methylene blue was investigated in order to optimize the experimental parameters. The statistical functions were used to estimate the error deviations between experimental and theoretically predicted adsorption values, including linear and non-linear method. The optimization procedure required a defined error function in order to evaluate the fit of equation to the experimental data.

Experimental

Materials

Methylene blue (3,7-bis (Dimethylamino)-phenazathionium chloride tetramethylthionine chloride, $C_{16}H_{18}N_3SCl{\cdot}3H_2O$, Mw =373.9 g/mol, Figure 1) used in the present study was purchased from Merck (Germany), being selected from the list of dyes normally used in Algeria. *Retama raetam* plants were collected in Mostaganem region (Algeria), washed several times with deionized water to remove the color and dried at 105°C for 5 h in a convection oven. The residual organics and lipids were respectively removed by methanol and petroleum ether. After this procedure, *Retama raetam* was washed again with distilled water.

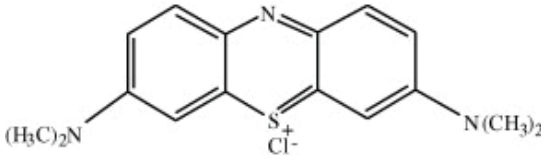

Figure 1. Structure of methylene blue [15].

Methods

The *Retama raetam* was characterized by pH measurement of the pH_{PZC} (point of zero charge). The pH_{PZC} of an adsorbent is a very important characteristic that determines the pH, at which the adsorbent surface has net electrical neutrality [16].

The pH_{PZC} of *Retama raetam* was measured by pH drift method: 0.1 mg of *Retama raetam* is added to 100 mL of water with varying pH from 2 to 12 and stirred for 24 h. Final pH of the solution is plotted against initial pH of the solution and shown in Figure 2 [17]. The value of pH_{PZC} for *Retama raetam* was determined as pH 6.

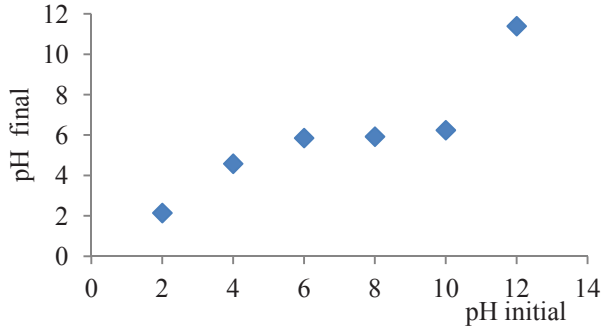

Figure 2. Point of zero charge (pH_{PZC}) of the *Retama raetam* used for the adsorption experiments.

Adsorption isotherms are important for the description of how adsorbates interact with an adsorbent being also critical in optimizing the use of adsorbent. Thus, the correlation of equilibrium data using either a theoretical or empirical equation is essential for interpretation of the adsorption data and prediction, as well. Several mathematical models can be used to describe experimental data of adsorption isotherms. Two famous isotherm equations, the Langmuir and Freundlich, were employed for further interpretation of the obtained adsorption data.

Adsorption kinetics of methylene blue onto *Retama raetam* was studied in a batch system. The effects of pH and equilibrium time were examined. The adsorption parameters were optimized. In each experiment pre weighed amount of adsorbent (0.04 g) was added to 200 mL of dye solution (20 mg/L) taken in a conical flask of 250 mL and 0.1 M NaOH or 0.1 M HCl were added to adjust the pH value. This solution was agitated at 300 rpm and centrifuged. The methylene blue concentration in solution was determined at λ_{max} = 665 nm by using UV-1700 PHARMA SPEC SHIMADZU spectrophotometer. The adsorbed amount of methylene blue per mass unit of adsorbent at time t, q (mg/g), (Eq.(1)) and the dye removal efficiency (R, %) (Eq.(2)) were calculated as:

$$q = (C_0 - C)\frac{V}{M} \quad (1)$$

$$R = \frac{(C_0 - C)}{C_0} \times 100 \quad (2)$$

where C_0 is the initial concentration of methylene blue (mg/L), C is the dye concentration at time t, V is the solution volume (L) and M is the adsorbent mass (g) [18].

The effect of pH was evaluated by mixing 0.2 g of adsorbent with 1 L of methylene blue simulated aqueous solution of 20 mg/L. The pH value of solution was varied from 2 to 13, by adding 0.1M NaOH or 0.1M HCl solutions. The suspension was shaken for 24h at 25°C.

Kinetic experiments were performed by mixing 200 mL of dye solution (20 mg/L) with 0.04 g of adsorbent for different time (5, 10, 30, 60, 90, 120, 150, and 180 min). The initial pH for each dye solution was set at 8. Methylene blue concentration in the supernatants was determined and the adsorbed amount of methylene blue was calculated.

Results and discussion

For studying the effect of every parameter, it is necessary to fix the values of other ones. The elimination of pollutant from simulated aqueous solution by adsorption is extremely influenced by the medium of solution, which affects the nature of the adsorbent surface charge, the ionization extent, the aqueous adsorbate species speciation and the adsorption rate. The adsorptive process through functional groups dissociation on the adsorbate and adsorbent were affected by a pH change [19]. The adsorption of methylene blue augments with increasing the pH of the solution. According to the data presented in Figure 3, the best value of adsorption capacity, q_e = 9.938 mg/g, was recorded at pH 8. From this study, it is obvious that in the basic medium, the negatively charged species tend to dominate leading to a more negatively charged surface. In this case, the adsorbent surface is negatively charged. The methylene blue adsorption increases due to the enhancement of electrostatic attractions between the negative charge of *Retama raetam* particles and the positive charge of methylene blue species.

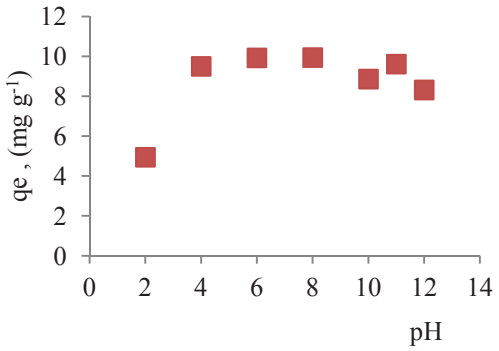

Figure 3. Effect of the initial pH of solution on equilibrium adsorption capacity of *Retama raetam*.

The experimental data for methylene blue adsorption on *Retama raetam* were analyzed with the Freundlich and Langmuir equations. Equations of these models [20] are presented in Table 1, where q is the equilibrium dye concentration on adsorbent (mg/g), q_m is the monolayer capacity of the adsorbent (mg/g), C is the equilibrium dye concentration in solution (mg/L), K_L is the Langmuir adsorption constant representing the energy constant related to the heat of adsorption, n and K_F are Freundlich constants related to adsorption intensity of the adsorbent and adsorption. A non-linear and linear fitting procedure using Excel and Origin software were used, respectively. The constants of all models were given in Table 2.

Table 1

Adsorption isotherms models and their linear and non linear forms [20].

Applied model	*Non linear form*	*Linear form*
Langmuir	$\frac{q}{q_m} = \frac{K_L C}{1 + K_L C}$	$\frac{C}{q} = \frac{C}{q_m} + \frac{1}{k_L q_m}$
Freundlich	$q = K_F C^{1/n}$	$\ln(q) = \ln(k_F) + n \ln(C)$

The coefficient of correlation indicated that Freundlich isotherm fitted the experimental data better than Langmuir isotherm. Good agreement between the experimental isotherms and the Freundlich model was found in the case of systems: pentachlorophenol/(M)Al-MCM-41 [21], and toluene/activated carbon [22].

The optimization procedure required a defined error function in order to evaluate the fit of equation to the experimental data. The best-fitting equation is determined using the well-known special functions to calculate the error deviation between experimental and predicted data. The mathematical equations of these error functions were illustrated in Table 3.

Table 2

Constants for linear and non-linear Langmuir and Freundlich isotherms related to the adsorption of methylene blue onto *Retama raetam*.

Model	*Linear method*	*Non-linear method*
Langmuir model		
q_m	- 142.857 < 0	$3.986 \cdot 10^{+6}$
K_1	- 0.350 < 0	$4.811 \cdot 10^{-44}$
R^2	0.609	0.799
Freundlich model		
k_F	115.353	96.837
n	1.806	0.483
R^2	0.989	0.967

Table 3

Mathematical equations of error functions.

Error functions	*Equations*	*Reference*
ARED	$ARED = \frac{100}{n}\sum_{i=1}^{n}\left\lvert\frac{q_{\exp}-q_{calc}}{q_{\exp}}\right\rvert_i$	[23]
ARE	$ARE = \frac{\sum\left\lvert(q_{calc}-q_{\exp})/q_{\exp}\right\rvert}{n}$	[24]
SAE = EABS	$SAE = EABS = \sum_{i=1}^{n}\left\lvert q_{\exp}-q_{calc}\right\rvert$	[25]
ARS	$ARS = \sqrt{\frac{\sum\left[\left(q_{\exp}-q_{calc}\right)/q_{\exp}\right]^2}{(n-1)}}$	[26]
MPSD	$MPSD = 100\sqrt{\frac{\sum\frac{\left[\left(q_{\exp}-q_{calc}\right)\right]^2}{q_{\exp}}}{n-p}}$	[27]
Δq(%)=100*ARS	$\Delta q(\%) = 100\sqrt{\frac{\sum\left[\left(q_{\exp}-q_{calc}\right)/q_{\exp}\right]^2}{(n-1)}}$	[28]
SSE	$SSE = \sum\left(q_{calc}-q_{\exp}\right)^2$	[29]
MPSED	$MPSED = \sqrt{\frac{\sum\left[\left(q_{\exp}-q_{calc}\right)/q_{\exp}\right]^2}{(n-p)}}$	[20]
HYBRID	$HYBRID = \frac{1}{(n-P)}\sum_{i=1}^{n}\left\lvert\frac{q_{\exp}-q_{calc}}{q_{\exp}}\right\rvert_i$	[30]

where n is the number of experimental data points, q_{calc} is the predicted (calculated) quantity of methylene blue adsorbed onto *Retama raetam*, q_{exp} is the experimental data, p is the number of parameters in each kinetic model, *ARED* is the average relative error deviation (dimensionless parameter), *ARE* is the average relative error (dimensionless parameter), *ARS* is the average relative standard error (dimensionless parameter), *HYBRID* is the hybrid fractional error function (dimensionless parameter), *MPSD* Marquardt's is the percent standard deviation (dimensionless parameter), *MPSED* Marquardt's is the percent standard deviation (dimensionless parameter), *SAE=EABS* is the sum of absolute error (mg/g), *SSE* is the sum of the squares of the errors $(mg/g)^2$, and $\Delta q(\%)$ is the normalized standard deviation (mg/g). The constants of all error analysis are represented in Table 4.

Table 4

Error deviation data related to the adsorption of methylene blue onto *Retama raetam* employing the most commonly used functions.

Error functions	*ARED*	*SAE = EABS*	*MPSED*	*SSE*	*HYBRID*	*ARE*	*ARS*	*Δq(%)= 100*ARS*	*MPSD*
Linear Freundlich model	113.162	1064.355	1.966	313447.05	1.383	1.131	1.865	186.493	1051.57
Non Linear Freundlich model	22.899	277.32	0.285	13850.819	0.28	0.229	0.27	27.028	254.777

The data of adsorption isotherm are essentially required for designing the adsorption systems. In order to optimize the design of a specific sorbate/sorbent system for removal of methylene blue from aqueous solution, it is important to establish the most appropriate correlation for the experimental kinetic data. Applicability of some statistical tools to predict the optimum adsorption isotherms of methylene blue onto *Retama raetam* after linear regression analysis showed that the highest R^2 value and the lowest *ARED, ARE, SAE, ARS, MPSD, Δq, SSE, MSPED* and *HYBRID* values can be suitable and meaningful tools to predict the best-fitting equation models.

The best fitting is determined based on the use of these functions for calculation of the error deviation between experimental and predicted equilibrium adsorption isotherm data, after linear analysis. Hence, according to Table 4, it seems that the linear Freundlich model was the most suitable mode to describe satisfactorily the studied adsorption phenomenon. Therefore, based on the mentioned results, the best useful error estimation statistical tools point out the non linear Freundlich model, followed by linear Freundlich model, as the best-fitting models.

In order to better understand the effect of temperature on the adsorption of methylene blue onto *Retama raetam*, the free energy change (ΔG°, J mol^{-1}), enthalpy change (ΔH°, J mol^{-1}) and entropy change (ΔS°, J K^{-1} mol^{-1}) were determined (such parameters reflect the feasibility and spontaneous nature of the process) using Eqs.(3)-(5).

$$\Delta G^\circ = \Delta H^\circ - T\Delta S^\circ \tag{3}$$

$$\Delta G^\circ = -RTLn\left(K_c\right) \tag{4}$$

The combination of Eqs.(3) and (4) gives Eq.(5):

$$Ln(K_c) = \frac{\Delta S^\circ}{R} - \frac{\Delta H^\circ}{RT}\frac{1}{T} \tag{5}$$

where R is the universal gas constant (8.314 J K^{-1} mol^{-1}), T is the absolute temperature (Kelvin) [31]. Experiments were performed using 20 mg/L dye solutions with 0.2 g of *Retama raetam* for 24 h at various temperatures. The apparent equilibrium constant K_c of the adsorption is defined as Eq.(6) [20]:

$$K_c = \frac{(C_o - C_e)}{C_e}\frac{V}{M} = \frac{q_e}{C_e} \tag{6}$$

The enthalpy and entropy can be obtained from the slope and intercept of the linear plot of lnK_c versus $1/T$. The obtained thermodynamic parameters are given in Table 5.

Table 5

Calculated thermodynamic parameters for adsorption of methylene blue onto *Retama raetam*.

	Temperature (K)					
	293	*303*	*323*	*333*	*343*	*363*
K_c (L/mol)	$5.174\cdot10^5$	$3.204\cdot10^5$	$1.150\cdot10^5$	$0.729\cdot10^5$	$0.435\cdot10^5$	$0.134\cdot10^5$
ΔG° (kJ mol^{-1})	-26.744	-26.117	-24.863	-24.237	-23.610	-22.356
ΔH° (kJ mol^{-1})	$-4.511\cdot10^5$					
ΔS° (J K^{-1} mol^{-1})	-62.687					
R^2	0.989					

A negative enthalpy value of $-4.511 \cdot 10^5$ kJ/mol indicates that adsorption was exothermic. A negative entropy value of -62.687 J/mol and a negatively decreasing Gibbs free energy indicates the increase in the randomness in the solid–liquid interface and adsorption spontaneity [32].

Figure 4 illustrates the effect of contact time on decolorization (dye adsorption) with *Retama raetam*. The plot (simulated aqueous solution) can be divided in three zones: (i) 0-30 min, which indicate the fast adsorption of methylene blue, suggesting a rapid external diffusion and surface adsorption; (ii) 30-60 min, show a gradual equilibrium, and (iii) 60-180 min, indicate the plateau of the equilibrium state. The adsorption was rapid at the initial stage of the contact, but it gradually slowed down until the equilibrium. The fast adsorption at the initial stage can be attributed to the fact that a large number of surface sites are available for adsorption. After a lapse of time, the remaining surface sites are difficult to be occupied.

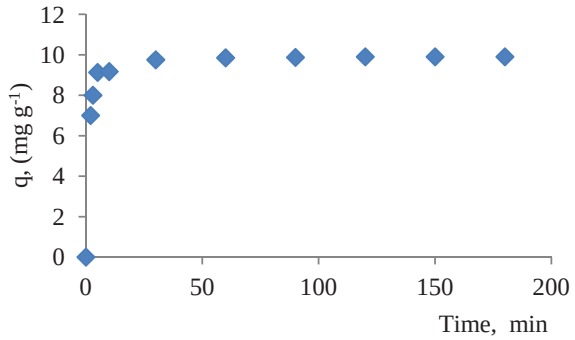

Figure 4. Adsorption kinetics of methylene blue on *Retama raetam*.

Adsorption is a complex process that is influenced by several parameters related to adsorbent and to the physicochemical conditions, under which the process is carried out [33]. For understanding the mechanism of the adsorption process, the following equations: pseudo-first order (Lagergren Model) [2], pseudo-second order [34], Esquivel [35], pseudo-third order [36], and Elovich [37] were selected to fit the experimental kinetic data. Equations of these models are presented in Table 6.

Table 6

Adsorption kinetics models and their linear and non linear forms.

Applied model	*Non Linear form*	*Linear form*	*Reference*
Pseudo-first order			
Pseudo-first order (type 1)	$q = q_e(1-e^{-k_1 t})$	$\log(q_e - q) - \log(q_e) = -\frac{k_1 t}{2.303}$	[38]
Pseudo-second order			
Pseudo-second order (type 9)	$q = q_e\left[1-\frac{1}{1+k_2 t}\right]$	$\frac{q_e}{q_e - q} - 1 = k_2 t$	[39]
Pseudo-second order (type 10)		$\frac{\theta}{1-\theta} = k_2 t$	[39]
Esquivel model (type 1)	$q = q_e\left(\frac{t}{t+K_E}\right)$	$\frac{1}{q} = \left(\frac{K_E}{q_e}\right)\frac{1}{t} + \frac{1}{q_e}$	[35]
Esquivel model (type 2)	$q = q_e\left(\frac{t}{t+K_E}\right)$	$(\frac{1}{q} - \frac{1}{q_e})q_e = K_E\frac{1}{t}$	[35]
Elovich (type1)	$\frac{dq}{dt} = k_4 \exp(-k_5 q)$	$q = k_5 \ln(k_5 k_4) + k_5 \ln(t)$	[37]
Elovich (Roginsky-Zeldovich) (type 2)	$\frac{dq}{dt} = k_7 \exp(k_6 q)$	$q = (1/k_6)\ln(k_6 k_7) + (1/k_6)\ln(t)$	[40]

where k_1 is pseudo-first order rate constant (min^{-1}), k_2 is pseudo-second order rate constant (g/(mg min)) k_3 is pseudo-third order rate constant ($g^2/(mg^2$ min)), K_E is Esquivel rate constant (min), k_4 is Elovich rate constant (mg/(g min)), k_5 is extent of surface coverage and activation energy of the process (g/mg), k_6 is extent of surface coverage and activation energy of the process (g/mg), k_7 is Elovich rate constant (mg/(g min)), q_e is amount of adsorption at equilibrium (mg/g), and θ is dimensionless parameter ($=q/q_e$). For the non-linear and linear fitting procedures Excel and Origin software were used, respectively. The constants of all models were given in Table 7.

Table 7

Kinetics constants related to the adsorption of methylene blue onto *Retama raetam*.

Model	*Linear Method*	*Non-linear Method*
Pseudo-first order (type 1)		**Non-linear Pseudo-first order (type 1)**
q_e	9.900	9.782
K_1	0.403	0.517
R^2	0.854	0.996
Equation	log(qe-q) - log(qe)= -0.175*t	q=9.782*(1-exp(-0.517*t))
Pseudo-second order (type 9)		
q_e	9.932	9.908
K_2	1.926	1.97
R^2	0.946	0.999
Equation	(qe/(qe-q))-1 = 1.926*t	q=9.908*(1-(1/(1+1.97*t)))
Pseudo-second order (type 10)		
q_e	9.933	
K_2	1.926	
R^2	0.946	
Equation	(θ/(1-θ)) = 1.926*t	
Esquivel Model (type 1)		
q_e	9.901	9.908
K_E	0.485	0.507
R^2	0.874	0.999
Equation	1/q = 0.049*(1/t)+0.101	q=9.908*(t/(t+0.507))
Esquivel Model (type 2)		
q_e	9.900	
K_E	0.492	
R^2	0.874	
Equation	(((1/q)-(1/q))*qe)= 0.492*(1/t)	
Elovich (type 1)		
K_4	$2.913\ 10^{+16}$	
K_5	0.240	
R^2	0.899	
Equation	q = 0.240*ln(t) + 8.756	
Elovich (type 2)		
K_4	$1.678\ 10^{+5}$	
K_5	4.167	
R^2	0.899	
Equation	q = 0.240*ln(t) + 8.756	

Table 7 shows that q_e, k_2 and R^2 values obtained from the two linear forms of pseudo-second-order expressions were the same. The value of q_e and k_2 were calculated to be, respectively, 9.932 mg g^{-1} and 1.926 g mg^{-1} min^{-1} for linear pseudo-second-order and 9.908 mg g^{-1} and 1.97 g mg^{-1} min^{-1} for non linear pseudo-second order biosorption. The constants of all error analysis are represented in Table 8.

Adsorption kinetic data are the basic requirements for the design of adsorption systems. In order to optimize the design of a specific sorbate/sorbent system to remove methylene blue from aqueous solution, it is important to establish the most appropriate correlation for the experimental kinetic data. Applicability of some statistical tools to predict optimum adsorption kinetics of methylene blue onto *Retama raetam* after linear regression analysis showed that the highest R^2 value and the lowest *ARED, ARE, SAE, ARS, MPSD, Δq, SSE, MSPED*, and *HYBRID* values could be suitable and meaningful tools to predict the best-fitting equation models.

The best fitting is determined based on the use of these functions to calculate the error deviation between experimental and predicted equilibrium adsorption kinetic data, after linear analysis. Hence, according to Table 4, it seems that the linear pseudo- second order type 9 and type 10 models were the most suitable models to describe satisfactorily the studied adsorption phenomenon. Therefore, based on these mentioned results, the best useful error estimation statistical tools should point out the linear pseudo- second order type 9 followed by linear pseudo- second order type 10 as the best-fitting models.

In the most studied adsorption systems, the pseudo-first-order model does not fit well over the entire adsorption period and is generally applicable over the first 20-30 min of the sorption process. The pseudo-second-order model is based on the biosorption capacity of the solid phase and it generally predicts the "chemisorption" behaviour over the whole time of adsorption [20].

Obtained results, presented in Table 4 show that the pseudo-first-order model data do not fall on straight lines indicating that this model was less appropriate. In contrast, the pseudo second order kinetics have shown very low *ARED, ARE, SAE, ARS, MPSD, Δq, SSE, MSPED,* and *HYBRID* and high R^2 values for type 9, 10 linear pseudo-second-order, and non linear pseudo-second-order expressions suggest that it is appropriate to use the pseudo-second-order model, suggesting that it is applicable to the adsorption kinetics. This suggests that, the biosorption of methylene blue onto *Retama raetam* is a chemisorption process involving exchange or sharing of electrons mainly between the dye ions and the sorbent functional groups [20]. Using linear method it was found that a theoretical pseudo-second order model represents well the experimental kinetic data of adsorption of methylene blue onto *Retama raetam* based on a Type 9 and 10 pseudo-second-order kinetic expression.

Studies regarding the use of *Retama raetam* as biosorbent are in progress. More technical and experimental optimisations and treatments should be realised to improve the adsorption capacity of *Retama raetam*. For example, use of more effective pre-treatment methods and reduction in particle size (larger specific adsorption area, m^2/g) may further improve the rate and the extent of adsorption of methylene blue onto *Retama raetam*. Besides, the methylene blue -loaded biomass itself has to be treated, in order to avoid a pollution transfer. Indeed, one of the more common questions aroused by biosorption processes involves the fate of the biosorbent after the process. Care must be taken that solving one problem, not to create another. The sorbed methylene blue can be recovered by extraction from the biomass in order to be concentrated and then stored, reused, or eliminated. Also, the decontamination of the methylene blue -loaded biomass by biodegradation is a very interesting approach.

Table 8

Error deviation data related to the methylene blue adsorption onto *Retama raetam* employing most commonly used functions.

Error functions	*ARED*	*SAE = EABS*	*MPSED*	*SSE*	*HYBRID*	*ARE*	*ARS*	*Δq(%)= 100*ARS*	*MPSD*
Linear Pseudo-first order type 1	1.801	1.334	0.035	0.635	0.024	0.018	0.033	3.283	10.741
Non Linear Pseudo-first order type 1	1.561	1.184	0.027	0.372	0.021	0.015	0.025	2.488	8.179
Linear pseudo- second order type 9	**0.599**	**0.442**	**0.013**	**0.092**	**0.008**	**0.006**	**0.012**	**1.251**	**4.090**
Linear pseudo- second order type 10	**0.599**	**0.442**	**0.013**	**0.092**	**0.008**	**0.006**	**0.012**	**1.251**	**4.090**
Non linear pseudo- second order type 1	0.701	0.523	0.013	0.088	0.009	0.007	0.012	1.225	4.012
Linear Esquivel type 1	0.708	0.530	0.013	0.090	0.009	0.007	0.012	1.232	4.036
Linear Esquivel type 2	0.729	0.546	0.013	0.089	0.009	0.007	0.012	1.227	4.022
Non linear Esquivel	0.700	0.522	0.013	0.088	0.009	0.007	0.012	1.225	4.012
Linear Elovich model type 1	0.827	0.64	0.012	0.078	0.011	0.008	0.011	1.098	3.682
Linear Elovich model type 2	0.827	0.64	0.012	0.078	0.011	0.008	0.011	1.098	3.682

Conclusions

Retama raetam plant was used for the adsorption of methylene blue in simulated aqueous solution. In batch mode, the adsorption was highly dependent on two operating parameters (pH, contact time). The obtained results revealed the following optimal conditions: pH value of 8 and 120 min of contact time, which lead to 90.38 % methylene blue removal.

Kinetics data correlated well with the pseudo second order kinetic model (type 9 and type 10), whereas equilibrium study was best described by non linear Freundlich isotherm model.

The adsorption kinetics of methylene blue onto *Retama raetam* can be better fitted by the pseudo- second order linear model (type 9 and type 10), as compared to the non-linear pseudo-second-order model, linear pseudo-second-order model, pseudo first order, pseudo third order, and Esquivel models. The entire experimental results showed that *Retama raetam* is suitable adsorbent for the removal of methylene blue.

The thermodynamic parameters such as: Gibbs free energy change $\Delta G°$, standard enthalpy $\Delta H°$, and standard entropy $\Delta S°$ indicated that methylene blue adsorption onto *Retama raetam* was exothermic and spontaneous.

This study identified *Retama raetam* – at its raw state and without any physical or chemical activation – as a suitable low cost adsorbent to be used for removal of methylene blue dye from aqueous solution. The very rapid adsorption and high uptake capacity for methylene blue (62.5 to 91.33 % removal rate in less than 4 minutes) make the *Retama raetam* a quite interesting alternative to more expensive materials such as activated carbons.

References

1. Shen, K.; Gondal, M.A. Removal of hazardous rhodamine dye from water by adsorption onto exhausted coffee ground. Journal of Saudi Chemical Society, 2013, doi:10.1016/j.jscs.2013.11.005.
2. Kushwaha, A.K.; Gupta, N.; Chattopadhyaya, M.C. Removal of cationic methylene blue and malachite green dyes from aqueous solution by waste materials of Daucus carota. Journal of Saudi Chemical Society, 2014, 18, pp. 200–207.
3. Prakash, N.B.; Sockan, V.; Jayakaran, P. Waste water treatment by coagulation and flocculation. International Journal of Engineering Science and Innovative Technology, 2014, 3(2), pp 479-484.
4. Petrovic, M.; Rarjenovic, J.; Barcelo, D. Advanced oxidation processes (AOPs): applied for wastewater and drinking water treatment. Elimination of pharmaceuticals. The Holistic Approach to Environment, 2011, 1(2), pp. 63-74.
5. Cesaro, A.; Naddeo, V.; Belgiorno, V. Wastewater Treatment by combination of advanced oxidation processes and conventional biological systems. Journal of Bioremediation and Biodegradation, 2013, 4(8), pp. 1-8.
6. Prince, J. A.; Bhuvana, S.; Anbharasi, V.; Ayyanar, N.; Boodhoo, K.V.; Singh, G. Self-cleaning metal organic framework (MOF) based ultra filtration membranes - A solution to bio-fouling in membrane separation processes. Scientific reports, 2014, 4, Article number: 65555, doi:10.1038/srep06555.
7. Abdel-Ghani, N.T.; El-Chaghaby, G.A.; Helal, F.S. Preparation, characterization and phenol adsorption capacity of activated carbons from African beech wood sawdust. Global Journal of Environmental Science and Management, 2016, 2(3), pp. 209-222.
8. Machado, F.M.; Bergmann, C.P.; Lima, E.C.; Adebayo, M.A.; Fagan, S.B. Adsorption of a textile dye from aqueous solutions by carbon nanotubes. Materials Research, 2014, 17 (Suppl. 1), pp. 153-160.
9. Suteu, D.; Zaharia, C. Sawdust as biosorbent for removal of dyes from wastewaters. Kinetic and Thermodynamic Study. Chemical Bulletin of "Politehnica" University of Timisoara, Romania, 2011, 56(70), pp. 85-88.
10. Prigione, V.; Grosso, I.; Tigini, V.; Anastasi, A.; Varese, G.C. Fungal waste-biomasses as potential low-cost biosorbents for decolorization of textile wastewaters. Water, 2012, 4, pp. 770-784.
11. Owoyokun, T.O.; Sc. M. Biosorption of methylene blue dye aqueous solutions on delonix regia (flamboyant tree) pod biosorbent. The Pacific Journal of Science and Technology; 2009, 10, (2), pp. 872-883.
12. Hameed, B.H.; El-Khaiary, M.I. Removal of basic dye from aqueous medium using a novel agricultural waste material: Pumpkin seed hull. Journal of Hazardous Materials, 2008, 155, pp. 601–609.
13. Bokhari-Taieb Brahimi, H., Faugeron, C.; Hachem, K.; Kaid-Harche, M.; Gloaguen, V. Investigation of parietal polysaccharides from *Retama raetam* roots. African Journal of Biotechnology, 2015, 14(29), pp. 2327-2334.
14. Djeddi, S.; Karioti, A.; Yannakopoulou, E.; Papadopoulos, K.; Chatter, R.; Skaltsa, H. Analgesic and antioxidant activities of Algerian *Retama raetam* (Forssk.) Webb & Berthel Extracts. Records of Natural Products, 2013, 7(3), pp. 169-176.
15. Al-Degs, Y.S.; Sweileh, J.A. Simultaneous determination of five commercial cationic dyes in stream waters using diatomite solid-phase extractant and multivariate calibration. Arabian Journal of Chemistry, 2012, 5, pp. 219–224.
16. El-Qada, E.N.; Allen, S.J.; Walker, G.M. Adsorption of methylene blue onto activated carbon produced from steam activated bituminous coal: a study of equilibrium adsorption isotherm. Chemical Engineering Journal, 2006, 124, pp. 103–110.
17. Ghazi Mokri, H.S.; Modirshahl, N.; Behnajady, M.A.; Vahid, B. Adsorption of C.I. Acid Red 97 dye from aqueous solution onto walnut shell: kinetics, thermodynamics parameters, isotherms. International Journal of Environmental Science and Technology, 2015, 12(4), pp. 1401–1408.
18. Santhi, T.; Manonmani, S.; Smitha, T.; Mahalakshmi, K. Adsorption kinetics of cationic dyes from aqueous solution by bioadsorption onto activated carbon prepared from Cucumis Sativa. Journal of Applied Sciences in Environmental Sanitation, 2009, 4(3), pp. 263-271.
19. Khattria, S.D.; Singh, M.K. Removal of malachite green from dye wastewater using neem sawdust by adsorption. Journal of Hazardous Materials, 2009, 167, pp. 1089–1094.
20. Mahjoub, B.; Ben Brahim, I. Biosorption performance of powdered waste sludge for removal of congo red: Equilibrium and kinetic modeling. Journal of Materials and Environmental Science, 2015, 6(11), pp. 3359-3370.

21. Marouf-Khelifa, K.; Khelifa, A.; Belhakem, A.; Marouf, R.; Abdelmalek, F.; Addou, A. The adsorption of pentachlorophenol from aqueuous solution onto exchanged Al-MCM-41 materials. Adsorption Science and Technology, 2004, 22 (1), pp. 1-12.
22. Benkhedda, J.; Jaubert, J.N.; Barth, D. Experimental and modeled results describing the adsorption of toluene onto activated carbon. Journal of Chemical and Engineering Data, 2000, 45 pp. 650-653.
23. Riahi, K.; Chaabane, S.; Ben-Thayer, B. A kinetic modeling study of phosphate adsorption onto Phoenix dactylifera L. date palm fibers in batch mode. Journal of Saudi Chemical Society, 2013, doi:10.1016/j.jscs.2013.11.007
24. Maderova, Z.; Baldikova, E.; Pospiskova, K.; Safarik, I.; Safarikova, M. Removal of dyes by adsorption on magnetically modified activated sludge International Journal of Environmental Science and Technology, 2016, doi: 10.1007/s13762-016-1001-8.
25. Subramanyam, B.; Das, A. Linearised and non-linearised isotherm models optimization analysis by error functions and statistical means. Journal of Environmental Health Science & Engineering, 2014, 12 (92), pp. 1-6.
26. Bajic, Z.J.; Djokc, V.R.; Velickovic, Z.S.; Vuruna, M.M.; Ristic, M.D.; Issa, N.B.; Marinkovic, A.D. Equilibrium; kinetic and thermodynamic studies on removal of Cd(II); Pb(II) AND As(V) from wastewater using CARP (Cyprinus Carpio) Scales. Digest. Journal of Nanomaterials and Biostructures, 2013, 8(4), pp. 1581–1590.
27. Alihosseini, A.; Taghikhani, V.; Safekordi, A. A.; Bastani, D. Equilibrium sorption of crude oil by expanded perlite using different adsorption isotherms at 298.15 K. International Journal of Environmental Science and Techology, 2010, 7(3), pp. 591-598.
28. Wang, L.; Zhang, J.; Zhao, R.; Li, Y.; Li, C.; Zhang, C. Adsorption of Pb(II) on activated carbon prepared from Polygonum orientale Linn.: Kinetics; isotherms; pH; and ionic strength studies. Bioresource Technology, 2010, 101(15), pp. 5808-5814.
29. Udoji, I.A.; Etim, E.E. Dynamics of M^{x+} salts of fatty acids adsorption onto metallic ores. International Journal of Environmental Science and Development, 2015, 6(3), pp. 205-210.
30. Gulipall, C.S.; Prasad, B.; Wasewar, K.L. Batch study; equilibrium; and kinetics of adsorption of selenium using Rice Husk Ash (RHA). Journal of Engineering Science and Technology, 2011, 6(5), pp. 586–605.
31. Chouchane, T.; Yahi, M.; Boukari, A.; Balaska, A.; Chouchane, S. Adsorption of the copper in solution by the kaolin. Journal of Materials and Environmental Science, 2016, 7(8), pp. 2825-2842. (in French).
32. Ezechi, E.H.; Kutty, S.R.M.; Malakahmad, A.; Isa, M.H. Characterization and optimization of effluent dye removal using a new low cost adsorbent: Equilibrium, kinetics and thermodynamic study. Process Safety and Environmental Protection. 2015, 98, pp. 16–32.
33. Dahri, M.K.; Kooh, M.R.R.; Lim, L.B.L. Water remediation using low cost adsorbent walnut shell for removal of malachite green: Equilibrium; kinetics; thermodynamic and regeneration studies. Journal of Environmental Chemical Engineering, 2014, 2(3), pp.1434-1444
34. Baek, M.H.; Ijagbemi, C.O.; Kim D.S. Removal of Malachite Green from aqueous solution using degreased coffee bean. Journal of Hazardous Materials, 2010, 176, pp. 820–828.
35. Shilpi, A.; Shivhare, U.S.; Basu, S. Supercritical CO_2 extraction of compounds with antioxidant activity from fruits and vegetables waste. Focusing on Modern Food Industry, 2013, 2(1), pp. 43-62.
36. Kyzas, G.Z.; Lazaridis, N.K.; Mitropoulos, A.C. Removal of dyes from aqueous solutions with untreated coffee residues as potential low-cost adsorbents: Equilibrium; reuse and thermodynamic approach. Chemical Engineering Journal, 2012, 189– 190, pp.148–159.
37. Secula, M.C.; Cagnon, B.; Creţescu, I.; Diaconu, M.; Petrescu, S. Removal of an acid dye from aqueous solutions by adsorption on a commercial granular activated carbon: equilibrium, kinetic and thermodynamic study. Scientific Study & Research – Chemistry and Chemical Engineering, Biotechnology, Food Industry, 2011, 12(4), pp. 307-322.
38. Santhi, T.; Manonmani, S.; Smitha, T. Kinetics And Isotherm Studies On Cationic Dyes Adsorption Onto Annona Squmosa Seed Activated Carbon. International Journal of Engineering Science and Technology, 2010, 2(3), pp. 287-295.
39. Oboh, I.O.; Aluyor, E.O.; Audu, T.O.K. Second-order kinetic model for the adsorption of divalent metal ions on Sida acuta leaves. International Journal of Physical Sciences, 2013, 8(34), pp. 1722-1728.
40. Abuh, M.A.; Akpomie, G.K.; Nwagbara, N.K.; Abia-Bassey, N.; Ape, D.I.; Ayabie, B.U. Kinetic rate equations application on the removal of copper (II) and zinc (II) by unmodified lignocellulosic fibrous layer of palm tree trunk single component system studies. International Journal of Basic and Applied Science, 2013, 1(4), pp. 800-809.

CHEMISTRY JOURNAL OF MOLDOVA. General, Industrial and Ecological Chemistry. 2016, 11(2), 84-92
http://cjm.asm.md
http://dx.doi.org/10.19261/cjm.2016.11(2).04

TOPOLOGICAL ANALYSIS AND FREQUENCY DEPENDENT HYPERPOLARIZABILITY CALCULATIONS OF FDDNP: A DFT STUDY

Keivan Akhtari[a*], Keyumars Hassanzadeh[b], Bahareh Fakhraei[a], Ghazal Akhtari[a]

[a]*Department of Physics, University of Kurdistan, P.O.Box 416, Sanandaj, Iran*
[b]*Young Researchers and Elites Club, Islamic Azad University, Sanandaj, Iran*
**e-mail: k1akhtari@yahoo.com; phone: (+98) 8733289430; fax: (+98) 8733247713*

Abstract. The topological and first-hyperpolarizability properties of 2-(1-{6-[(2-fluoroethyl)(methyl)amino]-2-naphthyl}ethylidene)malononitrile (FDDNP) were studied using DFTB3LYP method. The static and dynamic electronic (hyper)polarizabilities of conformers were calculated and a simple two-state model was employed to explain the first hyperpolarizability differences in two conformers. The second harmonic generation property was evaluated at the typical wavelengths of Cr:forsterite, Nd:YAG(neodymium-doped yttrium aluminium garnet) and Ti:sapphire lasers to predict the compound conformers potency for second harmonic generation imaging in biological studies.

Keywords: second-harmonic generation, FDDNP, near-infrared, QTAIM.

Received: August 2016/ Revised final: October 2016/ Accepted: October 2016

Introduction

Optical imaging techniques based on nonlinear optical phenomena have been widely incorporated in microscopy using ultra-fast pulsed lasers. There have been described many applications in cellular and tissue imaging due to the ability to spatially resolve subcellular details with high molecular contrast [1].

The employed near-infrared (NIR) wavelengths reduce scattering and maximize tissue penetration. These characteristics boost nonlinear microscopy as an elective method for imaging cells with micrometer-resolution deep into the living tissues. Both labeled and label-free second harmonic generation (SHG) imaging techniques have been employed in biological studies. For example, the non-centrosymmetric structure of fibrillar collagen is the major source of the SHG signals in different tissues [2,3], and for cellular and subcellular samples. For this purpose, several SHG labels have been used [4,5].

The 2-(1-{6-[(2-fluoroethyl)(methyl)amino]-2-naphthyl}ethylidene)malononitrile (FDDNP) is a functional fluorescent biomarker belonging to the family of dicyanovinyl naphthalene labels, which binds to its ligand through hydrophobic interactions [6]. FDDNP also binds to amyloid plaques with high affinity [7]. Fluorescence imaging microscopy of amyloid aggregates has a key role in diagnosing Alzheimer's disease and other neurodegenerative diseases [8,9].

According to the importance of second-harmonic generation, as one of the nonlinear excitation families with deep imaging, 3D capabilities and intrinsic contrast in certain tissues, the study of nonlinear optical properties of biomaterials and their labels plays an essential role in development of medicinal optic devices. So far, only a few electronic structure studies on FDDNP and other dicyanovinyl naphthalene biomarkers, based on *ab initio* calculations have been performed. Petrič *et al.* [6] performed a combined experimental and theoretical study on FDDNP and its analogs to explain the chemical modification effects on binding affinity of biomarkers to amyloid plaques and their fluorescence Quantum yields. Given the close relationship between the structure and nonlinear activities, and the functional importance of default molecule, it is necessary to develop a deeper vision on electron-topological properties, in order to predict its different optical capabilities. In the present work we consider both structural and nonlinear optical properties of FDDNP to introduce it as a potent material in nonlinear optical imaging of biological samples.

Thereupon in this work, beside the study of conformational effect on structural properties, the static and frequency-dependent electronic (hyper)polarizabilities of the FDDNP conformers were also computed. For this purposes, the nonlinear optical properties related to the excited-state dipole moment were studied using a simple two-state model (TSM) [10].

Computational details

The geometry optimization, frequency and single point energy calculations were carried out for all structures, using the Density Functional Theory method supplied in the GAUSSIAN98W suite of programs [11].

The B3LYP functional [12-14] with the 6-31G(d,p) basis set [15] were used.

The Time-Dependent Density Functional Theory (TD-DFT) was used to calculate the excited state energies and excited state dipole moments. The 10 lowest excited states were considered. The orbital transition contributions were obtained using GAUSSSUM 2.2 program [16].

To estimate the solvent effect on the studied optical parameters, polarizable continuum model (PCM) calculations were performed [17]. The topological analyses were carried out using Multiwfn program [18].

Results and discussion

Geometry and Natural Bond Orbital (NBO) studies

Two stable conformations of the FDDNP can theoretically exist [6]. The optimized structures are shown in Figure 1. The C2-C6-C9-C10 dihedral angles for two conformers are approximately 31° (*Syn* form) and 142° (*Anti* form). The *Syn* conformer has lower total energy than the *Anti* form by 4.98 kJ/mol.

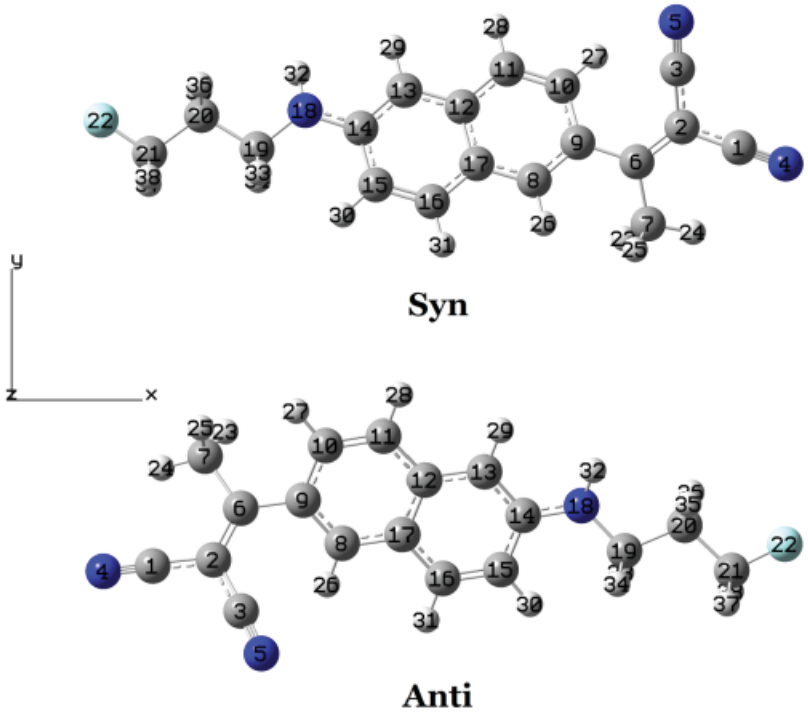

Figure 1. Structures of two possible minimum energy conformations of FDDNP.

Intra-molecular hyperconjugative interactions can be used as a measure of the interaction intensity between electron-acceptor orbitals. In fact, the larger the value of the hyperconjugative interaction, the more intensive the interaction between the donor and acceptor, and the greater the extent of conjugation of the whole system is [19].

The role of hyperconjugative interactions in the stabilization of *Syn* and *Anti* conformers has been studied using NBO analysis. For a better comparison of the conformers' stability, the same values of the donor-acceptor interactions with large differences (≥0.4 kJ/mol) have been summarized in Table 1. Upon the data, hyperconjugation interactions are more favored for the *Syn* form. The interactions such as πC8–C9→π*C2–C6 and πC2–C6→π*C8–C9 play an important role in conformational properties of FDDNP. In addition, the sum values of hyperconjugation interactions are in accordance with the total energy values.

Table 1

Important hyperconjugative interactions (kJ mol^{-1}) for FDDNP conformers.

Donor	*Acceptor*	*Syn*	*Anti*
πC2–C6→	π*C1–N4	85.19	85.94
	π*C3–N5	84.10	84.77
	π*C8–C9	30.92	27.74
σC6–C9→	σ*C8–C9	11.25	12.47
	σ*C9–C10	9.71	8.79
σC7–H23→	σ*C2–C6	10.17	10.63
σC8–C9→	σ*C6–C9	12.05	12.84
	σ*C9–C10	14.43	14.94
πC8–C9→	π*C2–C6	75.81	71.88
	π*C10–C11	69.08	72.01
	π*C12–C17	61.59	61.00

Continuation of Table 1

Donor	*Acceptor*	*Syn*	*Anti*
σC8–C17→	σ*C6–C9	13.81	14.89
σC8–H26→	σ*C8–C9	4.81	5.23
	σ*C9–C10	17.07	17.99
	σ*C12–C17	18.83	19.25
σC9–C10→	σ*C6–C9	10.50	9.92
πC10–C11→	π*C8–C9	63.47	60.50
	π*C12–C17	68.07	65.19
σC10–H27→	σ*C8–C9	15.27	14.68
	σ*C10–C11	5.69	5.23
	σ*C11–C12	18.62	18.16
σC11–C12→	σ*C10–H27	9.50	10.04
Sum		709.34	704.09

Topological analysis

The topological study of electron density based on *Quantum Theory of Atom In Molecules* (QTAIM) as a rigorous interpretative method can unambiguously describe atoms existing in the system. In this theory the chemical bonds can be defined as the set of lines known as bond paths (BPs) linking neighboring atoms. In addition, other concepts and quantities are also necessary to characterize a bonding interaction, namely critical point (CP), electron density $\rho(r)$, Laplacian of electron density $\nabla^2\rho(r)$, kinetic energy density [$G(r)$], potential energy density [$V(r)$], and total energy density [$H(r)$] [20].

Hydrogen bonding can be explained and classified as a main factor in determining the preferred conformers according to the Roza's criteria [21]:

1. weak hydrogen bonds: $\nabla^2\rho_{BCP}>0$ and $H_{BCP}>0$;
2. medium hydrogen bonds: $\nabla^2\rho_{BCP}>0$ and $H_{BCP}<0$;
3. strong hydrogen bonds: $\nabla^2\rho_{BCP}<0$ and $H_{BCP}<0$,

where $\nabla^2\rho_{BCP}$ and H_{BCP} are the Laplacian of electron density and the total electron energy density at critical point respectively.

The nature of hydrogen bonds can be specified using the following criteria [22]:

1. for $\frac{G_{BCP}}{|V_{BCP}|}>1$, the hydrogen bond has non-covalent nature;
2. for $0.5<\frac{G_{BCP}}{|V_{BCP}|}<1$, the hydrogen bond is partly covalent.

At the first step, we verified if C3····H27 and C3····H26 (see Figure 2) were in fact hydrogen bonds. Then, the strength of bonds was studied through the criteria above. Koch and Popelier [23] established some criteria for hydrogen atom that are involved in hydrogen bond as follows:

1. increasing the net positive charge [$q(H)$];
2. decreasing the first atomic dipole moment [$M(H)$];
3. decreasing the atomic volume [$V(H)$];
4. increasing the atomic total energy [$E(H)$].

To compare the atomic properties with a reference, the C2-C6-C9-C10 dihedral angle was fixed at 90° and QTAIM calculations were performed to obtain the atomic properties of H26 and H27 when they are not involved in hydrogen bond. The atomic QTAIM parameters related to H26 and H27 for *Syn* conformer, *Anti* conformer and the reference state are gathered in Table 2. As can be seen, all Koch's criteria for identification of C3····H26 and C3····H27 as hydrogen bonds are satisfied.

Table 2

Atomic properties of H26 and H27 obtained by QTAIM for different dihedral angles.

C2-C6-C9-C10 dihedral angle	*Hydrogen atom number*	*q(H)*	*M(H)*	*V(H)*	*E(H)*
31° (*Syn*)	27	0.029917	0.141198	43.083	-4.940696
142° (*Anti*)	26	0.027665	0.137417	43.477	-4.938453
90° (Reference)	27	0.004345	0.151833	49.105	-4.960837
	26	0.000881	0.146968	49.480	-4.960837

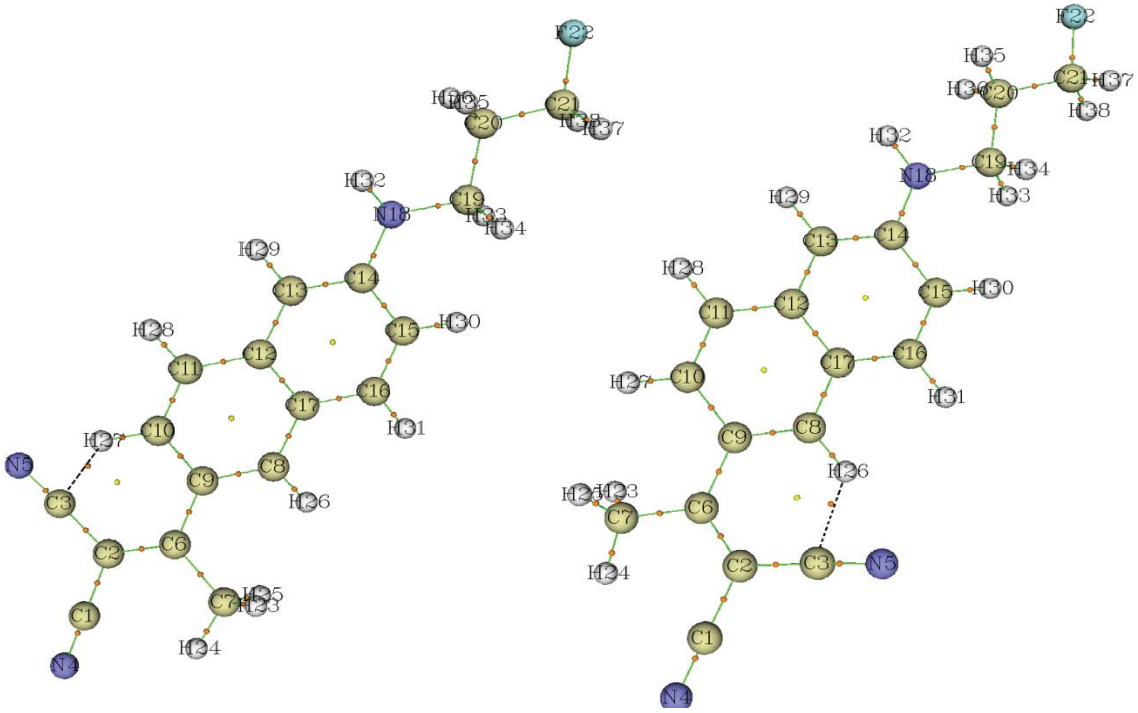

(a) **(b)**

Figure 2. Molecular graphs for the electron density topology of (a) *Syn* and (b) *Anti* forms, with their bond critical points (BCP) and ring critical points (RCP).

For classification of the intra-molecular hydrogen bonds in *Syn* and *Anti* conformers, the topological quantities at characteristic critical points (see Figure 2) have been calculated and summarized in Table 3. Both Laplacians of electron density at the bond critical points are positive, which reveals a depletion of electron charge in these bond critical points.

Table 3

Topological properties of FDDNP conformers.

Conformer	*Critical points*	*Atoms involved*	*ρ(r)*	*$\nabla^2\rho(r)$*	*G(r)*	*V(r)*		*H(r)*	*ε[a]*
Syn	BCP	C3, H27	0.01249	0.04874	0.00972	-0.00725	1.3400	0.00247	0.28697
	RCP	C2, C3, C6,C9, C10, H27	0.00995	0.05177	0.00976	-0.00659	1.4824	0.00318	-1.33429
Anti	BCP	C3, H26	0.01222	0.04780	0.00949	-0.00703	1.3504	0.00246	0.34337
	RCP	C2, C3,C6, C8, C9, H26	0.01019	0.05173	0.00979	-0.00665	1.4717	0.00314	-1.35175

[a]*Ellipticity (ε) is another topological parameter that measures the bond's stability. The high value of ellipticity indicates the lower bonds stability [22].*

In addition, the ratio of related to critical points of C3····H27 and C3····H26 are 1.34 and 1.35 respectively. Then according to Roza's criterion, both intra-molecular bonds can be classified as weak hydrogen bonds. Figure 2 shows that the formation of intra-molecular hydrogen bonds leads to a ring critical point (RCP) in each conformer.

Frequency dependence of linear and nonlinear optical properties

In order to investigate the linear and nonlinear optical performances of FDDNP conformers, polarizability (α), polarizability anisotropy ($\Delta\alpha$) and first hyperpolarizability (β) have been calculated according to the following relations [24-26]:

$$\alpha=1/3(\alpha_{xx}+\alpha_{yy}+\alpha_{zz}), \quad (1)$$

$$\Delta\alpha=2^{-1/2}[(\alpha_{xx}-\alpha_{yy})^2+(\alpha_{xx}-\alpha_{zz})^2+(\alpha_{yy}-\alpha_{zz})^2+6(\alpha_{xy}^2+\alpha_{xz}^2+\alpha_{yz}^2)]^{1/2}, \quad (2)$$

and

$$\beta=(\beta_x^2+\beta_y^2+\beta_z^2)^{1/2}, \quad (3)$$

where

$\beta_x=\beta_{xxx}+\beta_{xyy}+\beta_{xzz}$
$\beta_y=\beta_{yyy}+\beta_{yzz}+\beta_{xxy}$
$\beta_z=\beta_{xxz}+\beta_{yyz}+\beta_{zzz}$

Polarizability and hyperpolarizability parameters for some common frequencies in functional lasers are gathered in Table 4. As can be seen, the average polarizability, polarizability anisotropy, and Electro-Optic Pockels Effect (EOPE)-hyperpolarizability are increased with increasing frequency. SHG-hyperpolarizability has maximum value in ω=0.051770 au, which is the typical wavelength of the Ti:sapphire laser (880 nm).

Table 4

The SHG hyperpolarizability ($\beta(-2\omega,\omega,\omega)$), EOPE-hyperpolarizability ($\beta(-\omega,\omega,0)$) esu ($\times10^{-33}$), average polarizability ($\alpha(-\omega,\omega)$), and polarizability anisotropy ($\Delta\alpha(-\omega,\omega)$) esu ($\times10^{-24}$) calculated at B3LYP/6-31G(d,p) level of theory.

Linear and nonlinear optical parameters	*Syn*	*Anti*	*Frequency*
$\beta(-2\omega,\omega,\omega)$	81208.67	77573.81	
($\beta(-\omega,\omega,0)$)	81160.21	77564.57	ω= 0.000000
$\alpha(-\omega,\omega)$	37.90	37.14	
$\Delta\alpha(-\omega,\omega)$	48.72	44.83	
$\beta(-2\omega,\omega,\omega)$	180936.86	170314.51	
($\beta(-\omega,\omega,0)$)	102024.86	97054.33	ω= 0.037040
$\alpha(-\omega,\omega)$	39.18	38.32	**Cr:forsterite**
$\Delta\alpha(-\omega,\omega)$	51.98	47.68	
$\beta(-2\omega,\omega,\omega)$	271510.12	254866.48	
($\beta(-\omega,\omega,0)$)	111013.40	1094367.44	ω= 0.042820
$\alpha(-\omega,\omega)$	39.67	38.78	**Nd:YAG**
$\Delta\alpha(-\omega,\omega)$	53.19	48.80	
$\beta(-2\omega,\omega,\omega)$	1165261.93	1126879.80	
($\beta(-\omega,\omega,0)$)	130949.53	124041.44	ω= 0.051770
$\alpha(-\omega,\omega)$	40.65	39.69	**Ti:sapphire**
$\Delta\alpha(-\omega,\omega)$	55.82	51.08	
$\beta(-2\omega,\omega,\omega)$	699461.39	585507.27	
($\beta(-\omega,\omega,0)$)	162155.32	150656.64	ω= 0.059950
$\alpha(-\omega,\omega)$	41.89	40.84	**Ti:sapphire**
$\Delta\alpha(-\omega,\omega)$	59.10	53.98	

Nd:YAG is the neodymium-doped yttrium aluminium garnet.

Compared to other lasers, Ti:sapphire laser is at an advantage in terms of transparency considerations of melanin, hemoglobin and water when operating at near-IR wavelengths, and short pulse duration (~100 fs) of this laser. In such short duration, only a few nanojoules of energy transfers to samples [27,28]. Therefore, employing FDDNP label for biological microscopy, in addition to high performance in second harmonic generation, protects cells and tissues from photodamaging.

p-Nitroaniline (pNA) is prototypical compound used in the study of the nonlinear optical (NLO) properties as a reference one. Hence, we calculated SHG-hyperpolarizability of this molecule at λ= 880 nm. The calculated value is 43.99 times smaller than the same value of FDDNP (*Syn* form). Thus, we can conclude that the FDDNP has considerable nonlinear optical properties.

To study the medium effect on the optical properties of the FDDNP conformers, the water, DMSO, and benzene solvent were employed to simulate the protic polar, aprotic polar and nonpolar media. Similar method has been adopted to calculate thermodynamic and electronic properties in biological environments [29-31]. The linear and nonlinear optical parameters of FDDNP conformers have been shown in Table 5. The notable point is a large SHG-hyperpolarizability of title compound in nonpolar medium.

Table 5

Linear and nonlinear optical parameters in different solvents and ω= 0.051770 for FDDNP conformers. Units for polarizabilities are esu ($\times 10^{-24}$) and those for hyperpolarizabilities are esu ($\times 10^{-33}$), calculated at B3LYP/6-31G(d,p) level of theory.

Solvent	*Linear and nonlinear optical parameters*	*Syn*	*Anti*
Water	$\alpha(-\omega,\omega)$	47.85	46.38
	$\beta(-\omega,\omega,0)$	344924.10	320231.48
	$\beta(-2\omega,\omega,\omega)$	3153103.78	2450425.24
DMSO	$\alpha(-\omega,\omega)$	48.86	47.42
	$\beta(-\omega,\omega,0)$	359445.29	333351.67
	$\beta(-2\omega,\omega,\omega)$	2965299.81	2424596.108
Benzene	$\alpha(-\omega,\omega)$	48.40	47.06
	$\beta(-\omega,\omega,0)$	262042.98	244359.59
	$\beta(-2\omega,\omega,\omega)$	11873736.67	8434946.61

Two-state model

As shown from Table 5, the static first hyperpolarizabilities of *Syn* form are larger than the similar values in *Anti* form. A two-state model has been employed to explain these differences. According to this model, the first hyperpolarizability can be explained using the following relation [10]:

$$\beta \propto \Delta\mu_{ge} f_{os} / \Delta E^3 \quad (4)$$

In the above expression, β is proportional to the difference of dipole moment in the ground state and the crucial excited states ($\Delta\mu_{ge}$) and the oscillator strength (f_{os}), but inversely proportional to the third power of the transition energy (ΔE). Calculated parameters by using TD-DFT method (Table 6) for FDDNP conformers indicate that the largest dipole moment changes and oscillator strengths correspond to the HOMO→LUMO transition. The transition energies and corresponding oscillator strengths are almost the same for both conformers. The difference can be attributed to a larger dipole moment change in *Syn* form. The transition has $p \rightarrow \pi^*$character (Figure 3).

Table 6

Results of the TD-DFT calculations for FDDNP conformers*.

	λ_{max}	ΔE	f_{os}	$\Delta\mu_{ge}$	$\Delta\mu_{ge} f_{os} / \Delta E^3$	*major contribution*
Syn	416.83	2.8272	0.4904	15.8161	0.2947	HOMO→LUMO (97%)
	275.82	4.4952	0.3425	13.9161	0.0524	HOMO-2→LUMO (92%)
	230.69	5.3742	0.2198	6.6065	0.0093	HOMO-4→LUMO (56%)
Anti	418.20	2.9633	0.4485	13.8768	0.2391	HOMO→LUMO (98%)
	278.94	4.4435	0.2868	12.1143	0.0396	HOMO-2→LUMO (92%)
	236.51	5.2408	0.2337	4.8001	0.0078	HOMO-3→LUMO (48%)
	229.83	5.3932	0.2000	5.8542	0.0074	HOMO-4→LUMO (56%)

**wavelength λ_{max} (nm),*
oscillator strength ($f_{os} \geq 0.2$),
the transition energy ΔE (eV),
the difference of dipole moment between the ground state and the excited state $\Delta\mu_{ge}$ (Debye).

As seen in molecular orbital plots (Figure 3), the highest occupied molecular orbitals mainly concentrate on naphthalene group and nitrogen atom in the five-member chain, while for the lowest unoccupied molecular orbitals the population analysis of molecular orbitals indicates that the C2 and C6 atoms on rotating group contribute 13% and 28% for *Syn* conformer and 13% and 30% for *Anti* conformer. These orbitals play the crucial role in the intramolecular charge-transfer (ICT). In this way, the electron density transfers from the electron donor moiety to the electron acceptor group.

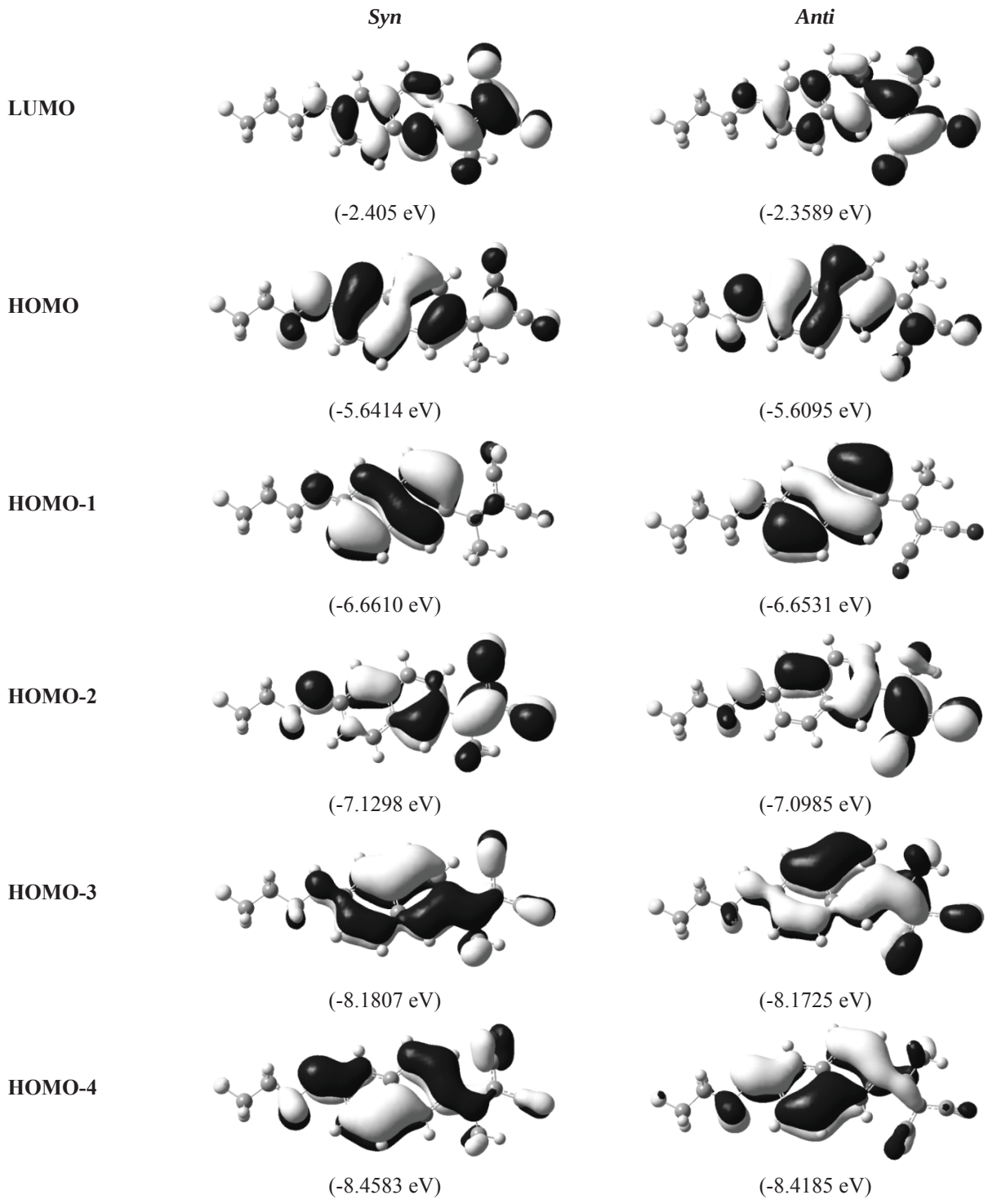

Figure 3. Energy graphic representation of molecular orbitals of FDDNP conformers.

Conclusions

Two FDDNP conformers have been studied in order to predict their conformational properties and second harmonic generation potency by using density functional theory. Upon the hyperconjugation values, the *Syn* conformer is a more favored form. The QTAIM parameters reveal the intra-molecular hydrogen bonds in both conformers, which are classified as weak hydrogen bonds. The frequency dependent hyperpolarizabilities indicate that both conformers have high performance in near-infrared region. The best predicted working wavelength belongs to Ti:sapphire laser (880 nm). The conformers' first hyperpolarizability differences were explained by using the two-state model. Calculated parameters indicate that the higher first hyperpolarizability of *Syn* form of FDDNP is related to a larger dipole moment change in crucial excited state. The solvent effect study indicates that SHG-hyperpolarizability of FDDNP in nonpolar medium is four times greater than the similar value in polar media.

References

1. Campagnola, P.J.; Loew, L.M. Second-harmonic imaging microscopy for visualizing biomolecular arrays in cells, tissues and organisms. Nature Biotechnology, 2003, 21, pp. 1356–1360.
2. Adur, J.; Pelegati, V.B.; de Thomaz, A.A.; Baratti, M.O.; Andrade, L.A.; Carvalho, H.F.; Bottcher-Luiz, F.; Cesar, C.L.; Cesar, C.L. Second harmonic generation microscopy as a powerful diagnostic imaging modality for human ovarian cancer. Journal of Biophotonics, 2014, 7, pp. 37–48.
3. Liu, J.; Cho, I.H.; Cui, Y.; Irudayaraj, J. Second harmonic super-resolution microscopy for quantification of mRNA at single copy sensitivity. ACS Nano, 2014, 8, pp. 12418-27.
4. Cox, G.; Kable, E.; Jones, A.; Fraser, I.; Manconi F.; Gorrell, M.D. 3-Dimensional imaging of collagen using second harmonic generation. Journal of Structural Biology, 2003, 141, pp. 53–62.
5. Jiang, J.; Yuste, R. Second-Harmonic generation imaging of membrane potential with photon counting. Microscopy and Microanalysis, 2008, 14, pp. 526–531.
6. Petric, A.; Johnson, S.A.; Pham, H.V.; Li, Y.; Ceh, S.; Golobic, A.; Agdeppa, E.D.; Timbol, G.; Liu, J.; Keum, G.; Satyamurthy, N.; Kepe, V.; Houk, K. N.; Barrio, J.R. Dicyanovinylnaphthalenes for neuroimaging of amyloids and relationships of electronic structures and geometries to binding affinities. Proceedings of the National Academy of Sciences U.S.A., 2012, 109, pp. 16492-16497.
7. Shoghi-Jadid, K.; Small, G.W.; Agdeppa, E.D.; Kepe, V.; Ercoli, L.M.; Siddarth, P.; Read, S.; Satyamurthy, N.; Petric, A.; Huang S.C.; Barrio, J.R. Localization of neurofibrillary tangles and beta-amyloid plaques in the brains of living patients with Alzheimer disease, The American Journal of Geriatric Psychiatry, 2002, 10, pp. 24-35.
8. Bresjanac, M.; Smid, L.M.; Vovko, T.D.; Petric, A.; Barrio J.R.; Popovic, M. Molecular-imaging probe 2-(1-[6-[(2-fluoroethyl)(methyl) amino]-2-naphthyl]ethylidene) malononitrile labels prion plaques in vitro. The Journal of Neuroscience, 2003, 23, pp. 8029–8033.
9. Thompson, P.W.; Ye, L.; Morgenstern, J.L.; Sue, L.; Beach, T.G.; Judd, D.J.; Shipley, N.J.; Libri, V.; Lockhart, A. Interaction of the amyloid imaging tracer FDDNP with hallmark Alzheimer's disease pathologies. Journal of Neurochemistry, 2009, 109, pp. 623-630.
10. Oudar J.L.; Chemla, D.S. Hyperpolarizabilities of the nitroanilines and their relations to the excited-state dipole moment. The Journal of Chemical Physics, 1977, 66, pp. 2664-2668.
11. Frisch, M.J.; Trucks, G.W.; Schlegel, H.B. et al. GAUSSIAN 98, (Revision A.7, Gaussian, Inc., Pittsburgh PA, 1998).
12. Lee, C.; Yang, W.; Parr, R.G. Development of the Colle–Salvetticonelation energy formula into a functional of the electron density. Physical Review B, 1988, 37, pp. 785–798.
13. Becke, A.D. Density-functional thermochemistry. III. The role of exact exchange. Journal of Chemical Physics, 1993, 98, pp. 5648–5652.
14. Stevens, P.J.; Devlin, F.J.; Chabalowski, C.F.; Frisch, M.J. *Ab initio* calculation of vibrational absorption and circular dichroism spectra using density functional force fields. Journal of Physical Chemistry, 1994, 98, pp. 11623–11627.
15. Hehre, W.J.; Ditchfield, R.; Pople, J.A. Self—Consistent Molecular Orbital Methods. XII. Further Extensions of Gaussian—Type Basis Sets for Use in Molecular Orbital Studies of Organic Molecules. Journal of Chemical Physics, 1972, 56, pp. 2257-2261.
16. Boyle, N.M.; Tenderholt, A.L.; Langner, K.M. A library for package independent computational chemistry algorithms. Journal of Computational Chemistry, 2008, 29, pp. 839-845.
17. Tomasi, J.; Persico, M. Molecular interactions in solution: an overview of methods based on continuous distributions of the solvent. Chemical Reviews, 1994, 94, pp. 2027-2094.
18. Lu, T.; Chen, F. Multiwfn: A multifunctional wave function analyzer. Journal of Computational Chemistry, 2012, 33, pp. 580-592.
19. Sebastian, S.; Sylvestre, S.; Jayabharathi, J.; Ayyapan, S.; Amalanathan, M.; Oudayakumar, K.; Herman, I.A. Study on conformational stability, molecular structure, vibrational spectra, NBO, TD-DFT, HOMO and LUMO analysis of 3,5-dinitrosalicylic acid by DFT techniques. Spectrochimica Acta Part A: Molecular and Biomolecular Spectroscopy, 2015, 136, pp. 1107-1118.
20. Akhtari, K.; Hassanzadeh, K.; Fakhraei, B.; Akhtari, G. Magnetic exchange coupling of chalcogen-centered radicals mediated via the 2D curved π-network: A broken-symmetry approach. Computational Materials Science, 120, 2016, pp. 53-59.
21. Rozas, I.; Alkorta, I.; Elguero, J. Behavior of ylides containing N, O, and C Atoms as hydrogen bond acceptors. Journal of the American Chemical Society, 2000, 122, pp. 11154-11161.

22. Shainyan, B.A.; Chipanina, N.N.; Aksamentova, T.N.; Oznobikhina, L.P.; Rosentsveig G.N.; Rosentsveig, I.B. Intramolecular hydrogen bonds in the sulfonamide derivatives of oxamide, dithiooxamide, and biuret. FT-IR and DFT study, AIM and NBO analysis. Tetrahedron, 2010, 66, pp. 8551- 8556.
23. Koch, U.; Popelier, P.L. A characterization of C-H-O hydrogen bonds on the basis of the charge density. The Journal of Physical Chemistry, 1995, 99, pp. 9747-9754.
24. Pati, S.K.; Ramasesha, S.; Shuai, Z.; Bredas, J.L. Dynamical nonlinear optical coefficients from the symmetrized density-matrix renormalization-group method. Physical Review B, 1999, 59, pp. 14827–14830.
25. Akhtari, K.; Hassanzadeh, K.; Fakhraei, B.; Hassanzadeh, H.; Akhtari, G.; Zarei, S.A. First hyperpolarizability orientation in [70]PCBM isomers: A DFT study. Computational and Theoretical Chemistry, 2014, 1038, pp. 1–5.
26. Librando, V.; Alparone, A.; Minniti, Z. Computational study on dipole moment, polarizability and second hyperpolarizability of nitronaphthalenes. Journal of Molecular Structure: THEOCHEM. 2008, 856, pp. 105–111.
27. Heisterkamp, A.; Maxwell, I.Z.; Mazur, E.; Underwood, J.M.; Nickerson, J.A.; Kumar, S. Pulse energy dependence of subcellular dissection by femtosecond laser pulses. Optics Express, 2005, 13, pp. 3690–3696.
28. Vogel A.; Venugopalan, V. Mechanisms of pulsed laser ablation of biological tissues. Chemical Reviews, 2003, 103, pp. 577–644.
29. Hassanzadeh, K.; Akhtari, K.; Hassanzadeh, H.; Zarei, S.A.; Fakhraei, N.; Hassanzadeh, K. The role of structural C-H single bond compared with phenolic OH sites on the antioxidant activity of oleuropein and its derivatives as a great non-flavonoid family of the olive components: A DFT study. Food chemistry, 2014, 164, pp. 251-258.
30. Markovic, Z.; Milenkovic, Đ.; Đorovic, J.; Dimitric Markovic, J.M.; Stepanic, V.; Lucic B.; Amic, D. PM6 and DFT study of free radical scavenging activity of morin. Food chemistry, 2012, 134, pp. 1754-1760.
31. Akhtari, K.; Hassanzadeh, K.; Fakhraei, B.; Fakhraei, N.; Hassanzadeh, H.; Akhtari, G.; Zarei, S.A.; Hassanzadeh, K. Mechanisms of the hydroxyl and superoxide anion radical scavenging activity and protective effect on lipid peroxidation of thymoquinone: A DFT study. Monatsheftefür Chemie, 2015, 146, pp. 601-611.

CHEMISTRY JOURNAL OF MOLDOVA. General, Industrial and Ecological Chemistry. 2016, 11(2), 93-98
http://cjm.asm.md
http://dx.doi.org/10.19261/cjm.2016.11(2).05

DISPOSAL OF POISONOUS ORGANIC HALIDES BY USING THE ELECTROCHEMICAL METHOD: DFT SIMULATION

Tudor Spataru[a], Francisco Fernandez[b], Joseph W. Sista[a], Petru Spataru[c], Igor Povar[c*]

[a]*Columbia University, Department of Chemistry, 3000 Broadway, New York 10027, United States*
[b]*Natural Sciences Department, Hostos Community College, 500 Grand Concourse, Bronx, New York 10451, United States*
[c]*Institute of Chemistry of the Academy of Sciences of Moldova, 3 Academiei str., Chisinau MD 2028, Republic of Moldova*
**e-mail: ipovar@yahoo.ca; phone: (+373 22) 73 97 36; fax: (+373 22) 73 99 54*

Abstract. Geometry optimizations at the UBP86/6-311++G** level of electronic structure theory have been performed for DDT, *β*-hexachlorocyclohexane, and heptachlor organic polychlorides as well for their positive and negative ions. The HOMO composition of these neutral molecules show no participation of the carbon-chlorine atomic orbitals, while LUMO of the calculated molecules include a major contribution of the anti-bonding character atomic orbitals from the two or three carbon-chloride bonds of each calculated molecule. Consequently, the negative ions were the most sensitive structure during the geometry optimization, showing the carbon-chloride bonds cleaving during the electronic structure calculations. Further geometry optimization of the obtained neutral intermediate molecules after the first and second reducing by two electrons show that the electrochemical dehalogenation of the organic poychlorides is sequential.

Keywords: poisonous pesticides, organic chlorides, electrochemistry, DFT, carbon-chloride bonds.

Received: September 2016/ Revised final: October 2016/ Accepted: October 2016

Introduction

The electrochemical method for disposal of halogenated organic compounds leads to complete mineralization of organic halides. Generally, the electro-reductive treatments using new, improved electrochemical sensors, lead to partial recovery/recycling of chemicals, are regarded as an advantageous [1]. Methods of chemical and electro-chemical oxidation applied to organic pollutants attain, in most cases, a complete mineralization, being considered to have high-energy requirements [2]. Reduction will not lead to a complete mineralization, but to a complete dehalogenation, with a possible formation of double bonds. This has been proven for organic halides with one [3,4], two [5,6], three [7], four [8] or six [9] halogen atoms in their structure.

Dehalogenation reactions of halogen-alkanes have been studied by direct and indirect electrochemical reductions and classical kinetics. The electrochemical redox processes can be divided into two categories: direct (heterogeneous) and indirect or mediated (homogeneous) ones. Direct electrochemical reduction involves electrons accepted directly by the analyte from the cathode surface, while indirect electrochemical reduction occurs between the analyte and an electrogenerated species, which serves as catalyst. Some authors use the term "mediator" as an alternative for catalyst [1]. The catalyst can exist in the electrolyte solution or can be immobilized on the electrode surface, namely CME's or chemically modified electrodes [1,10]. By modifying the surface of the electrodes by adsorption of molecules or ions, the surface reactivity and slow kinetics can be overcome [10].

Mechanistically, the halogen atoms are removed in a successive fashion, along with a two electron transfer at more and more cathodic (negative) potentials. This has been proven for polyhalogenated aromatics [11] and remains under question for polyhalogenated aliphatics. The difficulty of attaining sufficiently cathodic potentials would explain why complete dehalogenation does not always take place. The lower the number of halogens in the molecule, the lower the oxidation potential and, therefore, the molecule becomes more prone to oxidative biodegradation and as opposed to anaerobic reduction [12]. Baron *et al*. [12] have investigated the electrochemical reduction of (1,2,5,6,9,10 hexabromo cyclododecane) and (1,2 dibromo cyclododecane) at glassy carbon electrode, under catalytic (homogeneous) and non-catalytic (heterogeneous) conditions. Their results suggest elimination of bromine ion, in presence and absence of CoTPP (cobalt tetraphenylporphyrin) as catalyst, albeit no information on the nature of products is provided.

In literature, there are several mechanisms proposed for the dehalogenation process and those depended on the structure of the compound and medium conditions [13]. According to Huang *et al*. [14] polychloroethanes suffer sequential dehydrohalogenation, favoured by the presence of protic solvent and dehalogenation, in a dry aprotic solvent. Among the cathode materials used by Huang's group there were Ag, Cu and Pd, which exhibited good catalytic activity towards reduction of organic halides, displaying high current efficiencies and positive shifts of reduction potentials. The electrochemistry of 1,2–dibromo cyclohexane shows an irreversible reduction with the formation of an alkene [15]. Vitamin B12, a naturally occurring catalyst, has been tested in the reductive debromination of vicinal dibromides, yielding to the formation of corresponding olefins [15]. Even in presence of protic substances, vicinal dibromides failed to give monobromide or saturated hydrocarbons [16]. It is obvious that the electrochemistry is a perfect tool for dehalogenation of organic polyhalogenates.

Despite there being relevant experimental studies, theoretical studies of the dehalogenation have not been done for the organic polyhalides. Saveant [17] has developed a semi classical theory of concerted dissociative electron transfer based on the Morse curve approximation of the potential energy of the breaking bond and a Marcus-Hush solvent reorganization energy. Substantial literature on the transition between the concerted and stepwise types of dissociative ET processes has been developed [10]. Unfortunately, these studies followed by electronic structure calculations have described the excited dissociative curves [18,19] of only single carbon-halide σ bond cleavage in small organic compounds. No studies regarding the stepwise simulation of the electrochemistry of polyhalides have been done up to now to our knowledge. Generally, this paper is dedicated to the DFT simulation of the electrochemical behaviour of the organic polyhalides.

Computational details

The geometry optimizations at the UBP86/6-311++G** level of electronic structure theory of DDT, β-hexachlorocyclohexane, and heptachlor organic polychlorides and their positive (+1,+2) and negative ions (-1,-2) have been performed. The calculations were carried out with the Gaussian09 suite of programs [20]. All geometric optimizations were made to the default tolerances of Gaussian. Therefore, the structures of the initial calculated neutral pesticides were found during the geometry optimization. The obtained bond distances (and angles) are in excellent agreement with the general known values for single and double bonds (and for hybridization angles between them). CASSCF (MCSCF) calculations with various numbers of occupied and unoccupied orbitals taken into their "active space" were carried out to check for Cl interactions and for charge transfer from occupied to empty orbitals; these calculations did not show any significant charge transfer.

Results and discussion

Detection, decomposition and transformation of persistent organic pollutants in water, sediment and soil can be achieved at the laboratory level with electrochemical methods of high sensitivity and selectivity [1]. However, it is more efficient to undertake preventative measures to avoid excessive contamination of environment materials (water, soil, etc.) by polychlorinated organic compounds. Unfortunately, Republic of Moldova inherited (from the former Soviet Union) multiple stocks of extremely hazardous chemical waste. As environmental regulations become more stringent, it becomes absolutely necessary to minimize, recover and recycle industrial waste to the extent possible, lowering the amounts of generated pollutants and discovering new ecological ways of disposal. Large deposits of the pesticides DDT, heptachlor and *β*-hexachlorocyclohexane can be found in territories of the former Soviet Union. Therefore these three organic polychlorides will be the subject of our attention in this paper. The chemical structures of DDT, *β*-hexachlorocyclohexane and heptachlor are presented in Figure 1.

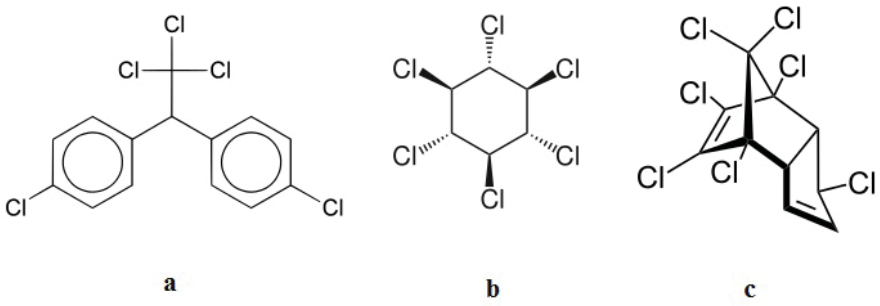

Figure 1. Molecular structures of (a) DDT, (b) *β*-hexachlorocyclohexane and (c) heptachlor.

Considering the adiabatic electron transfer between electrode (and catalyst) and organic polychlorides the DFT geometry optimization was done in order to follow their reactivity and structural modification under influence of the total charge modification. The behaviour of molecules after the receiving or leaving of one or two electrons depends decisively on the nature of frontier molecular orbitals. If the system receives one or two electrons, the nature of the lowest unoccupied orbital of the neutral molecule determines its further course, on the other hand, if the system is giving one or two electrons the nature of the highest occupied molecular orbital of the neutral molecule determines the further development of the system. The frontier molecular orbitals of the calculated systems are presented in Figure 2. One can observe from this figure that the highest occupied molecular orbital (HOMO) of every calculated organic polychloride compound does not include any significant bonding or anti-bonding contribution of the atomic orbitals to the carbon-chloride bonds. The HOMO of the DDT and *β*-hexachlorocyclohexane molecules is composed mainly from non-bonding *π*-orbital contributions of carbon and chloride atoms, while the HOMO of the heptachlor molecule is composed from a mixing of *π*- and *σ*- non-bonding orbitals. Therefore, one does not expect major modifications of the structural behaviour of the calculated positive charged ions as compared with the neutral molecules. Indeed, our DFT calculation of the +1 and even +2 ions do not show a significant structural modification of the calculated organic polychloride molecules. One can, therefore, predict little success when using the oxidation electrochemistry to dispose of these pesticides. Although, this conclusion may be affected by the nature of the electron transfer (ET) between electrode (or catalyst) and calculated organic compounds. Indeed, the electronic transfer between electrode orbitals

(or catalyst orbitals) and organic polychloride orbitals might have either adiabatic or non-adiabatic nature [20]. The determination of the nature of the ET can be made by comparing the measured k(ET) of the electron transfer with a value calculated from the Marcus-Hush theory of outer-sphere adiabatic ET. If the value of k(ET) is equal or close to $\kappa \approx 1$, the ET is adiabatic, and if $\kappa <<< 1$, it is non-adiabatic [21]. For non-adiabatic ET the DFT calculation of the electronic structure of the substrate is not valid and no conclusion regarding the reactivity of the substrate ions can be made [22,23]. More sophisticated electronic structure methods, like MCSCF must be applied to these studied processes [22,24,25]. Although, the true nature of the ET can be determined using the experimental data, along with theoretical ones [21].

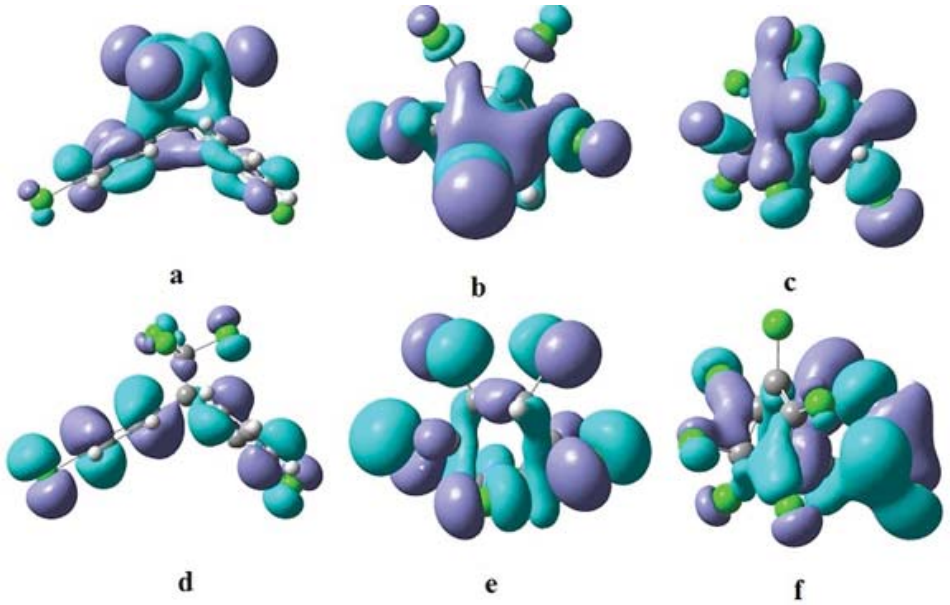

Figure 2. Frontier molecular orbital surfaces of UBP86/6-311++G DFT calculated neutral systems: a) LUMO-DDT; b) LUMO- *β*-hexachloro-cyclohexane; c) LUMO- heptachlor; d) HOMO-DDT; e) HOMO- *β*-hexachloro-cyclohexane; f) HOMO- heptachlor.**

The reactivity of the negative ions of organic polychlorides must be determined from the nature of Lowest Unoccupied Molecular Orbital (LUMO) of the neutral calculated compounds. If the LUMO of the studied compounds has an anti-bonding character along C-Cl bonds then one should expect the weakening (increasing of the C-Cl distances) or even breaking. One can observe from Figure 2 that the LUMO of the DDT molecule includes the huge antibonding contributions of the carbon and chloride atomic orbitals of the -C-Cl_3 group. Also, the LUMO of the heptachlor includes a consistent antibonding contribution of carbon and chloride atoms of the two side C-Cl bonds (Figure 2). The atomic orbitals of the other carbon and chloride atoms of DDT and heptachlor molecules have a negligible participation in the structure of their LUMO's. Therefore, one should expect that the transfer of an electron or two to the DDT would lead to the weakening or total cleavage of some C-Cl bonds of the CCl_3 group. Also, the transfer of an electron or two on heptachlor molecule would lead to the weakening or rupture of only two side C-Cl bonds. The rest of the C-Cl bonds in these geometry optimized systems remain at the C-Cl bond distance equal to the "normal" distance of the usual carbon-chlorine bond equal to about 1.77 Å. Indeed, our geometry optimizations of $(DDT)^{-1}$, $(DDT)^{-2}$, $(heptachlor)^{-1}$, and $(heptachlor)^{-2}$ negative ions show the one chlorine atom from $(DDT)^{-1}$ system and two chlorine atoms of the $(heptachlor)^{-1}$ depart away from carbon atoms up to the complete cleavage of the respective C-Cl bonds. This result is in full agreement with experimental [14]. The first conclusion, which must drawn is that DDT and heptachlor pesticides cannot be dehalogenated in one reducing electrochemistry step. This confirms the experimental data of the stepwise removal of the halogen atoms from polyhalogenated organic molecules [11,14]. A second conclusion regarding the geometry optimization of these four ions is that after the first dehalogenation step they form radicals at the carbon atoms of the former C-Cl bonds. These radicals would participate in various recombination and coupling reactions with the neighbouring molecules and ions. In conclusion, the next several steps of the dehalogenation of DDT and heptachlor pesticides must be studied only by using DFT method in straight connection with the results of the experimental electrochemical and analytical methods regarding the behavior of the formed ions after the first electrochemical dehalogenation.

The investigation of the direct electrochemical reduction of organic polyhalides with vicinal halogens in an aprotic medium (DMF) showed that the corresponding olefin is formed according to a two-electron stoichiometry [26]. In fact, alkyl halides do not follow a concerted mechanism in which a two electron transfer and bond rupture occur in a single step [5,14,26]. There is a clear trans- preference for the reaction in the case of dibromocyclohexane [27]. As one can observe in Figure 1, several two chloride combinations in *β*-hexachlorocyclohexane molecule can be considered as vicinal trans- atoms. Moreover, the LUMO of the *β*-hexachlorocyclohexane neutral molecule includes

the anti-bonding contribution of atomic orbitals participating into two vicinal carbon-chloride bonds (Figure 2). One should expect that two vicinal C-Cl bonds with significant anti-bonding contributions present in the LUMO of *β*-hexachlorocyclohexane neutral molecule would be cleaved upon receiving one or two electrons. Geometry optimization of the (*β*-hexachlorocyclohexane)$^{-1}$ and (*β*-hexachlorocyclohexane)$^{-2}$ has shown that, indeed, both vicinal chloride atoms move from their respective carbon atoms at a distance of 2.55 Å for -1 charged ion and completely remove for the -2 ion. The role of the solvent can be critical in the further trapping of the two chlorine atoms from the *β*-hexachlorocyclohexane negative ion. For instance, in their discussion of the mechanism for the reductive cleavage reaction of Me-Cl in homogeneous solution, Martin and Finke include the effect of solvent trapping [27]. On the basis of this mechanism, they suggest that the solvent effect is more likely an effect of the solvent acting as a good or bad radical trap. Especially, the polar solvents must play an important role in the further trapping of the "cleaved" C-Cl bond since, interestingly, each chlorine atom in these two bonds have Malliken charge very close to -0.5 a.u. in the -1 ion and very close to -1 a.u. in the -2 charged ion. Their full separation leads to a neutral trans-tetrachloro-cyclohexene molecule. The illustration of the first stage of the dehalogenation of *β*-hexachlorohexane is presented in the Scheme 1.

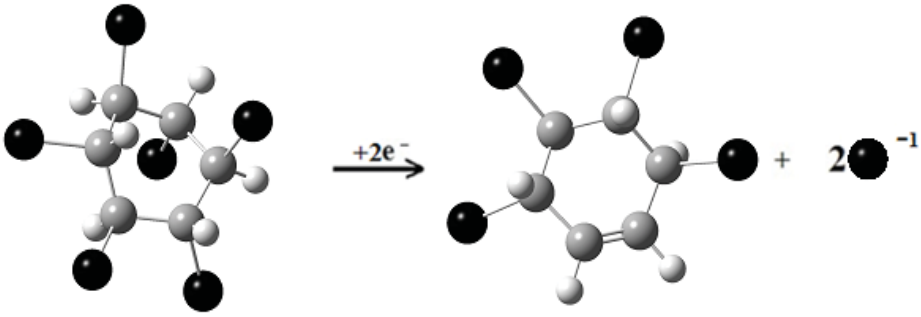

Scheme 1. Illustration showing the first stage of the dehalogenation of *β*-hexachlorohexane. Chlorine atoms are depicted as large black spheres; hydrogen atoms are small grey spheres; carbon atoms are large grey spheres.

Fortunately, the composition of the neutral trans-tetrachloro-cyclohexene LUMO exhibits a significant antibonding contribution from the atomic orbitals of the carbon and chlorine atoms of two other cobalt chlorine bonds (Figure 3). Interestingly, the presence of the double bond in the trans-tetrachloro-cyclohexene does not influence the LUMO structure. Note, that these two carbon-chlorine bonds are not vicinal anymore. Nevertheless, the formation of the diene bonds in the case of these two carbon-chlorine bond cleavage lowers the total energy of the next electrochemical reduced products. Indeed, the geometry optimization of the -1 negative ion of the trans-tetrachloro-cyclohexene molecule leads to stretching of the carbon-chlorine bonds at the distance of about 2.8 Å with the same Mulliken charge of about -0.5 a.u.

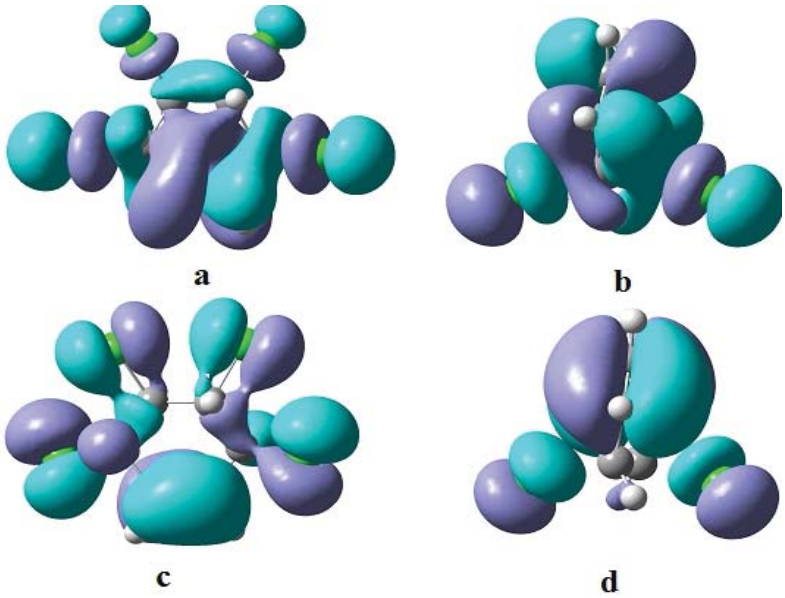

Figure 3. Frontier molecular orbital surfaces of UBP86/6-311++G DFT calculated neutral systems: a) LUMO-tetrachloro-hexene; b) LUMO- trans-dichloro-hexadiene c) HOMO-trans-tetrachloro-hexene); d) HOMO-trans-dichloro-hexadiene.**

The geometry optimization leads to complete C-Cl bond cleavage of the -2 charged ion and the Milliken charge on chlorine equal to about -1 a.u. Again, we expect that the solvent would further trap the chlorine atoms. This step is presented in Scheme 2.

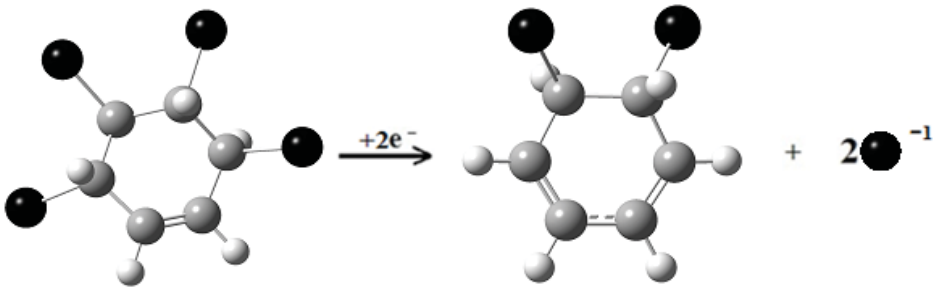

Scheme 2. Illustration showing the second stage of the dehalogenation of *β*-hexachlorohexane.

The formed trans-dichloro-cyclohexadiene neutral molecule can be again reduced by one or two electrons by using electrochemistry method. One can observe that the diene bonds do not influence the presence of the huge contribution of the carbon and chloride antibonding molecular orbitals of the last carbon-chloride bonds present in the LUMO of this last neutral chlorinated compound (Figure 3). The geometry optimization of its negative ion $(trans\text{-}dichloro\text{-}hexadiene)^{-1}$ leads to the stretching of the last carbon-chlorine bonds up to 3.00 Å, while the geometry optimization of -2 ion lead to complete C-Cl bond cleavage. The last reducing step of trans-dichloro-hexadiene intermediate compound is presented in Scheme 3. One can observe that the final product of the sequential dechlorination of the *β*-hexachlorocyclohexane molecule by using reducing electrochemistry is benzene, which after its purification can be reused for next economic needs.

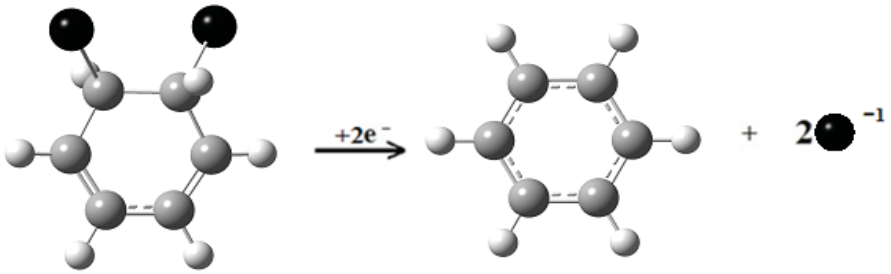

Scheme 3. Illustration showing the third stage of the dehalogenation of *β*-hexachlorohexane.

Conclusions

Geometry optimization of the DDT, *β*-hexachlorocyclohexane and heptachlor pesticide molecules and their positive and negative ions have been performed by using DFT method at UBV86/ 6-311++G** theory level. The positive ions of the studied molecules are quite stable during the geometry optimization. The negative ions of the studied molecules are not stable during the optimization procedure. Finally, one should conclude that the dehalogenation of the organic polychlorides is a several steps sequential procedure.

Acknowledgments

The study is produced as part of the Diaspora Professional Return Program, which is a part of the Diaspora Engagement Hub, implemented by the Diaspora Relations Bureau of the State Chancellery of the Republic of Moldova in partnership with the International Organization for Migration, Mission to Moldova, in the framework of the "Consolidating Moldova's Migration and Development Institutional Framework" project, funded by the Swiss Agency for Development and Cooperation. Also, this research was supported, in part, under National Science Foundation Grants CNS-0958379 and CNS- 0855217 and the City University of New York High Performance Computing Center at the College of Staten Island and by the National Science Foundation through TeraGrid resources provided by the TeraGrid Science Gateways program under grants CHE090082 and CHE0000036.

References

1. Rodinini, S.; Vertova, A. Electroreduction of halogenated organic compounds. Electrochemistry for the Environment, 2010, pp. 279 – 306.

2. Kulikov, S.M.; Juettner, K.M. electrochemical reductive dehalogenation of brominated organic compounds in water-methanol media on a boron doped diamond electrode: Bulk electrolysis. International Journal of Chemical Sciences, 2009, 7(2), pp. 625-631.
3. Beebower, M.L. Electrochemical reduction of 1-bromooctane catalyzed by a dicobalt complex. Honors Thesis, Texas State University-San Marcos, San Marcos, Texas, USA, 2010.
4. Wolf, N.L.; Peters, D.G.; Mubarak, M.S. Electrochemical reduction of 1-halooctanes at platinized platinum electrodes in dimethylformamide containing tetramethylammonium tetrafluoroborate. Journal of the Electrochemical Society, 2006, 153(1), pp. E1-E4.
5. Casanova, J.; Rogers, H.R. Electroorganic chemistry. II. Electroreduction of vicinal dibromides. Journal of Organic Chemistry, 1974, 39(16), pp. 2408–2410.
6. Rusling, J.F.; Zhou, D.L. Electrochemical catalysis in microemulsions. Dynamics and organic synthesis. Journal of Electroanalytical Chemistry, 1997, 439, pp. 89-96.
7. Bishop, G.W.; Karty, J.A.; Peters, D.J. catalytic reduction of 1,1,1-trichloro-2,2,2-trifluoroethane (CFC-113a) by Co(I) salen electrogenerated at vitreous carbon cathodes in dimethylformamide. Journal of the Electrochemical Society, 2007, 154(4), pp. F65-F69.
8. Scialdone, O.; Guarisco, C.; Galia, A.; Herbois, R. Electroreduction of aliphatic chlorides at silver cathodes in water. Journal of Electroanalytical Chemistry, 2010, 641, pp. 14-22.
9. Lo, K.W.; Saha-Roy, S.C.; Jans, U. Investigation of the reaction of hexabromocyclododecane with polysulfide and bisulfide in methanol/water solutions. Chemosphere 2012, 87, pp. 158-162.
10. Navaratne, A.; Priyantha, N. Chemically modified electrodes for detection of pesticides. 2011, pp. 453-464. http://cdn.intechopen.com/pdfs-wm/21000.pdf
11. Muthukrishnan, A.; Boyarskiy, V.; Sangaranarayanan, M.V.; Boyarskiy, I. Mechanism and regioselectivity of the electrochemical reduction in polychlorinatedbiphenyls (PCBs): Kinetic analysis for the successive reduction of chlorines from dichlorobiphenyls. Journal of Physical Chemistry C, 2012, 116, pp. 655-664.
12. Baron, L.; Kozlowska, A.; Kurek, S.S. Conditions of anaerobic biodegradation of common brominated flame retardants based on model electrochemical studies of hexabromocyclododecane(HBCD). CHEMIK, 2011, 10, pp. 1007-1010.
13. Sims, J.L.; Suflita, J.M.; Russell, H.H. Reductive dehalogenation of organic contaminants in soils and ground water. U.S. Environmental Protection Agency: Washington, DC, EPA/540/4-90/054 (NTIS 91-191056), 1991, 12p.
14. Huang, B.; Isse, A.A.; Durante, C.; Wei, C.; Gennaro, A. Electrocatalytic properties of transition metals toward reductive dechlorination of polychloroethane. Electrochimica Acta, 2012, 70, pp. 50-61.
15. Saveant, J. M. Molecular catalysis of electrochemical reactions. Mechanistic aspects. Chemical Reviews, 2008, 108, pp. 2348-2378.
16. Compton, R.G.; Banks, E.C. Understanding Voltammetry: Simulation of Electrode Processes. Imperial College Press: London, 2007, 249 p.
17. Saveant, J.M. A simple model for the kinetics of dissociative electron transfer in polar solvents. Application to the homogeneous and heterogeneous reduction of alkyl halides. Journal of the American Chemical Society, 1987, 109(22), pp. 6788–6795.
18. Shu-Yuan, Y.; Ming-Bao, H. CASPT2 study on electronic states of the $C_6H_5Cl^+$ ion. Chemical Physics, 2006, 328(1–3), pp. 291–298.
19. Shu-Yuan Y.; Cheng-Gen Z. Electronic states of the m-C6H4Cl2+ ion studied using multiconfiguration second-order perturbation theory. Journal of Molecular Spectroscopy, 2014, 295, pp. 58–61.
20. Frisch, M. J.; Trucks, G.W.; Schlegel, H.B. et al. Gaussian 09, Revision B.01; Gaussian, Inc.: Wallingford, CT, 2009.
21. Birke, R.L.; Qingdong, H.; Spataru, T.; Gosser, D.K. Jr. Electroreduction of a series of alkylcobalamins: mechanism of stepwise reductive cleavage of the Co-C bond, Journal of the American Chemical Society, 2006, 128(6), pp. 1922–1936.
22. Spataru, T.; Birke, R.L. Carbon−Cobalt bond distance and bond cleavage in one-electron reduced methylcobalamin: A failure of the conventional DFT method. The Journal of Physical Chemistry A, 2006, 110, pp. 8599-8604.
23. Bersuker, I.B. Limitations of density functional theory in application to degenerate states. Journal of Computational Chemistry, 1997, 108(2) pp. 260-267.
24. Bearpark, M.J.; Blancafort, L.; Robb, M.A. Molecular physics: the pseudo-Jahn–Teller effect: a CASSCF diagnostic. An International Journal at the Interface between Chemistry and Physics, 2002, 100, pp. 1735-1739.
25. Spataru, T.; Fernandez, F. The nature of the Co-C bond cleavage processes in methylcob(II)alamin and adenosylcob(III)alamin. Chemistry Journal of Moldova, 2016, 11(1), pp. 10-20.
26. Savéant, J.M. Molecular catalysis of electrochemical reactions. Mechanistic aspects. Chemical Reviews, 2008, 108, pp. 2348–2378.
27. Martin, B.D.; Finke, R.G. Methylcobalamin's full- vs. "half"-strength cobalt-carbon sigma bonds and bond dissociation enthalpies: A>10(15) Co-CH3 homolysis rate enhancement following one-antibonding-electron reduction of methylcobalamin. Journal of the American Chemical Society, 1992, 114(2), pp. 585-92.

CHEMISTRY JOURNAL OF MOLDOVA. General, Industrial and Ecological Chemistry. 2016, 11(2), 99-104
http://cjm.asm.md
http://dx.doi.org/10.19261/cjm.2016.11(2).09

STRUCTURAL DISTORTIONS OF COORDINATED KETENE MOLECULE INDUCED BY THE PSEUDO JAHN-TELLER EFFECT

Natalia Gorinchoy

Institute of Chemistry of Academy of Sciences of Moldova, 3, Academiei str., Chisinau MD-2028, Republic of Moldova
e-mail: ngorinchoy@yahoo.com

Abstract. It is demonstrated that the only reason of structural distortions of ketene molecule coordinated in the complexes VCp_2-H_2C_2O (**I**) and $Pt(PPh_3)_2$-H_2C_2O (**II**) is the pseudo Jahn-Teller effect (PJTE) induced by the orbital charge transfers (OCTs) by coordination. It is shown that the η^2-(C-O) coordination and the in-plane b_2-type distortion of ketene in the complex (**I**) is due to the PJTE induced by the back donation to its LUMO $3b_2$ (π_{CO}*). The η^2-(C-C) coordination mode, as well as the out-of-plane b_1-type distortion of the molecule in the complex (**II**) is caused by two OSTs: from the HOMO $2b_1(\pi_{CC})$ to the metal, and from the d_{xy}- atomic orbital (AO) of the atom of Pt to the vacant $3b_1(\pi_{CC}$*) molecular orbital (MO) of ketene, thus being the result of the diorbital Pt-ketene interaction. The necessary parameters of the PJTE were estimated by considering the excited states of free ketene molecule, and the values of the OSTs were obtained from the electronic structure calculations of the complexes.

Keywords: Pseudo Jahn-Teller effect, orbital charge transfers, ketene excited states, metal ketene complex.

Received: November 2016/ Revised final: December 2016/ Accepted: December 2016

Introduction

The case of coordinated ketene molecule is interesting in that ketenes can be bound to transition metal complexes in a variety of ways. To date, a number of complexes with ketenes were synthesized and structurally determined by X-ray diffraction [1-7]. It is generally accepted that early transition metal complexes favor the η^2-(C-O) bonding mode [3,6], the η^2-(C-C) mode is preferred by late transition metal complexes [2,7]. Moreover, in the first case the ketene molecule undergoes the in-plane distortion, while the η^2-(C-C) coordination mode leads to the out-of-plane distortion of ketene [1,7,8]. Some theoretical investigations of ketene binding to Ni, Pt [7], and Pd [8] were reported. These computational studies show that Ni binds ketene molecule through the η^2-(C-O) coordination mode, and Pd and Pt prefer the η^2-(C-C) binding mode. However, the origin of instability of coordinated ketene high-symmetry (C_{2v}) nuclear configuration and its distortions in different complexes were not considered.

In the present paper, we apply a new approach to handle instabilities and structural changes in coordinated and adsorbed molecules [9] in order to reveal the origin of structural distortions of ketene molecule coordinated in two transition metal complexes, VCp_2-H_2C_2O (**I**) and $Pt(PPh_3)_2$-H_2C_2O (**II**). It is based on an approximate evaluation of the Jahn-Teller effect (JTE), pseudo JTE (PJTE), and Renner-Teller effect (RTE) induced by the orbital charge transfers (OCTs) in such systems. This theoretical approach proved to be effective and predictable in rationalization of experimental data regarding the distortion of coordinated molecules [9-11]. It was shown that in-plane b_2-type distortion of ketene molecule, coordinated in the complex (**I**) is explained as due to the PJTE induced by the back donation to its LUMO $3b_2$ (π_{CO}*). The η^2-(C-C) coordination mode, as well as the out-of-plane b_1-type distortion of the molecule in the complex (**II**) is caused by the two OCTs: from the HOMO $2b_1(\pi_{CC})$ to the metal, and from the d_{xy}- atomic orbital (AO) of Pt to the vacant $3b_1(\pi_{CC}$*) molecular orbital (MO) of ketene.

Theoretical model and computational details

Coordination of a ligand to the transition metal complex is accompanied by the formation of bonding molecular orbitals (MOs) between the metal and the ligand. Due to formation of these bonding MOs the orbital charge transfers (OCT) to or from coordinated molecule take place. We assume that the influence of these small OCTs Δq ($\Delta q << ne$, where n is the number of electrons in the molecule) can be considered as a small perturbation to the integer-electron system. Then, in the first order of perturbation theory, it can be presumed that the additional charge occupies any vacant MO of the molecule or leaves one of the occupied MO without changing significantly the MO wavefunctions. These OCTs influence the PJTE in coordinated molecules leading to the instability and distortion of their high-symmetry nuclear configurations.

In the pseudo Jahn-Teller effect the problem of the stability or instability of molecular nuclear configuration with respect to any symmetrized coordinate Q may be reduced to the consideration of the curvature K of the adiabatic potential energy surface (APES) at $Q = Q_0$ in the direction of Q. In the second order perturbation theory with respect to small nuclear displacements from the reference point Q_0 the expression for K is given by Eq.(1) [12]:

$$K = K_0 - \sum_i 2\left|F_Q^{(1,i)}\right|^2/\Delta_i \qquad (1)$$

where

$$F_Q^{(1,i)} = \langle 1|(\partial H/\partial Q)_0|i\rangle \quad (2)$$

is the vibronic coupling constant between the reference $|1\rangle$ and higher in energy excited state $|i\rangle$, Δ_i is the energy gaps between the mixing states, K_0 is the primary force constant (the force constant without the PJTE), and H is the Hamiltonian of the electronic subsystem in the adiabatic approximation. In the particular case of two mixing states $|1\rangle$ and $|2\rangle$ the value of K is given by Eq.(3):

$$K = K_0 - 2\left|F_Q^{(1,2)}\right|^2/\Delta_{12} \quad (3)$$

and the distortion of a nondegenerate state $|1\rangle$ in the Q direction takes place when the inequality Eq.(4) holds:

$$\left(\left|F_Q^{(1,2)}\right|^2/\Delta_{12}\right) > K_0 \quad (4)$$

In the "frozen orbital" approximation it is assumed that the $|1\rangle \rightarrow |2\rangle$ excitation can be described by the one-electron excitation $|i\rangle \rightarrow |j\rangle$ that changes the occupations of molecular orbitals $|i\rangle$ and $|j\rangle$, while the other MOs remain unchanged. In this case the off-diagonal matrix element $F_Q^{(1,2)}$ can be simply expressed (Eq.(5)) by means of the off-diagonal orbital vibronic coupling constant (OVCC) $f_Q^{(i,j)}$ [12],

$$F_Q^{(1,2)} \approx f_Q^{(i,j)} = \langle i|(\partial H/\partial Q)_0|j\rangle \quad (5)$$

In [9] it was shown that in this case the curvature K^{coord} of the APES of coordinated molecule along the distortion coordinate can be expressed by Eq.(6).

$$K_Q^{coord.} = K_Q^{free} - 2\sum_{i,j}\left(\Delta q_i - \Delta q_j\right)\left|f_Q^{(i,j)}\right|^2/\Delta_{ij} \quad (6)$$

Here K^{free} is the curvature of the APES of free molecule in the Q direction, Δq_i and Δq_j are the OCTs to or from the molecular orbitals $|i\rangle$ and $|j\rangle$, and $f_Q^{(i,j)}$ is the off-diagonal OVCC between them. The condition of instability in the Q direction Eq.(4) in this case can be rewritten as

$$2\sum_{i,j}\left(\Delta q_i - \Delta q_j\right)\left|f_Q^{(i,j)}\right|^2/\Delta_{ij} > K_Q^{free} \quad (7)$$

If the inequality Eq.(7) holds then $K^{coord} < 0$ which shows that the molecule is unstable with respect to the symmetrized coordinate of nuclear displacements Q. To estimate the value of K^{coord} we need to calculate the curvature of the APES of free molecule (K^{free}) in this direction, to evaluate the PJT coupling constants $f_Q^{(i,j)}$ and the orbital charge transfers Δq_i induced by coordination.

To do this, we performed the electronic structure calculations of the free ketene molecule and the complexes VCp_2-H_2C_2O (**I**) and $Pt(PPh_3)_2$-H_2C_2O (**II**). All calculations were performed using the GAUSSIAN 09 program package [13]. The geometry optimization of all the considered species was carried out by means of the DFT (B3LYP) method [14] using the LANL2DZ basis set with non-relativistic effective core potential for Pt [15] and the split-valence basis sets 6-31G(d,p) [16] for all other atoms in the systems.

To estimate the values of the orbital charge transfers to and from coordinated ketene molecule, the calculated MOs of the complexes were rewritten in the basis of the eigenfunctions of the free ketene molecule and the atomic orbitals (AO) of other atoms. Then the changes in the occupations of MOs of coordinated molecule in the complexes are estimated from the difference in Mulliken populations of the corresponding orbitals.

Results and discussion

A general view of considered compounds, together with the relevant geometry parameters is shown in Figure 1. It can be seen that the geometry of the C_2H_2O molecule in the complexes is significantly different from that of the free molecule. In the ground $^1A_1$ electronic state it is planar with the nuclear configuration of C_{2v} symmetry. In the complex VCp_2-H_2C_2O the η^2-(C-O) binding mode takes place, the ketene molecule undergoes the in-plane distortion (∠C-C-O= 137.10º) with the significant elongation of the C-O bond (1.29Å *versus* 1.17Å in free molecule). The same C-O bond elongation and C-C-O moiety bending in η^2-(C-O) coordinated ketenes is also observed in other early transition metal complexes [1,3,7]. The η^2-(C-C) binding mode is preferred in the complex (**II**). The coordination is accompanied by the out-of-plane distortion of ketene molecule (∠C-C-O = 145.30º and

dih(C-CH_2) = 22.7º) and by significant elongation of the C-C bond (1.43 Å *versus* 1.30 Å in free molecule). The optimized geometry parameters agree well the experimental data for η^2-(C-C)-coordinated ketenes [1,8].

It should be noted that the molecule also undergoes similar distortions in its excited states. It was established [17,18] that in the lowest excited singlet $^1A_2$ and triplet $^3A_2$ electronic states ketene molecule undergoes the in-plane distortion leading to the planar C_s structure, wherein the oxygen is bent away from the C-C axis (Figure 1*d*). The second triplet excited $^3A_1$ state is stabilized by the out-of-plane distortion to the pyramidal nuclear configuration also of C_s symmetry, but the reflection plane in this case is perpendicular to the molecular plane of the C_{2v} structure (Figure 1*e*).

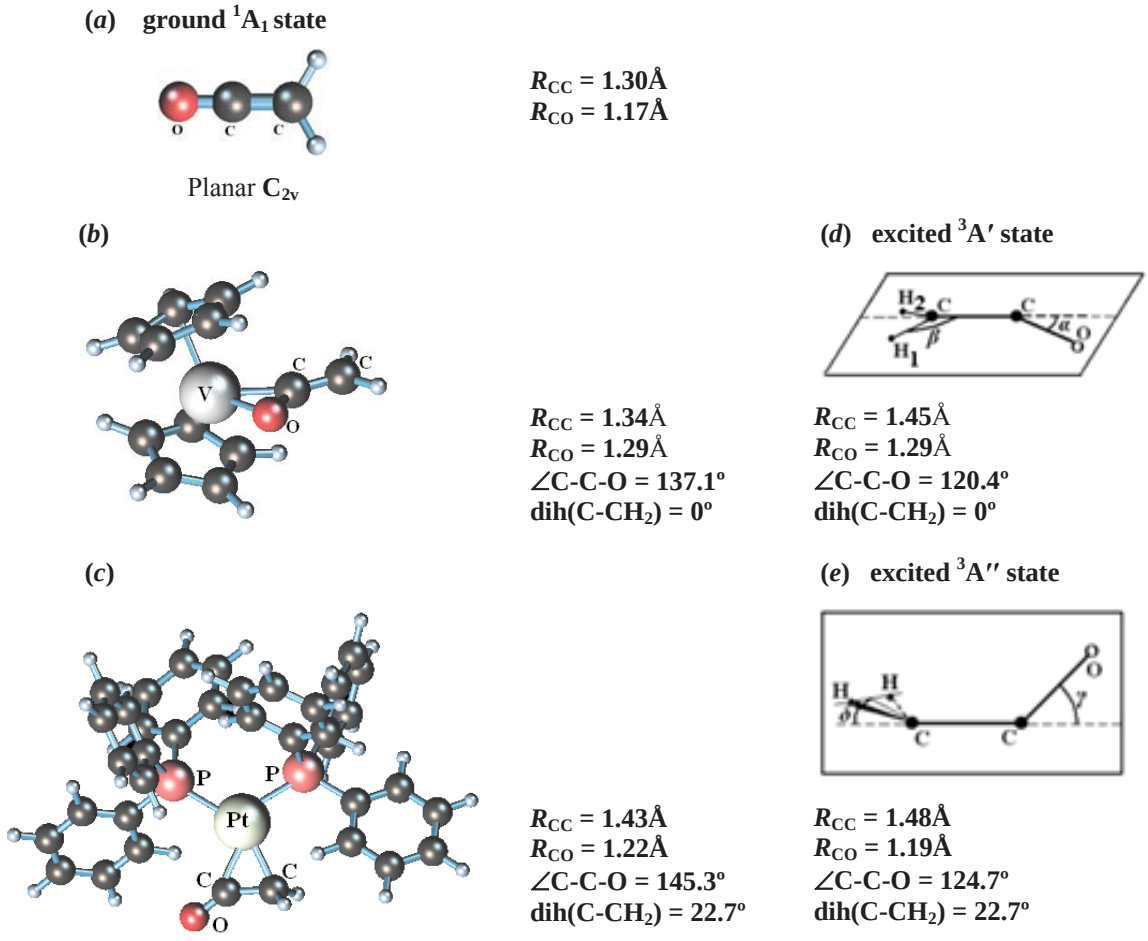

Figure 1. Optimized structures for (*a*) free ketene molecule in the ground $^1A_1$ electronic state (C_{2v}), (*b*)- VCp_2-H_2C_2O (I) complex, (*c*)- $Pt(PPh_3)_2$-H_2C_2O (II) complex, (*d*)- ketene molecule in the first excited $^3A'$ state, (*e*) ketene molecule in the second excited $^3A''$ state.

Previously [19] we have shown that instability of the high-symmetry C_{2v} nuclear configuration of ketene molecule in the $^3A_2$ and $^3A_1$ excited states and the corresponding low-symmetry in-plane and out-of-plane distortions are due to the pseudo Jahn-Teller mixing of these states with higher excited $^3B_1$ state. From this statement, some conclusions can be drawn, which may be useful in the analysis of distortions of coordinated ketene molecule. Given the fact that the $^3A_2$ and $^3B_1$ excited states, as well as the $^3A_1$ and $^3B_1$ states, differ from each other only by one spin-orbital, and the Hamiltonian H is the sum of one-electron operators, the vibronic coupling constants and between these states are respectively equal to the orbital vibronic constants $f_{b2}^{3b2,8a1}$ and $f_{b1}^{3b1,8a1}$ (Eqs.(8)) mixing the vacant molecular orbitals $3b_2$ and $8a_1$, and $3b_1$ and $8a_1$ MOs, respectively. The MO level scheme of free H_2C_2O molecule is shown in Figure 2 on the left.

$$F_{b2}^{A_2,B_1} = f_{b2}^{3b2,8a1} = \langle 3b_2|(\partial H/\partial Q_{b2})_0|8a_1\rangle$$
$$F_{b1}^{A_1,B_1} = f_{b1}^{3b1,8a1} = \langle 3b_1|(\partial H/\partial Q_{b1})_0|8a_1\rangle \quad (8)$$

From Eqs.(8) it is seen that the PJT contribution to the instability of the C_{2v} configuration of ketene molecule in considered $^3A_2$ ($2b_1 \rightarrow 3b_2$) and $^3A_1$ ($2b_1 \rightarrow 3b_1$) excited state is determined only by one OVCC, $f_{b2}^{3b2,8a1}$ in the first case and $f_{b1}^{3b1,8a1}$ in the second one. Therefore, we can assume that the corresponding anionic $^2B_2(...2b_2^2 2b_1^2 3b_2)$ and $^2B_1(...2b_2^2 2b_1^2 3b_1)$ states of ketene molecule are also unstable in the C_{2v} nuclear configuration with respect to considered b_2-type and b_1-type distortions due to the vibronic coupling of these states with the higher $^2A_{1(...2}b_2^2 2b_1^2 8a_1)$ anionic state, with the same OVCCs as in Eqs.(8). Indeed, this is confirmed by calculations of the AP curves for the $^2B_2$ and $^2B_1$ anionic states along the Q_{b2} and Q_{b1} coordinates, respectively.

Based on the above, we can draw some conclusions about the binding modes and the distortions of coordinated ketene. If the back donation occurs on the LUMO $3b_2$ (which is the antibonding with respect to the C-O bond), and if this charge transfer is large enough to satisfy the inequality (7), then the η^2-(C-O) coordination mode takes place, and the molecule undergoes the in-plane distortion of the b_2-type. The out-of-plane distortion of coordinated ketene can be realized only if the virtual $3b_1$ MO acquires some additional charge by coordination. In free ketene molecule, this $3b_1$ MO is much higher in energy (by 1.93 eV) than the LUMO $3b_2$. However, calculations of the ketene cation show that $3b_1$ MO is significantly stabilized by ionization (difference in energies of $3b_1$ and $3b_2$ MOs is reduced to 0.13 eV). In the context of the problem under discussion, this means that the η^2-(C-C) coordination mode, as well as the out-of-plane distortion of the molecule can occur only as the result of a diorbital metal-ketene interaction. If the metal is able to form a bond with the occupied $2b_1$ MO ($\pi_{C\text{-}C}$), then the C-C coordination mode is fixed, some electron density from the HOMO $2b_1$ is transferred to the complex, thereby stabilizing the unoccupied $3b_1$ MO, so the back donation to it becomes possible.

To reveal which orbital charge transfers to or from coordinated ketene molecule leading to its distortions take place in considered compounds, consider molecular orbitals of the complexes which are mainly involved in the vanadium-ketene and platinum-ketene binding (Figure 2). In the first case the V-H_2C_2O binding is provided by forming of only one bonding MO which is composed from the filled $3d_{xy}$ orbital of vanadium and the LUMO $3b_2$ of C_2H_2O (Figure 2), the orbital charge transfer is quite significant, $\Delta q(3b_2) = 0.46\bar{e}$. Due to forming of this MO the electron density transfers from the $3d_{xy}$-AO of the atom of V to the vacant $3b_2$-MO of the ketene molecule. Therefore, one can conclude that V-ketene bonding in the complex (**I**) is provided by the π-back donation from the transition metal to the ligand.

Then, the value of the curvature of the AP of coordinated ketene molecule with respect to the in-plane distortion of b_2-type can be estimated by Eq.(9):

$$K_{b2}^{coord} = K_{b2}^{free} - 2\Delta q_{3b2} \left| f_{b2}^{(3b2,8a1)} \right|^2 / \Delta_{3b2,8a1} \qquad (9)$$

Substituting the calculated values of all the parameters: $K^{free}(b_2) = 3.06$ eV/Å^2, $f_{b2}^{(3b2,8a1)} = 6.16$ eV/Å [19], and $\Delta = 5.53$ eV, we obtain $K^{coord}(b_2) = -3.25$ V/Å^2.

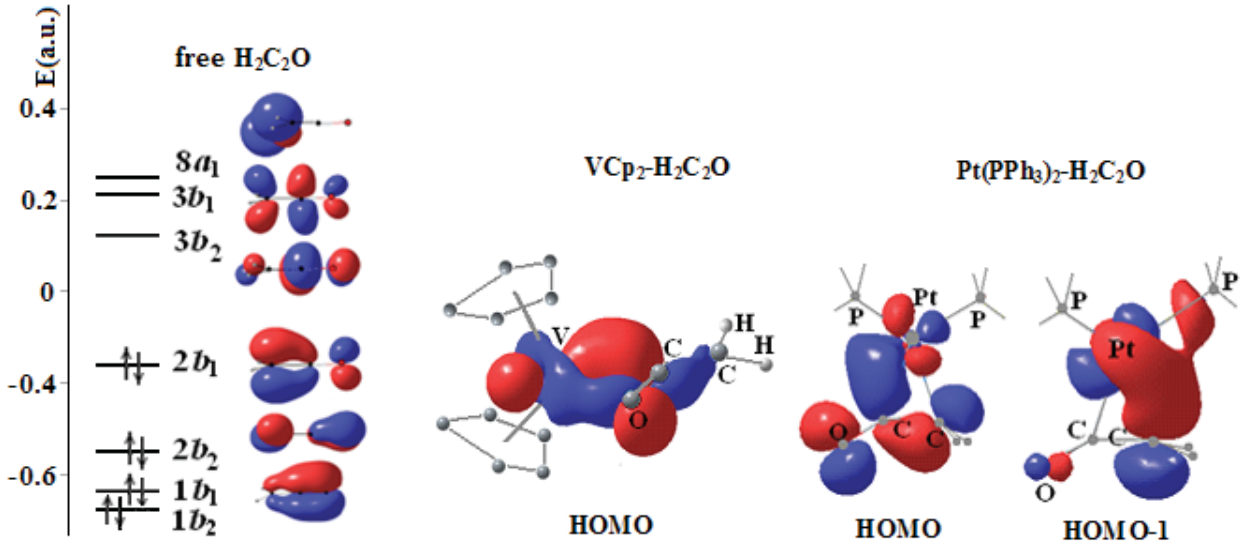

Figure 2. MO level scheme of free H_2C_2O molecule (left) and metal-ketene bonding molecular orbitals in VCp_2-H_2C_2O and $Pt(PPh_3)_2$-H_2C_2O complexes.

In the $Pt(PPh_3)_2$-H_2C_2O complex the two bonding molecular orbitals are formed between the metal and ketene molecule (Figure 2). The HOMO of the complex is the linear combination of $5d_{xy}$-AO of Pt and HOMO $2b_1$ of ketene. Due to formation of this MO, some electronic density is transferred from the HOMO $2b_1$ of ketene to the complex, thereby stabilizing the vacant $3b_1$ orbital, as noted above. Analysis of the second bonding MO (HOMO-1) show that the same $5d_{xy}$-AO of Pt interacts with the linear combination ($|2b_1\rangle$ - $|3b_1\rangle$) of ketene MOs, wherein the predominant contribution comes from the vacant $3b_1$ MO. This HOMO-1 of the complex provides the OCT to the unoccupied ketene MO $3b_1$, $\Delta q(3b_1) = 0.28$ ē. Thus, in this case, the corresponding metal orbitals can be considered as an interface in the electron density transfer from the HOMO $2b_1$ of ketene molecule to its excited $3b_1$ orbital. Then, the value of the $K^{coord}(b_1)$ with respect to the out-of-plane distortion of b_1-type can be estimated by Eq.(10).

$$K_{b1}^{coord} = K_{b1}^{free} - 2\Delta q_{3b1}\left|f_{b1}^{(3b1,8a1)}\right|^2/\Delta_{3b1,8a1} \quad (10)$$

Calculated value of $K^{free}(b_1)$ is equal to 1.70 eV/Å^2, $f_{b2}^{(3b1,8a1)}$ = 5.47 eV/Å [19], Δ = 3.56 eV, so that we obtain $K^{coord}(b_1)$ = -3.02 V/Å^2.

It is seen that in the coordinated state the curvature of the APES of the H_2C_2O molecule with respect to the bending modes becomes negative in both complexes. This explains the origin of the geometry of coordination of this molecule and provides for numerical estimates of the strength of distortion.

In the same approximation, by applying the JTE ideology to the ketene molecule with respect to the totally symmetric displacements of A_1 type, we can explain also the significant elongation of its C-O bond in the complex of vanadium, and elongation of C-C bond by coordination to the complex of platinum. The diagonal vibronic coupling constant has the physical meaning of the force with which the electrons affect the nuclei in the direction of Q; in the MO approximation [12]. In the ground state equilibrium configuration of free CH_2CO molecule the distorting force F_{A1} equals zero. After the charge transfers Δq_i this force changes by $\Delta F(\mathbf{I})=\Delta q(3b_2)f^{3b2,3b2}$, and $\Delta F(\mathbf{II})=\Delta q(2b_1)f^{2b1,2b1} + \Delta q(3b_1)f^{3b1,3b1}$. It was shown in [12] that for bonding MO $f^{(i)}>0$, and for antibonding MO $f^{(i)}<0$. Hence $f^{3b2,3b2}<0$ for the C-O bond, $f^{2b1,2b1}>0$, and $f^{3b1,3b1}<0$ for the C-C bond. Given that $\Delta q(2b_1)<0$, $\Delta q(3b_1)>0$, and $\Delta q(3b_2)>0$, we get $\Delta F(\mathbf{I})<0$ for the C-O bond in (**I**) and $\Delta F(\mathbf{II})<0$ for the C-C bond in (**II**). Thus, in the both cases the OCTs induce a JTE distorting force which pushes away the carbon and oxygen nuclei in (**I**), and the carbon nuclei in (**II**), thereby increasing the C-O and C-C and bond lengths, respectively.

Conclusions

In this study, we have demonstrated that structural distortions of ketene molecule caused by their coordination to transition metal complexes may be interpreted as the consequences of the PJTE induced by the orbital charge transfers It is shown that the curvature of the AP of coordinated ketene respectively in the b_2 (in **I**) and b_1 (in **II**) directions becomes negative in both complexes, that explains the origin of the geometry of coordination of the molecule. The η^2-(C-O) coordination and the in-plane distortion of ketene in the complex of vanadium is due to the PJTE induced by the back donation to its LUMO $3b_2$ (π_{CO}*). The η^2-(C-C) coordination mode, as well as the out-of-plane distortion of the molecule in the complex of platinum is caused by the two charge transfers: from the HOMO $2b_1(\pi_{CC})$ to the metal d_{xy}-AO, and from the same AO of Pt to the vacant $3b_1(\pi_{CC}$*) MO of ketene, thus being the result of diorbital Pt-ketene interaction.

The elongation of C-O and C-C bonds respectively in the complexes of vanadium and platinum as compared with the free ketene molecule is due to the change of the corresponding diagonal vibronic coupling constants which is induced by the orbital charge transfers by coordination.

References

1. Grotjahn, D.B.; Collins, L.S. B.; Wolpert, M.; Bikzhanova, G.A.; Lo, H.C.; Combs, D.; and Hubbard, J.L. First direct structural comparison of complexes of the same metal fragment to ketenes in both C,C- and C,O-bonding modes. Journal of American Chemical Society, 2001, 123, pp. 8260-8270.
2. Miyashita, A.; Shitara, H.; Nohira, H. Preparation and properties of platinum ketene complexes. Facile carbon-carbon bond cleavage of coordinated ketene. Organometallics, 1985, 4, pp.1463–1464.
3. Antiñolo, A.; Otero, A.; Fajardo, M.; Lopez-Mardomingo, C.; Lucas, D.; Mugnier, Y.; Lanfranchi, M.; Pellinghelli, M.A. Early-transition-metal ketene complexes: Synthesis, reactivity and structure of ketene complexes of bis(trimethylsilyl)niobocene, X-ray structure of [Nb(η^5-$C_5H_4SiMe_3)_2$Br(Ph_2C=C=O, η^2-C,O). Journal of Organometallic Chemistry, 1992, 435, pp. 55-72.
4. Miyashita, A.; Sugai, R.J.; Yamamoto, J.I. Synthesis and reactivities of novel η^2-(C,O) alkylphenylketene complexes of nickel. Coordination-mode switching reaction of the ketene ligand. Journal of Organometallic Chemistry, 1992, 428, pp. 239-247.
5. Wright, C.A.; Thorn, M.; McGill, J.W.; Sutterer, A.; Hinze, S.M.; Prince R.B.; and Gong, J.K. A first example of a

"Wittig Reaction" on a coordinated carbon dioxide nickel complex. Journal of American Chemical Society, 1996, 118, pp. 10305-10306.
6. Waymouth, R.M.; Santarsiero, B.D.; Grubbs, R.H. Trigonal-bipyramidal methyl group bridging two zirconocene-ketene centers. Journal of American Chemical Society, 1984, 106, pp. 4050–4051.
7. Hofmann, P.; Perez-Moya, L.A.; Stelgelmann, O.; Riede, J. η^2-(C,O) ketene coordination at nickel(0). Synthesis, bonding, and molecular structure of (dtbpm)Ni[η^2-(C,O)-Ph_2C_2O] [dtbpm = bis(di-tert-butylphosphino)methane]. Organometallics, 1992, 11, pp. 1167-1176.
8. Liu, X.; Gong, J.K.; Seyler, J.W. Theoretical investigation of ketene bonding modes in bis(phosphine) palladium ketene complexes. Journal of Coordination Chemistry, 2000, 52, pp. 47-56.
9. Gorinchoy N.N.; Balan I.I.; Bersuker I.B. Jahn-Teller, pseudo Jahn-Teller, and Renner-Teller effects in systems with fractional charges. Computational and Theoretical Chemistry, 2011, 976, pp. 113-119.
10. Gorinchoy N. Jahn-Teller and pseudo Jahn-Teller origin of structural distortions of coordinated molecules. Revue Roumaine de Chimie, 2014, 59(3-4), pp. 273-280.
11. Gorinchoy N. Bending of adsorbed FCN and FNC molecules induced be the Renner-Teller effect. Annals of the West University of Timisoara, Physics series, 2012, 56, pp. 15-23.
12. Bersuker I.B. The Jahn-Teller Effect, Cambridge University Press, Cambridge (UK), 2006, 616 p.
13. Frisch, M.J.; Trucks, G.W.; Schlegel, H.B.; Scuseria, G.E.; Robb, M.A. et al. Gaussian 09, Revision B.01; Gaussian, Inc.: Wallingford, CT, 2009.
14. Lee, C.; Yang, W.; Parr, R.G. Development of the Colle-Salvetti correlation-energy formula into a functional of the electron density. Physical Review B, 1988, 37, pp. 785-789.
15. Hay, P.J.; Wadt, W.R. Ab initio effective core potentials for molecular calculations. Potentials for K to Au including the outermost core orbitals. Journal of Chemical Physics, 1985, 82, pp. 299-310.
16. Hehre, W.J.; Ditchfield, R.; Pople, J.A. Self-Consistent Molecular Orbital Methods. XII. Further extensions of Gaussian-type basis sets for use in molecular orbital studies of organic molecules. Journal of Chemical Physics, 1972, 56 pp. 2257-2261.
17. Dykstra, C.E.; Schaefer III, H.F. Excited electronic states of ketene. Journal of American Chemical Society, 1976, 98, pp. 2689-2695.
18. Szalay, P.G;. Császár, A.G.; Namas, L. Electronic states of ketene. Journal of Chemical Physics, 1996, 105, pp. 1034-1045.
19. Gorinchoy N. Electronic control of molecular configuration instability *via* vibronic coupling. Pseudo Jahn-Teller stabilization of vertically excited states of F_2CO, N_2H_2 and H_2C_2O molecules. Chemistry Journal of Moldova, 2014, 9(2), pp. 80-89.

CHEMISTRY JOURNAL OF MOLDOVA. General, Industrial and Ecological Chemistry. 2016, 11(2), 105-108
http://cjm.asm.md
http://dx.doi.org/10.19261/cjm.2016.11(2).06

GC-MS ANALYSIS OF THE ESSENTIAL OIL OF *SATUREJA SUBSPICATA* BARTL. EX VIS. OF MOLDOVAN ORIGIN

Ion Dragalin[a*], Aculina Aricu[a], Nina Ciocarlan[b], Alexandru Ciocarlan[a,c], Victoria Codita[a,c]

[a]*Institute of Chemistry, Academy of Science of Moldova, 3, Academiei str., Chisinau MD 2028, Republic of Moldova*
[b]*Botanical Garden (Institute) of Academy of Sciences of Moldova,18, Padurii str., Chisinau MD 2002, Republic of Moldova*
[c]*Tiraspol State University, 5, Gh. Iablocikin str., Chisinau MD 2069, Republic of Moldova*
**e-mail: iondragalin@yahoo.com, phone: (+37322) 739769*

Abstract. For the first time the results of GC-MS analysis of *Satureja subspicata* L. oil of Moldovan origin are reported. The chemical profile includes forty-four constituents and consists mostly (97.86%) of phenolic monoterpenes, monoterpene hydrocarbons, bicyclic sesquiterpenes and their oxygenated derivatives. A substantial quantitative and qualitative chemical differentiation of *S. subspicata* oil of Moldovan origin and reported oil of Croatian origin were found. The essential oil of *S. subspicata* L. plants cultivated in Republic of Moldova belongs to the carvacrol chemotype.

Keywords: *Satureja subspicata* L., essential oil, chemical profile, GC-MS analysis.

Received: October 2016/ Revised final: November 2016/ Accepted: November 2016

Introduction

Numerous studies have been conducted on *Satureja* L. species, growing in different world regions, particularly on its volatile oil composition. According to these data, essential oils from *Satureja* species have a very complex composition, which includes phenolic monoterpenes, monoterpene hydrocarbons, bicyclic sesquiterpenes, other terpene derivatives and flavonoids [1-4].

A wide range of biological activities have been reported for different species of *Satureja* L.: anti-inflammatory [5], anti-HIV [6], antidiabetic, antioxidant, antimicrobial and antihyperlipidemic [7], antifungal [8], antispasmodic and antidiarrheal [9], vasodilatory [10] and cytotoxic [11].

The present studies are related to *Satureja subspicata* Bartl. ex Vis. cultivated in the Botanical Garden (Institute) of Academy of Science of Moldova (ASM), Collection of Medicinal Plants. Climate of the Republic of Moldova is favourable for *S. subspicata*, where plants have normal growth rhythms and successfully attain the generative period.

Up to date a few reports on essential oil composition and biological activity of *S. subspicata* species have been published. The volatile oil of *S. subspicata* possesses a big part of activities mentioned before, and is therefore a potential source of antimicrobial ingredients for the food and pharmaceutical industry.

The aim of this work is to reveal the chemical composition of *S. subspicata* essential oil cultivated in climatic and soil conditions specific for Republic of Moldova by means of GC-MS analysis.

Experimental

Materials

The plant material *Satureja subspicata* of Moldovan origin (aerial parts with inflorescence) for the chemical analyses was collected during flowering stage in July 2016 from experimental fields of the Botanical Garden (Institute) of ASM. The plants were cultivated in ecological conditions and without fertilizer use. Voucher specimen is deposited in the Herbarium of the Botanical Garden (Institute) of ASM.

Methods

Essential oil of *S. subspicata* was obtained by hydrodistillation (600 mL) of the aerial parts of the plant (200 g) for 2 hours in a Clevenger apparatus. After phase separation, volatile oil was dried over anhydrous sodium sulphate, and then used for chromatographic measurements.

The GC-MS analysis of the *S. subspicata* essential oil was carried out on an Agilent Technologies 7890A system with 5975C Mass-Selective Detector (GC-MSD) equipped with split-splitless injector (split, 250°C, split ratio 1:50, 1 μL) and HP-5 ms capillary calibrated column (30 m x 0.25 mm x 0.25 mm); The carrier gas: helium 1.1 mL/min; oven: 70°C-2 min, 5°C/min-200°C-20 min-300°C-5 min; MSD in scan 30-300 amu, 15 min, 30-450 amu, solvent delay 3 min.

Results and discussion

By hydrodistillation of plant material a whitish coloured volatile oil (n^{18}_D=1.5020) was obtained. The GC-MS analysis of *S. subspicata* oil resulted in identification of 44 components (see Figure 1 and Table 1). These components represent 97.86 % of the oil and were identified by comparison of the acquired mass spectra with those from apparatus database. The mass spectrum of the major component carvacrol (RT–13.54) is depicted in Figure 2.

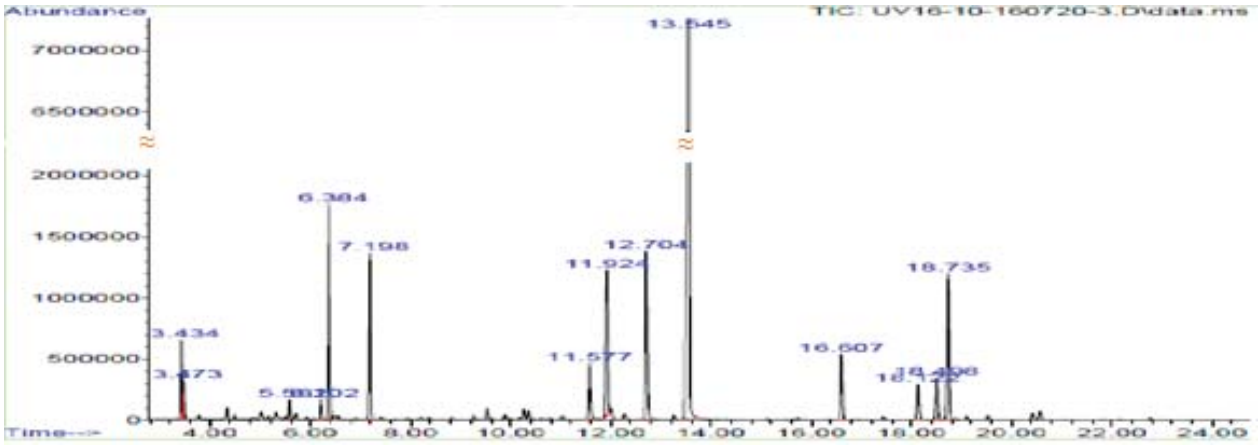

Figure 1. Cromatografic profile of *S. subspicata* essential oil.

Figure 2. Mass spectrum of carvacrol (1).

According to GC-MS analysis, the most abundant component of *S. subspicata* essential oil is phenolic terpene carvacrol **1** (47.56%), followed by monoterpene hydrocarbons *p*-cimen **2** (6.94) and *γ*-terpinene **3** (5.54%), alchohol nerol **4** (2.15%), aldehydes (*E*)-citral **5** (7.23%) and (*Z*)-citral **6** (5.73%) (Figure 3, Table 1); sesquiterpenes (+)-*β*-bisabolene **7** (5.80%), *β*-caryophyllene **8** (2.61%), germacrene B **9** (1.78%) and germacrene D **10** (1.42%) (Figure 4, Table 1). The reported compounds accounted for 97.86% of total content of the essential oil.

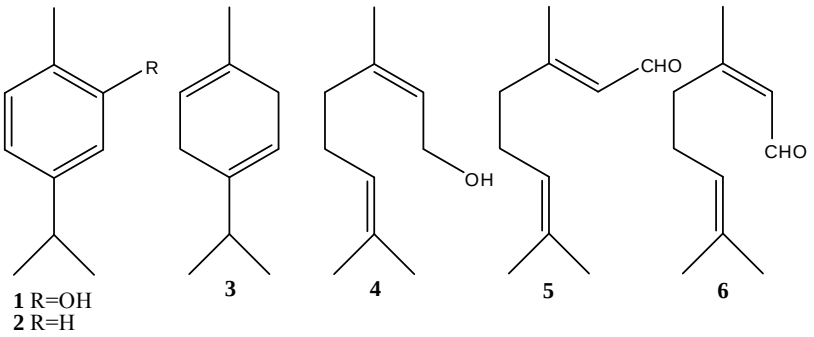

Figure 3. Monoterpenes.

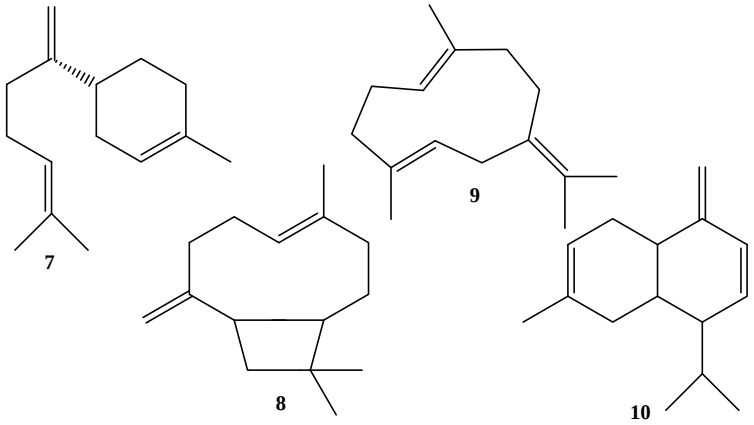

Figure 4. Sesquiterpenoids.

It must be mentioned, that the *S. subspicata* essential oil of Moldovan origin showed significant difference in qualitative and quantitative chemical composition in comparison with the reported from native area. *S. subspicata* essential oil of Croatian origin contains carvacrol (16.76%) as major constituent, followed by *α*-pinene (13.58%), *p*-cymene (10.75%) and *γ*-terpinene (9.54%) [12]. According to Dunkić V. *et al*., the major component of the essential oil of two *S. subspicata* subspecies (*S. subspicata* ssp. *subspicata* and *S. subspicata*s sp. *liburnica*) is monoterpenic hydrocarbon *α*-pinene (yield 52.9% and 42.6%, respectively) and it means that both taxa belong to *α*-pinene chemotype [13]. The carvacrol content (16.8% and 13.5%, respectively) reported by these authors is three times smaller than its content in *S. subspicata* oil of Moldovan origin.

Another team of researchers reported *α*-pinene (24.2%) as main compound of the essential oil from wild-grown *S. subspicata* in the Mediterranean part of Croatia, while carvacrol constitutes only 2.7% [14]. The *S. subspicata* species originating from Bosnia and Herzegovina contain thymol (28.6%) and carvacrol (27.9%) as main compounds of their essential oils [15].

Table 1

Phytochemical composition of *S. subspicata* essential oil of Moldovan origin.

No	*RT* (min)*	*Component*	*%*	***No***	*RT* (min)*	*Component*	*%*
1	3.434	Isoamyl acetate	1.98	***23***	9.885	Borneol	0.17
2	4.344	Origanene	0.36	***24***	10.271	1-Terpinen-4-ol	0.39
3	4.496	*α*-Pinene	0.14	***25***	10.360	(*Z*)-Verbenol	0.34
4	4.863	Isocumene	0.06	***26***	10.624	*α*-Terpineol	0.08
5	5.018	1-Ethyl-3-methylbenzen	0.31	***27***	10.787	Pulegone	0.10
6	5.270	Sabinene	0.04	***28***	11.038	Myrtenol	0.22
7	5.316	1-Octen-3-ol	0.25	***29***	11.577	Nerol	2.15
8	5.502	Heptenone	0.10	***30***	11.924	(*Z*)-Citral	5.73
9	5.581	*β*-Myrcene	0.59	***31***	11.999	Isothymol methyl ether	0.46
10	5.696	1,2,3-Trimethylbenzene	0.23	***32***	12.271	Geraniol	0.28
11	5.928	*α*-Phellandrene	0.09	***33***	12.704	(*E*)-Citral	7.23
12	6.202	*α*-Terpinene	0.63	***34***	13.252	Tymol	0.17
13	6.383	*p*-Cymene	6.94	***35***	13.545	Carvacrol	47.56
14	6.489	Limonene	0.73	***36***	15.729	*α*-Bourbonene	0.07
15	6.564	Eucalyptol	0.14	***37***	16.607	*β*-Caryophyllene	2.61
16	7.198	*γ*-Terpinene	5.54	***38***	17.447	*α*-Bisabolene	0.13
17	7.428	Terpinene-4-acetate	0.09	***39***	18.122	Germacrene D	1.42
18	8.202	Linalool	0.16	***40***	18.498	Germacrene B	1.78
19	8.370	*β*-Pinene oxide	0.10	***41***	18.735	(+)-β-Bisabolene	5.80
20	8.832	(*E*)-Sabinene-hydrate	0.11	***42***	19.535	*α*-Caryophyllene	0.21
21	9.261	Myrtanal	0.19	***43***	20.416	(-)-Spatulenol	0.36
22	9.533	2,2-Dimethylocta-3,4-dienal	0.42	***44***	20.555	Caryophyllene oxid	0.40

**RT - retention time.*

The list of secondary components of essential oils of Moldovan and Croatian origin, correspondingly, is comparable but differs quantitatively and includes: α-pinene, limonene, α-terpinene, thymol, linalool, β-myrcene, limonene, geraniol and others. In contrast with essential oil of Croatian origin, the studied by us oil is characterized by high content of unreported before components like γ-terpinene, (*E*)- and (*Z*)-citral, β-bisabolene, nerol, β -caryophillene, germacrenes (B and D) and others. As a result, biological activity, pharmaceutical and perfumery value of *S. subspicata* oil of Moldovan origin can be much higher.

Conclusions

The quantitative and qualitative chemical differentiation of essential oil obtained from *S. subspicata* plants growing in Moldova and Croatia can be correlated with different geographic location and ecological conditions. The high content of the phenolic terpene carvacrol as a main component (47.56%) suggests that *S. subspicata* plants cultivated in Republic of Moldova belong to a new high yielding carvacrol genotype.

References

1. Baser, K.H.C.; Tumen, G.; Satif, F.; Kirimer, N. Comparative morphological and chemical studies on *Satureja* species from west Anatolia. Book of abstracts, 2nd Balkan Botanical Congress, Istanbul, 2000, pp. 129-132.
2. Slavkovska, V.; Jancic, R.; Bojovic, S.; Miloslavjevic, S.; Djoković, D. Variability of essential oils from *Satureja montana* L. and *Satureja kitaibelii* Wierzb. Ex Heuff. from the central part of the Balkan Peninsula. Phytochemistry, 2001, 57, pp. 71-76.
3. Tumen, G.; Kirimer, N.; Baser, K.H.C. The essential oils of *Satureja* occuring in Turkey: Basic and Applied Research. Book of abstracts, 27th International Symposium on Essential Oils, Austria, 1997, pp. 250-254.
4. Tepe, B.; Cilkiz, M.A. Pharmacological and phytochemical overview on *Satureja*. Pharmaceutical Biology, 2016, 54(3), pp. 375-412.
5. Amanlou, M.; Dadkhah, F.; Salehnia, A.; Farsam, H.; Dehpour A. An anti-inflammatory and anti-nociceptive effects of hydrochloric extract of *Satureja khuzistanica* Jamzad extract. Journal of Pharmacy and Pharmaceutical Sciences, 2005, 8, pp. 102-106.
6. Yamasaki, K.; Nakano, M.; Kawahata, T.; Mori, H.; Otake, T.; Ueba, N.; Oishi, I.; Inami, R.; Yamane, M.; Nakamura, M.; Murata, H.; Nakanishi, T. Anti-HIV-l activity of herbs in *Labiatae*. Biological and Pharmaceutical Bulletin, 1998, 21, pp. 829-833.
7. Momtaz, S.; Abdollahi, M. An update on Pharmacology of *Satureja* species; From Antioxidant, Antimicrobial, Antidiabetes and Antihyperlipidemic to Reproductive Stimulation. International Journal of Pharmacology, 2010, 6(4), pp. 346-353.
8. Sokovic, M.; Sokovic, M.; Tzakou, O.; Pitarokili, D.; Couladis M. Antifungal activities of selected aromatic plants growing wild in Greece. Nahrung, 2002, 46, pp. 317-320.
9. Hajhashemi, V.; Sadraei, H.; Ghannadi, A.R.; Mohseni, M. Antispasmodic and antidiarrheal of *Satureja hortensis* L. essential oil. Journal of Ethnopharmacology, 2000, 71, pp. 187-192.
10. Sanchez de Pojas, V.R.; Somoza, B.; Ortega, T.; Villar, A.M.; Tejerina, T. Vasodilatory effect in rat aorta of eriodictyol obtained from *Satureja obovata*. Planta Medica, 1999, 65, pp. 234-238.
11. Stanojkovic, T.; Kolundzija, B.; Ciric, A.; Sokovic, M.; Nikolic, D.; Kundakovic, T. Cytotoxicity and antimicrobial activity of *Satureja kitaibelii* Wierzb. exHeuff (*Lamiaceae*). Digest Journal of Nanomaterials and Biostructures, 2013, 8, pp. 845-854.
12. Skočibusic, M.; Bezić, N.; Dunkić, V. Phytochemical composition and antimicrobial activities of the essential oils from *Satureja subspicata* Vis. growing in Croatia. Food Chemistry, 2006, 96(1), pp. 20-28.
13. Dunkić, V.; Bezić, N.; Ljubesić, N.; Bočina, I. Glandular hair ultrastructure and essential oils in *Satureja subspicata* Vis. ssp. s*ubspicata* and ssp. *liburnica* Šilić. Acta Biologica Cracoviensia, Series Botanica, 2007, 49(2), pp. 45-51.
14. Bezic, N.; Samanic, I.; Dunlic, V.; Besendorfer, V.; Puizina, J. Essential oil composition and internal transcribed spacet (ITS) sequience variability of four South-Croatian *Satureja* species (*Lamiaceae*). Molecules, 2009, 14, pp. 925-938.
15. Cavar, S.; Maksimović, M.; Šolić, M.E.; Jerković-Mujkić, A.; Bešta, R. Chemical composition and antioxidant and antimicrobial activity of two *Satureja* essential oils. Food Chemistry, 2008, 111, pp. 648-653.